INTENSIFICATION OF NH3 BUBBLE ABSORPTION PROCESS USING ADVANCED SURFACES AND CARBON NANOTUBES FOR NH3/LINO3 ABSORPTION CHILLERS

Carlos Fidel Amaris Castilla

Dipòsit Legal: T.66-2014

DOCTORAL THESIS

Intensification of NH_3 Bubble Absorption Process using Advanced Surfaces and Carbon Nanotubes for $NH_3/LiNO_3$ Absorption Chillers

Carlos Amaris Castilla

Supervisors: Dr. Manel Vallès
Dr. Mahmoud Bourouis

Department of Mechanical Engineering

UNIVERSITAT ROVIRA I VIRGILI

Tarragona
2013

UNIVERSITAT
ROVIRA I VIRGILI
DEPARTAMENT D´ENGINYERIA MECÀNICA
Escola Técnica Superior d´Enginyeria Química (ETSEQ)
Av. Països Catalans 26, 43007 Tarragona (Spain)

Los abajo firmantes, **Dr. Manel Vallès**, Profesor Titular del Departamento de Ingeniería Mecánica de la Universitat Rovira i Virgili y **Dr. Mahmoud Bourouis**, Profesor Agregado del Departamento de Ingeniería Mecánica de la Universitat Rovira i Virgili de Tarragona.

HACEN CONSTAR:

Que la presente memoria del trabajo titulado:

"*Intensification of NH_3 Bubble Absorption Process using Advanced Surfaces and Carbon Nanotubes for NH_3/$LiNO_3$ Absorption Chillers*"

presentado por el **Sr. Carlos Amaris Castilla** para optar al grado de Doctor de la Universitat Rovira i Virgili, ha sido realizado bajo su dirección inmediata en el CREVER – Grupo de investigación de Ingeniería Térmica Aplicada del Departamento de Ingeniería Mecánica de la Universitat Rovira i Virgili, que todos los resultados han sido obtenidos en las experiencias realizadas por dicho doctorando y que cumple los requisitos para poder optar a la Mención Europea.

Y para que así conste a los efectos oportunos, firmamos este documento.

Tarragona, 09 de Octubre de 2013.

Dr. Manel Vallès Dr. Mahmoud Bourouis

Dedicada a mi adorada familia, en especial a mis padres.

UNIVERSITAT ROVIRA I VIRGILI
INTENSIFICATION OF NH3 BUBBLE ABSORPTION PROCESS USING ADVANCED SURFACES AND CARBON NANOTUBES FOR NH3/LINO3 ABSORPTION CHILLERS
Carlos Fidel Amaris Castilla
Dipòsit Legal: T.66-2014

"The world is big enough to satisfy everyone's needs, but will always be too small to satisfy everyone's greed." Mahatma Gandhi.

UNIVERSITAT ROVIRA I VIRGILI
INTENSIFICATION OF NH3 BUBBLE ABSORPTION PROCESS USING ADVANCED SURFACES AND CARBON NANOTUBES FOR NH3/LINO3 ABSORPTION CHILLERS
Carlos Fidel Amaris Castilla
Dipòsit Legal: T.66-2014

Agradecimientos

En primer lugar quiero agradecer a mi amada familia por siempre estar ahí como fuente de motivación y apoyo durante todo el tiempo fuera de casa. En especial a mi querida madre Carmen Cecilia y querido padre Carlos Arturo por su amor, enseñanzas, consejos, ejemplos y palabras de aliento que han hecho de mi la persona que soy hoy en día. A todos mis hermanos, en especial a Jair F. y Arlys C. por su gran apoyo al principio de este viaje y en el transcurso de este. A mis viejitas queridas Eve y Maria, a mis primos Ever y Evelyn por su cariño y por ser mis mas grandes ejemplos de nobleza y humildad. A mis madrinas Elisabeth y Bertha por su apoyo cuando más lo necesite y a todos mis familiares que han estado pendientes de mí durante los últimos años.

Igualmente, quiero expresar mi más absoluta gratitud y agradecimiento a mis directores de tesis, al Dr. Manel Valles y al Dr. Mahmoud Bourouis. Quiero agradecerles por darme la oportunidad de trabajar con ellos, por la paciencia que tuvieron conmigo, por el tiempo dedicado, por su guía y dirección durante el desarrollo del trabajo que se resume en esta tesis, por todo lo que aprendí de ellos y por el respecto con el que siempre me trataron.

También quiero expresar mi sincera gratitud y agradecimiento al Dr. Alberto Coronas, por darme la gran oportunidad de venir a Tarragona desde un principio, por permitirme ser parte del CREVER y por ser artífice fundamental de los comienzos de mi historia por estas tierras la cual culmina con esta tesis doctoral.

Quiero agradecer además al Dr. Carlos Infante Ferreira (Delft University of Technology) y a la Dr. Nathalie Mazet (University of Perpignan) por servir como revisores externos de esta tesis, y por todos y cada uno de sus valiosos comentarios adicionales.

Al departamento de Ingeniería Mecánica de la Universitat Rovira i Virgili y a los miembros de secretaria, en especial a María José Duran por su colaboración cuando la necesite.

Mis agradecimientos van también al ministerio de Economía y Competitividad por la adjudicación de mi beca (BES-2009-015241), por la financiación del proyecto ENE2008-00863 para el desarrollo de esta tesis y por la financiación de mi estancia de investigación en el Austrian Institute of Technology (AIT) en Viena. Al AIT de Viena por permitirme realizar la estancia de investigación en sus instalaciones, en especial al Dr. Monsberger y Dr. Fleckl.

A Luis M. por haberme hecho participe de esa gran oportunidad a partir de la cual iniciamos esta gran aventura. A mi gente en Tarragona, los que están y los que se han marchado, en especial a María Eugenia A., John Z., Ivan T., Miguel A. M., Javier B., Ramón M., Pipe Gómez, Alejandro J., Pedro C., Fernando C., Cesar O., Jorge D., Jorge R., Barbara M., Isa S., Mafe. P., Oana M., Mihaela A., Taty S., Magdita y Carito B.. Muchísimas gracias a todos por su compañía, amistad y por ayudar a acortar un poco esa distancia que hay desde mi ciudad natal Barranquilla hasta Tarragona la cual a partir de ahora considerare mi segundo hogar.

Mis agradecimientos también van a mi ex compañeros Creverianos por haber compartido conmigo instantes de su tiempo, a David M., Yolanda C., Jordi O., Silvana T., Simona S., Jerko L., Javier M., Andrés M., Nuria Q., María P., Daniel S., Joaquín C., Arturo O., Jesús L..

Gracias a Dios por permitirme alcanzar a esta nueva meta, por cuidarme, por todas las bendiciones que me ha dado y por las que vienen. Muchas gracias a Todos!

Table of Contents

Abstract

In the last decade, the interest and necessity to progress on the development of absorption refrigeration systems have led to studies on several techniques to improve their performances and then, make them more competitive in comparison with mechanical compression systems. According to our current needs due to the climate change and economic crisis, use of absorption chillers would imply an important impact on environment and energy saving if they are driven by residual heat or solar thermal energy.

Absorption refrigeration systems with conventional working fluids present some drawbacks such as crystallization, corrosion and vacuum operating pressures for H_2O/LiBr systems, and rectification of the refrigerant vapor leaving the desorber and high activation temperatures for NH_3/H_2O systems. These well-know drawbacks have increased the interest of researchers for new working mixtures. Investigations with the $NH_3/LiNO_3$ mixture have resulted in considering this mixture as a promising alternative working pair for absorption refrigeration cycles driven by low temperature heat sources.

Absorption systems with $NH_3/LiNO_3$ can be air-cooled since high condensation temperatures can be achieved without crystallization problems. Cycle with $NH_3/LiNO_3$ can perfectly operate at low activation temperatures and rectification of the refrigerant vapor leaving the generator is not needed since the absorbent is a salt. Accordingly, refrigeration systems with $NH_3/LiNO_3$ are highly recommended for solar cooling applications. However, previous experimental studies found in the literature showed that the main drawback of the $NH_3/LiNO_3$ is its high viscosity which limits heat and mass transfer processes mainly in the absorber in comparison with NH_3/H_2O.

Studies applying intensification techniques such as the use of rough or extended surfaces or addition of small quantities of additives to working fluids, to improve heat and mass transfer processes have been carried out more frequently in the last years. Recently, optimization of nanoparticle synthesis and reduction in the acquisition prices has also allowed for the inclusion of nanotechnology in thermal systems to enhance heat and mass transfer processes.

This thesis deals with an experimental study on intensification of the ammonia absorption process in the $NH_3/LiNO_3$ mixture in vertical bubble mode absorbers using advanced surfaces and nanoparticles of carbon nanotubes (CNTs). The increase of ammonia absorption process would allow diminishing the absorber size or what is even more interesting, reducing the cycle driving temperature for solar thermal applications and/or increasing the heat sink temperature for the heat released in the absorber and condenser to avoid the use of humid cooling towers.

Operating conditions selected for the absorber test were obtained from a thermodynamic analysis of a single effect absorption cycle with $NH_3/LiNO_3$ driven by low temperature heat sources and head released by air.

The experiments were conducted in an experimental test facility designed for evaluating the absorber performance at the desired operating conditions. Intensification of the ammonia absorption process was studied using two types of heat exchangers working as bubble absorbers; a plate heat exchanger and a tubular heat exchanger.

Firstly, results from the absorption process with $NH_3/LiNO_3$ in a plate heat exchanger with Chevron H-type corrugations (with an angle of 30 degree from its horizontal axis) are shown and correlated. Then, main results using the plate absorber H-type are compared with results found in the literature with a plate absorber with Chevron L-type corrugations (with an angle of 60 degree from its horizontal axis). Secondly, results from the absorption process with $NH_3/LiNO_3$ in a 1 meter tubular heat exchanger with smooth and advanced surfaces are analyzed. Results with the advanced surface tube with different tube diameters and lengths are also reported. Thirdly, results from the absorption process in a tubular heat exchanger with the $NH_3/LiNO_3$ mixture with nanoparticles (binary nanofluid) are shown. Then, experiments from using simultaneously the advanced surface tube and nanoparticles are presented. Finally, a simplified model for bubble absorbers with $NH_3/LiNO_3$ to predict the ammonia absorption process as a function of inlet operating conditions is presented.

Experiments on the ammonia absorption process with the plate absorber H-type resulted in maximum absorption mass flux of 0.0038 and 0.0072 $kg.m^{-2}s^{-1}$ at an inlet cooling-water temperature of 40 and 35 ^oC, respectively, and at a solution mass flow of 40 $kg.h^{-1}$. Moreover, it was observed that mass absorption rates at an inlet cooling-water temperature of 35 ^oC in the plate absorber H-type were higher than those values in the plate absorber L-type and also that this enhancement was rather attributed to the higher cooling water flow rate set in the plate H-type. According to this, effect of the angle of corrugation in the plate H-type in the absorption rates with respect to that in the plate L-type was insignificant.

Regarding experiments in the tubular absorber, results showed that the advanced surfaces used significantly improve the ammonia absorption process in the tubular bubble absorber analyzed in comparison with the smooth tube. The effect of the advanced surfaces was larger when the solution mass flow was increased. At low cooling-water Reynolds numbers and solution mass flows of 40 and 50 $kg.h^{-1}$, absorption mass fluxes for the tube with advanced surfaces were around 1.46 and 1.57 times higher than the values achieved for the smooth tube, respectively. At high values of the cooling-water Reynolds number, absorption mass flux values for the tube with advanced surfaces were around 1.71 and 1.54 times higher than those achieved for the smooth tube, respectively.

Regarding experiments with nanoparticles, results showed that carbon nanotubes significantly improve the ammonia absorption process in the tubular bubble absorber with the $NH_3/LiNO_3$ mixture. With respect to the reference values, the maximum enhancements achieved in the absorption mass flux with the binary nanofluid were around 1.64 and 1.48 times higher at cooling-water temperature of 40 and 35 ^oC, respectively.

Effect of the simultaneous use of the carbon nanotubes and advanced surfaces was also studied. Results depicted an outstanding improvement in the absorption mass flux and solution heat transfer coefficient with respect to reference values.

In addition, results from the numerical model for each absorber configuration were compared with results from the experimental study showing good agreement. Furthermore, numerical model allowed predicting temperature and concentration profiles. The numerical results evidenced that the numerical model can be used as a useful tool to design bubble absorbers.

Resumen

En la última década, el interés y necesidad de progresar en el desarrollo de los sistemas de refrigeración por absorción a llevado a estudios sobre técnicas que mejoren el rendimiento de estas maquinas para hacerlas más competitivas en comparación con los sistemas de refrigeración por compresión mecánica. De acuerdo a nuestras necesidades actuales condicionadas al cambio climático y actual crisis económica, el uso de enfriadoras por absorción activadas con energía residual o energía solar implicaría un impacto muy importante sobre el medio ambiente y ahorro energético.

Los sistemas de refrigeración por absorción trabajando con los fluidos convencionales presentan ciertos problemas tales como: cristalización, corrosión y presiones de operación de vacio para los sistemas H_2O/LiBr, y rectificación del vapor generado en el generador y altas temperaturas de activación para los sistemas NH_3/H_2O. Estas desventajas, las cuales son bien conocidas, ha propiciado la investigación sobre nuevos fluidos de trabajos. Investigaciones con $NH_3/LiNO_3$, ha conllevado al reconocimiento de esta mezcla como un alternativa prometedora para ser usada en los sistemas de refrigeración por absorción activados con fuentes de energía a baja temperatura.

Los sistemas de absorción con $NH_3/LiNO_3$ pueden ser enfriados con aire ya que el proceso de condensación del refrigerante puede llevarse a cabo a altas temperaturas sin riesgos de cristalización. Además, el ciclo con $NH_3/LiNO_3$ puede operar a bajas temperaturas de activación y la rectificación del vapor generado en el generador no es necesaria ya que el absorbente es una sal. En consecuencia, el sistema de refrigeración por absorción con $NH_3/LiNO_3$ es altamente recomendado para aplicaciones de refrigeración solar. Sin embargo, estudios experimentales encontrados en la literatura mostraron que la principal desventaja de la mezcla $NH_3/LiNO_3$ es su alta viscosidad, la cual limita los procesos que transferencia de calor y masa principalmente en el absorbedor, si se compara con la mezcla NH_3/H_2O.

En los últimos años, es cada vez más frecuente encontrar estudios aplicando técnicas de intensificación de procesos tales como el uso de superficies extendidas o rugosas, o adición de pequeñas cantidades de surfactantes al fluido de trabajo para mejorar los procesos de transferencia de calor y masa. Recientemente, la optimización del proceso de síntesis de nanoparticulas y la disminución de los costos de su adquisición ha permitido el uso de esta nanotecnología en sistemas térmicos con el mismo objetivo.

En la presente tesis doctoral se realiza un estudio experimental de la intensificación del proceso de absorción de amoniaco por parte de la mezcla $NH_3/LiNO_3$ en absorbedores de burbuja por medio del uso de superficies avanzadas y nanotubos de carbono. El aumento del proceso de absorción de amoniaco permitiría reducir el tamaño del absorbedor o lo que es más interesante, reducir la temperatura de activación del ciclo para aplicaciones de refrigeración solar y/o aumentar la temperatura de condensación para eliminar el uso de las torres de enfriamiento húmedas.

Las condiciones de operación de los ensayos experimentales fueron obtenidas a partir de una simulación termodinámica de un ciclo de absorción de simple efecto con $NH_3/LiNO_3$ a las condiciones de operación de interés para una enfriadora por absorción activada por fuentes de energía a baja temperatura y enfriada por aire.

Los experimentos se llevaron a cabo en un banco de prueba experimental diseñado para la evaluación del desempeño de absorbedores a las condiciones deseadas. El estudio del proceso de absorción se realizo en dos tipos de intercambiadores de calor trabajando como absorbedores; un intercambiador de calor de placas y un intercambiador de calor tubular.

Primero, se realiza un estudio del proceso de absorción con $NH_3/LiNO_3$ en un intercambiador de placas con corrugaciones tipo H Chevron y los valores de transferencia de calor y masa son correlacionados. Luego, los resultados principales obtenidos en el intercambiador de placas se comparan con los resultados reportados en la literatura sobre el proceso de absorción con $NH_3/LiNO_3$ en un intercambiador de placas con corrugaciones tipo L. Segundo, se realiza un estudio del proceso de absorción, esta vez en un intercambiador de calor de doble tubo de 1 metro con superficie interna lisa y con superficies avanzadas. Luego, se estudia el proceso de absorción en el intercambiador de doble tubo con superficies avanzadas variando el diámetro interno y la longitud del absorbedor. Tercero, se realiza un estudio del proceso de absorción con $NH_3/LiNO_3$ y nanoparticulas de carbono en el intercambiador de doble tubo con superficie lisa. Seguidamente se estudia el efecto combinado de las nanoparticulas de carbono y superficies avanzadas en el proceso de absorción con $NH_3/LiNO_3$. Finalmente, se desarrolla un modelo simplificado para absorbedores de burbujas con $NH_3/LiNO_3$, en el cual se implementan las correlaciones obtenidas experimentalmente, para predecir el proceso de absorción en función de las condiciones de los parámetros de entrada y.

Los experimentos sobre el proceso de absorción en el intercambiador de placas con corrugaciones tipo H dio como resultado un flujo másico de absorción de 0.0038 y 0.0072 $kg.m^{-2}s^{-1}$ a una temperatura de entrada en el lado del agua de enfriamiento de 40 y 35 ^oC, respectivamente, con un flujo másico de solución de 40 $kg.h^{-1}$. Además, se observo que el flujo másico de absorción en el intercambiador de placas tipo H con una temperatura en el lado del agua enfriamiento de 35 ^oC fue mayor que aquellos valores obtenidos en el intercambiador de placas tipo L y también que esta mejora fue atribuida al flujo de agua más alto en el intercambiador de placas tipo H. De acuerdo a estas observaciones, el efecto del ángulo de la corrugación sobre el flujo de absorción es insignificante en los intercambiadores de placa estudiados.

De acuerdo a los experimentos en el absorbedor tubular, los resultados muestran que las superficies avanzadas usadas mejoran significativamente el proceso de absorción de amoniaco en el absorbedor de burbuja estudiado en comparación con un absorbedor de tubo liso y que el efecto de las superficies avanzadas es más notable cuando se incrementa el flujo de solución y agua. A bajos números de Reynolds en el lado agua y a flujos másicos de solución de 40 y 50 $kg.h^{-1}$, el flujo másico de absorción en el tubo con superficies avanzadas fue alrededor de 1.46 and 1.57 veces más alto que los valores alcanzados en el tubo liso, respectivamente. A altos números de Reynolds en el lado agua, el flujo másico de absorción en el tubo con superficies avanzadas fue alrededor de 1.71 and 1.54 veces más alto que los valores alcanzados en el tubo liso, respectivamente.

De acuerdo a los experimentos con nanoparticulas, los resultados mostraron que los nanotubos de carbono mejoran significativamente el proceso de absorción de amoniaco en el absorbedor de burbujas tubular con superficie lisa con la mezcla de $NH_3/LiNO_3$. Con respecto a los valores de referencia, la máxima mejora conseguida en el flujo másico de

absorción con los nanofluidos fue 1.64 y 1.48 veces más alto a temperaturas en el lado agua de 40 y 35 ^{o}C, respectivamente.

El efecto combinado de los nanotubos de carbono y las superficies avanzadas también se estudio. Los resultados muestran un más notable aumento en el flujo másico de absorción y el coeficiente de transferencia de calor de la solución con respecto a los valores de referencia.

Finalmente, se obtuvo una buena relación entre los resultados a partir de un modelo numérico simplificado para cada configuración del absorbedor y los resultados experimentales.

Por otra parte, el modelo numérico permitió predecir los perfiles de temperatura y concentración de la solución evidenciando su utilidad para el diseño de absorbedores de burbujas.

List of Figures

List of Tables

Symbols

A	*heat transfer area, m^2*
a_i	*specific interfacial area, $m^2.m^{-3}$*
Ap	*cross-sectional area, m^2*
C	*correction factor*
CNTs	*carbon nanotubes*
COP	*coefficient of performance*
Cp	*heat capacity, $kJ.kg^{-1}K^{-1}$*
D	*diameter, m*
dA_M	*differential mass transfer area, m^2*
dl	*differential length, m*
d_p	*bubble diameter, m*
dTa	*differential transfer area, m^2*
e	*wall thickness, m*
E_G	*gas hold up*
f	*Darcy friction factor*
F	*NH_3 absorption mass flux, $kg.m^{-2}s^{-1}$*
F_0	*adjustment factor*
g	*acceleration due to gravity,$m.s^2$*
H	*enthalpy, $kj.kg^{-1}$*
h	*heat transfer coefficient, $kW.m^{-2}K^{-1}$*
Km	*mass transfer coefficient, $m.h^{-1}$*
L	*length of the absorber, m*
LMTD	*logarithmic mean temperature difference, ^oC*
LMXD	*logarithmic mean concentration difference*
$\dot{m}$	*mass flow rate, $kg.s^{-1}$*
Mod	*model results*
MSE	*mean square error*
MWCNTs	*multi walled carbon nanotubes*
Nu	*Nusselt number*
OD	*outer diameter, m*
P	*pressure, kPa*
Pr	*Prandtl number*
Q	*thermal load per unit of area, $kW.m^{-2}$*
Q_{AB}	*thermal load in the absorber, kW*
Q_E	*thermal load in the evaporator, kW*
Q_G	*thermal load in the generator, kW*
R	*resistance*
Re	*Reynolds number*
s	*separation between plates, m*
Sc	*Schmidt number*
Sh	*Sherwood number*
T	*temperature, ^oC*
TEM	*transmission electron microscopy*
U	*overall heat transfer coefficient, $kW.m^{-2}K^{-1}$*
v	*specific volume,$m^3.kg^{-1}$*
$\dot{V}$	*volumetric flow rate, $m^3.h^{-1}$*

vel	*velocity, $m.s^{-1}$*
W	*pump consumption, kW*
w	*width of the plate, m*
x	*NH_3 concentration, kg $_{NH3}.kg^{-1}_{NH3/LiNO3}$*
z	*ratio of ammonia mass flux to the total mass flux absorbed*

Subscripts:

AB	*absorber*
ABS	*absorbent*
b	*bubble*
C	*cold side*
CNTs	*carbon nanotubes*
cte	*constant of heat transfer*
Cw	*cooling water*
Eq	*equilibrium*
Exp	*experimental result*
H	*hot side*
h	*hydraulic*
In	*absorber inlet*
Inner	*inner diameter of the tube*
Int	*interface*
liq	*liquid*
m	*average*
NH_3	*ammonia*
o	*outer tube*
Out	*absorber outlet*
Outer	*outer diameter of the tube*
PA	*plate absorber*
REF	*refrigerant*
Sat	*saturation state*
SEN	*sensible*
Sol	*solution of $NH_3/LiNO_3$*
Steel	*stainless steel*
Sub	*subcooling*
TA	*tubular absorber*
vap	*ammonia vapor*

Greek letters:

ΔP	*pressure difference, kPa*
ΔT	*temperature difference, ^oC*
β	*diffusivity coefficient, $m^2.s^{-1}$*
λ	*thermal conductivity, $kW.m^{-1}K^{-1}$*
μ	*dynamic viscosity,$kg.s^{-1}m^{-1}$*
ρ	*density, $kg.m^{-3}$*
σ	*superficial tension, $N.m^{-1}$*

UNIVERSITAT ROVIRA I VIRGILI
INTENSIFICATION OF NH3 BUBBLE ABSORPTION PROCESS USING ADVANCED SURFACES AND CARBON NANOTUBES FOR NH3/LINO3 ABSORPTION CHILLERS
Carlos Fidel Amaris Castilla
Dipòsit Legal: T.66-2014

Chapter 1

Introduction

1.1 Introduction

The over-exploitation of natural resources, ozone depletion and global warming together with the increment of the energy consumption and its costs are some of the problems that humanity faces. Over-exploitation of important natural resources such as fossil fuels due to the large increment of the population and global energy consumption has caused excessive pollution which at the same time has resulted in the depletion of ozone layer and imbalances in the environment.

Energy consumers sectors include the buildings, industry and transport sectors. The first one, the building sector which involves the residential and commercial buildings, consumes up to 40 % of final energy used globally. Significant part of the buildings consumption is for heating, ventilation, cooling and lighting. It means that large amount of the energy demand of buildings is for air-conditioning of spaces (United Nations Environment Programme). The air-conditioning systems are responsible of around 50 % of the total building consumption, which represent around 20 % of total energy consumption in developed countries (Perez-Lombard et al. 2008). These issues also show the greatest opportunities for significantly reduce gases emissions in both developed and developing countries.

The International Energy Agency (IEA), in its report of Energy Technology Perspectives 2010, showed some insights into the future of global energy consumption and CO_2 emissions in the sectors of industry, buildings and transport, (Figure 1.1 and Figure 1.2). In this report is analyzed the current status and future energy options taking into account two main scenarios. A baseline and a BLUE map scenario. The baseline scenario assumes that no new policies are introduced and follows the world energy outlook 2009 reference scenario to 2030, and the BLUE map scenario which assumes optimistically that global energy-related CO_2 emissions are reduced to half their 2005 levels by 2050.

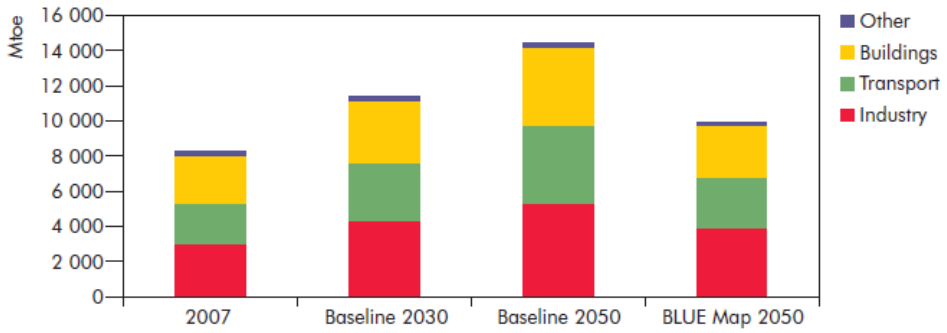

Figure 1.1 – Final energy use by sector (International Energy Agency, 2010).

According to the IEA, energy consumption in the transport, buildings and industry sectors together, increases on average by 1.3 % a year between 2007 and 2013. This trend was mainly attributed to continued strong population and income growth in developing countries. In 2050, global energy consumption is projected to be higher than 14000 Mtoe if new policies are not introduced. The report also showed that comparing both scenarios in 2050, total final energy demand can be reduced up to 31 % in the Blue map scenario if new control policies are implemented.

Furthermore, it is also commented that the most significant reductions in energy consumption can be achieved in the buildings and transport sectors and highlighted that in the buildings sector, savings of 1 509 Mtoe in 2050 show the extraordinary technical opportunity to optimize space heating and cooling needs in both existing and new buildings, as well as to improve the energy efficiency of lighting, electric appliances and air-conditioning technologies.

The IEA also reported that about 84 % of current CO_2 emissions are energy-related and about 65 % of all greenhouse-gas emissions can be attributed to energy supply and energy use. The IEA showed that the baseline scenario projects a doubling of the 2007 emissions over the period to 2050. On the other hand, almost a 90 % reduction of CO_2 emissions compared to 2007 levels can be achieved if strong control policies are implemented.

According to the Figure 1.2, direct emissions from buildings are for around 10 % of global CO_2 emissions which become almost 30 % if indirect emissions from the use of electricity are included. IEA explained that from an energy perspective, buildings are complex systems consisting of the building envelope and its insulation, lighting, appliances, consumer products, business equipment, water heating system and spaces that require air-conditioning systems.

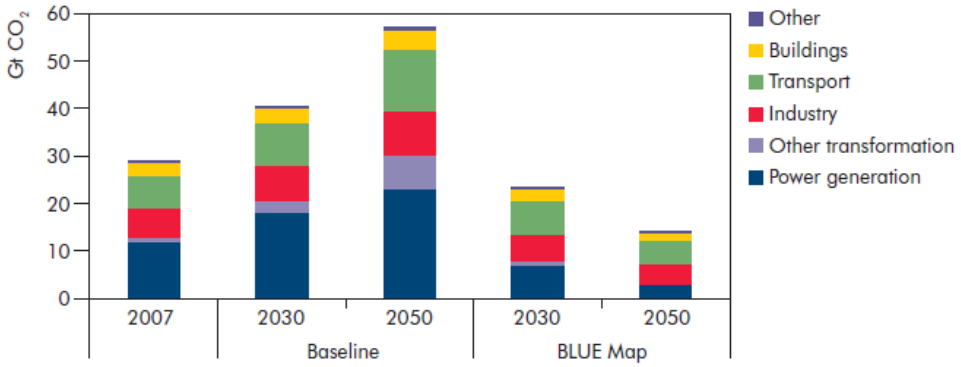

Figure 1.2 - Global CO_2 emissions in the Baseline and BLUE Map scenarios (International Energy Agency, 2010).

Air-conditioning systems such as mechanical compression technologies need high electrical power and a suitable refrigerant for their operation. Both of these requirements can have high environmental impacts and contribute to global warming.

Many ozone-depleting substances (ODS) such as chlorofluorocarbons (CFCs) and the fluorocarbon gases such as hydrofluorocarbons (HFCs) used to replace CFCs are potent greenhouse gases and are between 90 to 12,200 times more powerful than CO_2 in causing climate changes. In 2007, the Parties to the Montreal Protocol on Substances that Deplete the Ozone Layer decided to accelerate the gradual elimination of HCFCs, which are mainly used in the refrigeration and air-conditioning systems. Because of their lower ozone depletion potential, HCFCs were promoted as transitional replacements to enable the CFCs gases to be quickly excluded (United Nations Environment Programme).

The accelerated elimination of HCFCs shows an unprecedented opportunity to adopt ozone and climate-friendly technologies and policies. However, these outstanding climate benefits depend on the replacement of old and obsolete technologies by energy efficient alternative ones together with more efficient servicing practices. Undoubtedly, these efforts will lessen direct and indirect gas emissions through increased energy efficiency.

Countries need to work on the development of advanced air-conditioning technologies in order to adapt to the effects of climate change and to progress onto low gases emission development choices. For that, there is a need to distinguish which technologies can best be adapted to our actual necessities, as well as to remove obstacles preventing the widespread diffusion of advanced air-conditioning technologies in markets.

Absorption air-conditioning technologies have been identified as an attractive technology option to replace conventional electrically driven mechanical compression systems. Absorption air-conditioning technologies have demonstrated to provide high potential for energy saving due to the fact that they can be thermally driven to produce cooling or heating in comparison with conventional electrically driven mechanical compression technologies. Also, absorption technologies use environmentally friendly working fluids which do not deplete the ozone layer and do not contribute to global warming, contrary to most refrigerants used in mechanical compression technologies.

On the other hand, thermally driven absorption technologies for buildings are still in the early periods of market development. The main obstacles that impede their wide diffusion are high initial costs, lack of consumer awareness of technologies, few regulations, the low priority on energy efficiency, import and export restrictions, deficient government policies and lack of experience/knowledge to operate these technologies (The International Energy Agency, 2010). In order to overcome these obstacles, comprehensive policies that may include fiscal and financial incentives, information campaigns, and other development policies, as well as minimum energy performance standards and requirements are indispensables to be adopted.

Recent years show some hopeful signs of a change in consumer preferences towards new technologies that can reduce energy consumption and CO_2 emissions. Investigations have also been increasing rapidly on solar thermal systems that can provide low-temperature heating and cooling for air-conditioning of spaces.

1.2 Justification

In the last decade, the interest and necessity to progress on the development of absorption refrigeration systems have led to studies on several techniques to improve their performances and then, make them more competitive in comparison with mechanical compression systems. According to our current needs due to the climate change and economic crisis, use of absorption chillers would imply an important impact on environment and energy saving if they are driven by residual heat or solar thermal energy. Absorption refrigeration systems with conventional working fluids present some drawbacks such as crystallization, corrosion and vacuum operating pressures for H_2O/LiBr systems, and rectification of the refrigerant vapor leaving the desorber and high activation temperatures for NH_3/H_2O systems. These well-know drawbacks have

increased the interest of researchers for new working mixtures. Investigations with the $NH_3/LiNO_3$ mixture have resulted in considering this mixture as a promising alternative working pair for absorption refrigeration cycles driven by low temperature heat sources.

The absorption systems with the $NH_3/LiNO_3$ mixture can be air-cooled since high condensation temperatures can be achieved without crystallization problems. Cycles with the $NH_3/LiNO_3$ mixture can perfectly operate at low activation temperatures and rectification of the refrigerant vapor leaving the generator is not needed since the absorbent is a salt. Accordingly, refrigeration systems with the $NH_3/LiNO_3$ mixture are highly recommended for solar cooling applications. However, previous experimental studies found in the literature showed that the main drawback of the $NH_3/LiNO_3$ mixture is its high viscosity which limits heat and mass transfer processes mainly in the absorber in comparison with NH_3/H_2O working pair. The absorber is considered the key component into the absorption systems due the complex heat and mass transfer phenomena that take place there.

Studies applying intensification techniques such as the use of rough or extended surfaces or addition of small quantities of additives to working fluids, to improve heat and mass transfer processes have been carried out more frequently in the last decade. Recently, optimization of nanoparticle synthesis and reduction in the acquisition prices have also allowed for the inclusion of nanotechnology in thermal systems to enhance heat and mass transfer processes.

In this thesis is proposed and experimentally studied the intensification of the ammonia absorption process into the $NH_3/LiNO_3$ mixture in vertical bubble mode absorbers using advanced surfaces and nanoparticles of carbon nanotubes (CNTs). The increase of ammonia absorption process would allow diminishing the absorber size or what is even more interesting, reducing the cycle driving temperature for solar thermal applications and/or increasing the heat sink temperature for the heat released in the absorber and condenser to avoid the use of humid cooling towers.

1.3 Research Objective

The objective of this research is to contribute to the technological development of absorbers for the $NH_3/LiNO_3$ absorption chillers. The research objective involves the main objective of the thesis and a series of specific objectives proposed for achieving the main goal.

1.3.1 General objective

The primary objective of this thesis is to study experimentally the intensification of the ammonia absorption process in bubble absorbers with the $NH_3/LiNO_3$ mixture using advanced surfaces and nanoparticles at operating conditions of interest for absorption chillers driven by low temperature heat sources and heat released by air.

1.3.2 Specific objectives

Based on the general objective of this thesis, the next specifics objectives are drawn:

- To review the experimental and theoretical studies dealing with the use of the $NH_3/LiNO_3$ mixture and bubble absorbers for absorption refrigeration systems.
- To review the experimental studies dealing with the use of advanced surfaces in absorbers.
- To review the experimental studies dealing with the use of nanoparticles in the absorption process in order to recognize the different kinds of nanoparticles and the key parameters that make them suitable for use to intensify the heat and mass transfer processes.
- To perform a thermodynamic simulation of the absorption refrigeration cycle with $NH_3/LiNO_3$ and obtain the operating conditions in the absorber based on an air-cooled absorption system driven by low temperature heat sources.
- To conduct experimental studies of the ammonia absorption process in a plate bubble absorber H-type with $NH_3/LiNO_3$ and analyze the heat and mass transfer processes during the absorption.
- To correlate and propose dimensionless correlations for the determination of heat and mass transfer coefficients in the plate absorber tested.
- To conduct experimental studies of the ammonia absorption process in a tubular absorber with inner smooth surface and analyze the heat and mass transfer processes during the absorption.
- To study experimentally and quantify the effect of advanced surfaces, length and tube diameter on ammonia absorption process in a tubular absorber with $NH_3/LiNO_3$ and analyze the heat and mass transfer processes during the absorption.
- To correlate and propose dimensionless correlations for the determination of heat and mass transfer coefficients in the tubular absorber with and without advanced surfaces.
- To study experimentally and quantify the effect of nanoparticles on the ammonia absorption process in a tubular absorber with $NH_3/LiNO_3$ and analyze the heat and mass transfer processes during the absorption.
- To conduct experimental studies of the ammonia absorption process in a tubular absorber with nanoparticles and advanced surfaces and analyze if a synergic effect takes places.
- To develop a numerical model for bubble absorbers and implement the heat and mass transfer correlations obtained from experiments in order to predict the heat and mass transfer rates, and temperatures and concentration profiles during the absorption in the studied configurations.

1.4 Structure of the thesis

Apart of the present chapter, this thesis consists of five additional chapters which are briefly described in the following lines.

In Chapter 2 presents a brief description of the absorption refrigeration technologies, and a review mainly focused on researches dealing with the working pair $NH_3/LiNO_3$, the absorption process in bubble mode and state of the art of researches on the passive intensification of heat and mass transfer in the absorption process.

Chapter 3 describes the experimental test facility used for the study of the absorption process and shows in detail the different geometries of bubble absorbers tested. In addition, description of the instrumentation and control system, experimental procedure, data reduction and description of the method for the uncertainty determination of results from the experiments are presented.

Chapter 4 presents the thermodynamic simulation of a single stage absorption refrigeration cycle with $NH_3/LiNO_3$ developed for selecting the operating conditions of the experimental studies. Then, main experimental results of intensification of the NH_3 absorption process in bubble mode absorbers with the $NH_3/LiNO_3$ mixture are shown and discussed. Experimental results involve the analysis of parameters such as NH_3 absorption mass flux, absorber thermal load, solution heat transfer coefficient, solution mass transfer coefficient and degree of sub-cooling in the absorbers tested. It includes the experimental test of a plate heat exchanger, and a tubular absorber with smooth and advanced surfaces with different tube diameters and lengths. It also involves the experimental test of the tubular absorber with nanoparticles into the $NH_3/LiNO_3$ mixture.

Chapter 5 is devoted to the numerical description and simulation of a one-dimensional model of the ammonia absorption process in bubble absorbers with the $NH_3/LiNO_3$ mixture. It includes a review of the main numerical bubble absorber models found in the literature. Then, main aspects of the numerical model developed are described. Finally, results obtained from the numerical model are directly compared with those from the experiments using plate and tubular bubble absorbers with the $NH_3/LiNO_3$ mixture for the model validation.

Finally, Chapter 6 gives the conclusions about the work done in the present thesis and some comments about future actions.

Chapter 2

Absorption Refrigeration Technology and the Absorption Process

2.1 Introduction

This chapter is devoted to review the main characteristics of the current absorption refrigeration technologies, working fluids, and the object of study of this thesis.

First, a brief description of the basic absorption refrigeration technology and its historical evolution are given. Second, classification of the absorption refrigeration technology is summarized and configurations of single, double, triple, half effect and GAX systems are briefly described. Third, description of the conventional working fluids for absorption systems and a review of researches dealing with the mixture of NH_3/$LiNO_3$, which is used as the working fluid in this thesis, are done. Then, the review is focused on the absorption process and classification of absorbers, paying special attention to the bubble absorption mode, which is of our interest in this thesis. Finally, state of art of researches dealing with intensification of the heat and mass transfer that take place during the absorption process is presented.

2.2 Absorption Refrigeration System

In terms of operation, absorption refrigeration systems are cooling units partially similar to mechanical vapor compression systems. Refrigerant vapor at high temperature and pressure is condensed and throttled to a very low temperature and pressure toward an evaporator where it is boiled to provide cooling. Difference between these systems lies in the way how refrigerant vapor is compressed from a low pressure to a high pressure, Figure 2.1. In the case of the absorption refrigeration system with respect to the vapor compression system, mechanical compressor is replaced by ``thermal compressor´´ which consists mainly of an absorber, a solution pump, a solution heat exchanger, a generator and an expansion valve. In the absorber, refrigerant vapor coming from the evaporator is absorbed by a solution mixture composed by a proportion of the refrigerant and absorbent with high affinity in liquid state (solution weak in refrigerant). The refrigerant absorption process is an exothermic process and in order to maintain the absorption potential, the heat released by the absorption must be rejected to surroundings. The solution strong in refrigerant leaving the absorber is then pumped to a high pressure generator. In the generator, refrigerant absorbed is one more time boiled and separated from the solution mixture by applying heat, which drives the cycle, at a high temperature and then, the refrigerant vapor is sent to the condenser. Finally, the remaining solution mixture leaving generator is sent to the absorber to repeat the cycle. The Coefficient Of Performance (COP) of an absorption refrigeration system is defined as the relation between the ratio of the cooling performance [Q_E] and the amount of heat input (Q_G) plus the pump consumption (W), equation 2.1. Since the pump energy consumption is relatively small in comparison with the heat flow applied to the generator, this parameter is often neglected.

$$COP = \frac{Q_E}{Q_G + W} \tag{2.1}$$

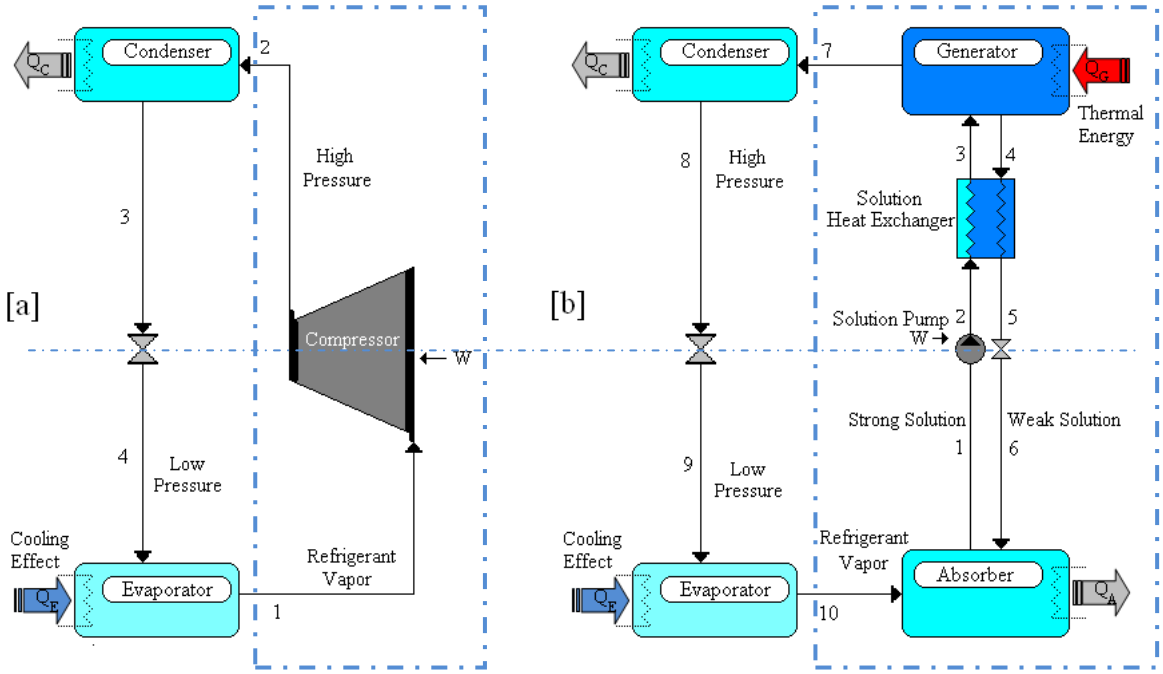

Figure 2.1 - Mechanical vapor compression system [a] and absorption refrigeration system [b].

Although absorption refrigeration systems are not yet competitive with mechanical vapor compression systems in terms of efficiency and cost, the relevance of the absorption refrigeration systems lies in the next facts: Small electricity consumption by the solution pump, few moving parts leading to low noise, very low vibration levels, use of natural refrigerants and cycle activation by thermal energy. The most interesting points of the absorption refrigeration systems is the use natural refrigerants which means zero ozone depleting as well as a zero global warming potentials and also the fact that the system can be activated by thermal energy such as solar energy (Best and Pilatowsky, 1998) or residual energy from industrial processes or cogeneration/trigeneration processes (Ge at al., 2009). In the cases that locations cannot support the use of vapor compression system due to the unavailability of electricity from a power grip, absorption refrigeration systems activated by solar energy appear to be an important alternative. Last studies have also shown that absorption refrigeration systems have good prospect to geothermal application (Wang et al., 2013).

Further development of absorption refrigeration systems would lead to an important change in the cooling production world, and will definitely imply an important impact on environment and energy saving.

The beginnings of absorption principle date from the 1700s. In 1755, the Scottish professor William Cullen experimented with water vapor in a vessel at a low pressure to produce a small quantity of ice in the laboratory. Based on experiments of Cullen, Gerald Nairne in 1777 introduced H_2SO_4 (sulfuric acid), which has very high affinity for water, to a vessel with water. Nairne observed that H_2SO_4 improved the water evaporation by its absorption, which at the same time resulted in a substantial reduction in the temperature of the remaining water. In 1810, John Leslie used water in a couple of vessels connected together in the presence of H_2SO_4 obtaining a production of 3 kg of ice per hour (www.absorsistem.com). In 1850, Edmond Carré developed the first absorption machine with water and sulfuric acid as the working fluids basing his model on Perkins design

(Jacob Perkins was in 1834 the first in patenting a refrigerating machine that used a vapor compression cycle); however, this design did not succeed because of problems of air leakages and corrosion into the vessel under vacuum conditions. In 1859, his brother Ferdinand Carré, who continued working on improving the absorption system, proposed and implemented the use ammonia as refrigerant and water as absorbent in the absorption refrigeration machine. As result, Ferdinand Carré was in 1860 the first in obtaining a U.S. patent for a commercial absorption system suitable for industrial applications such as ice production as well as storing food. Carré technology was popular until it was surpassed by vapor compression systems around the early 1900s.

Just until the 1945, thanks to a development program encouraged by the U.S. for absorption chillers, the first absorption system for space cooling which used water as the refrigerant and lithium bromide as absorbent made its appearance in the market (Srikhirin et al. 2001). In this opportunity, the Carrier Corporation was the responsible of the mass production of water/lithium bromide absorption machines. This absorption machines were initially electric-driven, but later the gas natural industry promoted effectively the use gas-fired heaters resulting in a better system performance. Due to the success of this system, in few years others companies joined the production. In 1970, the Trane Company gave a step forward in advanced absorption chillers with the first mass-produced double-effect water/lithium bromide system first patented by Carl V. Loweth and James M. Porter in the same year (Wang and Chua, 2009). The absorption machines industries in the U.S. were prosperous until 1975 when a significant fall on sales started. The causes of this issue were the technical evolution of vapor compression systems, low cost of electricity and the prohibited use of natural gas in new developments due to the concerns in the U.S. government about a possible diminution on the natural gas supplies (Kalogirou and Florides, 2012).

Meanwhile, Japanese government aware of their tight electricity supply, promoted the development and production of direct/indirect-fired single and double-effect water/lithium bromide absorption chillers resulting in a constant increase on the sales and in becoming the world leader in absorption technology. In 1985, Oouchi et al. from Hitachi patented the first triple effect absorption refrigeration system with three generators. Similarly, China and Korea joined the development of absorption machines providing significant advances on absorption chillers. In 2005, Kawasaki Thermal Engineering Co., Ltd. (KTE) announced that it will release the world's first triple-effect gas absorption chiller with a reduction on energy consumption by 30 % with respect to the double-effect chiller. It have been only a matter of time before absorption systems gained considerable acceptance in the commercial HVAC and industrial cooling sectors of these Asian countries.

The latest report about market trends provided by Global Industry Analysts Inc. highlight the growth of the absorption chiller market in the next years. According to the report, global market for absorption Chillers is projected to reach US$ 921.8 million (€ 705 million) by 2018, being the Asian-Pacific countries the largest and fastest growing market. Sales in these countries are projected to grow at a compound annual growth rate of about 4.1 %. The report also points that Chinese investment in efficient technologies would increase at over 18 % per annum.

2.3 Classification of Absorption Refrigeration Systems

Absorption systems are mainly classified according to the next criteria:

- With respect to the system activation method.
- With respect to the heat dissipation method.
- With respect to the range of application.
- With respect to the number of effects.

With respect to the system activation method, absorption systems can be classified as direct or indirect-fired units:

Direct-fired systems: The heat source can be gas or any other fuel that is burned in the system to directly heat the generator. According to the cost of the natural gas, this is the most usually used fuel.
Indirect-fired systems: These systems use a heat exchanger as a medium to heat the generator with hot fluid currents that bring in heat from another energy source, such as a boiler or heat recovered from solar thermal collectors, cogeneration or industrial processes. Fluids usually used are steam, thermal oil or superheated water or exhaust gases.

With respect to the heat dissipation method, absorption systems can be water-cooled or air-cooled:

Water-cooled systems: These systems use water as medium to dissipate the heat released from the absorption process and condensate refrigerant vapor in the condenser. The heat gained by the water is usually dissipated by a humid cooling tower. Main inconvenient of these systems is the growth of legionella in the cooling tower and the increase in the initial cost of the installation. Although cooling towers are highly used in large commercial and industrial applications, cooling towers are not accepted for smaller size applications because of cooling tower maintenance requirements.

Air-cooled systems: The heat dissipation in the absorber and condenser is directly performed by induced air currents. These systems can also be indirect air-cooled (heat is first dissipated with water and then, heat gained by the water is dissipated by induced air currents).

With respect to the range of application, absorption systems can be for industrial refrigeration applications or for air-conditioning applications:

Absorption systems for refrigeration applications: These absorption systems are capable to produce refrigeration at temperatures lower than 0 ^{o}C and usually used for food conservation, and ice production. The working fluid commonly used is NH_3/H_2O due to the very low freezing point of ammonia (refrigerant).

Absorption systems for air-conditioning applications: These absorption systems produce chilled water at temperatures higher than 0 ^{o}C to be used for air-conditioning of spaces. The working fluid commonly used is H_2O/LiBr, which provides a better performance in comparison with the NH_3/H_2O system for this application.

With respect to the number of effects, absorption systems can be single effect, half effect, double effect and triple effect:

Single effect absorption systems: In principle, the term ``effect´´ refers to the number of generator used to thermally drive the absorption cycle. The most basic absorption system configuration consists of a condenser, an evaporator, an absorber, a refrigerant expansion valve, a solution expansion valve, a solution heat exchanger, and a generator. The single effect absorption systems (Figure 2.2), which operate as described in section 2.1, usually use NH_3/H_2O or H_2O/LiBr as the working fluids depending of the application and have COPs between 0.5 and 0.7 at their most favorable conditions. These systems are characterized by their small size, low maintenance and the use of relatively low temperature heat sources as driving energy.
Methods for the improvement of the absorption systems have included the implementation of additional components into the basic cycle. For instance, the use of additional generators (double-effect and triple-effect absorption systems) and absorbers. In the case that the single effect systems have additional absorbers; configurations are called as double or multi stage systems. Although multi-stage systems have shown to have important improvements over the basic cycle (Wang et al. 2000), studies on the development of multi-effect absorption systems have been more relevant.

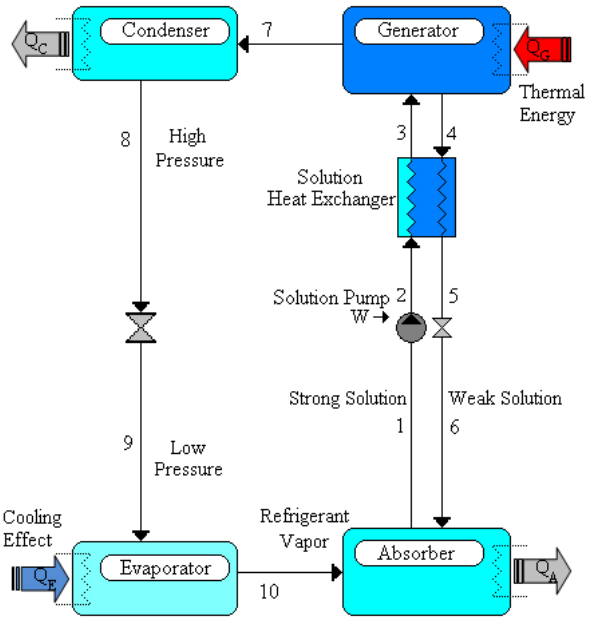

Figure 2.2 - Diagram of a single effect absorption system.

Double effect absorption systems: As mentioned earlier, efforts to improve the absorption systems and use of heat sources at different temperature levels have resulted in the development of double effect absorption systems. The double effect absorption systems are activated by heat sources around 170 ^oC and use H_2O/LiBr as the working fluid. Their applications are for air-conditioning and the COP usually ranges between 1.0 and 1.2. As shown in Figure 2.3, this configuration consists of the same number of components in the single effect systems plus a high temperature generator and condenser operating at a higher temperature and pressure than the components in the conventional single effect system. In this configuration, absorption system operates between three pressure levels defined by the conditions in the evaporator, in the low

temperature condenser and in the high temperature condenser. High temperature energy for driving the cycle is applied into the high temperature generator and refrigerant vapor generated is sent to the high temperature condenser where heat exchanged is later used as driving energy in the low temperature generator at an intermediate pressure. Double effect absorption systems can be found in the market mainly with two solution flow arrangements; in series and in parallel. In the configuration in series (Figure 2.3a), the solution strong in refrigerant is sent directly from the absorber to the high temperature generator and refrigerant vapor is generated at a high temperature level, then the remaining solution is sent to the low temperature generator where the solution is reheated to a lower pressure to generate more refrigerant vapor. The main inconvenient with this configuration is the proximity to the crystallization limits in the low temperature absorber. With regards to the configuration in parallel (Figure 2.3b), the solution strong in refrigerant coming from the absorber is separated after the low pressure heat exchanger outlet and sent simultaneously to the high and low temperature generators. In this way, condition of the weak solution in refrigerant is not as close from the crystallization limits in comparison to the series flow configuration.

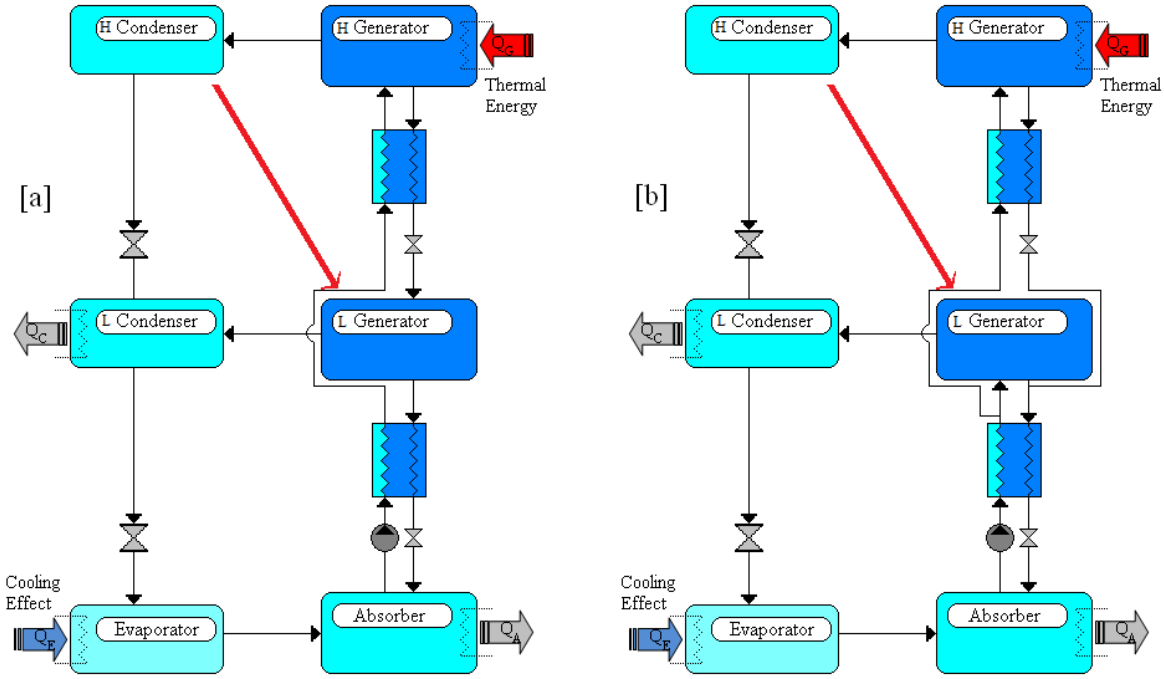

Figure 2.3 - Diagram of the double effect absorption system with solution flow in series [a] and in parallel [b] configuration.

Triple effect absorption systems: Due to the large industrial processes that reject waste heat at temperatures higher than 180 ^{o}C, interest on the development of efficient absorption systems driven at very high temperatures increased in the last decade. Triple effect absorption systems are capable to make good use of high temperature heat sources around 250 ^{o}C for their activation and achieve COPs up to 1.7. A triple effect system is basically the extension of the double effect absorption system by adding one more generator and condenser which operate at a much higher temperature and pressure (Figure 2.4). Thus, the whole system consist of three generators; a low temperature generator, an intermediate temperature generator and a high temperature generator, and operates between four pressure levels. Similar to the double effect

system, heat exchanged in the high temperature condenser is used as driving energy in the medium generator and heat exchanged in the medium temperature condenser is used as driving energy in the low temperature generator.

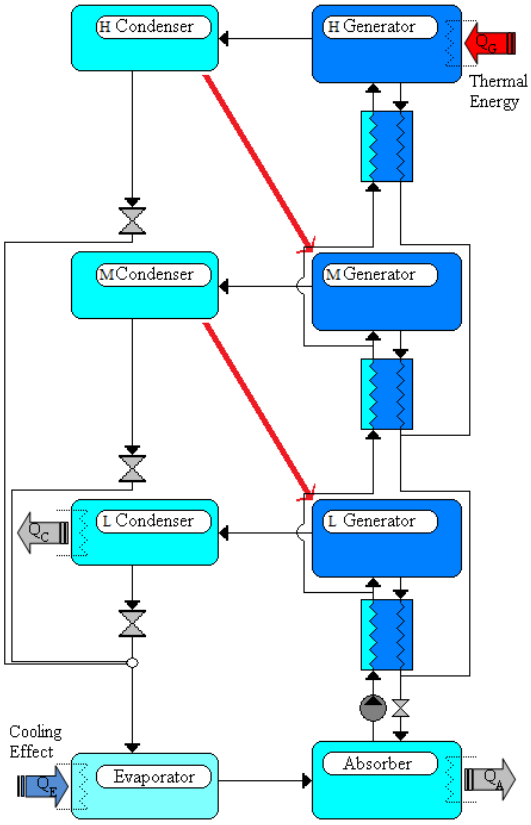

Figure 2.4 - Diagram of the triple effect absorption system (Oouchi et al. 1985).

Additional to the previously described cycles, necessity for absorption systems capable to operate at lower temperature heat sources than that for driving the single effect system with H_20/LiBr and development of the NH_3/H_20 absorption systems resulted in the design of the half effect system, and GAX absorption system with higher COP.

Half effect absorption systems: The half effect system (also called double-lift) includes two solution circuits. This configuration was proposed in order to make use of relatively lower temperature heat sources than those necessary for driving the single effect system with H_20/LiBr but at the cost of a lower COP. As can be observed in Figure 2.5a, the half effect absorption system consists mainly of a condenser, a refrigerant valve, an evaporator, a low pressure absorber, a low pressure generator, a high pressure absorber and a high pressure generator, therefore, the whole system operates between three pressure levels. The low pressure generator and high pressure absorber operate at intermediate pressure, and the high pressure generator and condenser at high pressure. According to this configuration, the refrigerant vapor generated in the low pressure generator is one more time absorbed in the high pressure absorber, then solution is pumped from the high pressure absorber to the high pressure generator. The thermal energy to drive the cycle can be supplied in parallel to the two generators at the same temperature. Although this system is basically a double-stage absorption system, it is

known as half effect due to its low COP in comparison to the single effect absorption system. Another half effect configuration involves the heat exchange between an intermediate pressure evaporator and the low pressure absorber, Medrano et al. (2001).

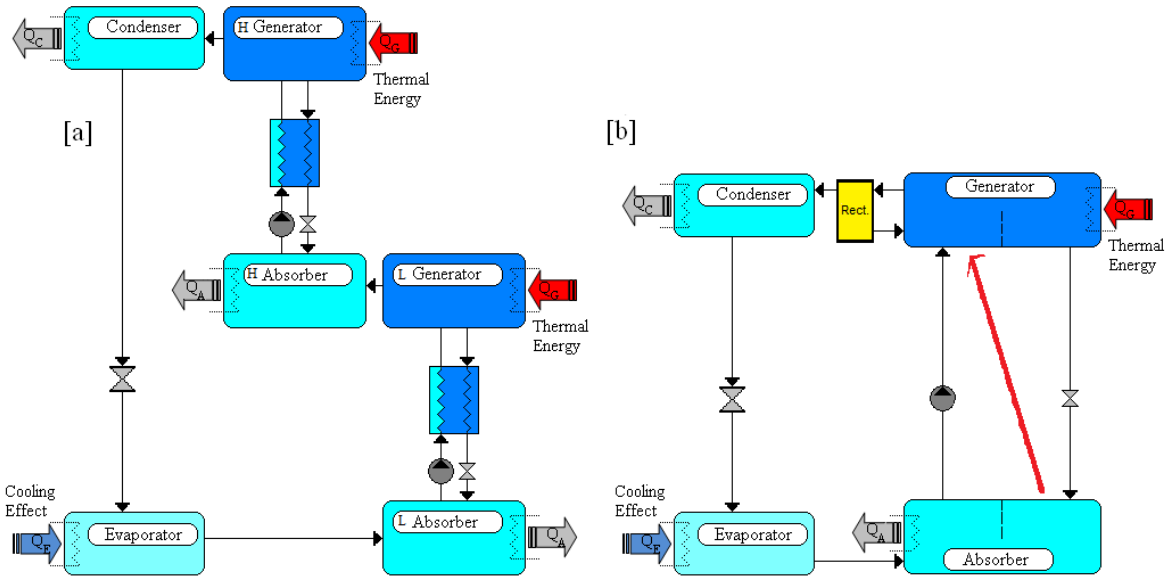

Figure 2.5 - Diagram of the half effect [a] and GAX [b] absorption systems.

GAX absorption systems: The term GAX refers to system generator/absorber heat exchange. This absorption configuration (Figure 2.5b) is similar to the single effect absorption system working with NH_3/H_20; however, the absorber and generator are divided into two sections. In one section of the absorber heat released by the absorption process has a low temperature, and in the other section heat released has at higher and usable temperature. In the low temperature absorber section heat released by the absorption process is rejected to surroundings while heat released by the high absorber section is used to preheat the strong solution entering the generator. This configuration, which results in less heat input to the generator and less heat rejected by the absorber, was first described and patented by Altenkirch and Tenckhoff in 1914.

As summary, Table 2.1 shows a list of the absorption refrigeration technologies available in the market with their available range of cooling capacity. This list was elaborated from studies of Gluesenkamp et al. (2011) and Labus (2011) and websites of absorption systems companies.

2.4 Conventional Working Fluids

The main characteristics to select a refrigerant and absorbent mixture to be used in absorption systems are:

- Total miscibility within the operating conditions range in the absorber.
- Mixture has to be chemically stable.
- Non-toxic and non-explosive.
- Non-corrosive and environmental friendly.

- Refrigerant has to be much more volatile than absorbent; therefore difference in boiling point between the pure refrigerant and the mixture at the same pressure should be as large as possible.
- Refrigerant should have low freezing point.
- Favorable transport properties (viscosity, diffusion coefficient, thermal conductivity) for heat and mass transfer.
- Low cost.

Table 2.1 - Absorption refrigeration technologies available until today.

Company	Country	Type	Working pair	Cooling capacity [kW]
AGO	Germany	Single effect	NH_3-H_2O	30 – 1000
Broad	China	Single and double effect	H_20-LiBr	150 – 23260
Carrier	U.S.A	Single and double effect	H_20-LiBr	352 – 15977
Century Corporation	Corea	Single effect	H_20-LiBr	350 – 5200
Climatewell	Sweden	Single effect With storage	H20-LiCl	10 – 20
Cooltec5	U.S.A	GAX	NH_3-H_2O	17,6 – 35
EAW Wergcall	Germany	Single effect	H_20-LiBr	15 – 200
Ebara corporation	Japan	Single and double effect	H_20-LiBr	158 – 2462
Entropie	France	Single Effect	H_20-LiBr	300 – 6000
Hitachi	Japan	parallel double effect	H_20-LiBr	106 – 19690
Kawasaki	Japan	Double and triple-effect	H_20-LiBr	141 – 2462
LG	Corea	Single and double effect	H_20-LiBr	352 – 5275
McQuay International	U.S.A	Single and double effect	H_20-LiBr	350 – 5275
Pink	Austria	Single effect	NH_3-H_2O	12
Rinnai Osaka gas	Japan	Double effect	H_20-LiBr	6.7
Robur	Italy	Single effect	NH_3-H_2O	12,8 – 17,7
Sanyo	China	Single and double effect	H_20-LiBr	105 – 5274
Shuangliang	China	Single and double effect	H_20-LiBr	211 – 11605
Solarice	Germany	Single effect	NH_3-H_2O	25 – 40
SolarNext	Germany	Single effect	H_20-LiBr and NH_3/H_20	18 – 50
Sonnenklima	Germany	Single effect	H_20-LiBr	10
Thermax	India	Single and double effect	H_20-LiBr	35 – 12000
Trane	USA	Single and double effect	H_20-LiBr	390 – 5925
Yazaki	Japan	Single and double effect	H_20-LiBr	17,6 – 703
York	U.S.A	Single and double effect	H_20-LiBr	422 – 4840

According to the open literature, many working fluids have been suggested to be used in absorption systems but due to problems such as high corrosion, toxicity and chemically instability most of them have been discarded. Moreover, the working fluids ammonia/water (NH_3/H_2O) and water/lithium bromide (H_2O/LiBr) have shown important characteristics and nowadays are the most widely used pair in the absorption systems market.

According to the properties and limitations of the conventional working fluids, the absorption system with NH_3/H_2O, the first one in being patented, is mainly used for refrigeration applications (< 0 ^oC) due to the very low ammonia freezing point (-77 ^oC at 1 atm). In addition, NH_3/H_2O mixture allows the system to operate at high heat dissipation temperatures, and thus the system can be air-cooled and the use of humid cooling towers can be eliminated.

Systems with NH_3/H_2O require high activation temperatures (> 110 ^oC) to keep the refrigerant cooling capacity at the desired low evaporation temperatures. Furthermore, due to the fact that NH_3 and H_2O are volatile at the conditions of interest, rectification of the refrigerant vapor leaving the generator is required in order to avoid water in the evaporator. It makes necessary the use of an extra component to perform the rectification process and ensure the highest vapor refrigerant quality. The use of a rectifier, which size increases reducing the evaporation temperature and thus increasing the generation temperature, and the fact that the refrigerant vapor coming to the condenser is not pure ammonia significantly affects the performance of the cycle with NH_3/H_2O. Another important aspect of the NH_3/H_2O system is the high pressure achieved in the generator which is the main reason why there are no double-effect absorption systems with NH_3/H_2O. Although other disadvantages of the NH_3/H_2O system include toxicity and incompatibility with copper based metals, NH_3/H_2O mixture is environmental friendly and has low cost.

With regards to absorption systems with H_2O/LiBr, these machines appeared in the market some years later than NH_3/H_2O machines in response to the low performance of NH_3/H_2O systems. Performance of a H_2O/LiBr system at lower activation temperatures is higher in comparison with NH_3/H_2O systems, which make H_2O/LiBr systems suitable for solar cooling. Besides, the fact that LiBr is a salt (non-volatile) with great affinity for water allows the system to be operated without the need of the refrigerant vapor rectifier. Moreover, H_2O/LiBr systems are only used for air-conditioning applications (> 0 ^oC) due to the water (the refrigerant) freezing point (0 ^oC at 1 atm). Use of water as refrigerant implies also that the evaporator and absorber must be operated under vacuum conditions which results in high vapor specific volumes, and thus in bigger components.

Although the aspects previously commented, main problems of the LiBr based absorption systems are the solution crystallization that takes place at low refrigerant concentrations in the absorber, the high corrosion to some metals and the high cost of the salt. The crystallization limits for H_2O/LiBr are very close to the operating concentrations required for practical H_2O/LiBr absorption chillers. Due to the crystallization limits, H_2O/LiBr system cannot be air-cooled, thus use of humid cooling towers for heat dissipation is required and the cost of the whole system increases. In the case of small capacity H_2O/LiBr systems, cooling towers are not suitable because of the cooling tower maintenance requirements.

In order to overcome the crystallization and corrosion problems, implementation of several control strategies such as chemical inhibitors additives, heat and mass transfer enhancements and thermodynamic cycle modifications have been investigated in the last years (Wang et al. 2011). Advances in the mitigation of the crystallization and corrosion problems have allowed the H_2O/LiBr systems to be developed under the objective to improve their performance at higher activation temperature. H_2O/LiBr systems with double and triple effects are a sign of the improvements achieved in the last years.

Recently, Alvarez (2013) conducted a series of experimental and theoretical studies and proposed the use of Water/alkaline nitrite solution ($LiNO_3$+KNO_3+$NaNO_3$) as a potential alternative to conventional working fluid for air-conditioning applications with high temperature heat sources (up to temperatures of 260 ^oC). According to the author, this working fluid offers high thermal stability and non-corrosive action in comparison with the H_2O/LiBr.

2.5 Interest on the $NH_3/LiNO_3$ as an Alternative Working Fluid

Conventional working fluids such as H_2O/LiBr or NH_3/H_2O mixtures for absorption heat pumps and chillers have well known disadvantages as commented before according to their field of application.

In order to overcome the disadvantages and limitations of the conventional working fluids, one of the alternative working fluids proposed in the open literature is the ammonia/lithium nitrate ($NH_3/LiNO_3$).

In this case ammonia was again used as refrigerant due to its outstanding thermodynamic and thermophysical properties and also due to the fact that ammonia is environmentally friendly and any possible emissions will not contribute to global warming. Furthermore, ammonia has a great potential to be used in low charge systems by using plate heat exchangers or advanced surfaces heat exchangers and thus, the impact of its toxicity can be reduced (Paerson, 2012). In addition, Gluesenkamp et al. (2011) analyzed the mass flow and volumetric flow rate of refrigerant required for a given evaporator capacity in function of the ration of the specific heat capacity to the latent heat of evaporation. The authors showed that ammonia provides the lowest values in these relations in comparison with those of the other refrigerants such as water, CO_2, methanol etc… The authors explained that low values of these relations are desired to maximize the cooling capacity with more compact components.

The advantages of the $NH_3/LiNO_3$ working mixture over conventional H_2O/LiBr are therefore: a) it does not cause crystallization at the conditions of interest for solar air-conditioning systems so it allows the cycle to be air-cooled; b) the absorption cycle with $NH_3/LiNO_3$ does not operate under vacuum conditions which mean low refrigerant specific volumes, and thus smaller components.

Compared with the NH_3/H_2O working pair, $NH_3/LiNO_3$ a) does not require a rectifier for the vapor refrigerant at the generator outlet because the absorbent is a salt, and b) can be used at a lower temperature in the generator, according to the results of the thermodynamic simulation (Antonopoulos and Rogdakis 1996, Sun 1998, Infante Ferreira 1995, Abdulateef et al. 2008). The great advantages of this mixture, therefore, are the cycle simplicity and a greater potential for solar cooling. This mixture is expected to help the practical implementation of solar refrigeration technologies by the use of thermal chillers driven at lower temperatures and with direct heat rejection to the ambient without cooling towers.

According to the open literature, in 1921, being the ammonia of a wide use in the refrigeration industry, Davis et al. investigated a list of 19 substances suitable as liquid absorbent for ammonia. From this study, lithium nitrate resulted to have the highest absorptive value. Therefore, they determined the vapor pressure of the binary mixture $NH_3/LiNO_3$ at temperatures from 286 to 308 K and ammonia mass fraction of 0.36. The results showed that lithium nitrate is very soluble in ammonia and that the corrosion action on ordinary iron or steel is not appreciable after several months.

Gensch (1937) reported measurements of the vapour-liquid equilibrium of the $NH_3/LiNO_3$ at ammonia mass fractions ranging from 0.24 to 0.42. Blytas et al. (1962) extended the range up to 0.60. Later on, Infante Ferreira (1984), collected and reported

thermodynamic and thermophysical properties of the $NH_3/LiNO_3$ mixture and proposed a series of correlations for their determination. Equations were presented for solubility, equilibrium pressure, density, viscosity, thermal conductivity, specific heat and liquid enthalpy. These correlations were used later by several authors to simulate various absorption cycles such as single-effect (Antonopoulos and Rogdakis 1996, Sun 1998), and double-effect and half- effect (Bourouis et al. 2003, Arzoz et al. 2003, Ayala et al. 1994).

The viscosity as a function of composition, from 0 to 0.30 in lithium nitrate mole fraction and temperatures from 223 to 308 K, and the density at 223 K and 293 K for various compositions, were determined by Uchibayashi et al. (1985). Aggarwal and Agarwal (1986) measured the vapor-liquid equilibrium up to 0.7 in ammonia mass fraction over a temperature range of (248 - 429) K and up to 2.2 MPa. Also, the enthalpy, latent heat of vaporization, liquid specific volume, vapor specific volume, differential heat of solution and enthalpy of superheated ammonia were calculated.

Thanks to the increasing interest on the $NH_3/LiNO_3$, the first experimental studies in experimental test facilities were performed. Prototypes of absorption refrigeration machines working with $NH_3/LiNO_3$ were evaluated and their performances were compared with those of absorption machines working with mixtures such as NH_3/H_2O and NH_3/NaSCN (Infante Ferreira 1995, Ayala et al. 1994, Heard at al. 1996). The authors of these experimental studies obtained poor results and agreed that the main reason for the poor performance of the $NH_3/LiNO_3$ prototypes lie in the absorber due to the high viscosity of this mixture at the studied conditions compared with results using NH_3/H_2O. The authors concluded that the high viscosity of $NH_3/LiNO_3$, which increases drastically at low temperatures, penalizes the heat and mass transfer processes especially in the absorber, and therefore reduces the performance predicted by the thermodynamic models.

The high viscosity of the $NH_3/LiNO_3$ in comparison with the NH_3/H_2O had been already noted by some researchers. To overcome this drawback, Ehmke and Renz (1983), Bokelmann (1985), and Reiner and Zaltash (1991, 1993) proposed the addition of a small amount of water to the binary mixture of $NH_3/LiNO_3$. Ehmke and Renz (1983) studied the effect of water on the solubility and viscosity of the ternary $NH_3/(LiNO_3+H_2O)$ mixture and suggested an optimal water mass fraction of between 0.20 and 0.25 in the absorbent mixture. The authors also determined and correlated density and vapour pressure data of the mixture at a water mass fraction of 0.25 in the absorbent. Later, Bokelmann (1985) carried out an experimental study on the performance of an absorption heat pump with the $NH_3/(LiNO_3+H_2O)$.

Bothe (1989) compared the performance of an absorption system in refrigeration and heat pump mode with $NH_3/LiNO_3$ and $NH_3/(LiNO_3+H_2O)$. Comparison resulted in higher operation temperatures and interesting efficiency improvements for the $NH_3/(LiNO_3+H_2O)$ compared with the $NH_3/LiNO_3$. The author also noted that rectification for the $NH_3/(LiNO_3+H_2O)$ was a minor need.

Reiner and Zaltash (1991, 1993) measured the densities and viscosities of the ternary mixture $NH_3/(LiNO_3+H_2O)$ with ammonia mass fraction of 0.04 NH_3 + 0.355 $LiNO_3$ + 0.605 H_2O, which is a typical composition for GAX systems. The authors expressed these properties as function of temperature using the least-squares method. In addition, the boiling point of this mixture was measured at atmospheric pressure. $NH_3/(LiNO_3+H_2O)$

resulted to have lower viscosity and presented minor corrosion problems than the $NH_3/LiNO_3$.

Heard and Ayala (2003) studied the corrosion of carbon and stainless steel in solutions of lithium nitrate in ammonia, for a series of concentrations and temperatures from 323 to 423 K. This study showed that 304 and 316 stainless steel and A37 carbon steel can be used in the construction of absorption refrigeration and heat pump systems containing this working pair.

To improve and complete the available experimental data, Libotean et al. (2007, 2008) measured the vapour-liquid equilibrium, density, viscosity and heat capacity at several temperatures and compositions for the binary mixture $NH_3/LiNO_3$ and ternary mixture $NH_3/(LiNO_3+H_2O)$ and proposed analytical equations for calculating each property, besides a thermodynamic method (Electolyte-NRTL) for predicting the vapour-liquid equilibrium.

Cuenca et al. (2013a) presented experimental measurements and correlations of the thermal conductivity for $NH_3/LiNO_3$ and $NH_3/(LiNO_3+H_2O)$ solutions for several compositions and temperatures. Results presented for $NH_3/LiNO_3$ showed important differences with those values obtained from the correlations reported by Infante Ferreira (1984). In addition, the thermal conductivity of the $NH_3/(LiNO_3+H_2O)$ solution was found to be up to 8 % and 11 % higher than values of the $NH_3/LiNO_3$ with water mass fractions of 0.20 and 0.25 respectively. Cuenca et al (2013b) measured the thermal conductivity of the working pair NH_3+LiNO_3+Carbon nanotubes. Experimental measurements were conducted at concentrations of NH_3 and CNTs in weight, ranging from 30 % to 50 % for NH_3, and 0.005 % to 0.2 % for CNTs. The thermal conductivity of the binary nanofluid was measured at temperatures from 303.15 K to 353.15 K, at 1.5 MPa. In this study, the highest thermal conductivity value was obtained with 40 wt. % of NH_3 concentration and 0.01 wt. % of CNTs. The maximum value was 7.5 % higher than that of $NH_3/LiNO_3$ solution.

Table 2.2 summarizes the thermophysical properties available in the open literature for $NH_3/LiNO_3$ mixture.

Table 2.2 - Summary of the thermophysical properties available in the literature for $NH_3/LiNO_3$ mixture, versus the temperature and ammonia mass fraction (x) ranges.

Reference	Property (ranges)
Davis et al. (1921)	P (286-308 K; x = 0.36)
Gensch (1937)	P (x = 0.24-0.42)
Blytas et al. (1962)	P (x = 0.4-0.6)
Infante Ferreira (1984)	P, x, ρ, μ, λ, Cp, H (correlations)
Aggarwal and Agarwal (1986)	P (248-429 K; x up 0.7)
Uchibayashiet et al. (1985)	μ(223-308 K; x up 0.3) ρ (223-293 K)
Heard and Ayala (2003)	Corrosion (323-423 K)
Libotean et al. (2007,2008)	P, ρ, μ, Cp (293-353 K; x = 0.35-0.65)
Cuenca et al. (2013a)	λ (303.15-353.15 K; 1.5 MPa; x = 0.35-0.60)

Altamush (1997) performed an economic analysis of the individual components in absorption systems working with $NH_3/LiNO_3$ and others mixtures such as $H_2O/LiBr$, NH_3/H_2O and $NH_3/NaSCN$, and activated by different renewable energies sources. In this study, the costs of the components in a system with $NH_3/LiNO_3$ activated by solar energy were close to those with $H_2O/LiBr$ and lower than those of the $NH_3/NaSCN$ system.

Ayala et al. (1997, 1998) simulated and experimentally evaluated an $NH_3/LiNO_3$ absorption refrigeration combined with mechanical vapor compression in the same circuit. The authors concluded that the combined absorption/compression refrigeration systems increase in overall efficiency and the use of the $NH_3/LiNO_3$ absorption system is an attractive alternative.

Wang et al. (1998) simulated a solar-driven ejection absorption refrigeration cycle with $NH_3/LiNO_3$. In this configuration, the ammonia vapor is injected and pressurized together with the ejection of solution to enhance the absorption process. From this study, the authors conclude that incorporation of an injector at the inlet of the absorber improves the COP of the cycle when this is driven by low-grade unsteady heat source.

Rivera and Best (1999) and Rivera et al. (2000) presented heat transfer coefficients of the $NH_3/LiNO_3$ and NH_3/H_2O working fluids in forced convective boiling flowing upward in a vertical tube uniformly heated. According to results, average heat transfer coefficients for the NH_3/H_2O mixture were between two and three times higher than those obtained with the $NH_3/LiNO_3$. Rivera and Rivera (2003) simulated the performance of an intermittent absorption refrigeration system operating with $NH_3/LiNO_3$ mixture. The authors from this study concluded that the efficiency of the system at different generation and condensation temperatures is satisfactory considering the simplicity of the system.

Wang et al. (2000) simulated a one, two and three staged absorption system with $NH_3/LiNO_3$ mixture. Based on the results, the authors concluded that the conventional system can be improved by incorporating a series of evaporator-absorbers. The improved system was able to produce refrigeration temperatures as low as -40 ^oC and also be run at driven heat sources as low as 65 ^oC.

Venegas et al. (2002) simulated the $NH_3/LiNO_3$ absorption systems in two different applications, refrigeration and heat pump cycles, activated by low temperature heat sources, and compared their performances with the systems using H_2O/NH_3 and $NH_3/NaSCN$. In this study, double and triple-stage absorption systems were modeled and simulated. Results showed that $NH_3/LiNO_3$ absorption systems achieved the highest COP in both refrigeration and heat pump mode.

Venegas et al. (2003, 2004, 2005) theoretically studied the ammonia absorption by using the spray absorption method with the $NH_3/LiNO_3$ mixture in an adiabatic chamber. Operating conditions of this study were those of a low-pressure absorber of a double-stage absorption refrigeration system. In these studies, the authors concluded that a mean mass transfer coefficient of 0.67 $m.h^{-1}$ may be attained. Studies performed by Venegas et al. (2004) were focused on both the low and high-pressure absorbers of a double-stage absorption refrigeration system.

Zacarías et al. (2010) and Venegas et al. (2012) presented experimental results of the boiling heat transfer in a plate heat exchanger (PHE) with the $NH_3/LiNO_3$ mixture. From this study, the effect of the heat and mass flux on boiling heat transfer coefficient is

analyzed resulting in boiling heat transfer coefficients ranging between 0.6 and 1.1 $kW.m^{-2}K^{-1}$ at heat fluxes between 1.4 and 5.0 $kW.m^{-2}$.

Herrera et al. (2010) characterized and evaluated numerically and experimentally the performance of a horizontal tube falling film generator working in a 10 kW $NH_3/LiNO_3$ absorption refrigeration system. The falling film generator was made of Carbon steel and operated at a pressure of 15.56 bar. The generator consisted of 3 rows, 4 tubes per row and a length of 0.9 m.

Oronel et al. (2010) reported an experimental study of the saturated boiling process heat transfer process in a plate heat exchanger for $NH_3/LiNO_3$ and $NH_3/(LiNO_3+H_2O)$. The authors analyzed the different boiling regimes (convective, nucleate and film boiling) that take place and effect of parameters such as mean vapor quality, heat flux and solution mass flux on the boiling heat transfer coefficient for both $NH_3/LiNO_3$ and $NH_3/(LiNO_3+H_2O)$. Results for the pressure drop and friction factor were also reported in this study. The authors of this study concluded that lower viscosity of the ternary mixture $NH_3/(LiNO_3+H_2O)$ with 20 wt. % of water in the absorbent compared with the binary mixture $NH_3/LiNO_3$, caused an improvement of the boiling heat transfer coefficient. For instance, at a vapor quality of 10 %, pressure of 15 Bar, solution mass flux of 100 $kg{\cdot}s^{-1}{\cdot}m^{-2}$ and a heat flux of 10 $kW{\cdot}m^{-2}$, the boiling heat transfer coefficients were about 3.8 and 5.3 $kW{\cdot}m^{-2}{\cdot}K^{-1}$ for $NH_3/LiNO_3$ and $NH_3/(LiNO_3+H_2O)$ mixtures, respectively. It indicated that the boiling coefficient for the ternary mixture was about 39 % higher than that achieved with the binary mixture. Oronel et al. (2012) also performed a comparison between the boiling coefficients for NH_3/H_2O, $NH_3/LiNO_3$ and $NH_3/(LiNO_3+H_2O)$ mixtures at similar conditions with the same generator and noted that the boiling coefficients for NH_3/H_2O remains higher than those obtained with $NH_3/LiNO_3$ and $NH_3/(LiNO_3+H_2O)$.

Eysseltová and Orlova (2010) compiled solubility data of lithium nitrate and confirmed that adding water improves the solubility of the solution, making the ternary mixture more suitable for high generation temperatures or low cooling temperatures.

Ventas et al. (2010a) numerically evaluated the performance of an $NH_3/LiNO_3$ absorption chiller with an integrated low-pressure compression booster between the evaporator and the absorber. From the evaluation conducted, configuration studied allowed to reduce the activation temperature keeping the same COP that could be achieved with the conventional configuration at a higher activation temperature. Results also showed that the electrical COP obtained seems to be higher than that in an ammonia vapor compression cycle. Ventas et al. (2010b) also numerically evaluated the performance of an $NH_3/LiNO_3$ absorption chiller incorporating an adiabatic absorber. This configuration makes necessary the use of additional components and thus, the cost of the system could increase.

Rivera et al. (2011) experimentally evaluated the performance of an intermittent refrigeration system operating with $NH_3/LiNO_3$ mixture. The system developed has a nominal capacity of 8 kg of ice/day and was capable to obtain evaporation temperatures as low as -11 ^oC. The experimental study was performed at three different solution concentrations 48 %, 49 % and 50 % and the cooling-water temperature in the condenser varied between 26 ^oC and 30 ^oC. In this study was obtained that the solar coefficient of performance increased with the increment of solar radiation and the solution concentration.

Cerezo et al. (2011) simulated the absorption process in the plate bubble absorber with the $NH_3/LiNO_3$ mixture and compared the results with those obtained with NH_3/H_2O and NH_3/NaSCN. In this study, absorber performance results obtained with $NH_3/LiNO_3$ were lower than those obtained with the others mixtures due to its higher viscosity.

Bourouis et al. (2011) obtained the first patent for a water-cooled or air-cooled single stage absorption chiller using $NH_3/LiNO_3$ for solar cooling applications. These absorption chillers have as main characteristic the use of brazed plate heat exchangers in all components.

Zacarías et al. (2011) conducted an experimental evaluation of an adiabatic absorber working with the $NH_3/LiNO_3$ mixture using a flat fan nozzle at the absorber top and a plate heat exchanger as sub-cooler for the solution coming from the generator. From this study, maximum mass transfer coefficient obtained was around 3.60 $m.h^{-1}$. Similarly, Ventas et al. (2012) and Zacarías et al. (2013) report experimental results of the adiabatic absorption process with the $NH_3/LiNO_3$ mixture this time using by a fog-jet injector. With this configuration, maximum mass transfer coefficient obtained was around 1.69 $m.h^{-1}$.

Vereda et al. (2012) reported a numerical model of an ejector-absorption refrigeration system with $NH_3/LiNO_3$. According to the configuration studied, the ejector was located at the absorber inlet replacing the solution expansion valve. The authors of this study concluded that the use of an ejector allows improving the absorber performance, and thus the activation temperature of the cycle can be lower in comparison with the conventional absorption cycle. Acuña et al. (2013) developed a mathematical model of a diffusion absorption cooling system with $NH_3/LiNO_3$, NH_3/H_2O and NH_3/NaSCN. Cycle performance results showed that the $NH_3/LiNO_3$ mixture is the best working mixture between the three options for most of the operating conditions established.

Moreno-Quintanar et al. (2012) published the experimental performance of a solar powered intermittent absorption refrigeration system with both $NH_3/LiNO_3$ and $NH_3/(LiNO_3+H_2O)$ for ice production. The authors concluded that the ternary mixture produced a higher amount of ammonia during the generation for water concentrations of 20 % and 25 % in the absorbent. The authors also observed that for a water concentration of 10 % in the absorbent, there is not any difference in the performance of the $NH_3/(LiNO_3+H_2O)$ system with respect to the $NH_3/LiNO_3$ system. It was also found that with the $NH_3/(LiNO_3+H_2O)$ mixture the solar coefficients of performance were up to 24 % higher than those obtained with the $NH_3/LiNO_3$ mixture (varying from 0.066 to 0.093) and that the initial generation temperatures were up to 5.5 ^oC lower than those required for the $NH_3/LiNO_3$ mixture. The authors finally highlighted that no traces of water in the ammonia vapor were observed at any point during the experimental test.

Oronel et al. (2013) conducted an experimental study of absorption process in a plate heat exchanger L-type as bubble absorber using the $NH_3/LiNO_3$ and $NH_3/(LiNO_3+H_2O)$ mixtures. The authors analyzed the effect of the solution mass flow, cooling water temperature and ammonia concentration on the absorber performance parameters (absorption mass flux, solution heat and mass transfer coefficient, and outlet subcooling degree) with $NH_3/LiNO_3$. Then, main results were compared with those obtained with the $NH_3/(LiNO_3+H_2O)$. Experimental results with the $NH_3/LiNO_3$ were correlated and Nusselt and Sherwood numbers correlations were reported. Main conclusion from this study highlights that the lower viscosity of the $NH_3/(LiNO_3+H_2O)$ improved the heat and mass

transfer processes taking place in the absorber. For instance, the absorption mass flux achieved with the ternary mixture ranged from 0.00400 to 0.00595 $kg \cdot m^{-2} \cdot s^{-1}$. In the case of the solution heat transfer coefficient, it ranged from 3.5 to 8.1 $kW \cdot m^{-2} \cdot K^{-1}$. Results indicated that the absorption mass flux and the solution heat transfer coefficient achieved with the ternary mixture were around 1.3-1.6 and 1.4 times higher, respectively, than those of the binary mixture under similar operating conditions.

2.6 Absorption Process

Although each one of the components that constitute the absorption system is important in terms of design and efficient use of the heat transfer area, the present thesis is focused on the absorber since it plays a particular and critical role into the whole system. The heat transfer and the even more important mass transfer taking places in the absorber greatly affect the performance and size of the whole absorption system. The enhancement of the pure refrigerant vapor rate absorbed in the absorber allows positive effects on the next items:

- Cooling capacity of the absorption system.
- Absorber and system size.
- Driving temperature of the system.
- Heat dissipation temperature.

2.6.1 Classification of absorbers

Absorbers can be found in three modes of design and operation: Falling film mode absorber, spray mode absorber and bubble mode absorber. Depending of the mode, the way how the refrigerant vapor coming from the evaporator is introduced into the absorber and has contact with the solution varies. The falling film mode absorber is the most commonly used in absorption systems available in the market, while the spray mode and bubble mode absorber are still under investigation, being this last one (under study in this thesis) strongly recommended for several researchers due to its high mass transfer performance in comparison with the falling film mode.

2.6.1.1 Falling film absorber

There are mainly two configurations for absorbers in falling film mode; in horizontal and vertical tube configuration. In horizontal tube configuration, the solution is introduced into the absorber by using a distributor located in the upper section of the absorber (Figure 2.6). The solution flows in falling film along the cooling-water tube surfaces. The solution leaving the distributor has immediate contact with the saturated vapor phase of refrigerant which occupies the volume of the absorber. The weak solution falling film, which falls from one tube to the next one, is cooled by the bundle of tubes and thus, the capacity of solution to absorb refrigerant increases. The strong solution in refrigerant leaves the absorber through the lower section.

According the configuration of the absorbers used in the commercial absorption machines, the horizontal configuration is found to be the most common in comparison

with the vertical tube configuration. In vertical configuration, cooling water usually flows upward through the tubes while the weak solution and refrigerant flows downward through the outer space. This configuration is also studied for the design of air-cooled absorbers, in which case solution and refrigerant flow inside the tubes arrangement.
It is important to highlight the fact that even thought falling film absorber in horizontal configurations is commonly used due to the insignificant pressure drop it involves; its design is really complicated due to solution distribution limitations and inconvenient in the wetting of the cooling-water tube surfaces area which affects the mass transfer. Studies on the absorption process in falling film mode with $NH_3/LiNO_3$ have not been found.

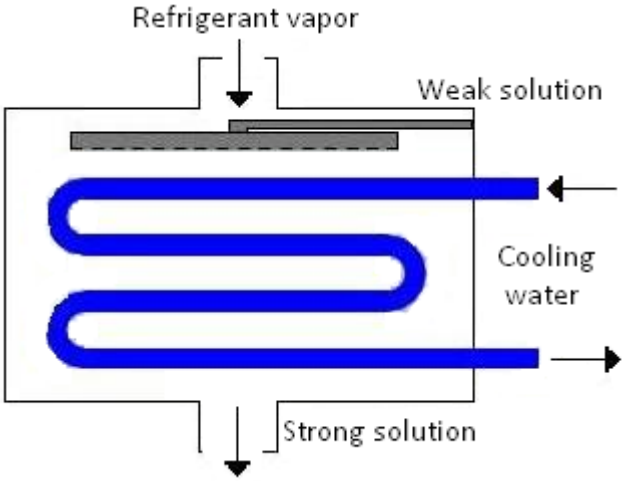

Figure 2.6 - Diagram of a falling film absorber with horizontal tube configuration.

2.6.1.2 Spray absorbers

The spray absorption mode consists of an adiabatic chamber and solution sprayer, Figure 2.7. The solution weak in refrigerant coming from the generator is introduced into the adiabatic chamber in a fine spray mode where it gets in contact with the refrigerant vapor coming from the evaporator. Once the absorption process takes place, the solution strong in refrigerant leaves the absorber through the lower section of the adiabatic chamber.

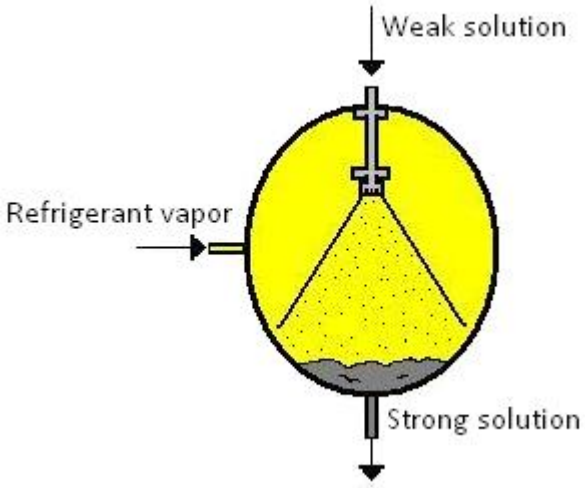

Figure 2.7 - Diagram of a spray absorber.

The use of the spray mode to disperse the solution into the chamber in very fine drops helps to the reduction the solution resistance for mass transfer and improves the absorption potential. As can be noted in Figure 2.7, spray absorption occurs without simultaneous heat transfer in an adiabatic chamber which makes necessary the use of additional components to sub-cool the weak solution in order to enhance its absorption potential. Also, it is necessary the recirculation of part of the strong solution through the adiabatic absorber in order to increase the absorption and get close to the solution equilibrium conditions. As mentioned in section 2.4, numerical and experimental studies on the absorption process in spray mode with $NH_3/LiNO_3$ have been lastly conducted by Venegas et al. (2003, 2004, 2005), Ventas et al. (2010b), Zacarías et al. (2011), Ventas et al. (2012) and Zacarías et al. (2013).

2.6.1.3 Bubble absorbers

The bubble mode absorber, which is studied in this thesis, consists of vertical absorber where the solution weak in refrigerant flows upward through the solution channel and pure refrigerant vapor is injected at the bottom of the absorber (Figure 2.8). The refrigerant vapor enters the absorber in bubble mode and is absorbed as this goes up. The heat released during the absorption process is removed by cooling fluid circulated on the outside of the solution channel.

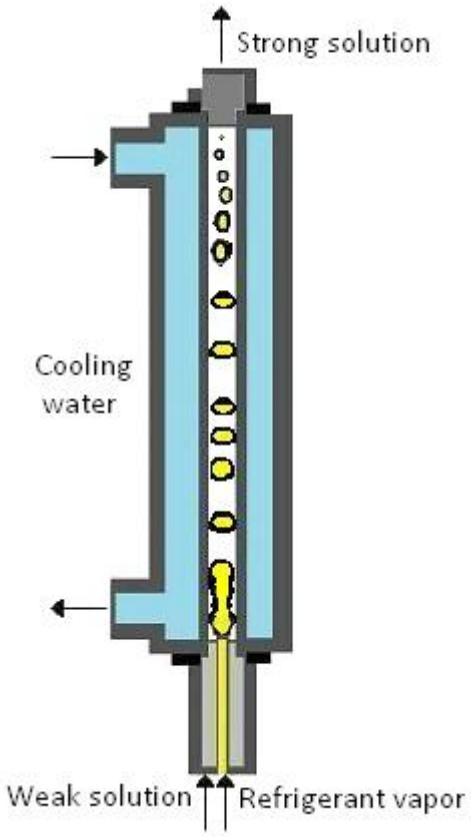

Figure 2.8 - Diagram of a bubble absorber.

Interest on investigation of the bubble absorption process for absorption systems have been increasing in the last years. Description and explanation of phenomena that take places in the absorption and its improvement have been the focus of the researchers in this area in order to contribute to the technological development of the absorption systems. Experimental investigations on bubble absorbers for absorption refrigeration systems found in the literature are reviewed as follows. Numerical studies found in the literature are reviewed in chapter 5.

Infante Ferreira et al. (1984) conducted experiments in a tubular bubble absorber with NH_3/H_2O with solution and vapor flowing upwards in concurrent flow. Experiments in the absorber were performed with and without heat removal. The tubular absorber with heat removal was tested with internal tube diameters of 10.0, 15.3 and 20.5 mm. During experiments, the authors observed two-phase flows patterns (slug and bubbly flow) and a formation of a kind of churn flow directly after to the vapor injection tube. The authors affirmed that the churn flow was observed about 20 % of the tube, followed by a slug flow in a 65 % of the tube length. From the experimental results, the authors reported a mass transfer correlation in terms of modified Sherwood number which was used in a numerical model in the same document.

Sujatha et al. (1999) reported experimental heat and mass transfer and pressure drop data of a tubular bubble absorber working with HCFC22-DMF. In this study, the authors evaluated the effect of the solution flow, coolant flow and cooling water temperature on the pressure drop, heat and volumetric mass transfer coefficient. To conclude, the authors reported a Sherwood correlation obtaining deviation up to ± 25 % with respect to experimental values.

Staicovici (2000a) carried out experiments by injecting single gas ammonia bubbles into the NH_3/H_2O solution with a small molar fraction in a pool at normal pressure (1.0 bar), varying the temperatures of the gas (5.1-19.4 ^oC) and liquid phases (1.2-17.0 ^oC). According to results and observations, the author concluded that at low and continuous gas mass flow rates, bubble dynamics takes place in two stages: periodic bubble growth to a maximum volume and collapse to a zero volume without detaching itself from the nozzle. At high and continuous gas mass flow rates, bubble collapse does not occur.

Helbing et al. (2000) performed a comparative analysis of the absorption process using NH_3/H_2O in both falling film and bubble mode. Experiments in falling film mode were conducted in a vertical tube with a heat transfer area of 0.076 m^2 while experiments in bubble mode in a narrow plate channel with a heat transfer area of 0.048 m^2. In this study, the authors concluded that the absorption in bubble mode resulted in a significant advantage in heat and mass transfer due to a more effective and intensive interaction of both liquid and vapor phase if compared with the falling film mode. Also, the authors identified the gas distribution system as a key element to improve heat transfer for this type of bubble absorber.

Terasaka et al. (2002) conducted an experimental study of the absorption process with NH_3 and N_2 into distilled water in a tubular gas chamber. The objective of this study was to investigate the mechanism of gas absorption from a bubble including the measurement of the bubble growth curve, volume, surface area and shape of the growing bubbles by an analysis of video images using a computer. The authors of this study described the mass transfer by separating it into three mass transfer resistances; gas

phase resistance, interface resistance and liquid phase resistance. The authors concluded that the mass transfer resistance in the liquid phase governed the mass transfer rate throughout the bubble formation.

Kang et al. (2002a, 2002b) visualized the bubble behavior during absorption and studied the effect of parameters such as orifice diameter, liquid concentration and vapor velocity on absorption performance for NH_3/H_2O. Experiments were conducted in a test cell simply filled with NH_3/H_2O solution where the pure ammonia vapor in bubble mode was introduced through the bottom section. In this study, the authors observed that during the absorption, bubble presents a growth and a disappearance process, and concluded that when surface tension forces were dominant the departing bubbles tended to be spherical, and when inertial forces were dominant, the bubbles tended to be hemispherical, especially as the vapor velocity increases. The authors also noted that the absorption driving potential is reduced when the liquid concentration increases. It was also observed an increase in the initial bubble diameter when the liquid concentration and orifice diameter increase. The authors reported experimental correlations of mass transfer coefficient for both processes observed and also for the initial bubble diameter, however, the validity of these correlations is not clear when the solution is in motion.

Lee et al. (2002a) experimentally analyzed the NH_3/H_2O absorption in a plate type absorber and Lee et al. (2002b) reported also a comparative study of the absorption process with NH_3/H_2O in falling film and bubble mode in the plate type absorbers. The objective of these studies was to analyze the effects of solution and gas flow rate on the performance of the absorber. From these studies, the authors noted that the mass transfer increased slightly, while the heat transfer showed a more pronounced increase when the solution flow was varied from 0.002 to 0.015 $kg.s^{-1}$. In addition, the gas flow rate showed an important effect in both mass and heat transfer coefficients. In bubble mode, the authors found that increasing the gas flow rate produced slugging. Comparing the two absorption modes, the authors confirmed that the absorber in bubble mode showed a better heat and mass transfer performance especially at low solution flow rates and high gas flow rate. To conclude, the authors reported Nusselt and Sherwood numbers correlations for the falling film and bubble mode.

Issa et al. (2002) estimated the mass transfer in the absorption process with NH_3/H_2O in a rectangular test cell where the ammonia vapor was injected through the top of the absorber. Tests were performed at two pressure differences; 380 and 50 kPa. For this study, the effect of the inlet ammonia concentration in the test section was studied. As main results, the authors noted also that the ammonia absorption process decreases when increasing the inlet ammonia concentration. Also, it was observed almost no absorption when the ammonia concentration was about 60 %.

Lee et al. (2003) performed an experimental and numerical study of the absorption process with NH_3/H_2O in bubble mode. The absorber was a column with a diameter of 3 cm with a height of 100 cm without heat removal. The refrigerant vapor was injected from the bottom of the absorber while the solution flowed both up and down. From the experimental study, the authors concluded that the absorption is sensitive to the inlet gas and solution flow, temperature and concentration of solution, and direction of flows. The authors compared with a good fitting the experimental results with a numerical study.

Kim et al. (2003a,b) experimentally studied a counter-current slug flow absorber with NH_3/H_2O at the operating conditions for a GAX cycle. The authors performed a sensitivity study by varying parameters such as ammonia gas flow rate (0.6, 0.9 and 1.2 $kg.hr^{-1}$), solution flow rate (1.0 - 3.5 $kg.hr^{-1}$), inlet solution concentration in ammonia (2.5, 10.3 and 21.6 %), coolant inlet temperature (20, 30, 40 ^oC) and flow rate (0.08 - 0.4 $L.min^{-1}$), and also visualized the vapor behavior flowing up through the absorber. The absorber used was a glass tube with an inner diameter of 1 cm and a length of 150 cm, and seven annulus jackets made of poly-carbonate resin where the coolant flowed to remove the heat released by the absorption. From this study, the authors confirmed that the flow inside the absorber is mostly in slug flow mode with well-shaped Taylor bubbles and observed the presence of a churn flow, just after the gas injection. The authors also found that the mass transfer coefficient in the churn flow region, which is extended with increasing the vapor flow, is higher than that in the slug region, and they attributed it to the severe turbulence and mixing effect. Finally, the authors concluded that the absorber size can be reduced by increasing the solution flow, decreasing the gas flow and improving the coolant side heat transfer.

Cerezo et al. (2009) reported an experimental study of the heat and mass transfer processes in a plate bubble absorber with NH_3/H_2O. The absorber was corrugated plate heat exchanger L-type with three channels where ammonia vapor was injected in bubble mode through the bottom of the central channel in co-current configuration with the solution flow. Vapour bubbles were injected at the inlet of the weak solution through a 1.7-mm orifice. Experiments were performed varying parameters such as inlet solution flow rate, solution concentration (29-33 %), inlet solution temperature (38-42 ^oC), absorber pressure (160-200 kPa), and cooling water flow rates (30-35 ^oC) and to quantify their effects on the absorption mass flux, solution heat transfer coefficient, solution heat transfer coefficient and degree of subcooling of the solution leaving the absorber. Sensitivity study performed resulted in an increase of the heat and mass transfer coefficients with increasing the cooling water flow rate, solution flow rate and absorber pressure. The opposite effect was observed when increasing the solution concentration and cooling water temperature. When the solution temperature was varied, just a very slight effect was observed on the heat and mass transfer performance of the absorber. To conclude, the absorption mass flux varied in the range between 0.0025 and 0.0063 $kg.m^{-2}s^{-1}$, solution heat transfer coefficient between 2.7 and 5.4 $kW.m^{-2}K^{-1}$, the absorber thermal load between 0.5 and 1.3 kW, and the mass transfer coefficient between 3.6 and 7.2 $m.h^{-1}$.

Oronel (2010) experimentally studied the bubble absorption process with the $NH_3/LiNO_3$ and $NH_3/(LiNO_3+H_2O)$ mixtures in a plate heat exchanger L-type. The author studied the effect of inlet solution flow rate, solution concentration, inlet solution temperature, absorber pressure, inlet cooling water temperature and cooling water flow rate on absorber performance parameters such as absorption mass flux, solution heat and mass transfer coefficient with the $NH_3/LiNO_3$. Results of the sensitivity study agreed with trends of the absorber performance parameters previously obtained by Cerezo et al. (2009) with NH_3/H_2O.

Suresh and Mani (2012a,b) visualized the bubble behavior and effect of gas flow rate and liquid concentration on the bubble characteristics of Tetrafluoro ethane (R134a) in a liquid R134a–Dimethyl Formamide (DMF) solution in a glass absorber and also conducted

an sensitivity study of the heat and mass transfer processes. The absorber was a double pipe heat exchanger. The inside tube had an inner and outer diameter of 33 and 37 mm, respectively. The outside tube had an inner and outer diameter of 46 and 50 mm, respectively. The absorber measured 1000 mm in length and the refrigerant vapor was injected from the bottom of the absorber through a nozzle with an inner diameter of 2.2 mm. For the study of heat and mass transfer, effects of parameters such as gas flow, solution flow, inlet solution concentration, absorber pressure, solution temperature and cooling water flow rate on absorber performance were analyzed. From the bubble visualization study, Suresh and Mani (2012a) concluded that at lower gas flows, bubbles tend to be spherical due to the dominance of surface tension and at higher gas flow rates, bubbles tend to be hemispherical due to the dominance of inertia force (previously observed by Kang et al. 2002a, 2002b with NH_3/H_2O). The authors also noted that the bubble diameter during detachment increases with the increase in the gas flow rate and solution concentration, but when solution concentration is increased further from a limit, effect of surface tension is dominant resulting in a decrease in bubble diameter. Finally, the authors proposed a correlation for bubble diameter during detachment. From the sensitivity study, Suresh and Mani (2012b) concluded that absorption rate and heat transfer rate increase as the gas flow, solution flow, cooling water flow rate and absorber pressure increase whereas they decrease as the solution initial concentration and solution temperature increase. Finally, the authors proposed a correlation for the mass transfer based on a modified Sherwood number correlation.

Suresh and Mani (2013) studied the heat and mass transfer characteristics of Tetrafluoro ethane (R134a) in Dimethyl formamide (DMF) solution in a compact bubble absorber (plate heat exchanger) of a vapor absorption refrigeration system of 1 TR capacity. In this paper, the authors studied the effect of parameters such as circulation ratio, absorber and generator temperatures on heat and mass transfer effectiveness, overall heat transfer coefficient and volumetric mass transfer coefficient. From this study the authors concluded that heat and mass transfer effectiveness of absorber are better at lower circulation ratios and higher generator temperatures. Also, the authors proposed a correlation for the mass transfer in the plate absorber based on a modified Sherwood number correlation which takes into account the Reynolds number, Schmidt number as well as non- dimensional temperature gradients.

Experimental studies to enhance the bubble absorption by using intensification techniques have been also conducted in the last years. Review of the main studies dealing with bubble absorption, which have been reported by Kim et al. (2006a,b), Kim et al. (2007a,b), Ma et al. (2007, 2009), Pang et al. (2011, 2012), are included in the next section.

2.6.2 Intensification of the heat and mass transfer processes

The intensification of the heat and mass transfer processes taking place in the absorber can be achieved by applying three techniques: mechanical treatment, chemical treatment, and nanotechnology (Kim et al. 2003). Due to the fact that the dominant resistance to the transfer processes is mainly found in the solution side, intensification

techniques are usually applied in this side to enhance the interaction of both liquid and vapor phase and their heat and mass transfer.

The intensification of heat and mass transfer coefficients in the absorber would allow diminishing the absorber size or what is even more interesting, reducing the cycle driving temperature for solar cooling applications and/or increasing the heat sink temperature for the heat released in the absorber and condenser avoiding therefore the use of humid cooling towers.

Studies on intensification techniques to improve heat and mass transfer processes in the absorber have been carried out more frequently in the last years. A brief description of the different intensification techniques to enhance the absorption process is presented as follows. In addition, experimental studies dealing with the use of these techniques in absorbers for absorption refrigeration systems are reviewed.

2.6.2.1 Use of mechanical treatment

In falling film mode absorbers, mechanical treatment includes both scratching the tube surface to increase the surface roughness as well as the use of advanced surface tubes such as constant curvature tubes, fluted tubes or micro-finned tubes.

In bubble mode absorbers, mechanical treatment includes the use internal micro-finned area for tubular absorbers and the use of corrugated surfaces for plate absorbers. Main works dealing with the use of mechanical treatment to enhance the absorption process have been reported by Moller and Knoche (1996), Miller (1999), Kang et al. (1999a), Yoon et al. (2002), Kim et al. (2003), Park et al. (2003), Park et al. (2004) for falling film mode absorber and by Merrill et al. (1995), Lee et al. (2002a), Cerezo et al. (2009), Amaris et al. (2012), Oronel et al. (2013) for bubble mode absorbers.

2.6.2.2 Use of chemical treatment

The chemical treatment, that has been extensively investigated, consists in the addition of small quantities of surface active agents (surfactants) to induce surface tension gradients in the solution in order to cause Marangoni effect (interfacial turbulence, Figure 2.9) and lead to higher heat and mass transfer coefficients.

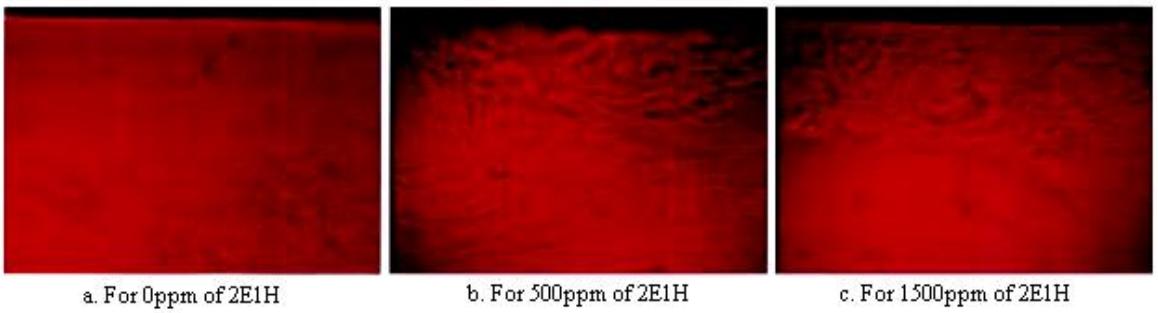

Figure 2.9 - Visualization results of Marangoni convection by Kang et al. (1999b)

The surface tension affects in a large degree the flow patterns. In the bubble mode absorption, the interfacial area between the liquid and vapor phase is significantly affected by the surface tension of the liquid. The higher the surface tension is, the lower the interfacial area for mass transfer is.

In falling film mode, the wettability on the tubes is also affected by the surface tension which limits the heat transfer, and thus the mass transfer. The higher the surfaces tension is, the lower the wettability is.

Main experimental investigations dealing with the use of surfactants to improve the absorption process for absorption systems have been reported by Nordgrent and Setterwall (1996), Moller and Knoche (1996), Kim et al. (1996), Kang et al. (1999b), Kang and Kashiwagi (2002), Yoon et al. (2002), Cheng et al. (2004), Park et al. (2004), Kim et al. (2006a), Kim et al. (2007a,b), Nakoryakov et al. (2008).

2.6.2.3 Use of nanotechnology

Recently, optimization of nanoparticles synthesis and reduction in the acquisition prices has also allowed for the inclusion of nanotechnology in absorption refrigeration systems as a technique for enhancing heat and mass transfer processes. In this case, the working fluids including nanoparticles is usually called binary nanofluids, which means binary mixtures with evenly suspended nano-sized particles (d_p < 100 nm),(Choi, 1995).

According to the last studies, nanoparticles can enhance not only the effective thermal conductivity of the base fluid but also affect directly the heat and mass transfer characteristic of fluid.

Researchers have studied and discussed the mechanisms that may justify the increase in the thermal conductivity and convective heat transfer coefficient of nanofluids with respect to the base fluid [Keblinski et al. (2002), Das et al. (2003), Buongiorno (2006), Haddad et al. (2012), Ding et al. (2007)].

In their study, Das et al. (2003) concluded that a potential explanation for the behavior of nanofluids could be the nano-convection of fluid around the particles due to their motion. The authors explained that the particles could transport some amount of heat with them and contribute to the total heat transfer through agitation in the liquid.

Buongiorno (2006) explained that the nanoparticles absolute velocity can be viewed as the sum of the base fluid velocity and a relative slip velocity, and analyzed seven slip mechanisms, some of them with higher effects than the others: inertia, Brownian diffusion, thermophoresis, diffusiophoresis, Magnus effect, fluid drainage, and gravity settling. The author defined each one as follows: Inertia, defined as the particle inertia developed by slip velocities due to turbulence in the fluid. Brownian motion, defined as a random motion of nanoparticles within the base fluid, and results from continuous collisions between the nanoparticles and the molecules. Thermophoresis, defined as the diffusion of the particles under the effect of a temperature gradient. Diffusiophoresis, defined as the migration of particles suspended in a solution due to net forces promoted by a concentration gradient. Magnus effect, if a relative axial velocity exists between the particle and the fluid, a force perpendicular to the main flow direction will arise due to the pressure gradient around the particle, created by its rotation. Fluid drainage, as a particle approaches the wall, there is a resistance caused by the pressure in the draining

fluid film between the two approaching surfaces. Gravity, the nanoparticles settling velocity due to gravity.

Meanwhile, Ding et al. (2007) suggested that the particle migration could be the major factor responsible for the heat transfer enhancement and also the enhanced thermal conductivity due to nanoparticles does not guarantee a significant enhancement in the convective heat transfer.

Based on the proposed mechanisms and explanations above, it is clear that heat transfer enhancement with nanofluids is not only due to the increase in thermal conductivity but also to the slip mechanisms, such as the Brownian motion, which refers to the random motion of nanoparticles, and thermophoresis caused by the temperature gradients, with the effect of the slip mechanisms being more predominant.

Since heat and mass transfer are analogues processes, investigations on nanofluids have also shown outstanding mass transfer enhancements [Kim et al. (2012), Kim et al. ((2006b), Kim et al. (2007a,b), Ma et al. (2007, 2009), Lee et al. (2010), Pang et al. (2012), Krishnamurthy et al. (2006), Linek et al. (2008), Fang et al. (2009), Veilleux and Coulombe (2011), Lee et al. (2011), Torres Pineda et al. (2012)]. These studies reported that possible reasons for the mass transfer enhancements in bubble absorbers are the induced micro disturbances and the increase in the gas-liquid interfacial bubble area due to motion and nanoparticles interaction (Figure 2.10).

Moreover, Krishnamurthy et al. (2006) showed that an optimum volume fraction of nanoparticles could result in a mass transfer enhancement higher than that observed in thermal conductivity.

It is worthwhile to highlight that because of the different operating conditions and methodologies employed in investigations dealing with mechanisms of transport phenomena in nanofluids, agreement with possible theories has not been established.

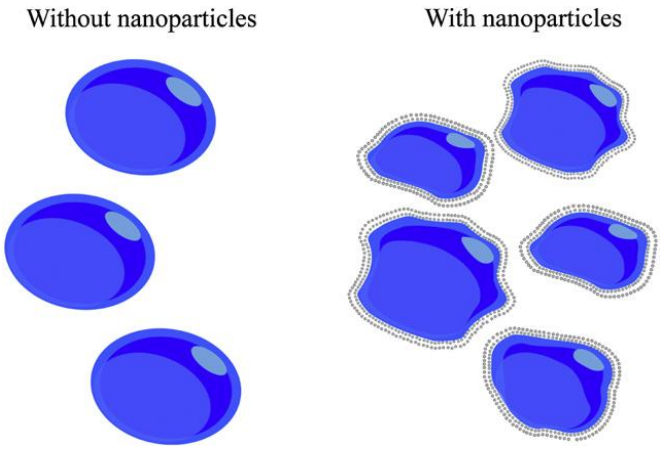

Figure 2.10 - Bubble breaking model, the nanoparticles cover the bubble surface area and break them into smaller bubbles, by Torres Pineda et al. (2012).

2.6.2.4 Experimental studies on intensification of the absorption process

Merrill et al. (1995) evaluated the performance of three compact bubble absorbers developed for generator-absorber heat exchange absorption cycles (GAX). The absorbers

tested involved roughness, spiral flutes, and internal spacers. Experimental results showed that the enhancement increased the GAX load, increased the vapor flow rate, and decreased the approach temperature difference when compared to the base values. The authors also concluded that the vapor injection process needs further improvement to improve the absorption.

Nordgrent and Setterwall (1996) studied the effect of the addition of surfactant (1-Octanol) to a mixture of water and glycerol on the wave pattern that take places in the falling film mode absorption process. Experiments were conducted with different mass flow rates (Re 40-260) and varying the surface tension of the mixture by changing the surfactant concentration. The absorber was a column of 6 m with an outside diameter of 51 mm and a wall thickness of 1.2 mm placed within a glass cylinder. From this study, the authors concluded that interfacial tension of the fluid decreases sharply when the surfactants was added and caused calmer and more uniforms waves in the falling film. The authors also observed the surfactant concentrations under the saturation limit stabilize the falling film meanwhile concentrations over the limit destabilize the film.

Moller and Knoche (1996) evaluated the effect of different surfactants on the absorption process in a compact absorber working with NH_3/H_2O. The compact absorber was a compact brazed plate heat exchanger with offset strip fin (OSF), (Figure 2.11). The authors employed surfactants to reduce the surface tension of the solution and the interfacial tension between solid surface and solution to improve the walls wettability of the channels and the mass transfer. The surfactants used were Marion PS (0.25 wt. %, 0.4 wt. %), Marion A (0.25 wt. %, 0.5 wt. %), Dehydol LT 14 (0.5 wt. %), Emulgin B1 (0.5 wt. %, 0.91 wt. %), l-Octanol (50, 100 and 500 ppm). From this study, the authors confirmed that the surfactants used reduce the surface tension strongly and improve the wettability of the compact heat exchanger plates and mass transfer. The authors also found that the best result in terms of the measured absorption rates was achieved with the 1-octanol.

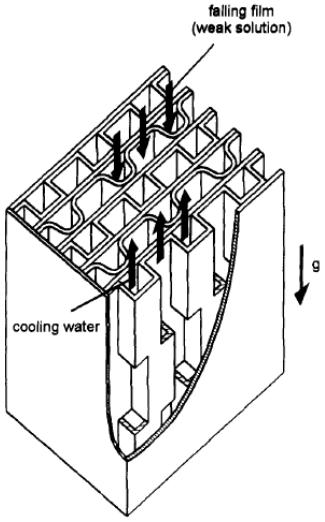

Figure 2.11 - Compact absorber tested by Moller and Knoche (1996).

Kim et al. (1996) analyzed the absorption of water vapor to aqueous lithium bromide in vertical falling film mode adding 2-ethyl-l-hexanol (1 to 100 ppm). The absorber tested

consisted of two concentric tubes with an inner stainless-steel tube (measuring 1.83 m in length) and an outer Pyrex tube to facilitate the observation (Figure 2.12). In this absorber, the LiBr solution flows down the outside of the inner tube. According to this configuration, the absorption takes place at the outer wetted surface of the inner tube and the heat released by the absorption is removed by cooling water flowing upward inside the inner tube. Experiments were conducted at solution concentration of 60 wt. %, inlet solution temperature of 40 ^{o}C, absorber pressure of 1 kPa and inlet cooling water temperature of 30 ^{o}C. From this study, the authors observed that the film becomes highly turbulent during the absorption, starting from a surfactant concentration of 3-6 ppm and reaching a maximum effect near to 30 ppm. As a consequence, the heat and mass transfer is significantly enhanced. The authors explained that the interfacial turbulence obtained is due to the surface-tension gradients caused by LiBr concentration, heat-transfer additive concentration and the high temperature achieved in the interface.

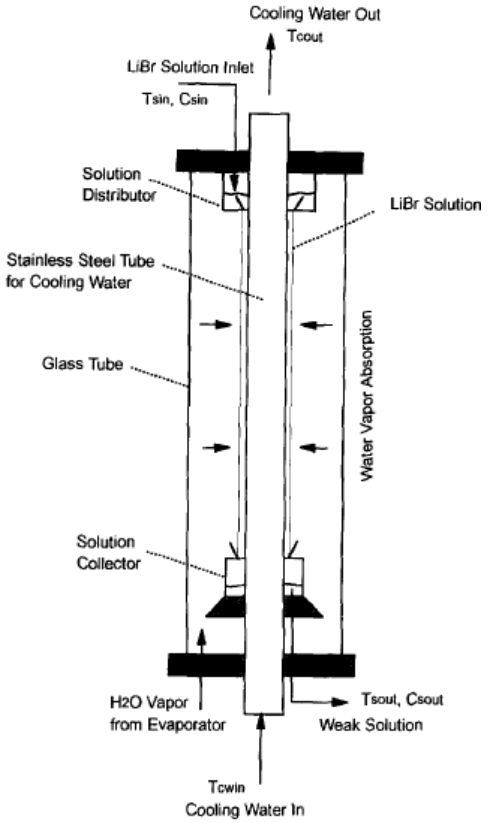

Figure 2.12 - Vertical Falling film absorber tested by Kim et al. (1996).

Kang et al. (1999a) carried out experiments for NH_3/H_2O falling film absorption process in a plate heat exchanger with enhanced surfaces. The plate heat exchanger had offset strip fin between two plates in the absorption side, and rectangular plain fins between two plates in the coolant side (Figure 2.13). In this study, the solution and vapor entered at the top of the plate heat exchanger and flowed down meanwhile the coolant entered the test section from the bottom, flowed up in the counter-cross direction to the liquid solution flow. The inlet liquid temperature was varied between 17.0 and 37.2 ^{o}C, the inlet solution concentration in ammonia was varied between 5 % and 15 % while the inlet vapor concentration was varied from 64.7 % to 79.7 %. The authors examined the effects

of solution and vapor flow characteristics, inlet subcooling of the solution flow and inlet concentration difference on heat and mass transfer performance. The authors concluded that Nusselt number is more significantly affected by falling film solution flow than by the vapor flow while Sherwood number is more significantly affected by the vapor flow than by solution flow. Finally, the authors presented correlations for heat and mass transfer coefficients.

Kang et al. (1999b) reported surface tension and interfacial tension data for NH_3/H_2O systems and various surfactants. The authors also visualized the Marangoni convection effect due to the use of surfactants. For this study, the authors performed experiments for eight additives; 2-ethyl-1-hexanol (2E1H), n-Octanol (n-O), 2-Octanol (2-O), 3-Octanol (3-O), 4-Octanol (4- O), n-Decanol (n-D), 2-Decanol (2-D) and 3-Decanol (3-D). The authors found that the solubility limits of the additives in NH_3/H_2O ranged from 500 to 3000 ppm depending on the additives which are much higher than those in H_2O/LiBr solution (70 to 400 ppm). The authors also reported that the surface tension increased with increasing ammonia concentration for 2E1H, n-O, 2-O, 2-D and 3-D while it decreased for 3-O, 4-O, and n-D. Finally, the authors reported a new model of Marangoni convection for the best selection of heat transfer additive in NH_3/H_2O absorption systems.

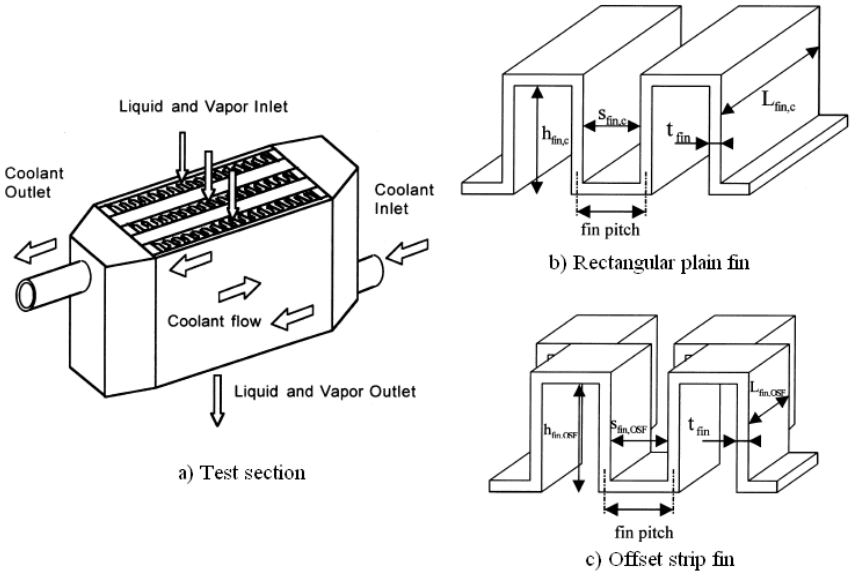

Figure 2.13 - Absorber with rectangular fin and OSF studied by Kang et al. (1999a).

Miller (1999) measured the absorption rate and the heat transfer coefficient in a H_2O/LiBr horizontal tube absorber comparing several advanced surface tubes. The author also analyzed the synergism of the effects of advanced surfaces and additives such as 2-ethyl-1-hexanol. The bundle of tubes consisted of six copper tubes, each tube with an outside diameter of 15.9 mm and a length of 320 mm. The experimental study was performed over a pressure of 3.33 kPa, coolant temperature ranging from 20 to 35 ^oC and solution concentration ranging from 0.6 to 0.62. The author reported that the tested advanced surfaces increased the mass transfer around 1.75 times higher than those values with the smooth surface tubes. The author also reported that the mass absorbed and the overall falling film heat transfer coefficient achieved with the advanced surface tubes were doubled when the additive and the advanced surfaces were simultaneously tested. From

this study, the author concluded that the enhancement caused by the mechanical mixing of advanced surfaces was not as effective as the enhancement induced by the chemical agitation of the additive and found a synergistic effect rather small.

Lee et al. (2002a) studied the effect of solution and vapor flow rates on a plate-type NH_3/H_2O bubble absorber. Three types of plates were tested: smooth plate, hair lined plate treated by laser, and plate treated by sand paper. In a comparative study, the plate treated by sand paper was selected due to its laminar flow and better wettability. To perform the study, the solution flowed down from the top of the absorber while ammonia gas flowed up in counter-current. The coolant flowed up in counter current to the solution flow. From this study, Nusselt and Sherwood numbers were correlated as functions of solution Reynolds and gas Reynolds numbers to establish the solution and gas characteristics on the absorption rate.

Kang and Kashiwagi (2002) studied the effect of the surfactant n-octanol on the absorption performance for the NH_3/H_2O absorption process. The authors also visualized Marangoni convection induced by the additive. During the experiments temperature of the solution and the pressure were kept almost constant about 20 ^oC and 200 kPa, respectively. From this study, the authors visualized the Marangoni convection near the interface only when additive was into the solution and achieved an absorption heat transfer enhancement as high as 3.0 - 4.6 times with respect to the base solution by adding the additive.

Yoon et al. (2002) studied the enhacement of the heat transfer by surfactants into H_2O/LiBr solutions. The authors also studied the effect of tube surfaces using a bare tube, a floral tube and a hydrophilic tube in a horizontal configuration (Figure 2.14). Experiments were conducted at a solution concentration of 60 wt. %, inlet solution temperature of 45 ^oC, inlet cooling-water temperature of 32 ^oC and varying the surfactant concentration (500 - 5500 ppm of n-Octanol). From this study, the authors obtained the highest wettability and heat transfer coefficient with the hydrophilic tube, however, higher heat trasnfer coefficients were achieved with the floral tube when the additives were used. The authors also explained that the addition of surfactant concentration higher than 3500 ppm did not show improvements in the heat transfer coefficient.

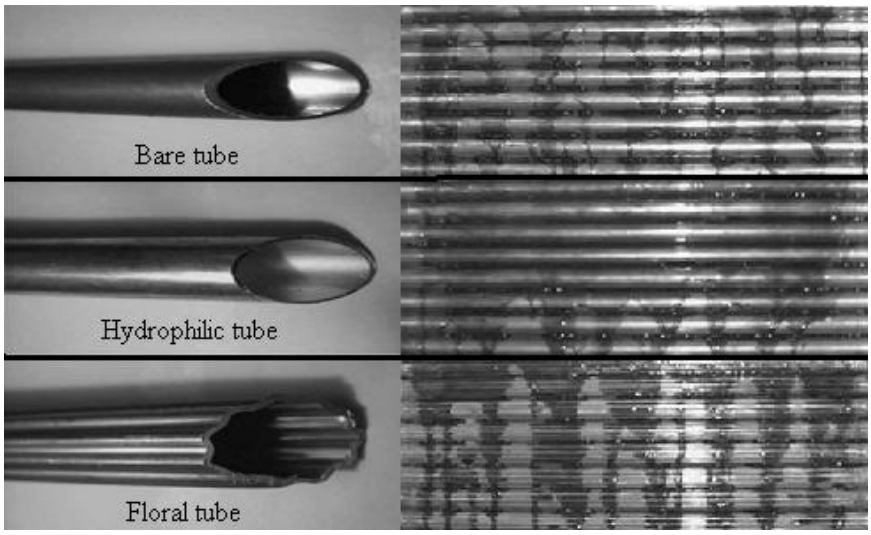

Figure 2.14 - Tubes tested by Yoon et al. (2002) and flow patterns on them.

Kim et al. (2003) and Park et al. (2003) analyzed the effect of micro-scaled surface treatment on the wettability and absorption performance in a H_2O/LiBr falling film absorber. For this study, three types of tubes with surface treatment were tested; a smooth tube, a tube N. 600 with a roughness of 0.384 μm and a tube N. 24 with a roughness of 6.986 μm (Figure 2.15). In the studied configuration, the solution enters the test section from the top of the absorber through a liquid distributor. The absorber consists of 28 copper tubes with diameter of 16 mm and a length of 205 mm. Experiments were conducted at an inside absorber pressure of 0.94 kPa, solution temperature ranging from 30 to 50 ^oC, solution concentrations from 55 to 62 wt. % and mass flow rates ranging from 0.74 to 2.71 $kg.min^{-1}$. The results obtained from this study corroborated that the wettability for the micro-scale hatched tubes was higher than for the smooth tubes and also that absorption performance of the absorber with the micro-hatching tubes was improved up to two times compared with the smooth tubes.

Cheng et al. (2004) studied the enhancement effects of additives (2-ethyl-1-hexanol and 1-octanol) on a vertical falling film absorber with H_2O/LiBr. The absorber consists of two concentric tubes in a vertical disposition. The outer tube, which had an outer diameter of 90 mm and thickness of 5 mm, was made of acryl glass. The inner tube, which was made of stainless steel, had an outer diameter of 15.88 mm and thickness of 1 mm. The effective length of the absorption tube was 1 m. The cooling water flowed upward through the inner tube and the solution in falling film on the outer surfaces of the inner tube. According to the experimental results, the authors confirmed that small amounts of an additive (5, 10, 30, 50, 100 ppm) enhance the heat transfer during the absorption process significantly and also that the additive concentration is a key parameter that should be taken into account.

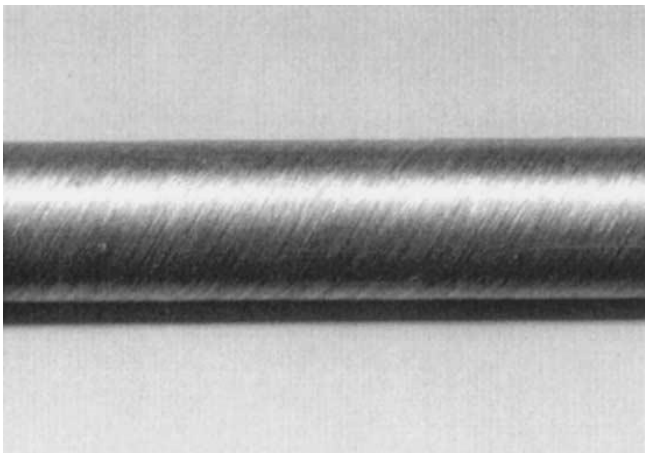

Figure 2.15 - Micro-scaled hatched tubes N. 24 used by Kim et al. (2003).

Park et al. (2004) studied the effect of heat transfer additive (Normal Octanol with the concentration of 400 ppm) and surface roughness of micro-scale hatched tubes on the absorption performance for a H_2O/LiBr horizontal tube absorber. The test facility was the same used by Kim et al. (2003) and Park et al. (2003). From this study the authors concluded that for the bare tube, absorption rate with additive was enhanced up to 3.76 times of that without the additive. Also, the effect of additive on the heat transfer rate was found to be more significant in the bare tube than that in the micro-scale

hatched tubes. Finally, the authors found that the absorption performance for the micro-hatched tube with additive became up to 4.5 times higher than that for the bare tube without additive.

Kim et al. (2006a,b) and Kim et al. (2007a) evaluated the effect of different kinds of nanoparticles (Cu, CuO, and Al_2O_3, Figure 2.16) and surfactants (2-ethyl-1-hexanol, n-octanol, and 2-octanol) on the absorption performance during NH_3/H_2O bubble absorption process. The experimental test facility consisted of the absorber test section made of transparent acrylic resin plates. The bubble behavior was observed with a visualization equipment. In this study, the solution was filled in the test section and bubbles are injected from the bottom through a vapor orifice. The temperature of test solution was kept at 20 ^oC. The average diameters of all nanoparticles used were under 50 nm and concentration was varied from 0.0 to 0.10 wt. %. In the case of the surfactants, the surfactants concentration was varied between 0 and 1000 ppm.

Regarding the addition of surfactant, Kim et al. (2006a) observed that surfactants also enhanced the absorption rates during the bubble absorption process and that 2-Ethyl-1-hexanol showed the highest effect on the absorption rates among the considered surfactants. In addition, results showed that the addition of 700 ppm of 2-ethyl-1-hexanol enhanced the absorption performance up to 4.81 times in an ammonia solution with a concentration of 18.7 %.

According the results with nanoparticles reported by Kim et al. (2006b), Cu showed the most effective effect on the absorption among the considered nanoparticles. The addition of nanoparticles enhanced the absorption up to 3.21 times with respect to the base fluid when 0.1 wt. % Cu nanoparticles concentration was added in an ammonia solution with a concentration of 18.7 %. In a visual study, the authors observed that bubble shape was spherical in the case with nano-particles, while it became hemi-spherical shape in the case without nano-particles (Figure 2.17). The authors also explained that the bubble size in the binary nanofluids is smaller than that in the base mixture because it was absorbed faster than that in the base mixture.

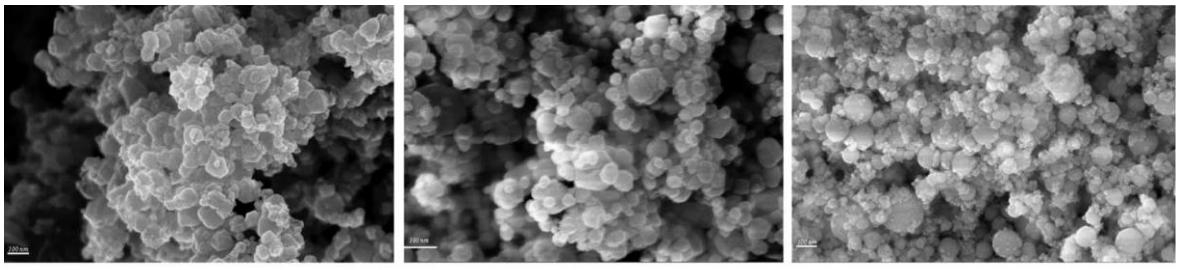

(a) Copper (b) Copper oxide (c) Aluminum oxide

Figure 2.16 - SEM pictures of nano particles used and reported by Kim et al. (2006b).

Kim et al. (2007a) also showed that the addition of both surfactants and nanoparticles improved mass transfer performance during the ammonia bubble absorption process. When 2-ethyl-1-hexanol and Cu nanoparticles were used simultaneously, the absorption performance enhanced up to 5.32 times. Finally, the authors concluded that the concentration of ammonia solution, the kind of nanoparticles and concentration, the kinds and the concentrations of surfactants are considered as the key parameters. The

authors also concluded that the effect of the nanoparticles and surfactant in the absorption rate increases with increasing concentration of both and with increasing the ammonia concentration.

Ma et al. (2007, 2009) studied the experimental enhancement of the heat and mass transfer processes in a bubble absorber with NH_3/H_2O. For this, the authors used multi-wall carbon nanotubes (MWCNT, diameter of 10-20 nm) into the NH_3/H_2O solution. The authors also measured the thermal conductivity of the NH_3/H_2O solution with the nanoparticles. The authors justified the use of carbon nanotubes due to the fact that carbon nanotubes do not chemically react with ammonia as it could occur with metal-based nanoparticles. The experimental test facility consisted of an absorber (200 mm in length and 20 mm in diameter) without a heat removal system where the ammonia gas is injected from an orifice located at the bottom of the absorber. Temperature of the inlet solution and the pressure in the absorber were kept about 14 ^oC and 140 kPa, respectively. From this study, the authors concluded that the thermal conductivity of the NH_3/H_2O solution with the nanoparticles increased by 16 % and also that the maximum effective absorption rate was 1.16 for an ammonia concentration of 23.29 % and a nanotubes concentration of 0.23 %. As previously concluded by Kim et al. (2006b), Ma et al. (2007, 2009) also observed that the nanofluids improve the bubble absorption when the absorption potential is lower (high solution concentrations).

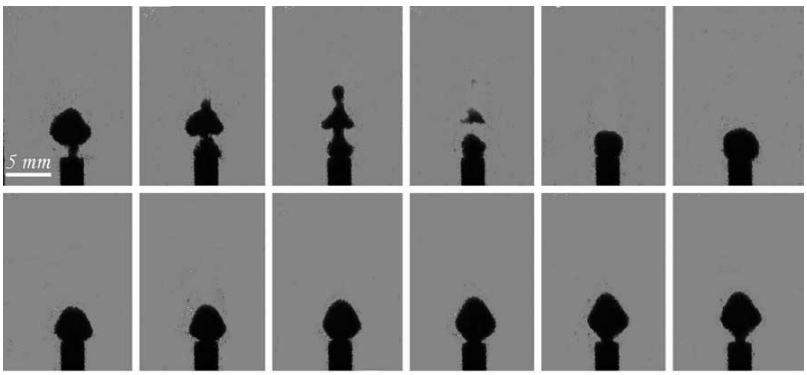

(a) without nano-particles

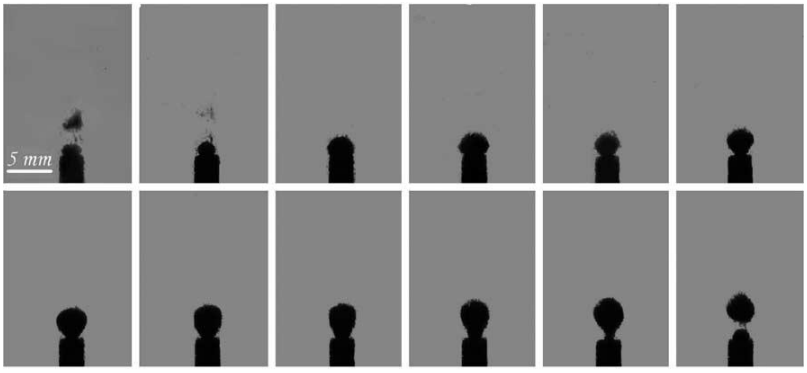

(b) with Cu nano-particles 0.1% (binary nanofluid)

Figure 2.17 - The bubble behavior with and without nanoparticles (Cu, 0.1 wt. %) for an ammonia concentration of 8.0 % reported by Kim et al. (2006b).

Kang et al. (2008) evaluated the horizontal falling film absorption process with H_2O/LiBr with the addition of nanoparticles. For this study, the authors used nanoparticles of Fe (with diameter of 100 nm) and Carbon nanotubes (CNT) (with diameter of 25 nm and length of 5 mm) with the concentrations of 0.0, 0.01 and 0.1 wt. %. The test section consisted of eight copper tubes (with length of 500 mm and diameter of 15 mm) installed in column disposition. The system pressure was kept at 10 kPa, the inlet solution concentration was 55 wt. %, the inlet temperature of solution was 40 ^oC and the inlet temperature of the cooling water was varied between 24 and 28 ^oC. In this absorber, the cooling water flowed inside the tubes from the bottom to the top. In this study, the authors found that the absorption rate using CNT into the H_2O/LiBr solution became higher than that with the Fe nanoparticles. A maximum mass transfer enhancement was achieved using 0.01 wt. % of CNT. This enhancement was 2.48 higher than that with the base solution while it was 1.90 higher with the Fe nanoparticles. Finally, the authors concluded that absorption rate increased with increasing the solution mass flow rate and the concentration of nanoparticles. Interestingly, the heat transfer rate increase obtained was not much affected by the concentration of nanoparticles and also was found that the use of nanoparticles had a much more significant effect in mass transfer than in heat transfer.

Nakoryakov et al. (2008) measured the heat and mass transfer intensification of the steam absorption into H_2O/LiBr using additives of n-octanol (25 - 400 ppm). Experiment were conducted in a vacuum cylindrical chamber made of stainless steel (165 mm in diameter and 87 mm in length) which was filled with a solution of H_2O/LiBr (58 %) and additives. The steam was introduced into the chamber from the top of it. The steam pressure in the vacuum chamber was kept of about 2 kPa. The local characteristics of heat and mass transfer and surfactant effect was visualized through an infrared glass and recorded by a high resolution camera. From this study, the authors confirmed that addition of surfactants into a solution generates surface convection even in the initially immobile layer.

As commented earlier, Cerezo et al. (2009) carried out a sensitivity study of the heat and mass transfer in a three channels plate heat exchanger as a bubble absorber and NH_3/H_2O as the working fluid. In this study can be highlighted the use of a compact absorber with advanced corrugated surfaces to improve the ammonia absorption process.

Lee et al. (2010) analyzed the effect of nanoparticles on the absorption enhancement for NH_3/H_2O absorption systems. Al_2O_3 and carbon nanotube (CNT) were selected for this study. Experiments were performed in a chamber filled with the nanofluids. The vapor entered the test section through the distributor located at the top of the test section. The ammonia concentration used was 20 % and the concentration of the CNT was varied from 0 to 0.08 vol % and from 0 to 0.06 vol % for the Al_2O_3 nanoparticles. The system pressure for the test section was 5.0 bar. From this study, the authors obtained that the maximum heat transfer and absorption rate enhancement was obtained with a nanoparticles concentration of 0.02 vol %. Heat transfer and absorption rate enhanced 17 % and 16 % when the CNTs were used, respectively. Also, heat transfer and absorption rate increased 29 % and 18 %, respectively, when the Al_2O_3 were used.

Yang et al. (2011) used Al_2O_3, Fe_2O_3 and $ZnFe_2O_4$ into a mixture of NH_3/H_2O to experimentally study the falling film absorption process. Additionally, sodium dodecyl benzene sulfonate (SDBS) was added with the nanoparticles in the NH_3/H_2O mixture to

reduce the nanofluids viscosity. Experiments were performed for NH_3/H_2O mass fraction of 0 %, 5 %, 10 %, and 15 %. The mean size of Al_2O_3, $ZnFe_2O_4$ and Fe_2O_3 nano-particles were less than 20 nm, 30 nm and 30 nm, respectively. The absorber used is a container with a falling film liquid distributor located at the top. The container is made of stainless steel with a plexi glass to observe the falling film flow. From this work, the authors concluded that absorption performance can be enhanced by adding a small mass fraction of nanoparticles with matched surfactants, which avoid the viscosity of nanofluids to increase. Finally, the authors achieved an effective absorption ratio enhancement by 70 % and 50 % with Fe_2O_3 and $ZnFe_2O_4$ nanofluids, respectively, when the initial ammonia mass fraction was 15 %.

Pang et al. (2011) studied the effect of Al_2O_3 nanoparticles on the absorption performance in NH_3/H_2O bubble absorption process. The nanoparticles size was 20 nm and the mass fraction was varied from 0.2 % to 1.0 % in the experimental study. The absorber size was 20 mm × 20 mm × 200 mm and the diameter of the ammonia injector was 2 mm. The ammonia initial concentration was varied from 0 to 20 % and the pressure was about 200 kPa. From this study, the authors obtained a maximum effective absorption rate of 2.017 with an initial ammonia concentration of 20 % and the Al_2O_3 nanoparticles mass fraction of 0.5 %.

Pang et al. (2012) evaluated the effect of mono silver (Ag) nanoparticles into the NH_3/H_2O mixture for application of NH_3/H_2O absorption in a bubble absorber. Experiments for this study were performed with and without heat removal. During experiments, the pressure of the absorber, which was made of stainless steel 316 was kept about 200 kPa. The size of the nanoparticles was 15 nm and the concentration used was varied from 0 to 0.02 wt. %. The NH_3/H_2O solution concentration in the absorber was varied from 0 to 20 wt. %. For experiments with heat removal, the inlet cooling-water temperature was set to 15 ^oC. After analyzing the results, the authors concluded that mass transfer in nanofluids with heat removal was enhanced more than that without heat removal. The maximum absorption rate achieved was 1.55 times higher than values with the base mixture at Ag nanoparticles concentration of 0.02 wt. %. Finally, the authors justified that the mass transfer enhancement by nanofluids was attributed to two main reasons, the enhanced heat transfer and gas bubble breaking.

Kim et al. (2012) visualized the dispersion of nano-particles in H_2O/LiBr solution, and determined the absorption and heat transfer rates for falling nanofluids film flows. SiO_2 nanoparticles with size between 10 and 20 nm were selected for this study. Experiments were also conducted without and with 2E1H in a concentration of 150 ppm to reduce the surface tension of the solution. The test section consisted of an absorber with eight copper tubes, with a length of 500 mm and diameter of 15 mm installed in a column, inside. According to the flows configuration studied, the cooling water flowed inside the tubes from the bottom to the top while the solution was distributed on the top of the absorber. To conduct the experiments, the absorber pressure was kept at 1 kPa, the inlet concentration of H_2O/LiBr solution was set to 53 %, the concentration of nanoparticles into the solution was varied from 0, 0 to 0.01 vol %, the inlet solution temperature was 40 ^oC, and the inlet cooling water temperature was set to 25 ^oC. After experiments, the authors recommended the use of SiO_2 nanoparticles into the H_2O/LiBr solution with concentrations lower than 0.01 wt. % and found that the maximum improvements of mass transfer and heat transfer rate reached 18 % and 46.8 %, respectively, when the

concentration of SiO_2 nanoparticles was 0.005 vol %. The authors also observed that the maximum enhancement achieved with the nanofluids was obtained without surfactant.

Recently, Amaris et al. (2012) studied the effect of inner advanced surfaces in tubular bubble absorbers on the NH_3 absorption process using $NH_3/LiNO_3$ as working pair. Experiments in the bubble absorber with an internal smooth tube were also performed and the results were compared with those achieved with the advanced surface tube. The absorber performance with advanced surfaces using two tube lengths (1 and 3 m) and two tube diameters (8 and 9.5 mm) have also been investigated. Results from this work have shown that the maximum absorption rate achieved with the advanced surfaces was up to 1.7 times higher than that of the smooth tube.

As reviewed before, Oronel et al. (2013) carried out an experimental study on the absorption processes with the $NH_3/LiNO_3$ and $NH_3/(LiNO_3+H_2O)$ mixtures in a three channels plate heat exchanger with L type corrugations (Figure 2.18) and conducted a sensitivity study of the main operating conditions. The main conclusion from this study highlighted that the addition of a small amount of water in the absorbent (25 wt. %) resulted in the lower viscosity of the $NH_3/(LiNO_3+H_2O)$ which improved the heat and mass transfer processes taking place in the absorber.

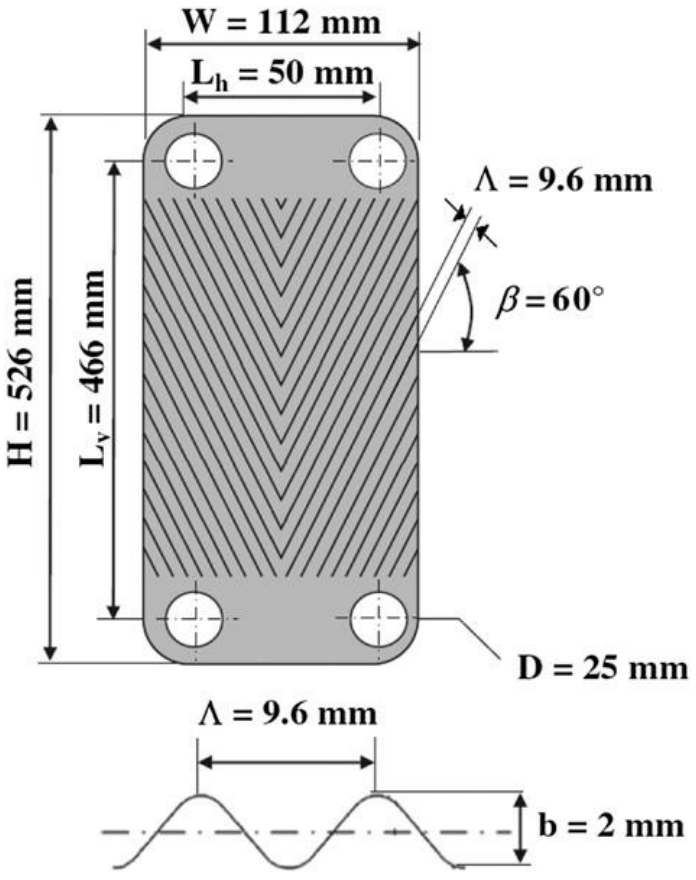

Figure 2.18 - Plate with L-type corrugations tested by Oronel et al. (2013).

2.7 Conclusions

In this chapter, a review of the main characteristics of the current absorption refrigeration technologies, conventional working fluids and the absorption process configurations have be presented.

Also, thermophysical properties available and experimental studies found in the literature dealing with $NH_3/LiNO_3$ as the working fluid have been reviewed as well as experimental investigations on bubble absorption and experimental studies on intensification of the absorption process for absorption systems.

According to the review performed, $NH_3/LiNO_3$, which is focus of this thesis, has been recognized as a promising working fluid for air-cooled absorption refrigeration systems driven by low temperature heat sources such as solar and waste heat.

Ammonia is used as refrigerant since it has a great potential for use in low charge systems using compact components such as plate heat exchangers or advanced surface heat exchangers.

The bubble mode absorption has been recommended and studied due to its high mass transfer performance and more compact designs in comparison with the falling film mode.

Intensification techniques such as the use of advanced surfaces and nanoparticles have shown outstanding heat and mass transfer enhancements. In some cases, mass transfer enhancements can be much more significant that those obtained in the heat transfer.

For the selection of nanoparticles to be used in absorption systems, key parameters such as the kind of nanoparticles and concentration, and base mixture should be taken into account.

Carbon nanotubes (CNTs) are suitable nanoparticles to be used in ammonia based working fluids due to the fact that CNTs do no chemically react with ammonia and have high thermal conductivity.

Chapter 3

Experimental Test Facility and Procedure

3.1 Introduction

Several bubble absorbers configurations were analyzed to evaluated their performance at conditions of interest for solar refrigeration systems with the $NH_3/LiNO_3$ mixture.

The following chapter describes the experimental test facility used for the study of the absorption process and shows in detail the different geometries of bubble absorbers tested.

In addition, description of the instrumentation and control system, experimental procedure, data reduction and description of the method for the uncertainty determination of results are presented.

3.2 Experimental Test Facility

Figure 3.1 and Figure 3.2 show a diagram and a picture of the experimental test facility used to study the absorption process in bubble mode absorbers. This experimental test facility, initially built up for the characterisation of plate absorbers with NH_3/H_2O (Cerezo, 2006), was modified and adapted to study the ammonia absorption process into the $NH_3/LiNO_3$ mixture in plate and tubular bubble absorbers.

The facility allows operating conditions of interest to be monitored and controlled including solution and cooling-water flow rates, solution and cooling-water temperatures, ammonia concentration in the solution, and operating pressure in the absorber. According to test facility design, hot and cold side currents in the absorber can be set in co-current and counter-current configuration, however all experiments were conducted in counter-current configuration. The test facility consists of the following circuits: solution circuit, heating-water circuit, cooling-water circuit and ammonia circuit.

Measuring instruments such as RTD temperature sensors (T), pressure transmitter (P), magnetic flow meters (F) and Coriolis flow meters (C) were located in the experimental test facility as shown in Figure 3.1. Measuring equipments were connected to a data acquisition unit. Density, temperature and mass flow rate of the weak and strong solutions were measured by Coriolis flow meters. Thermophysical properties of the $NH_3/LiNO_3$ mixture at the conditions under study were calculated using the correlations presented by Libotean et al. (2006, 2007). Regarding the thermal conductivity of the $NH_3/LiNO_3$, correlation reported by Cuenca et al. (2013a) was used.

3.2.1 Solution circuit

The circuit of the $NH_3/LiNO_3$ solution (dark and pea green lines) consists mainly of two stainless-steel tanks (ST1 and ST2), a solution pump (B1), a heat exchanger (SHE), a vapor-liquid separator (VLS) and the test section where the absorption process takes place.

In the solution circuit, the solution weak in refrigerant (pea green line) that has previously been heated in the heat exchanger (SHE) until conditions of interest is pumped from the

storage tank 1 (ST1) to the bottom side of the test section. The solution rises through the central channel of the absorber in counter-current with the cooling-water absorbing the ammonia vapor fed from an ammonia bottle. The solution strong in refrigerant (dark green line) leaves the test section at the top and flows to the vapor-liquid separator tank (VLS), and then the solution flows to be stored in the storage tank 2 (ST2).

The test facility operates in discontinuous mode since weak solution in refrigerant is pumped from the storage tank 1 to the test section and the strong solution in refrigerant from the absorption process is sent to the storage tank 2. Therefore, it can be easily set the desired operating condition at the inlet of the test section and the maximum ammonia absorption capacity can be obtained.

When storage tank 1 gets empty, the tank is filled with the strong solution from the storage tank 2 and excess of ammonia is send to a neutralization tank (NT) until getting the desired initial solution concentration for later start a new test.

Tubing of the solution circuit is made of stainless steel with an inner and outer diameter of 10 and 12 mm, respectively.

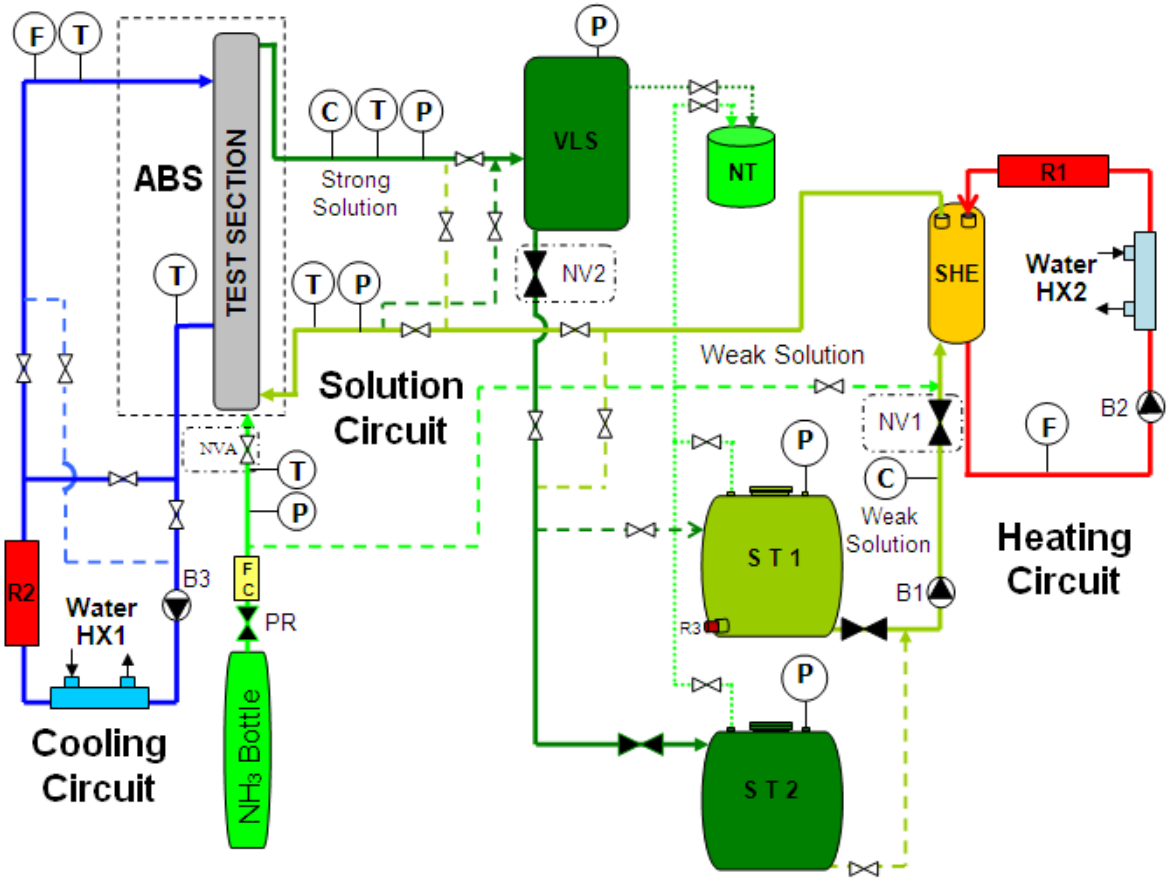

Figure 3.1 - Diagram of the experimental test facility.

Storage tank 1 (ST1) and 2 (ST2) are made of stainless steel with an individual capacity of 132 litres. Each storage tank has at the top a pressure transmitter, a manometer and a ball valve to purge the excess of ammonia to the neutralization tank (NT). In front of each storage tank is localized a transparent type glass plate level gauge (Suincasa, Glass DIN

7081) that allows observing the solution level. Storage tank 1 has an electric resistance (R3) set at the bottom to increase the pressure of the solution and to reduce the pressure increase by the solution pump (B1).

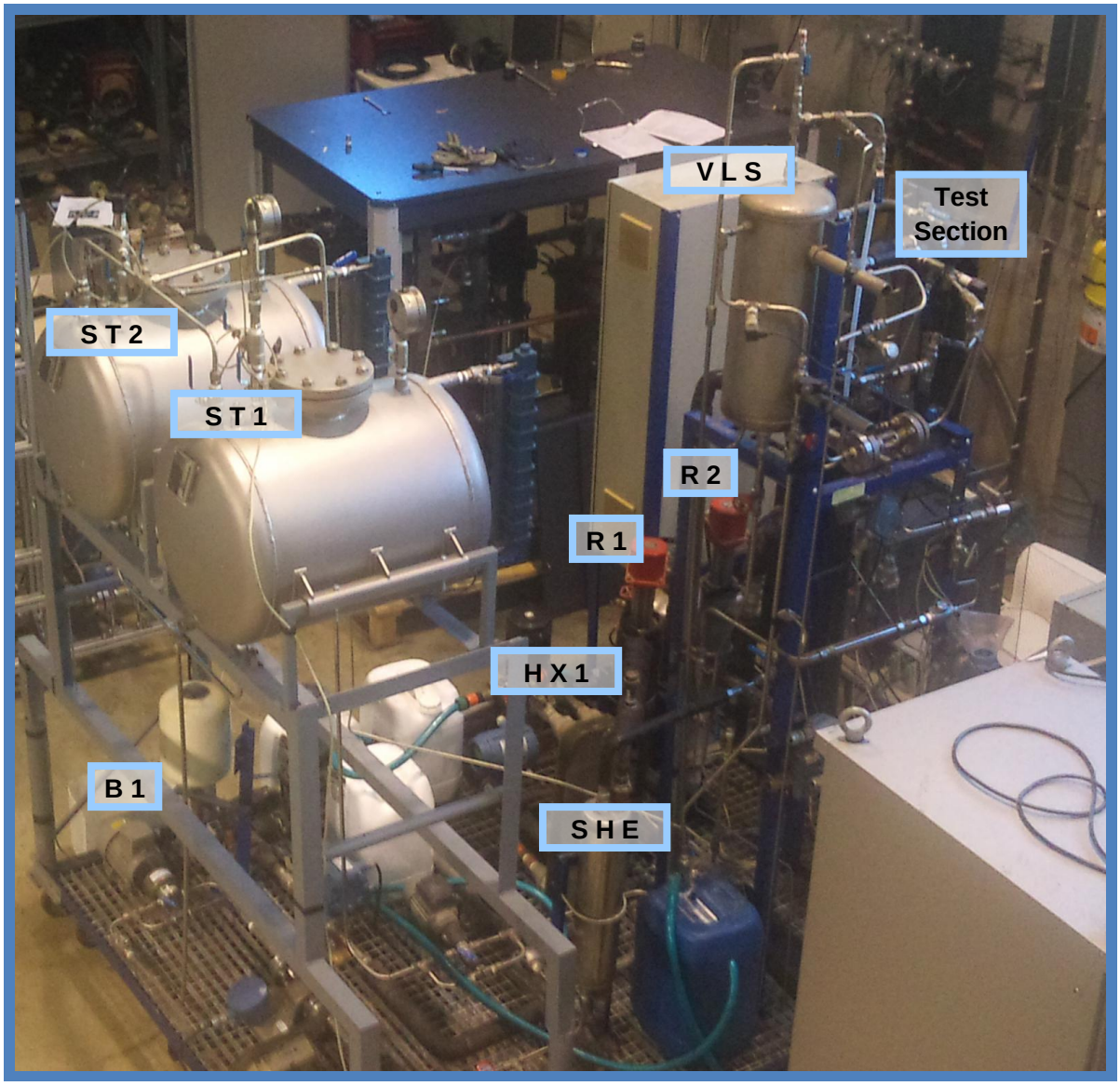

Figure 3.2 - Picture of the experimental test facility.

Solution Pump (B1) (with flexible rotary vane) is a magnetically coupled internal gear pump (Leroy Somer, LS71M/T, 2800 rpm/min) with a power of 0.37 kW. Solution mass flow is controlled by manipulating two needle valves (NV1 and NV2) which are localized in the test facility as shown in Figure 3.1.

Heat exchanger (SHE), which is used to heat or cool the solution to the conditions of interest before entering the test section, is a spiral heat exchanger (model Spirex k4 CC) made of stainless steel with an outer diameter of 12 cm, 51.4 cm in length and a heat exchange area of 1.4 m^2.

Vapor-liquid separator tank (VLS) is a stainless steel cylinder with an outer diameter of 23 cm and 50 cm in length. It has a purge and a security valve at the top and a transparent teflon tube as level.

3.2.2 Heating-water circuit

Heating-water circuit consists of a 5 kW circulation heater (R1), a recirculation pump (B2), a magnetic flow meter (F), a water-water heat exchanger (HX2) and the heat exchanger (SHE). This circuit allows heating the solution to the required temperature before it enters the absorber. The circuit tubing is made of copper with an outer diameter of 2.82 cm.

Circulation heater (R1), IES, model RFP-E24405, is 600 mm in length, thermally insulated by mineral wool and protected by a galvanized sheet. It is controlled by a relay (RN2448D50) with a proportional-integral-derivative controller (PID controller, Shimaden, model SR 71-8P1-1C) that receives signals of a thermocouple which measures the solution temperature.

Recirculation pump (B2), GRUNDFOS, model CR1, is made of stainless steel AISI 304. Water- water heat exchanger (HX2) has the same characteristics that the heat exchanger (SHE) previously described. The water-water heat exchanger (HX2) only allows cooling the heating water with tap water when the solution temperature is higher than desired temperature at the absorber inlet; else, the water-water heat exchanger is not used.

3.2.3 Cooling-water circuit

Cooling-water circuit consists of a 5 kW circulation heater (R2), a magnetic flow meter (F), a recirculation pump (B3), and a heat exchanger (HX1), a magnetic flow meter (F) and two temperature sensors Pt-100 (T). Heat released by the absorption process in the test section is removed by the cooling-water circuit. The circuit tubing is made of copper with an outer diameter of 2.82 cm.

Circulation heater (R2), which has the same characteristics and control system than the circulation heater (R1), is used to heat the cooling-water to the required temperature at the water-side test section inlet. Recirculation pump (B3), GRUNDFOS, model CR1, is made of stainless steel AISI 304. Heat exchanger (HX1) is a plate heat exchanger; model CB76, provided by Alfa Laval with twenty brazed plates and H-type corrugations. Cooling-water-side design allows setting the water flow in co-current or in counter-current configuration with respect to the solution flow.

3.2.4 Ammonia circuit

Ammonia circuit consists of a pressure regulator (PR), a mass flow controller (FC), an ammonia bottle, a needle valve (NVA) and a non-return valve. The pressure regulator (PR) allows controlling the ammonia pressure at the bottle outlet. Needle valve (NVA) and the

mass flow controller (FC), Aalborg, model GFC67, is used to obtain a better control of the ammonia vapor mass flow at the inlet of the test section. The non-return valve avoids that solution flows to the ammonia circuit. Ammonia vapor is injected in bubble mode at the bottom of the test section using a thin tube with an inner diameter of 1.7 mm.

3.3 Test Section

Two kinds of absorbers were set in the test section of the experimental test facility for the experimental study presented in this thesis. The first one is a plate bubble absorber and the second one is a tubular bubble absorber. Geometrical characteristics of each design and relevant details are presented below.

3.3.1 Plate bubble absorber

The plate bubble absorber is a plate heat exchanger (PHE) provided by Alfa Laval with four brazed plates, thus making three channels. Plates are made of stainless steel AISI 316 and have Chevron-H type corrugations with an angle of 30 degrees from the plate horizontal axis. Plates are brazed with nickel which allows the absorber operates up to a maximum working pressure of 21 bar. In the plate absorber, solution mixture and ammonia vapor flow upward in the central channel in co-current configuration and cooling-water flows downward in the two side channels in counter-current configuration. Major characteristics of the plate and absorber are shown in Figure 3.3 and Table 3.1, respectively. A picture of the plate absorber is shown in Figure 3.5a.

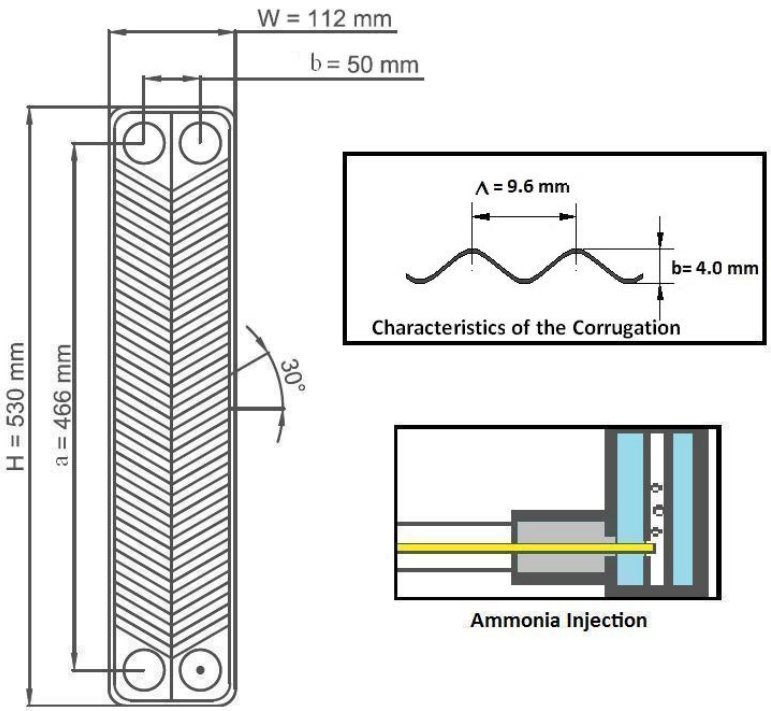

Figure 3.3 - Main characteristics of the plate absorber H-type.

Table 3.1 - Geometrical characteristics of the plate absorber H-type.

Plate Absorber	
Model	Type H, NB51
Absorbers Length, m	0.53
Absorber Width, m	0.112
Heat exchange area, m^2	0.1
Channel hydraulic diameter, m	0.004
Separation between plates, m	0.002
Plate thickness, m	0.0004
Diameter of ports, Int/Ext, m	0.018/0.025
Channel volume, lt	0.095

3.3.2 Tubular bubble absorber

The tubular bubble absorber is a vertical double pipe heat exchanger. The absorption process takes place in the inner tube. The outer tube of the tubular absorber is made of stainless steel. Two types of inner tubes were used for this study. One was made of stainless steel with an inner smooth surface and the other one is an advanced surface tube made of aluminum. The advanced surface tube has internal helical micro-fins measuring 0.3 mm in length and a helix angle of 20^o with respect to the vertical. Bubble absorber with the inner advanced surface tube of 1 meter was initially tested using two tube diameters (9.5 and 8.0 mm, OD). Advanced surface tube with a tube diameter of 9.5 mm was also tested using a bar inside with a diameter of 5.0 mm and the same length of the tube with the objective of reducing the passage area and increase the flow velocity. Additionally, bubble absorber with the inner advanced surface tube with an inner tube diameter 8.0 mm and three tube lengths (1, 2 and 3 meters in series, Figure 3.5b,c,d) were tested. The inner diameter (internal equivalent diameter) of the advanced surface tubes was measured at the fin tip diameter. In the tubular absorber, solution and ammonia vapor flow upward in the inner tube in co-current configuration and cooling-water flows downward in the annulus space in counter-current configuration. Major characteristics of the tubular absorber and advanced tubes are shown in Table 3.2 and Figure 3.4. A cross-section view of the advanced surface tube is also shown in Figure 3.5e.

Table 3.2 - Geometrical characteristics of the tubular absorber.

Tubular Absorber				
Advanced surface tube Manufacturer	HYDRO			
Absorber Length, m	1.0		2.0	3.0
Outer tube diameter, m	0,0150	0,0150	0,0150	0,0150
Inner tube diameter, m	0,0095	0,0080	0,0080	0,0080
Heat exchange area, m^2	0.0300	0,0250	0.0510	0.0760
Hydraulic diameter of the inner tube, m	0,0075	0,0060	0,0060	0,0060
Hydraulic diameter of annular space , m	0,0035	0,0050	0,0050	0,0050
Fin length, m	0.0003			

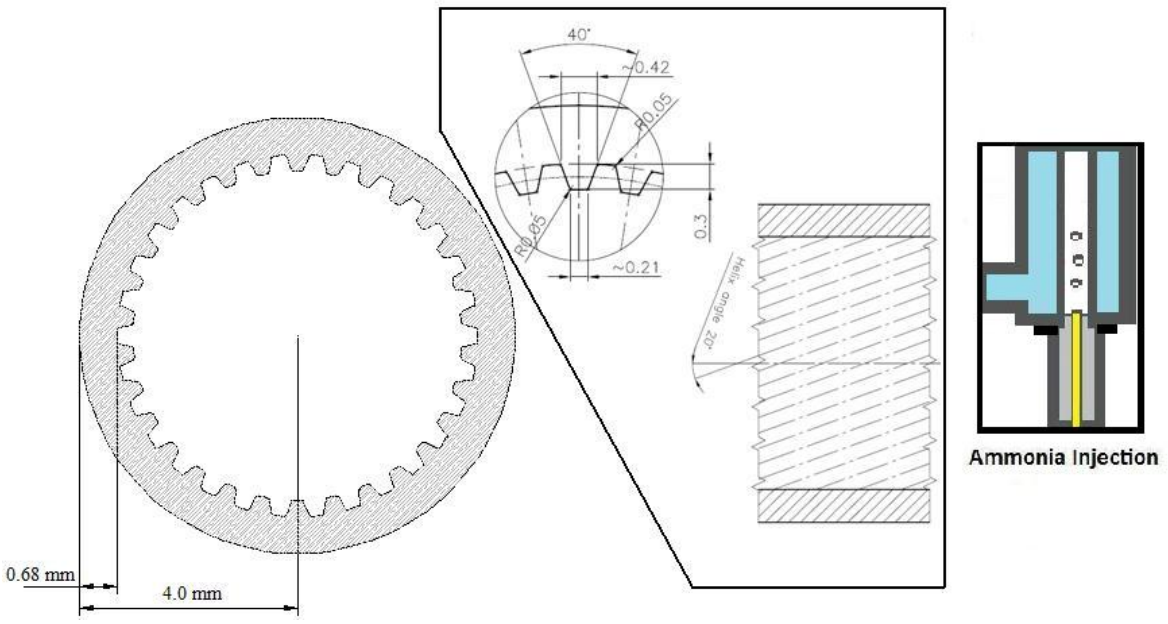

Figure 3.4 - Main characteristics of advanced surface tube of 8.0 mm.

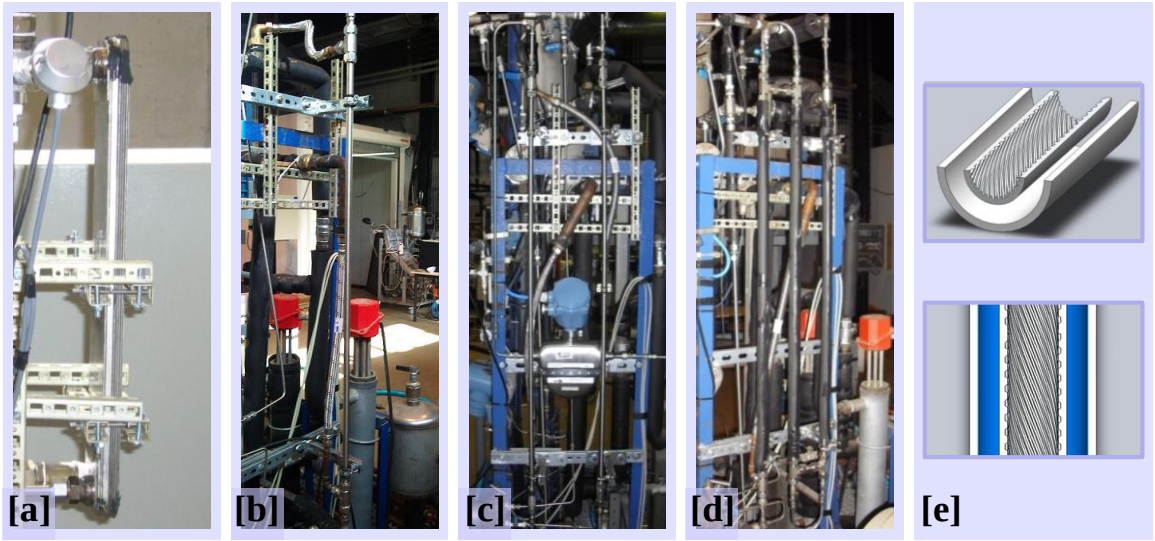

Figure 3.5 - [a] PHE, [b] 1m tubular absorber, [c] 2m tubular absorber, [d] 3m tubular absorber and [e] Cross-section view of the advanced surface tube.

3.4 Instrumentation and Control System

This section details the Instruments used (Figure 3.6) for the measurement and data acquisition of parameters such as mass and volumetric flows, temperatures, pressures, and solution densities of the NH_3/$LiNO_3$ mixture at the inlet and outlet of the test section.

3.4.1 Solution flow meters

Solution flow rates at the inlet and outlet of the test section were measured by Coriolis flow meters, Micro Motion Elite, model CMF025M and model CMF010M, respectively.

The first one, which has a flow rate operation range up to 2.18 $m^3.h^{-1}$, was connected to a transmitter Micro Motion 1700, while the second one, which has an operation range up to 0.108 $m^3.h^{-1}$, was connected to a transmitter Micro Motion RFT9739. Coriolis flow meters (C) were located in the test facility as shown in Figure 3.1. Coriolis flow meters with theses specifications are also capable of processing signals of density (up to 5000 $kg.m^{-3}$), temperature (measurements between -40 to 60 ^oC) of the fluid. The Coriolis have an accuracy of ± 0.1 % in mass/volume flow rate measurements and ± 0.5 $kg.m^{-3}$ in density measurements. Accuracy of the temperature sensor measurement is ± 0.2 ^oC taking as reference the temperature sensor at the outlet of the absorber.

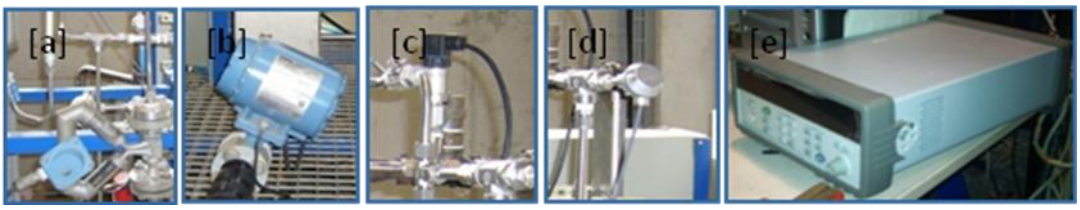

Figure 3.6 - [a] Solution flow meter, [b] water flow meter, [c] Pressure Transmitter, [d]Temperature sensor, and [e] Data logger.

3.4.2 Water flow meters

Water flows in the cooling and heating circuits were measured by magnetic flow meters, Emerson, model 8732C, with an accuracy of 0.0015 $m.s^{-1}$ ($2.4x10^{-4}$ $m^3.h^{-1}$) and capable of processing signals from fluids that are traveling between 0.01 to 10 $m.s^{-1}$ for both forward and reverse flow in all flow tube sizes. Orifice diameter of the flow meter is 7.6 mm.

3.4.3 Temperature sensors

Solution and cooling-water temperatures at the inlet and outlet of the test section were measured by RTD temperature sensors Pt 100, model CR-BNN, with four wires with an accuracy of ± 0.1 ^oC after calibration. Calibration of the RTD temperature sensors was performed in a thermostatic bath, Huber, model CC308, varying the bath temperature from 35 to 80 ^oC with respect to temperature measuring instrument, Testo, model 735, with a system accuracy of 0.05 °C**.** Correction factors obtained for the temperature sensors at the inlet and outlet of the test section were implemented in the data acquisition device

$$T_{Sol,in}[^oC] = 0.9977 \cdot T - 0.6898 \quad (3.1)$$

$$T_{Sol,out}[^oC] = 0.9998 \cdot T - 0.0443 \quad (3.2)$$

$$T_{Cw,in}[^oC] = 1.0001 \cdot T + 0.0013 \quad (3.3)$$

$$T_{Cw,out}[^{o}C] = 1.0032 \cdot T - 0.1546 \quad (3.4)$$

3.4.4 Pressure transmitters

Pressures in the solution circuit were measured by pressure transmitters, WIKA, model S-10, with an accuracy of 0.25 % of span. Pressure transmitters located at the inlet and outlet of the test section operate in a range between 0 and 4 bar (Relative). Additional pressure transmitters located in ST1 and Vapor-liquid separator operates in a range between 0 and 10 bar (Absolute).

3.4.5 Data acquisition

Data measured by the measuring instruments previously detailed were collected by a data logger, model Agilent 34970A. Data logger system includes 3-slot mainframe with built-in GPIB and RS-232 interface for simple connection to the PC. It accepts signals in dc volts or ac volts, sensor with 2- and 4-wire Ohms, dc current, ac current, frequency, and period. Additionally, data logger includes BenchLink Data Logger Software to configure and control tests, display results and collect data for further analysis. Figure 3.7 shows a screen of the BenchLink Data Logger Software during a data process acquisition.

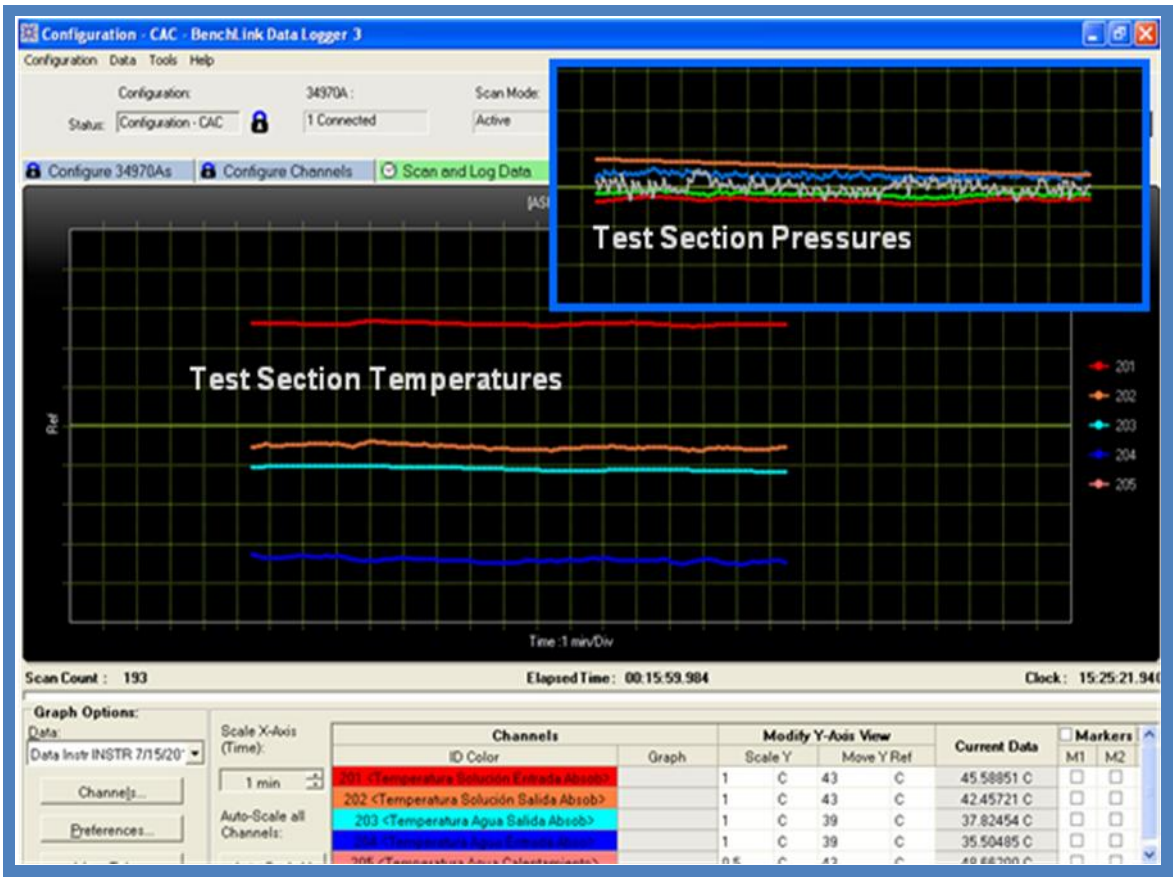

Figure 3.7 – Measuring and control of temperatures and pressures at the inlet and outlet of the test section.

3.5 Experimental Procedure

In this section, procedure to conduct the experimental study of the NH_3 absorption process in bubble absorbers is detailed.

3.5.1 Security measures

When working with NH_3 and $LiNO_3$, extreme caution must be taken in order to avoid injuries. Exposure to high concentrations of NH_3 and $LiNO_3$ can result in irritation of the nose and throat, burns in the skin and eyes, coughing, shortness of breath, difficult breathing and tightness in the chest, and in the worst cases, lung damage and death. Long-term damage may result from a severe short-term exposure.

In order to avoid high ammonia concentrations in the laboratory caused by a possible leak, an ammonia gas detector and a system of local exhaust was installed to keep exposures as low as possible. Local exhaust ventilation can control the emissions of the ammonia at its source, preventing dispersion of it into the general work area. Typical safety measures in a lab like the use of protective clothing, including boots, gloves, lab coat, apron or coveralls, eye chemical safety goggles were taken into account. A positive pressure full-face mask was also used when direct contact with the $NH_3/LiNO_3$ was required. An emergency shower and eyewash station was also installed near to the work area. A portable single gas detector (Micro IV) was also used.

3.5.2 Preparation of $NH_3/LiNO_3$ mixture

Once the circuits were cleaned and possible leaks were eliminated, storage tank 1 was filled with $NH_3/LiNO_3$ mixture. For this, 40 kg of $LiNO_3$ was firstly introduced through the top of storage tank 1, followed by a vacuum process through the solution circuit to remove the excess of air and humidity. Then, ammonia liquid was slowly introduced through the bottom of storage tank 1 until obtaining the desired solution concentration in ammonia. During ammonia injection, temperature and pressure in the storage tank increased because of the exothermic process that occurs from the absorption process. To avoid a high pressure and temperature in the tank, it was important to eventually stop the ammonia injection and cool the storage tank with city water until pressure decreased. Parallel, heating and cooling water circuits were filled with demineralized water and pressurized to 2 bar. Finally, measuring instruments were checked.

For the implementation of the carbon nanotubes (CNTs) into the $NH_3/LiNO_3$ mixture, solution in the storage tank 1 was sent to storage tank 2. Then, excess of ammonia in storage tank 1 was sent to the neutralization tank. Once storage tank was empty, the top of the storage tank was carefully opened, the inside of the tank was cleaned and the CNTs were introduced inside taking into account the required security measures. Top of the storage tank 1 was closed followed by a vacuum process. Finally, solution in storage tank 2 is pumped back to storage tank 1.

3.5.3 Test procedure

Procedure followed for the experimental data acquisition is described as follow:

To initiate experimentation all solution mixture must be accumulated in storage tank 1. Measuring equipments and data acquisition system are first turned on and checked. Next, pump of the heating circuit and pump B1 are turned on and then, solution is pumped at established flow rate through the sub-circuit shown in Figure 3.8 in order that solution concentration becomes homogeneous.

During the solution recirculation process, electric resistance at the bottom of the storage tank 1 is turned on and pressure of the solution is set through the PID controller to the desired initial condition. Solution concentration is periodically calculated by using the density and temperature values measured by the Coriolis flow meter (C) and correlations reported by Libotean et al. (2008). Depending on the solution concentration, more ammonia is injected from the ammonia bottle or extracted to the neutralization tank until obtaining the desired concentration. If solution concentration does not change during 20 minutes, next step can be followed. Previously to injection or extraction of ammonia, pump B1 is turned off.

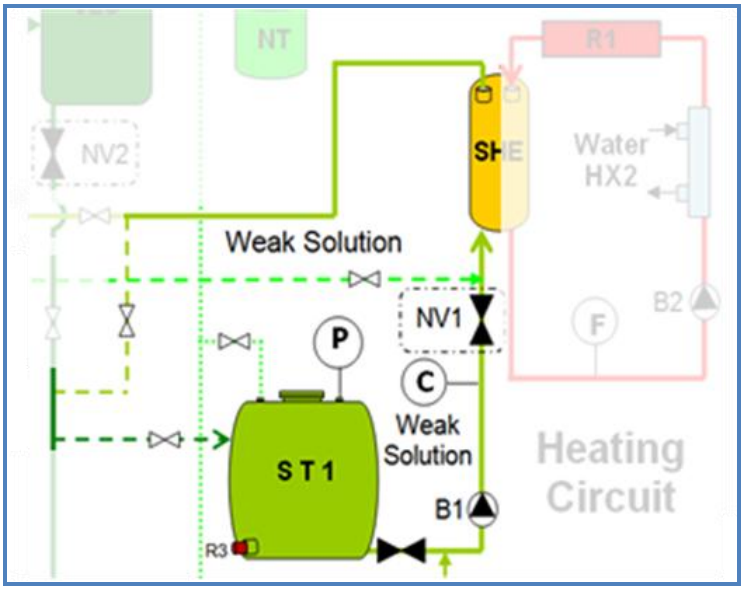

Figure 3.8 – Diagram of the sub-circuit for the homogenization of the solution.

Once initial conditions in the solution are obtained, valves are configured to send the solution to the test section and return it to the storage tank 1. Pump of the cooling water circuit is turned on and cooling water temperature and flow are established. Flow rates and temperatures at the inlet and outlet of the test section are monitored until achieve steady state. During the process to get steady state, pump B1 is turned off for a couple of seconds and pressure in the storage tank 2 is equated to the pressure in storage tank 1 by manipulating the valves that connect both tanks in the top. Equalizing pressure between the tanks facilitates the control of the solution flow during the absorption process

Once achieved stable conditions in flows and temperatures in the test section, experiments on the NH_3 absorption process can be started. For this, valves are configured to send the solution to storage tank 2. Next, pressure regulator is manipulated to inject the ammonia vapor through bottom of the test section. Ammonia vapor flow is controlled with the pressure regulator (PR) and a needle valve (NVA) located just before the inlet of the test section. When the ammonia vapor starts to be absorbed, monitored solution density at the outlet of the test section tends to gradually decrease until a point where solution density presents a sharp fall. Sharp fall in the monitored density value at the outlet of the absorber is due to the fact ammonia vapor is not been fully absorbed in the test section, and therefore there is ammonia vapor leaving the absorber. In this case, ammonia flow is reduced by using the needle valve until the density is reduced to a minimum value just before the sharp fall appears.

Finally, once temperatures, flows, pressures and densities reach steady state during the absorption, data acquisition can be started. During the data acquisition, solution flows and pressure tends to vary because of the pressure control by the PID and also due to the fact that solution circuit during absorption is discontinuous. According to this, success of each test depends on the skill of the user for controlling the solution flow and pressure to keep the steady state. Control of the solution flow and pressure is obtained by carefully manipulating valves NV1 and NV2, respectively. After data acquisition is completed, injection of ammonia is stopped. Depending on the amount of solution remaining in the storage tank 1, the next test can be immediately carried out or not. If there is still available solution in storage tank 1, next conditions of interest can be established and injection of the ammonia can be restarted when steady states in temperatures, flows, pressures are one more time obtained. If not, the electric resistance in the storage tank 1, pumps and heaters in the cooling and heating-water circuits are turned off. Then, solution in storage tank 2 is pumped back to storage tank 1 to start the experimental procedure from the beginning.

3.6 Data Reduction

In each experiment, once a steady-state regime was reached, measured data of the operating conditions such as temperatures, flow rates, pressures and densities at the outlet and inlet of the test section, were maintained and recorded each 5 seconds for around 15 minutes. After the data acquisition process, measured operating conditions are averaged. The parameters calculated from measured data and considered to assess the performance of the plate and tubular absorbers are defined below.

3.6.1 NH_3 absorption mass flux

The NH_3 absorption mass flux (F_{AB}), which quantifies the capacity of the system to absorb ammonia vapor from the evaporator, is defined as the absorbed ammonia mass flow rate per unit of heat transfer area.

$$F_{AB} = \frac{\dot{m}_{NH3,Absorbed}}{A_{Exchange}} \tag{3.5}$$

where $A_{Exchange}$ is the heat exchange area for each case study. In the case of the tubular absorber, heat transfer area was calculated by using the tube outer diameter. $\dot{m}_{NH3,absorbed}$ is calculated as follow.

$$\dot{m}_{NH3,Absorbed} = \dot{m}_{Sol,out} \cdot x_{Sol,out} - \dot{m}_{Sol,in} \cdot x_{in} \tag{3.6}$$

$$A_{Exchange\_PA} = 2 \cdot w \cdot L_{AB} \tag{3.7}$$

$$A_{Exchange\_TA} = \pi \cdot D_{outer} \cdot L_{AB} \tag{3.8}$$

w in Equation (3.7) refers to the width of the plate and D_{outer} in Equation (3.8) is the outer diameter of the inner tube.

3.6.2 Solution heat transfer coefficient

The absorber thermal load is determined from the measured data on the water-side which involves the cooling water flow rate and temperatures at the inlet and outlet of the test section. Since the absorbers tested were well covered with foam material for thermal insulation, there were no heat losses to surroundings.

$$Q_{AB} = \dot{m}_{Cw} \cdot Cp_{Cw} \cdot (T_{Cw,out} - T_{Cw,in}) \tag{3.9}$$

The overall heat transfer coefficient *U* is given by Equation (3.10).

$$U = \frac{Q_{AB}}{A_{Exchange} \cdot LMTD} \tag{3.10}$$

where *LMTD* is the standard definition of the logarithmic mean temperature difference involving solution and cooling-water temperatures at the inlet and outlet of the absorber in counter-current configuration.

$$LMTD = \frac{(T_{Sol,in} - T_{Cw,out}) - (T_{Sol,out} - T_{Cw,in})}{Ln\left(\frac{T_{Sol,in} - T_{Cw,out}}{T_{Sol,out} - T_{Cw,in}}\right)} \tag{3.11}$$

LMTD is not the most appropriate parameter to represent the temperature difference between solution and cooling flow currents because there is a heat generation during the absorption process. However, traditional heat exchanger analysis definition of LMTD has been used in this thesis to be consistent with current works found in literature on absorbers with different working fluids where it is the most commonly used (Kang et al., 1999a, Lee et al., 2002a, Park et al., 2003, Kwon and Jeong, 2004, Kim et al., 2012, Oronel et al., 2013, Suresh and Mani, 2013). Other definitions for the temperatures difference in an absorber have been proposed. For instance, Miller (1998) used the maximum temperature difference $(T_{Sol,Eq,in} - T_{Cw,in})$ in the absorber; however, this definition, which

takes into account the maximum absorption potential of the solution, does not include the outlet temperatures. Another definition is the LMTD based on inlet and outlet solution temperature in saturation state. This definition is only valid when the solution temperatures in the absorber are close to its saturation state. It is not the case for experiments conducted for this thesis since solution currents always presented a subcooling degree at the inlet and outlet of the absorber.

The solution heat transfer coefficient (h_{Sol}) for each case study is obtained from Equation (3.12) which is found based in the heat transfer resistances from the bulk solution to the cooling water side.

$$\frac{1}{U \cdot A_{Exchange}} = \frac{1}{h_{Sol} \cdot A_{Sol\_Side}} + R_{Wall} + \frac{1}{h_{Cw} \cdot A_{Cw\_Side}} \tag{3.12}$$

U is calculated as shown in Equation (3.10). R_{Wall} refers to the resistance of the wall which depends on the thickness and the thermal conductivity of the wall material between the fluids.

The cooling-water heat transfer coefficient (h_{Cw}) is calculated using Equation (3.13).

$$h_{Cw} = \frac{\mathrm{Nu}_{Cw} \cdot \lambda_{Cw}}{D_{h\_Cw}} \tag{3.13}$$

where λ_{Cw} refers to the thermal conductivity of the cooling water and Nu_{Cw} is the Nusselt number. Nusselt number in the plate absorber H-Type is obtained as detailed in Chapter 4 and the cooling-water Nusselt number in the tubular absorber was determined by using the Gnielinski´s correlation (Gnielinski, 1976) found in the Heat Exchanger Design Handbook (HEDH), (1983). This correlation has been proved valid for smooth tubes over a large Reynolds number interval ($0.5 \le Pr \le 2000$ and $3000 \le Re \le 5x10^6$) taking into account the transition region and also the entrance effects, Equation (3.14). In some experiments Reynolds numbers lower than 3000 were achieved, however, Gnielinski correlation was considered for use in those experiments to obtain a reasonable Nusselt number value taking into account the fact that Reynolds values were still in the transition region ($2300 \le Re \le 10^4$).

$$\mathrm{Nu}_{Cw\_TA} = \left[\frac{(f/8)\cdot(\mathrm{Re}-1000)\cdot \mathrm{Pr}}{1+12.7\cdot(f/8)^{0.5}\cdot(\mathrm{Pr}^{2/3}-1)} \right] \cdot \left[1+\left(\frac{D_{h\_annular}}{L} \right)^{2/3} \right] \tag{3.14}$$

f in Equation (3.14) is the friction factor taken from the correlation found in the book published by Bergman et al. (2011) and developed by Petukhov (1970) for the interval $3000 \le Re \le 5x10^6$, (Equation 3.15).

$$f = \frac{1}{(0.79 \cdot Ln(\mathrm{Re}) - 1.64)^2} \tag{3.15}$$

Investigations on heat transfer in concentric annular spaces have showed that heat transfer coefficients are also dependent on the ratio of diameters D_{outer} and $D_{inner,o}$. For that, Petukhov and Royzen (1964) recommended multiplying the Nusselt correlation by a correction factor for flows in annular spaces. Equation (3.16) is used in cases of heat transfer at the inner wall and outer tube wall insulated.

$$C = 0.86 \cdot \left(\frac{D_{outer}}{D_{inner,o}} \right)^{-0.16} \tag{3.16}$$

Recently, correlation used for heat transfer in turbulent flows in concentric annular spaces reported by Gnielinski (1976) has been extended by Gnielinski (2009).

Reynolds number Re in both solution and cooling water channels is calculated as in its more common definition.

$$\mathrm{Re} = \frac{vel \cdot \rho \cdot D_h}{\mu} \tag{3.17}$$

Hydraulic diameters in the plate absorber were obtained using Equation (3.18) while for the tubular absorber Equations (3.19) and (3.20) were used.

$$D_h = \frac{4 \cdot w \cdot s}{2 \cdot (w + s)} \tag{3.18}$$

$$D_{h\_inner} = D_{inner} \tag{3.19}$$

$$D_{h\_annular} = D_{inner,o} - D_{outer} \tag{3.20}$$

D_{inner} is the inner diameter of the tube where the absorption process takes place and $D_{inner,o}$ is the inner diameter of the external tube. Inner diameter of the advanced surface tubes was measured at the fin tip diameter.

3.6.3 Solution mass transfer coefficient

The overall mass transfer coefficient was obtained as follows:

$$K_m = \frac{\dot{m}_{NH3,Absorbed}}{A_{Exchange} \cdot LMXD} \tag{3.21}$$

The logarithmic mean concentration difference (*LMXD*) expresses the nominal log-mean concentration difference along the absorber channel.

$$LMXD = \frac{(x_{Sol,Eq} \cdot \rho_{Sol,Eq} - x_{Sol} \cdot \rho_{Sol})_{in} - (x_{Sol,Eq} \cdot \rho_{Sol,Eq} - x_{Sol} \cdot \rho_{Sol})_{out}}{Ln\left(\frac{(x_{Sol,Eq} \cdot \rho_{Sol,Eq} - x_{Sol} \cdot \rho_{Sol})_{in}}{(x_{Sol,Eq} \cdot \rho_{Sol,Eq} - x_{Sol} \cdot \rho_{Sol})_{out}} \right)} \tag{3.22}$$

$x_{Sol,Eq}$ and $x_{Sol,Eq}$ refer to concentration and density at equilibrium conditions. Equilibrium concentrations in Equation (3.22) were calculated from measured temperature and pressure values, using the correlations reported by Libotean et al. (2007). Equilibrium densities were calculated from measured temperature and equilibrium concentration values, using the correlations reported by Libotean et al. (2008).

In order to correlate the overall mass transfer coefficient in terms of a dimensionless number, experimental Sherwood number was obtained using Equation (3.23). The

correlation used in calculating the solution diffusivity coefficient was that reported by Infante Ferreira (1985).

$$\mathrm{Sh}_{Sol,Exp} = \frac{K_m \cdot D_h}{\beta_{Sol}} \tag{3.23}$$

3.6.4 Subcooling degree

Finally, the degree of subcooling of the solution at the absorber outlet (ΔT_{Sub}) indicates the degree of the available absorption potential.

$$\Delta T_{Sub} = (T_{Sol,Eq,out} - T_{Sol,out}) \tag{3.24}$$

$T_{Sol,Eq,Out}$ is the equilibrium solution temperature at the absorber pressure and actual concentration of the outlet solution. Solution concentrations in ammonia at the absorber inlet and outlet were determined from the density and temperature values measured by Coriolis flow meters using the density correlation reported by Libotean et al. (2008).

3.7 Uncertainty Calculation Method

Uncertainties propagation of calculated parameters were obtained by using the method proposed in the Technical Note 1297 of the National Institute of Standards and Technology Technical, NIST, and implemented in the EES software (Taylor and Kuyatt, 1994). This method takes into account the uncertainties in each of the measured variables (temperatures, flow rates, densities, pressures) to quantify their propagations into the values of the calculated parameters. For instance: Assuming the individual measurements are uncorrelated and random, the uncertainty in the calculated quantity can be determined as:

$$U_Y^2 = \sum_{i=1}^{n} \left(\frac{\partial Y}{\partial x_i} \right)^2 \cdot U_{X_i}^2 \tag{3.25}$$

$$Y = f(x_1, x_2, x_3, \ldots x_n) \tag{3.26}$$

where U_Y represents the uncertainty of the calculated parameter *Y* and U_X represents the uncertainty of the measured variable *x* (Table 3.3).

Table 3.3 - Summary of uncertainty of the measured variables.

Instrument	Variable	Accuracy
Coriolis flow meters	Temperature	± 0.2 °C
	Density	± 0.5 kg.m^{-3}
	Solution flow	± 0.1 %
RTD sensors Pt 100	Temperature	± 0.1 °C
Magnetic flow meters	Water flow	2.4x10^{-4} m^3.h^{-1}
Pressure transmitter	Pressure	0.25 %

Chapter 4

Experimental Study of the NH_3 Absorption Process

4.1 Introduction

This chapter presents an experimental study on intensification of the NH_3 absorption process in vertical bubble mode absorbers with the $NH_3/LiNO_3$.mixture.

Initially, main results from a thermodynamic simulation of a single stage absorption refrigeration cycle with $NH_3/LiNO_3$ are summarized and operating conditions for the experiments in the absorbers under study are defined.

Then, experimental results from the different proposal for the intensification of the NH_3 absorption process are reported. Experimental results involve the analysis of parameters such as NH_3 absorption mass flux, absorber thermal load, solution heat transfer coefficient, solution mass transfer coefficient and degree of subcooling at the absorber outlet.

Intensification of the NH_3 absorption process is studied using two types of bubble absorbers. Firstly, results from the absorption process in a plate heat exchanger with Chevron H-type corrugations (with an angle of 30 degree from its horizontal axis) are shown and correlated. Then, main results using the plate absorber H-type are compared with results found in the literature with a plate absorber with Chevron L-type corrugations (with an angle of 60 degree from its horizontal axis).

Secondly, results from the absorption process in a tubular heat exchanger with smooth and advanced surfaces are analyzed. Results using the advanced surface tube with different tube diameters and lengths are also reported.

Finally, results from the absorption process in a tubular heat exchanger with smooth surface and the $NH_3/LiNO_3$ mixture with nanoparticles are shown. Additionally, experiments from using simultaneously the advanced surface tube and nanoparticles are presented.

4.2 Simulation of the Absorption Refrigeration Cycle with $NH_3/LiNO_3$

Thermodynamic simulation of a single stage absorption refrigeration cycle with $NH_3/LiNO_3$ was performed in order to obtain an approach of the operating conditions of a real system. Operating conditions in the absorber are used as inlet conditions in the bubble absorbers under study in this chapter. Figure 4.1 shows a diagram of the cycle simulated. Thermodynamic cycle simulation is based on energy and mass balances on each one of the components shown in Figure 4.1. Detailed description and balances of the thermodynamic cycle model is presented in Appendix A. Equilibrium and transport properties of the $NH_3/LiNO_3$ mixture used for this study were those measured, correlated and reported by Libotean et al. (2007, 2008). Equations of state for calculating the thermodynamic properties for ammonia were those developed by Tillner-Roth et al. (1993) and implemented in the software Engineering Equations Solver (EES). Summary of correlations to determine the properties of the $NH_3/LiNO_3$ mixture are presented in Appendix B.

Software used for the simulation of the thermodynamic cycle was the Engineering Equation Solver (EES). EES is a general equation-solving program that can numerically

solve thousands of coupled non-linear algebraic and differential equations in any order. EES best characteristic is its high accuracy and thermodynamic and transport property database that is provided for hundreds of substances. Additionally, thermodynamic and transport properties of new substances can be easily integrated.

4.2.1 Assumptions for simulation of the absorption cycle

Some assumptions are usually considered for simulation of absorption cycles. Main assumptions are summarized below.

- System operates in steady state.
- Strong and weak solutions leaving the absorber and generator, respectively, are in saturated state.
- Ammonia vapor leaving the generator is in saturated state. Vapor is in equilibrium with the weak solution.
- Ammonia liquid leaving the condenser is in saturated state.
- Isenthalpic processes in the expansion valves.
- There are no heat loss or heat gain in the components and pipes from and to surroundings.
- There are not pressure drops in components and pipes.

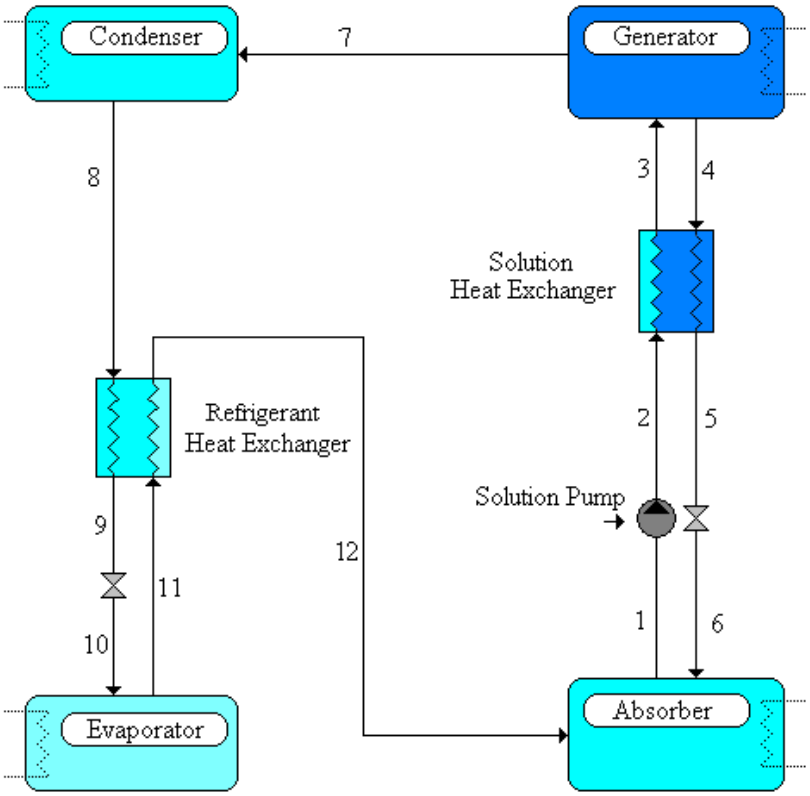

Figure 4.1 - Diagram of a single stage absorption refrigeration cycle with $NH_3/LiNO_3$.

4.2.2 Results from Simulation

Main results from the thermodynamic simulation of the absorption refrigeration cycle with $NH_3/LiNO_3$ are shown in Figure 4.2. A complete sensitivity analysis of the absorption refrigeration cycle with $NH_3/LiNO_3$ was previously detailed by Oronel (2010). Input data for the cycle simulation are summarized as follows:

- An evaporator with cooling capacity of 10 kW.
- A solution pump with an isentropic efficiency of 0.7.
- A solution heat exchanger with a thermal efficiency of 0.9.
- A refrigerant heat exchanger with a thermal efficiency of 0.7.
- Evaporation, absorption, condensation and generation temperatures were set as shown in Figure 4.2.

Figure 4.2 shows the coefficient of performance (COP) of the cycle as a function of the generation, evaporation, absorption, condensation temperatures and solution heat exchanger efficiency. Figure 4.2a illustrates the effect of the heat rejection temperature (absorption, condensation) on the COP at an evaporation temperature of 5 °C.

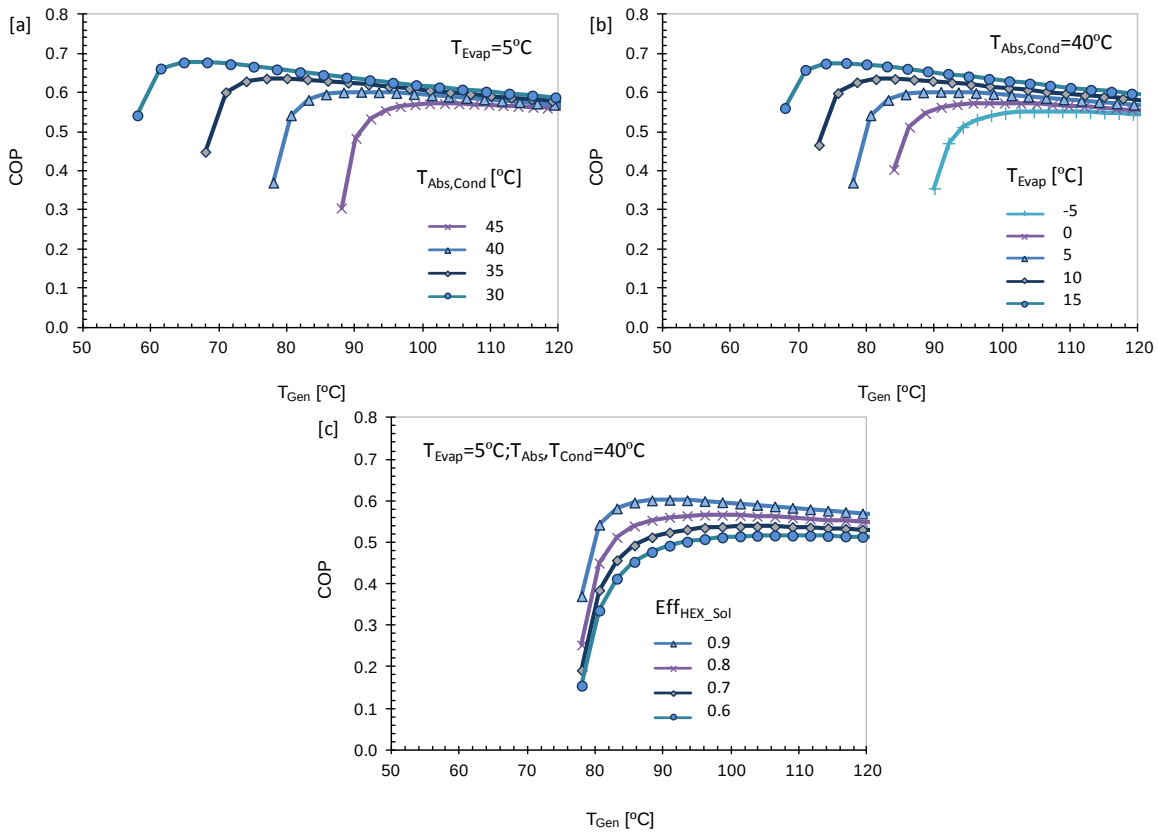

Figure 4.2 - Effect of generation, evaporation and absorption/condensation temperatures and solution heat exchanger efficiency on the absorption system COP with $NH_3/LiNO_3$.

In Figure 4.2a can be noted that maximum COP values of 0.68, 0.64, 0.60 and 0.57 were obtained at vapor generation temperatures of 68, 80, 90 and 103 °C, for a heat rejection temperature of 30, 35, 40, 45 °C, respectively. Given generation temperatures are close to

the minimum vapor generation temperatures to run the cycle at the conditions shown in Figure 4.2a. It is observed, therefore, that when decreasing the heat rejection temperature, a lower minimum generation temperature to run the cycle is needed and a higher COP is achieved. However, low heat rejection temperatures imply the use of wet cooling towers with well know problems as legionella.

Figure 4.2b shows the effect of evaporation temperature on the COP at a heat rejection temperature of 40 °C. Figure 4.2a shows that maximum COP values of 0.68, 0.64, 0.60, 0.57 and 0.55 were obtained at generation temperatures of 77, 84, 90, 98 and 106 °C, for an evaporation temperature of 15, 10, 5, 0 and -5 °C, respectively. According to Figure 4.2b, when low evaporation temperatures are set, higher generation temperatures and heat flux in the generator are required, and therefore COP of the cycle is reduced. Moreover, Figure 4.2c shows the effect of the solution heat exchanger efficiency on the COP at a heat rejection temperature of 40 °C and at an evaporation temperature of 5 °C. In Figure 4.2c can be observed that that maximum COP values of 0.60, 0.56, 0.53 and 0.51 were achieved at generation temperatures of 90, 96, 103 and 109 °C, for solution heat exchanger efficiencies of 0,9, 0,8, 0,7 and 0,6, respectively. Results in Figure 4.2c show that a solution heat exchanger with low efficiency affects negatively the COP of the cycle due the fact that higher heat fluxes in the generator are required.

Due to the interest in the design of air-cooled absorbers to avoid the use of wet cooling towers for the heat dissipation, inlet operating conditions for the experimental study shown in the next sections are those operating conditions of the absorber (Figure 4.3) resulting from thermodynamic simulation of the absorption refrigeration cycle with $NH_3/LiNO_3$ at absorption/condensation, evaporation and generation temperatures of 40 °C, 5 °C and 90 °C, respectively. In addition, the fact that the cycle can be activated at a generation temperature of 90 °C, make the absorption refrigeration system with $NH_3/LiNO_3$ suitable to operate with low temperature heat sources such as solar energy (flat solar collectors) or waste heat.

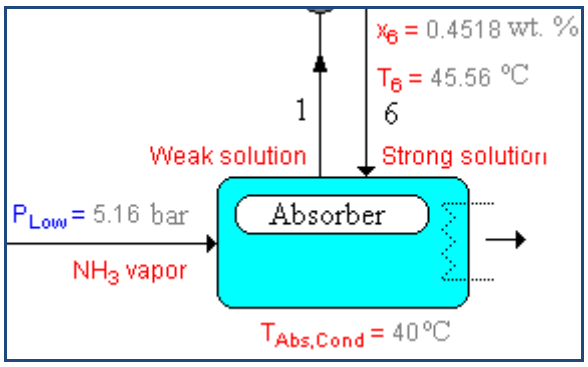

Figure 4.3 - Absorber inlet conditions from the thermodynamic simulation.

4.3 Experimental Results

In this section, experimental results on intensification of the NH_3 absorption process are reported. Experimental results involve the analysis of parameters (previously described in Chapter 3) such as overall NH_3 absorption mass flux, absorber thermal load,

solution heat transfer coefficient, solution mass transfer coefficient and degree of subcooling at the absorber outlet. Intensification of the NH_3 absorption process is studied using two types of bubble absorbers. Firstly, results from the absorption process in plate heat exchangers are shown. Secondly, results from the absorption process in tubular heat exchangers with smooth and advanced surfaces are analyzed. Finally, results from the absorption process in a tubular heat exchanger with smooth surface and the $NH_3/LiNO_3$ mixture with nanoparticles are shown and additionally, experiments from using simultaneously the advanced surface tube and nanoparticles are presented. Detailed descriptions of the bubble absorbers are presented in Chapter 3. Equilibrium and transport properties of the $NH_3/LiNO_3$ mixture used were those reported by Libotean et al. (2007, 2008). To determine the thermal conductivity of the $NH_3/LiNO_3$, correlation reported by Cuenca et al. (2013a) was used.

4.3.1 NH_3 absorption process in a plate absorber H-type

In this sub-section, experimental results of the heat and mass transfer processes in a plate bubble absorber with Chevron H-type corrugations (angle with 30 degree from its horizontal axis) are shown and correlated. Effects of parameters such as solution mass flow, cooling-water flow and cooling-water temperature on the absorber performance are analyzed. Then, main results using the plate absorber H-type are compared with results found in the literature with a plate absorber with Chevron L-type corrugations (with angle of 60 degree from its horizontal axis). In appendix C can be found all data of tests performed.

4.3.1.1 Experimental results water/ water

Preliminary experiments were performed using water in both cold and hot side of the plate bubble absorber H-type in order to determine and correlate the water-side Nusselt number (Nu_{Cw}) at the conditions of interest.

Heat transferred in the plate absorber is obtained by averaging the values of heat exchanged in both hot *(Q_H)* and cold side *(Q_C).*

$$Q_H = \dot{m}_H \cdot Cp_H \cdot (T_{H,in} - T_{H,out}) \tag{4.1}$$

$$Q_C = \dot{m}_C \cdot Cp_C \cdot (T_{C,out} - T_{C,in}) \tag{4.2}$$

$$Q_m = \frac{Q_H + Q_C}{2} \tag{4.3}$$

Once the heat transferred is determined, the experimental overall heat transfer coefficient can be obtained from Equation (4.4).

$$U_{Exp} = \frac{Q_m}{A_{Exchange} \cdot LMTD} \tag{4.4}$$

where $A_{Exchange}$ is the total heat transfer area and *LMTD* is the logarithmic mean temperature difference involving hot and cold side temperatures at the inlet and outlet of the plate absorber.

$$LMTD = \frac{(T_{H,in} - T_{C,out}) - (T_{H,out} - T_{C,in})}{Ln\left(\frac{T_{H,in} - T_{C,out}}{T_{H,out} - T_{C,in}}\right)} \tag{4.5}$$

The experimental overall heat transfer coefficient obtained by Equation (4.4) is compared against the overall heat transfer coefficient calculated from heat transfer resistances relationship given by Equation (4.6), Figure 4.4a.

$$\frac{1}{U} = \frac{1}{h_H} + \frac{e}{\lambda_{Steel}} + \frac{1}{h_C} \tag{4.6}$$

Nusselt numbers were correlated in function of the Reynolds and Prandtl numbers as shown in Equation (4.7), by minimizing the mean square error (*MSE*) between the two overall heat transfer coefficients, Equation (4.8).

Figure 4.4b shows the calculated water Nusselt number (Nu_{Cw}) from the experimental study water/water using Equation (4.7). Inlet temperatures were varied between 30 and 60 ^{o}C and the water mass flows between 50 and 352 kg.h^{-1}. The correlation is valid for a turbulent regime (Re: 400-1400).

$$\mathrm{Nu}_{Cw} = 0.858 \cdot \mathrm{Re}^{0.555} \cdot \mathrm{Pr}^{1/3} \tag{4.7}$$

$$MSE = \sqrt{\sum (U_{Exp} - U)^2} \tag{4.8}$$

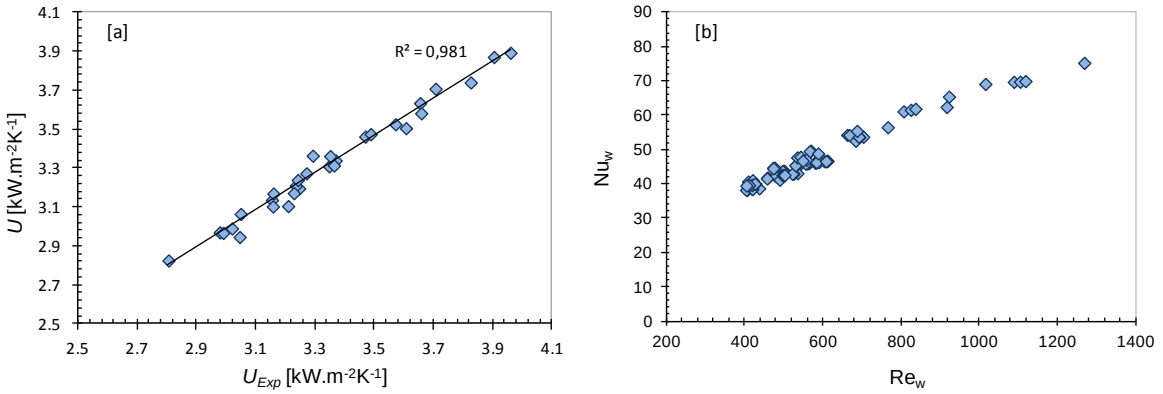

Figure 4.4 – [a] Theoretical overall heat transfer coefficient vs. Experimental overall heat transfer coefficient and [b]Nusselt number as a function of the Reynolds number.

4.3.1.2 Operating conditions

Operating conditions of interest to perform the experimental study of the NH_3 absorption process in the plate absorber were obtained from the thermodynamic simulation of the absorption refrigeration cycle with $NH_3/LiNO_3$ at absorption/condensation, evaporation and generation temperatures of 40 ^{o}C, 5 ^{o}C and 90 ^{o}C, respectively, as shown in sub-section 4.2.2.

Table 4.1 - Experimental operating conditions.

Parameters	Range
Solution temperature at the absorber inlet, °C	45
Cooling-water temperature at the absorber inlet, °C	35 and 40
Ammonia mass fraction in the solution at the absorber inlet, $kg_{NH3}.kg^{-1}_{NH3/LiNO3}$	0.45
Absorber pressure, kPa	510
Solution mass flow rate, $kg.h^{-1}$	10-50
Cooling-water flow rate in the plate absorber, $m^3.h^{-1}$	0.130-0.450

4.3.1.3 Effect of the solution flow and cooling-water temperature on the absorber performance

Results of a sensitivity study carried out to assess the effect of the solution flow rate and cooling-water temperature on the absorber performance are shown in this sub-section. Cooling-water flow rate was set around 0.267 $m^3.h^{-1}$ (Re_{cw}≈1060).

Figure 4.5 shows the ammonia absorption mass flux as a function of the solution Reynolds number and cooling-water temperature, respectively. In this figure can be observed that when the solution Reynolds number is increased from 11 to 40 at a cooling-water temperature of 40 °C at the absorber inlet, absorption mass flux increases from 0.0021 to a maximum of 0.0038 $kg.m^{-2}s^{-1}$ while for solution Reynolds numbers higher than 40, absorption mass flux tends to decrease slightly.

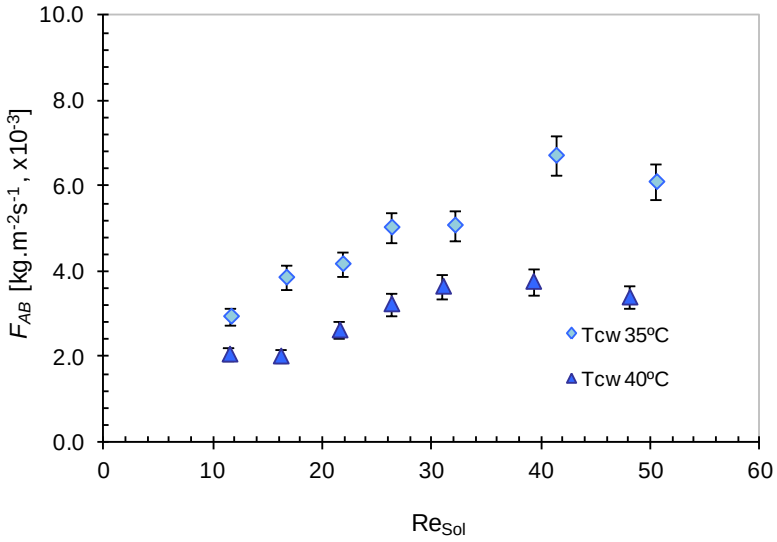

Figure 4.5 - Effect of the solution flow rate and cooling-water temperature on NH_3 absorption mass flux.

A similar trend is obtained when the cooling-water temperature is set to 35 °C, however, absorption mass flux values are significantly higher than those at a cooling-water temperature of 40 °C ranging from 0.0029 to a maximum of 0.0067 $kg.m^{-2}s^{-1}$. Therefore, absorption mass flux values at a cooling-water temperature of 35 °C are around 1.38 and 1.78 times higher than values at 40 °C. On the other hand, Figure 4.6 illustrates the absorber thermal load as a function of the solution Reynolds number and cooling-water

temperature, respectively. It can be observed that thermal load values significantly increase from 3.4 to 7.6 kW.m^{-2} and from 4.8 to 13.1 kW.m^{-2} at cooling-water temperatures of 40 and 35 ºC, respectively, when the solution Reynolds number is varied from 11 to approximately 50. It represents increments in the thermal load at a cooling-water temperature of 35 ºC around 1.45 and 1.71 times higher than values at 40 ºC.

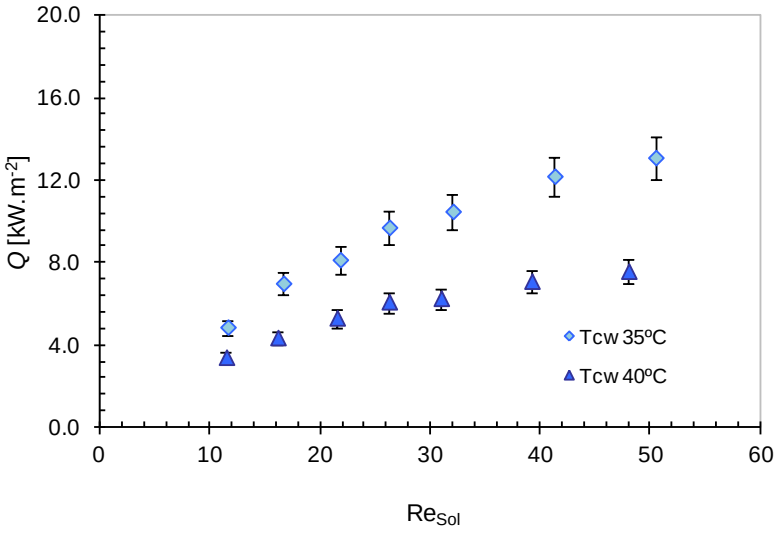

Figure 4.6 - Effect of the solution flow rate and cooling-water temperature on absorber thermal load.

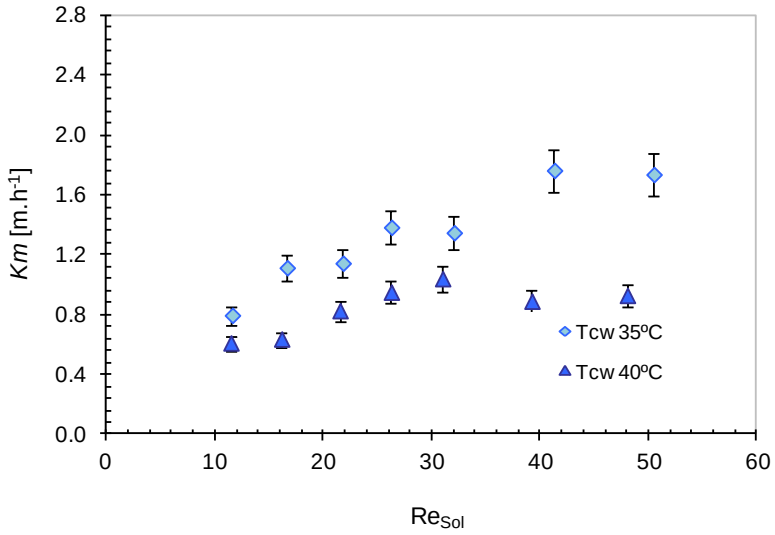

Figure 4.7 - Effect of the solution flow rate and cooling-water temperature on solution mass transfer coefficient.

Increment of the solution mass flow affects positively the heat and mass transfer in the corrugated plate absorber due to an increase in the turbulence of the solution flow which improves the mixing between the solution and the ammonia vapour. In addition, improvement in the absorption mass flux as the cooling-water inlet temperature decreases is attributed to an increase in the absorption potential by cooling much more the solution. Dissipating the heat released from the absorption process and cooling the

solution allow extending the difference between the actual and equilibrium states at the conditions under study, and therefore the solution is able to absorb much more ammonia.

Figure 4.7 illustrates the solution mass transfer coefficient as a function of the solution Reynolds number and cooling-water temperature, respectively. As could be expected, the solution mass transfer coefficient follows a trend similar to the absorption mass flux. When the solution Reynolds number is varied from 11 to 50, solution mass transfer coefficient increases from 0.6 to 0.9 $m.h^{-1}$ at an inlet cooling-water temperature of 40 ^oC and from 0.8 to 1.7 $m.h^{-1}$ at an inlet cooling-water temperature of 35 ^oC. Consequently, results in Figure 4.8 show that concentration difference values obtained at a cooling-water temperature of 35 ^oC are wider than at a cooling-water temperature of 40 ^oC. However, when increasing solution mass flow, concentration difference decreases because ammonia absorbed is not proportional to the solution flow increment. Concentration difference values range between 0.044 and 0.020 $kg_{NH3}.kg^{-1}_{NH3/LiNO3}$ and between 0.029 and 0.011 $kg_{NH3}.kg^{-1}_{NH3/LiNO3}$ at inlet cooling-water temperatures of 35 ^oC and 40 ^oC, respectively.

Moreover, Figure 4.9 presents the solution heat transfer coefficient as a function of the solution Reynolds number and cooling-water temperature, respectively. It is observed that at the conditions under study, reducing the cooling-water temperature has an opposite effect on the solution heat transfer coefficient in comparison with results of the mass transfer coefficient. This effect of the cooling-water temperature on the heat transfer coefficient is caused by a higher increase in the logarithmic mean temperature difference (LMTD) (Figure 4.10) than in the absorber thermal load. Figure 4.9 shows that solution heat transfer coefficients increase from 1.9 to 3.1 $kW.m^{-2}.K^{-1}$ and from 1.9 to 4 $kW.m^{-2}.K^{-1}$ for cooling-water temperatures of 35 and 40 ^oC, respectively. Furthermore, LMTD increases from 3.2 to 5.8 ^oC at a cooling-water temperature of 35 ^oC while at a cooling-water temperature of 40 ^oC, LMTD presents a very slight increment which values vary from 2.2 to 2.8 ^oC.

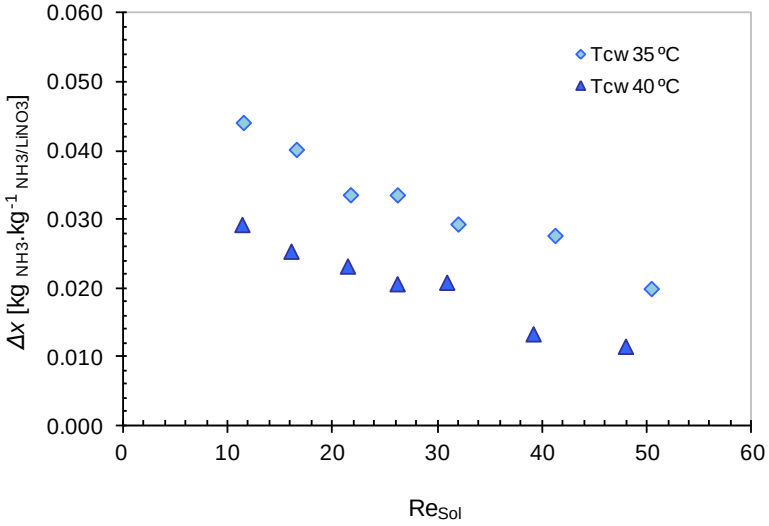

Figure 4.8 - Effect of the solution flow rate and cooling-water temperature on concentration difference.

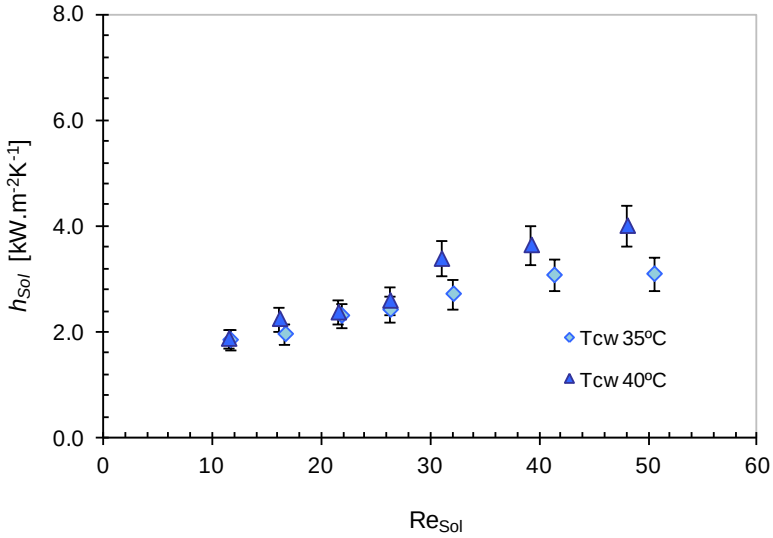

Figure 4.9 - Effect of the solution flow rate and cooling-water temperature on solution heat transfer coefficient.

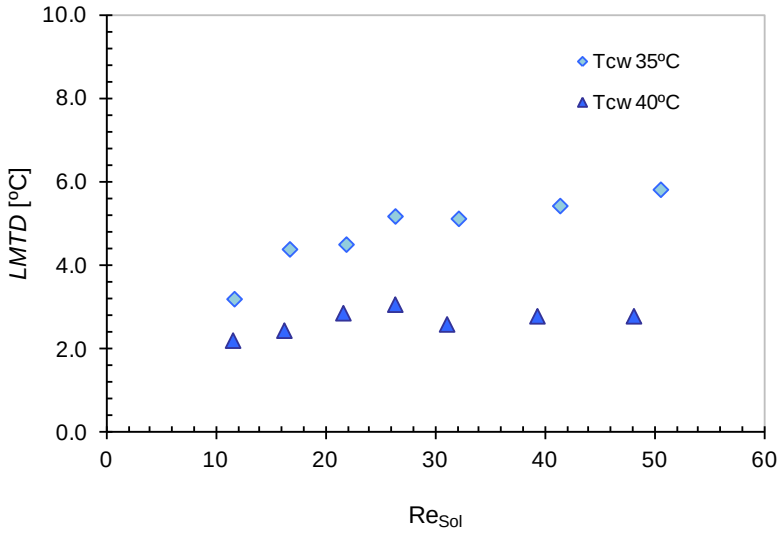

Figure 4.10 - Effect of the solution flow rate and cooling-water temperature on LMTD.

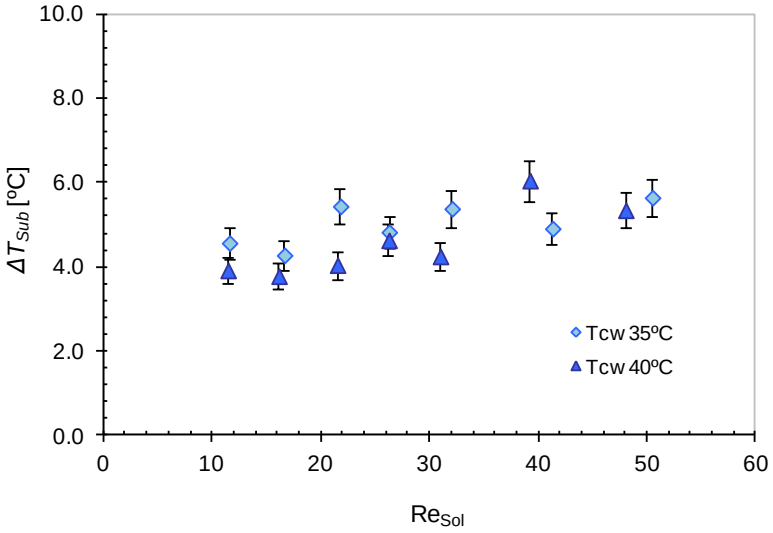

Figure 4.11 - Effect of the solution flow rate and cooling-water temperature on subcooling at the absorber outlet.

Regarding the degree of subcooling of the solution at the outlet of the absorber, results in Figure 4.11 depicts that solution mass flow and cooling-water temperature have a rather small effect on the degree of subcooling which slightly increases when increasing the solution mass flow and when cooling-water temperature is reduced. Results for both cooling-water temperatures are between 3.7 and 6 °C, which means solution flow at the outlet of the absorber was near to its saturations conditions and thus, close to its maximum absorption potential at the conditions under study.

4.3.1.4 Effect of the cooling-water flow on the absorber performance

Results of the effect of the cooling-water flow rate and cooling-water temperature on the absorber performance are shown in this sub-section. In this case, solution flow rate was set to 40 $kg.h^{-1}$.

Initially, Figure 4.12 shows the ammonia absorption mass flux as a function of the cooling-water Reynolds number and cooling-water temperature. Results presented in this figure indicates that at the conditions studied in this sub-section, ammonia absorption mass flux is improved by increasing the cooling-water flow and as shown in the last sub-section, by decreasing cooling-water temperature. However, improvements obtained by increasing the cooling-water flow rate are not as significant as improvements achieved with the solutions flow rate. Figure 4.12 shows that when varying the cooling-water Reynolds number from 550 to 1510, ammonia absorption mass flux increases from 0.0056 to 0.0066 $kg.m^{-2}s^{-1}$ at an inlet cooling-water temperature of 35 °C and from 0.0034 to 0.0044 $kg.m^{-2}s^{-1}$ at an inlet cooling-water temperature of 40 °C. According to results in Figure 4.12, absorption mass flux values at a cooling-water temperature of 35 °C are around 1.50 times higher than values at 40 °C. Similarly, Figure 4.13 shows that thermal load in the absorber slightly increases from 6.0 to 8.0 $kW.m^{-2}$ and from 10.3 to 12.87 $kW.m^{-2}$ at cooling-water temperatures of 40 and 35 °C, respectively. It gives an increment in the thermal load at a cooling-water temperature of 35 °C around 1.65 times higher than thermal load values at 40 °C.

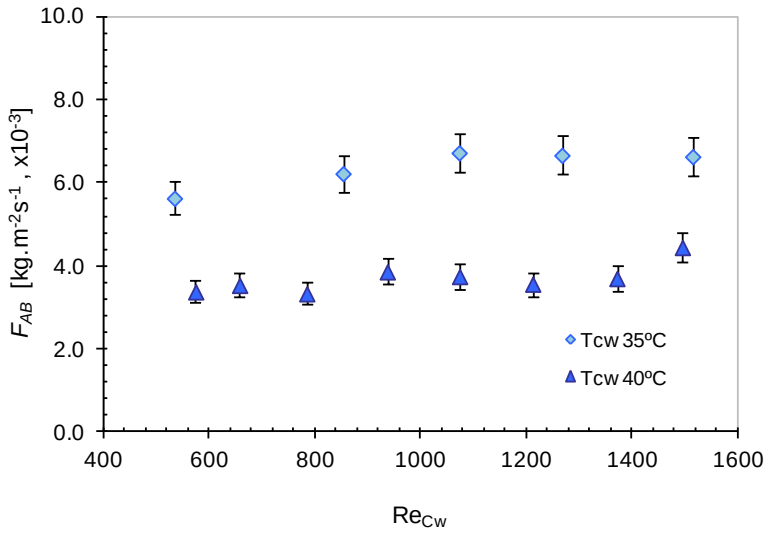

Figure 4.12 - Effect of the cooling-water flow rate and cooling-water temperature on NH_3 absorption mass flux.

Slight effect of the cooling-water flow at the conditions under study on the heat and mass transfer is due to the fact that flows established in the cooling-water are in fully developed regime. Once achieved a fully developed regime, increment in the cooling-water flow seems not to have remarkable effect on the absorption mass flux and thermal load and global heat transfer coefficient is determined by the solution heat transfer coefficient.

In consequence, Figure 4.14 shows that improvement in the solution mass transfer coefficient when increasing the cooling-water flow is also moderated. Mass transfer coefficient mildly increase from 1.4 to 1.7 $m.h^{-1}$ and from 0.9 to 1.1 $m.h^{-1}$ at cooling-water temperatures of 35 ^oC and 40 ^oC, respectively. Mass transfer coefficient values at a cooling-water temperature of 35 ^oC are 1.55 times higher than values at 40 ^oC. In addition, concentration difference shows a relatively low increase ranging from 0.023 to 0.028 $kg_{NH3}.kg^{-1}_{NH3/LiNO3}$ and from 0.013 to 0.018 $kg_{NH3}.kg^{-1}_{NH3/LiNO3}$ at cooling-water temperatures of 35 ^oC and 40 ^oC, respectively (Figure 4.15).

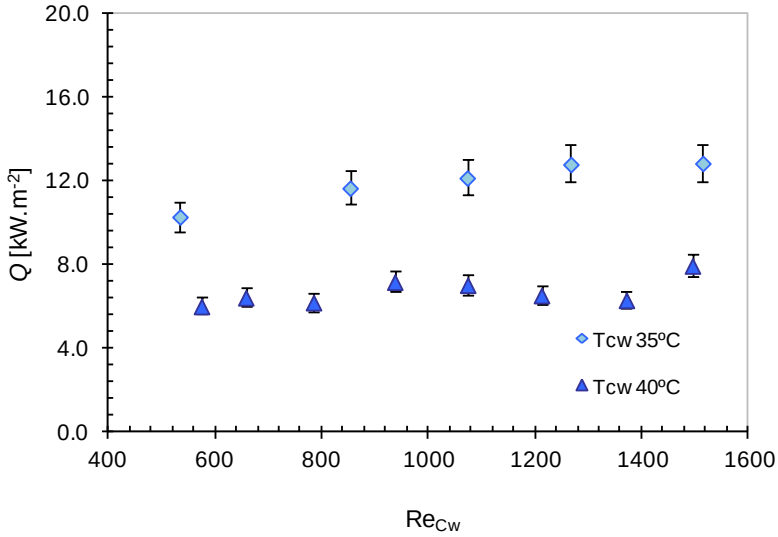

Figure 4.13 - Effect of the cooling-water flow rate and cooling-water temperature on absorber thermal load.

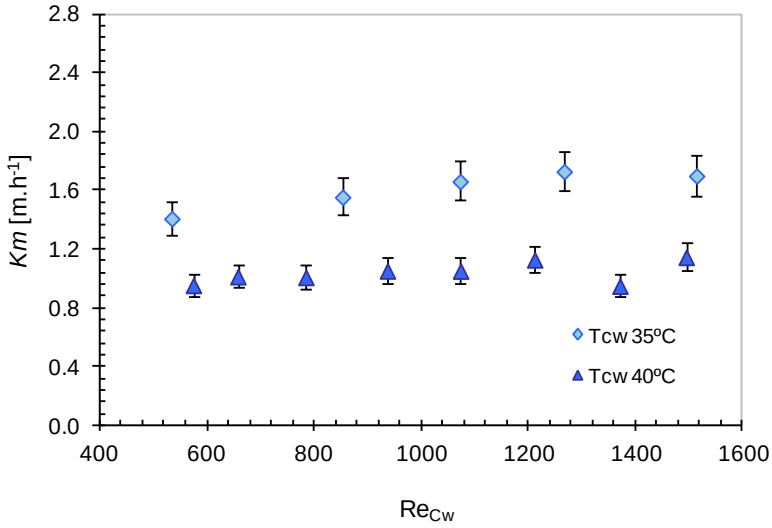

Figure 4.14 - Effect of the cooling-water flow rate and cooling-water temperature on solution mass transfer coefficient.

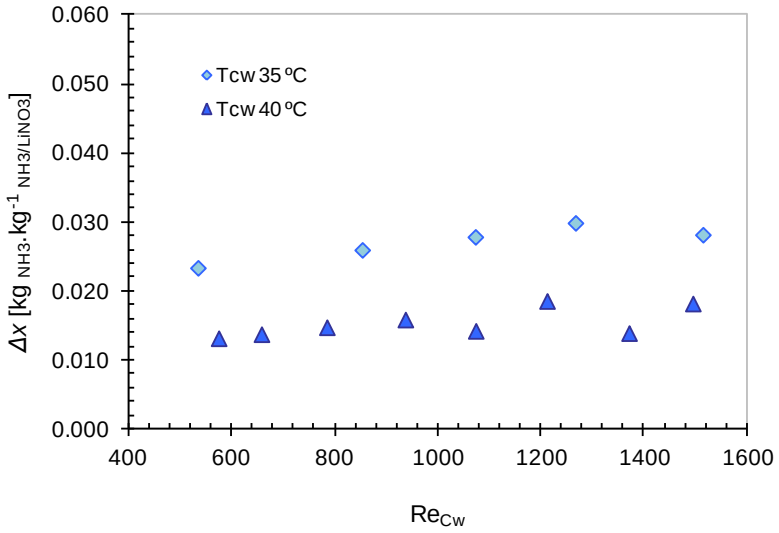

Figure 4.15 - Effect of the cooling-water flow rate and cooling-water temperature on concentration difference.

Figure 4.16 illustrates solution heat transfer coefficient as a function of the cooling-water Reynolds number and cooling-water temperature. According to results and in contrast to tendencies in the mass transfer coefficient shown earlier, solution heat transfer coefficient at these operating conditions decreases when increasing cooling-water flow rate. The solution heat transfer coefficient decreases from 5.1 to 3.6 $kW.m^{-2}.K^{-1}$ and from 4.2 to 2.9 $kW.m^{-2}.K^{-1}$ at cooling-water temperatures of 35 ºC and 40 ºC, respectively. This trend is due to a significant decrease in the cooling-water resistance and overall heat transfer coefficient when increasing the cooling-water flow rate. According to results in Figure 4.13 and Figure 4.17, calculated overall heat transfer coefficient tends to decrease slightly when the cooling-water Reynolds number is increased. This effect is due to a higher increase in the LMTD in comparison with that in the thermal load. This in turn, results in a gradual increment in the solution resistance when the cooling-water Reynolds number is increased. In addition, Figure 4.16 also shows that from a cooling-water Reynolds number of 1100, the solution heat transfer coefficient presents a minor variation which means that from this point cooling-water resistance is negligible.

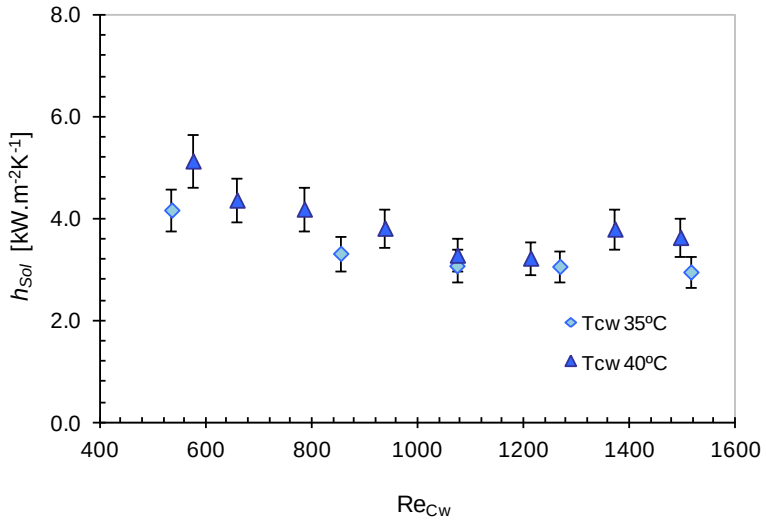

Figure 4.16 - Effect of the cooling-water flow rate and cooling-water temperature on solution heat transfer coefficient.

Figure 4.18 shows that at the conditions under study, the degree of subcooling at the outlet of the absorber ranges between 5.4 and 3.8 ºC and also that this is not significantly affected when increasing the cooling-water flow rate.

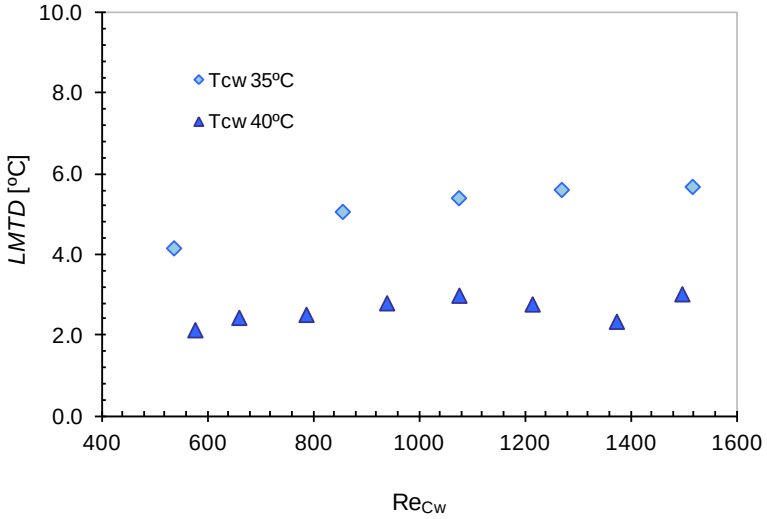

Figure 4.17 - Effect of the cooling-water flow rate and cooling-water temperature on LMTD.

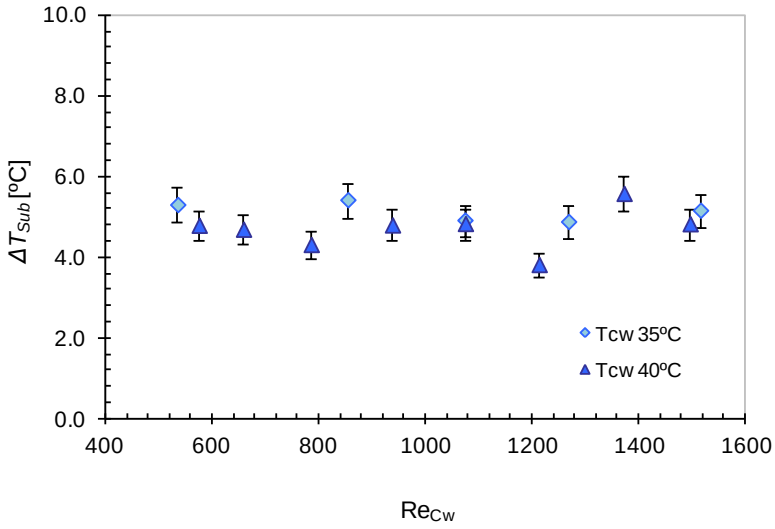

Figure 4.18 - Effect of the cooling-water flow rate and cooling-water temperature on subcooling at the absorber outlet.

According to results, solution resistance is more dominant than the cooling-water resistance. However, results also show that cooling-resistance remains important. An optimum value in the cooling-water flow would imply a better absorption capacity without unnecessary exceeding the cooling-water pump energy consumption. Moreover, results have shown that any attempts to improve the absorption rate are more efficient if they are addressed directly to the solution side. In addition, at the operating conditions and absorber configuration under study, the limiting mechanism to improve the absorption capacity of the absorber is the heat transfer. However, it can be observed in the next sub-sections that the implementation of passive intensification techniques directly to the solution side can improve the solution and vapor mixing and thus the intensification affect is more positive in the mass transfer than in the heat transfer.

4.3.1.5 Comparison between plate absorbers

This sub-section presents a comparison between main experimental results of the NH_3 absorption process performed in this study and those obtained in the sensitivity study performed by Oronel et al. (2013) in a plate heat exchanger with L-type corrugations (angle with 60 degree from its horizontal axis) with the $NH_3/LiNO_3$ mixture. Comparison was performed taking in count the same inlet operating conditions. Inlet solution temperature of 45 °C, solution concentration of 0.45 $kg_{NH3}.kg^{-1}_{NH3/LiNO3}$ and an inlet pressure of 510 kPa. Solution flow rate and cooling-water temperature was varied as shown in Figure 4.19. Regarding the cooling-water flow rate, in the case of the plate heat exchanger L-type, water flow was varied between 0.139 and 0.218 $m^3.h^{-1}$, while in the plate heat exchanger H-type, water flow was kept around 0.270 $m^3.h^{-1}$.

In experiments reported using the plate heat exchanger L-type, absorption mass flux values range from 0.0017 to a maximum of 0.0043 $kg.m^{-2}s^{-1}$ and from 0.0029 to 0.0062 $kg.m^{-2}s^{-1}$ when the solution Reynolds number increases from 15 to 49 at cooling-water temperatures of 40 and 35 °C, respectively (Figure 4.19). According to this, there are not significant differences between absorption mass flux values in the plate heat exchanger H-type and L-type at a cooling-water temperature of 40 °C. However, absorption mass flux results at a cooling-water temperature of 35 °C in the plate heat exchanger H-type are in average around 1.26 times higher than those values obtained in the plate heat exchanger L-type when the solution Reynolds number is varied from 15 to 40. Similarly, Figure 4.20 shows that solution mass transfer coefficient values in the plate heat exchanger L-type range from 0.52 to 0.99 $m.h^{-1}$ and from 0.78 to 1.42 $m.h^{-1}$ when the solution Reynolds number increases from 15 to 49 at cooling-water temperatures of 40 and 35 °C, respectively. It means that mass transfer coefficient values in the plate heat exchanger H-type are around 1.32 times higher than those values obtained in the plate heat exchanger L-type at a cooling-water temperature of 35 °C but at a cooling-water temperature of 40 °C mass transfer coefficients values were relatively close.

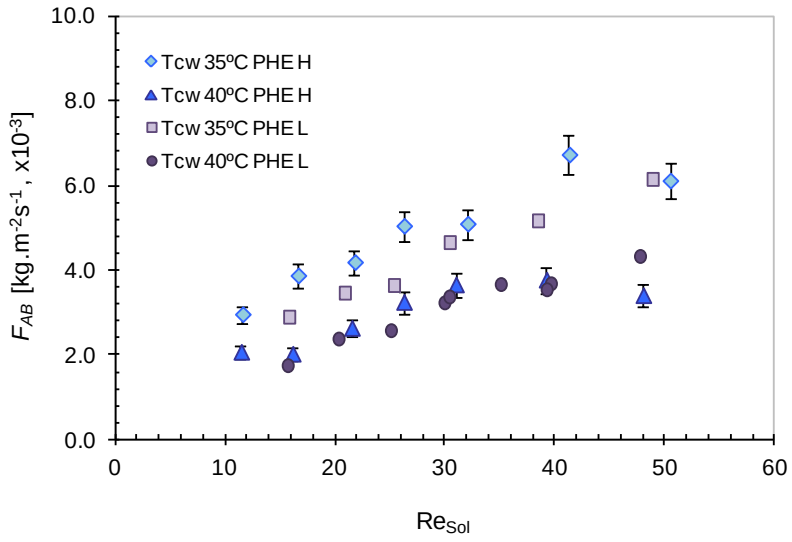

Figure 4.19 - Comparison between absorption mass flux results in plate absorbers L-type and H-type.

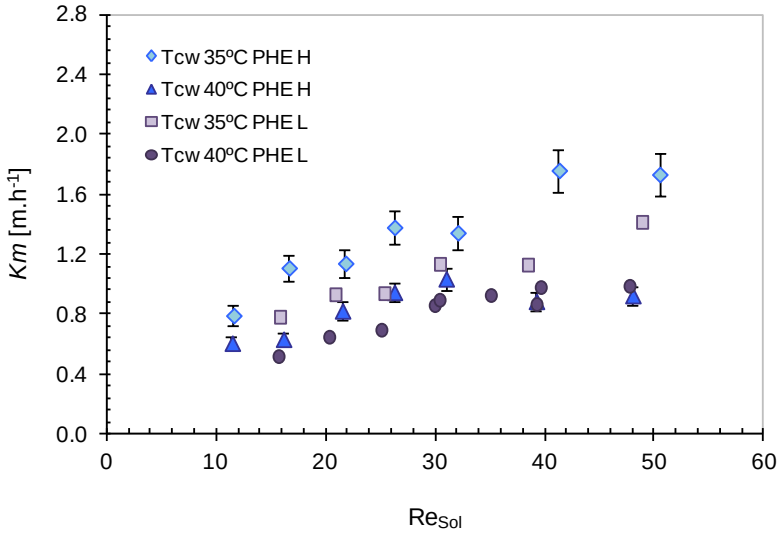

Figure 4.20 - Comparison between solution mass transfer coefficient results in plate absorbers L-type and H-type.

Figure 4.21 shows that thermal load values in the plate heat exchanger H-type are higher than those values obtained in the plate heat exchanger L-type. Thermal load in plate exchanger L-type increase from 5.56 to 12.1 $kW.m^{-2}$ and from 3.5 to 7.0 $kW.m^{-2}$ at cooling-water temperatures of 40 and 35 ^{o}C, respectively.

Furthermore, Figure 4.22 shows that experimental results using the plate absorber L-type for the solution heat transfer coefficient range from 1.8 to 4.0 $kW.m^{-2}.K^{-1}$ and from 2.1 to 5.5 $kW.m^{-2}.K^{-1}$ at cooling-water temperatures of 35 and 40 ^{o}C, respectively. Results show that solution heat transfer coefficients obtained using the plate absorber L-type are between 1.13 and 1.37 times higher than those values obtained in the plate exchanger H-type at a cooling-water temperature of 40 ^{o}C. In the same order, results at a cooling-water temperature of 35 ^{o}C show that solution heat transfer coefficients in the plate absorber L-type are around 1.09 and 1.28 times higher than those obtained in the plate exchanger H-type.

Taking into account that cooling-water flow rates used for experiments in the plate heat exchanger H-type were higher than those cooling-water flow rates in the plate L-type, enhancements achieved in the mass absorption rates using the plate absorber H-type were due to the higher cooling-water flow established for experiments. Furthermore, solution temperatures at the outlet of the plate absorber with H-type corrugations were lower than values in the plate absorber with L-type corrugations. It meant that more heat was extracted from the solution due to the higher cooling-water flow rate resulting in a higher absorption potential.

Regarding the solution heat transfer coefficient, lower coefficients obtained with the plate H-type are due to the fact that LMTD and cooling-water heat transfer coefficients values were higher than those values in the plate L-type. In conclusion, it can be affirmed that the effect of the angle of corrugation in the plate H-type on the absorption rates with respect to the plate L-type is not significant and also that improvements obtained in the absorption rates presented in this comparison are attributed to the higher cooling-water flow rates established for experiments in the plate H-type.

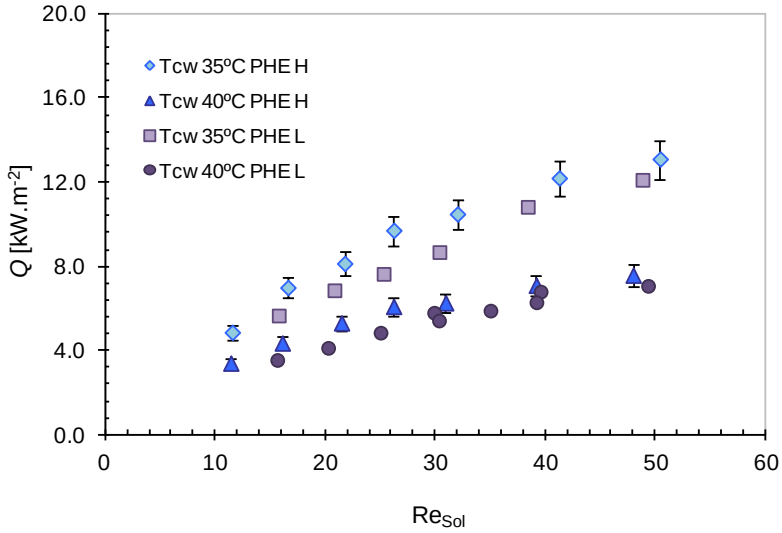

Figure 4.21 - Comparison between thermal load results in plate absorbers L-type and H-type.

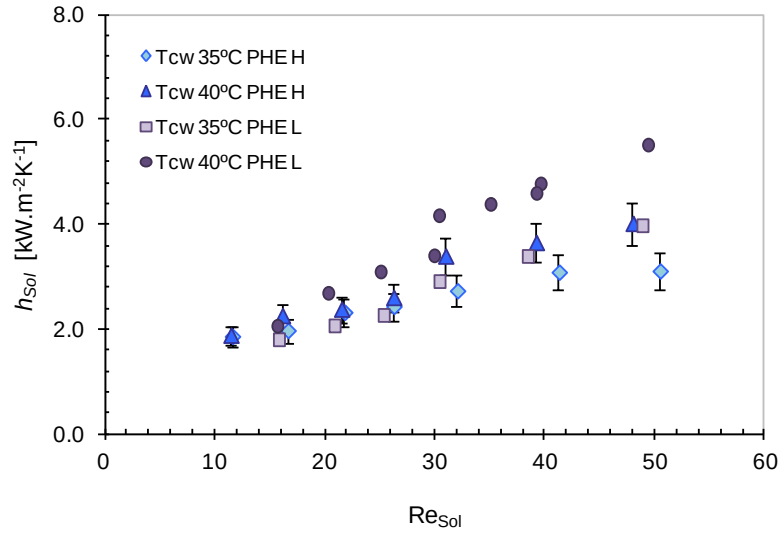

Figure 4.22 - Comparison between solution heat transfer coefficient results in plate absorbers L-type and H-type.

4.3.1.6 Experimental uncertainty of results

Based on the accuracy of the measuring instruments and the method for calculating uncertainties propagation described in Chapter 4, Table 4.2 shows the uncertainty intervals of the calculated parameters presented above for the plate absorber H-type taking into consideration a 95 % confidence interval.

Table 4.2 - Summary of uncertainty of the calculated parameters.

Parameters	Uncertainty
Width, thickness and pitch, L (%)	± 0.5 %
Area of plate, A (%)	± 0.5 %
Calculated parameters	
Solution Reynolds number, Re	± 0.92 %
NH_3 absorption mass flux, F_{AB} (%)	± 4.3 %
Thermal Load, Q_{AB} (%)	± 6.6 %
Solution mass transfer coefficient, *Km* (%)	± 5.6 %
Solution heat transfer coefficient, h_S (%)	± 10.3 %
Subcooling, ΔT_{Sub} (%)	± 7.3 %

4.3.1.7 Experimental correlations

Equations (4.9), (4.10) and (4.11) are the empirical correlations for the NH_3 absorption mass flux, solution Nusselt and Sherwood number, respectively, based on experimental results of the NH_3 absorption process into $NH_3/LiNO_3$ in the plate heat exchanger H-type. Correlations include variables such as solution equilibrium temperature ($T_{Sol,Eq,in}$, ^oC), solution temperature ($T_{Sol,in}$, ^oC), and cooling-water temperature ($T_{Cw,in}$, ^oC) at the absorber inlet. These variables have been observed to have an important effect on the correlated parameters (Cerezo, 2006 and Oronel, 2010). Reynolds and Prandtl numbers are calculated taking into account a mean value between the inlet and outlet conditions of the properties involved. Due to the importance of the NH_3 absorption mass flux parameter for a preliminary design of absorbers, the correlation presented in Equation (4.9) is very useful for obtaining a good estimation of this parameter. To be consistent with this term, the adjustment factor F_0 has units of $kg.m^{-2}s^{-1}$.

$$F_{AB} = F_0 \cdot \mathrm{Re}^{0.48} \cdot \left(\frac{T_{Sol,Eq,in}}{T_{Sol,in}}\right)^{4.39} \cdot \left(\frac{T_{Sol,in}}{T_{Cw,in}}\right)^{3.53}, F_0 = 22.07\times10^{-5}\,\mathrm{kg.m^{-2}s^{-1}} \tag{4.9}$$

$$\mathrm{Nu}_{Sol} = 1.24 \cdot \mathrm{Re}^{0.60} \cdot \mathrm{Pr}^{1/3} \cdot \left(\frac{T_{Sol,Eq,in}}{T_{Sol,in}}\right)^{1.12} \cdot \left(\frac{T_{Sol,in}}{T_{Cw,in}}\right)^{-1.41} \tag{4.10}$$

$$\mathrm{Sh}_{Sol} = 872358 \cdot \mathrm{Re}^{0.51} \cdot \mathrm{Sc}^{-1.08} \cdot \left(\frac{T_{Sol,Eq,in}}{T_{Sol,in}}\right)^{3.87} \cdot \left(\frac{T_{Sol,in}}{T_{Cw,in}}\right)^{2.97} \tag{4.11}$$

Additionally, Figure 4.23a,b,c show that correlations obtained predict the experimental results satisfactorily. With 93 %, 90 % and 90 % of the experimental absorption mass

fluxes, solution heat transfer coefficients and Sherwood numbers, respectively, were predicted with an error lower than 15 %.

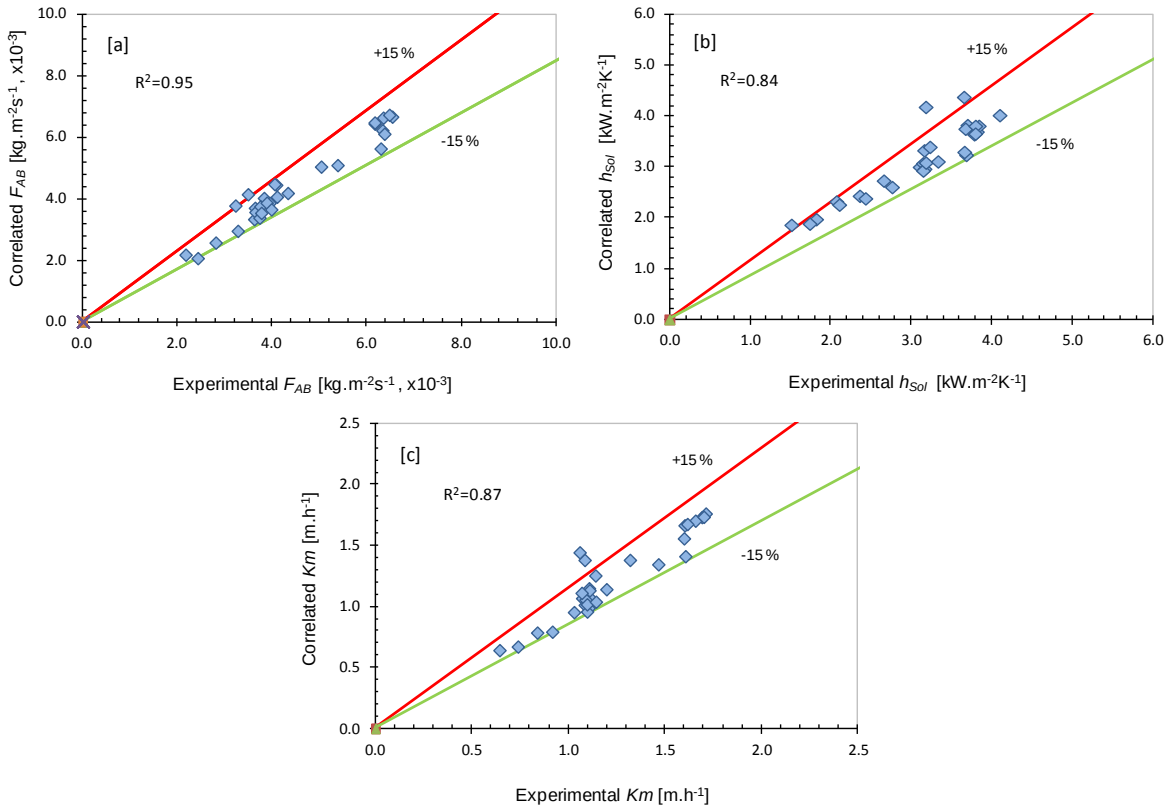

Figure 4.23 - Correlated data in the plate absorber H-type for: [a] NH_3 absorption mass flux, [b] solution heat transfer coefficient; and [c] solution mass transfer coefficient.

4.3.2 NH_3 absorption process in a tubular absorber with advanced surfaces

In this sub-section, experimental results obtained from the study of the effect of the advanced surfaces on the ammonia absorption process in tubular bubble absorbers with ammonia/lithium nitrate are presented. The tubular bubble absorber is a vertical double pipe heat exchanger in which absorption takes place in the inner tube.

In order to quantify the effect of advanced surfaces, a smooth tube and an internally micro-finned tube were tested. The advanced surface tube is made of aluminium with an outer diameter of 8.0 mm and has internal helical micro-fins measuring 0.3 mm in length. Additionally, the absorber performance using different tube diameters and lengths was investigated. In appendix C can be found a summary of tests performed.

4.3.2.1 Operating conditions

Operating conditions of interest for assessment of the tubular absorber configurations are shown in Table 4.3. These operating conditions were determined from the thermodynamic simulation of the absorption refrigeration cycle with $NH_3/LiNO_3$ as shown in sub-section 4.2.2. The tubular absorber with the different configurations was tested at the same operating conditions to perform a direct comparison.

Table 4.3 - Experimental operating conditions.

Parameters	Range
Solution temperature at the absorber inlet, °C	45
Cooling-water temperature at the absorber inlet, °C	35 and 40
Ammonia mass fraction in the solution at the absorber inlet, $kg_{NH3}.kg^{-1}_{NH3/LiNO3}$	0.45
Absorber pressure, kPa	510
Solution mass flow rate, $kg.h^{-1}$	10-70
Cooling-water flow rate in the tubular absorber, $m^3.h^{-1}$	0.080-0.345

4.3.2.2 Effect of the diameter of the advanced surface tube

The effects of the diameter of the advanced surface tube on NH_3 absorption mass flux, mass transfer coefficient, solution concentration difference and degree of subcooling are depicted in the next figures. Studies were conducted at an inlet cooling-water temperature of 40 °C and cooling-water flows in a fully turbulent regime. Initially, experiments were conducted using the advanced surface tube with an outer diameter of 9.5 mm. Then, additional tests were conducted introducing a bar of 1.0 meter in length and 5.0 mm of diameter inside the advanced surface tube with an outer diameter of 9.5 mm to reduce the passage area and increase the solution flow velocity. In consequence, hydraulic diameter in the tube with an outer diameter of 9.5 mm is reduced from 7.5 mm to approximately 2.5 mm. Finally, the advanced surface tube with a diameter of 8.0 mm was tested.

Figure 4.24 shows that higher absorption mass fluxes were achieved when the tube diameter is reduced. NH_3 absorption mass flux values obtained with the 9.5 mm tube diameter range from 0.0034 to a maximum 0.0059 $kg.s^{-1}m^{-2}$ while values obtained when the tube hydraulic diameter is reduced range between 0.0033 and 0.0080 $kg.s^{-1}m^{-2}$. In addition, it can be noted that absorption mass flux values are similar when using the tube with a diameter 9.5 mm including the bar inside and the tube with a diameter 8.0 mm, and also that absorption mass flux values vary slightly after a solution mass flow of 40 $kg.h^{-1}$.

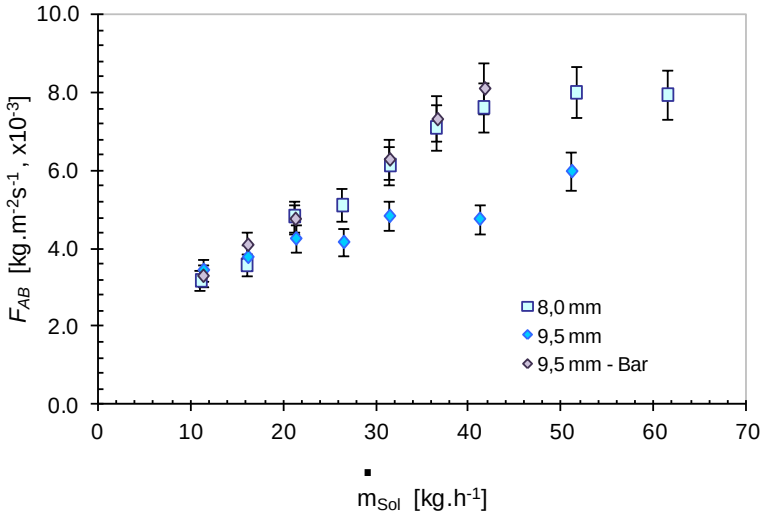

Figure 4.24 - Effect of advanced surface tube diameter on NH_3 absorption mass flux.

In the same way, Figure 4.25 and Figure 4.26 show the mass transfer coefficient and solution concentration difference as a function of the different internal tube diameter under study. Results presented in these figures for the mass transfer coefficient and concentration difference are in agreement with tendencies obtained in the absorption mass flux. For instance, mass transfer coefficient increases from 1.0 to 1.4 $m.h^{-1}$ in the advanced surface tube with a diameter 9.5 mm and from 1.2 to a maximum of 2.6 $m.h^{-1}$ when the tubes hydraulic diameter are smaller.

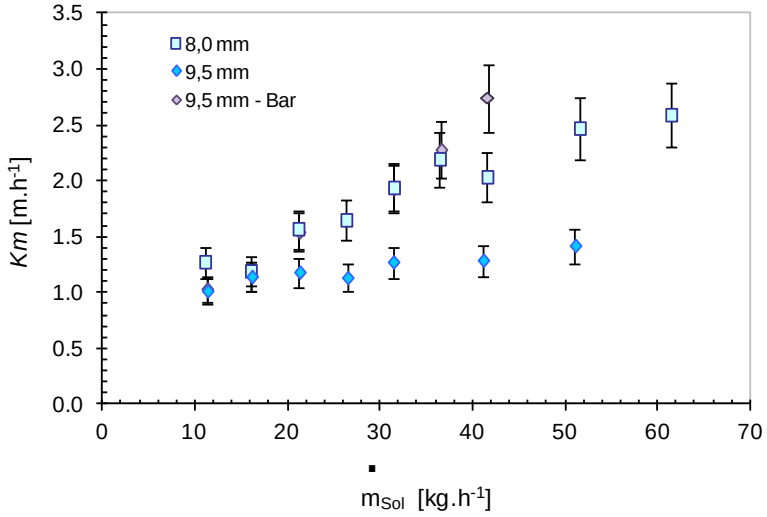

Figure 4.25 - Effect of advanced surface tube diameter on solution mass transfer coefficient.

The subcooling degree values for the solution in these experiments are presented in Figure 4.27. Subcooling values of the solution leaving the absorber are lower when the internal diameter of the tube is smaller. In addition, the maximum value obtained in the tube with a diameter of 9.5 mm was approximately 5.9 ^{o}C.

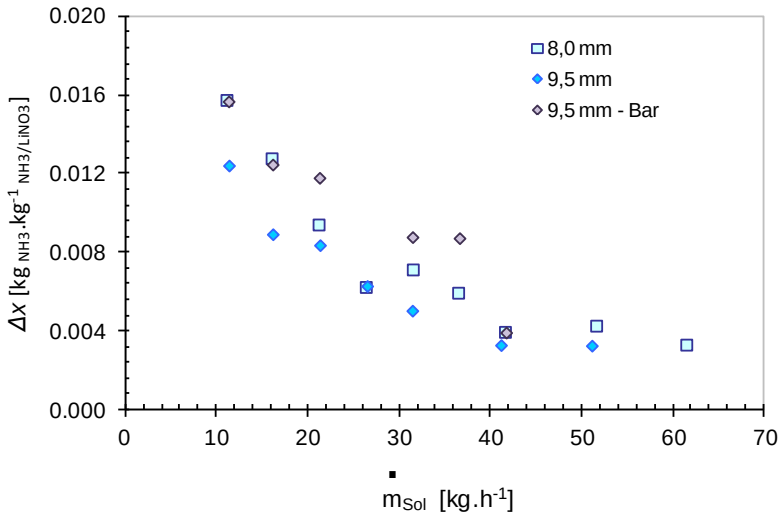

Figure 4.26 - Effect of advanced surface tube diameter on solution concentration difference.

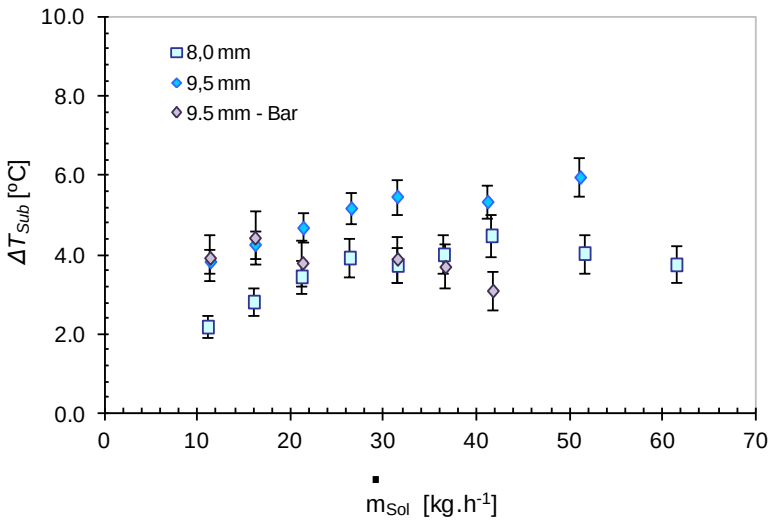

Figure 4.27 - Effect of advanced surface tube diameter on subcooling at the absorber outlet.

The results for the heat transfer performance of the absorber for these experiments are not presented due to the high uncertainty propagation obtained in the thermal load, and therefore in the solution heat transfer coefficient as well.

The experimental results described in this sub-section indicate that, as expected, the higher solution and ammonia vapor velocities achieved by reducing the tube hydraulic diameter result in an increase in mass transfer rate. However, the increased mass transfer rate was offset by the reduction in the transfer area, resulting in a similar absorption capacity for both tubes. Results are in good agreements with the experimental data reported by Infante Ferreira (1985).

4.3.2.3 Effect of advanced surfaces on the absorber performance.

In this sub-section, experimental results of the effect of advanced surfaces on the performance of a tubular absorber are analyzed through the comparison of these results with those obtained with a smooth tube. Both advanced surface tube and smooth tube have an exterior diameter of 8.0 mm and a length of 1 meter. Results were achieved at a cooling-water temperature of 40 ºC.

Figure 4.28 shows the NH_3 absorption mass flux as a function of the solution and cooling-water mass flows for the $NH_3/LiNO_3$ mixture. In this case, the NH_3 absorption mass flux results in both advanced and smooth surfaces tubes were obtained for cooling-water flows at the beginning of the transition and turbulent regimes. With the cooling-water flow in a transition regime, the NH_3 absorption mass flux increases from 0.0037 to 0.0061 $kg.s^{-1}m^{-2}$ when the solution mass flow in the advanced surface tube is changed from 20 (Re≈221) to 70 $kg.h^{-1}$ (Re≈746). In the case of the smooth tube, the corresponding values are between 0.0032 until a maximum of 0.0035 $kg.s^{-1}m^{-2}$ at the same operating conditions. With the cooling-water flow in a turbulent regime, the absorption mass flux in the advanced surface tube increases from 0.0048 to 0.0080 $kg.s^{-1}m^{-2}$ when the solution mass flow is varied from 20 (Re≈221) to 60 $kg.h^{-1}$ (Re≈640). Moreover, the corresponding values for the smooth tube range from 0.0036 to 0.0055 $kg.s^{-1}m^{-2}$.

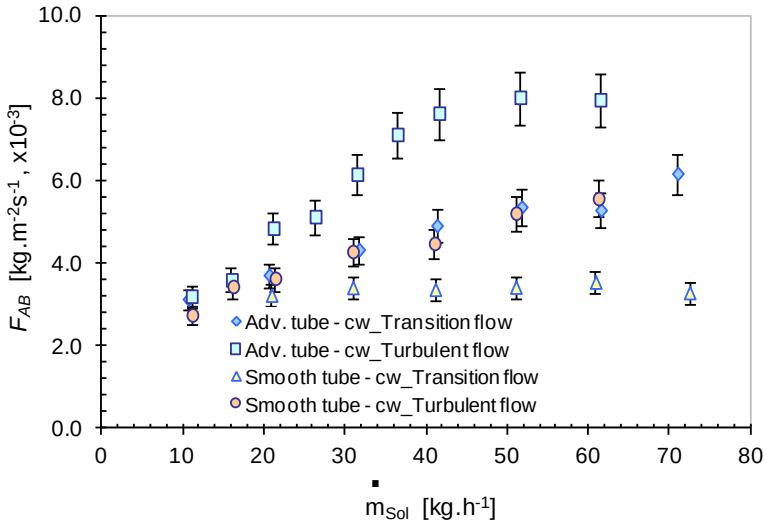

Figure 4.28 - Effect of advanced surfaces on NH_3 absorption mass flux.

According to results, absorption mass flux values achieved using the advanced surface tube are even higher than the values achieved with the plate absorber H-type and those results reported by Oronel et al. (2013) with the plate absorber L-type. At the same operating conditions and the cooling-water flow in a turbulent regime, the absorption mass flux values using the advanced surface tube are approximately twice higher than the values achieved with the corrugated plate absorber L-type. Lower mass transfer in the plate absorbers could probably be attributed to the inefficient use of the mass transfer area since bubbles could follow a preferential way upward through the center of the channel.

Infante Ferreira (1985) also conducted an experimental study with a tubular bubble absorber with an $NH_3/LiNO_3$ mixture and four different smooth tubes with internal diameters of 10, 15.3, 20.5 and 25.7 mm. The author reported a maximum absorption mass flux of 0.0038 $kg.s^{-1}m^{-2}$ with a 10 mm internal diameter smooth tube, but the operating conditions were quite different. Although the solution inlet temperature and concentration were quite close, solution flow rates were much higher while the absorber pressure and inlet coolant-water temperature were lower.

It was initially studied of the absorption process with the cooling-water flow in a fully developed turbulent regime (Figure 4.28); however, the results for the absorber load and heat transfer coefficient at these conditions are not shown because of their high uncertainty propagation due to the small difference in the cooling-water side temperatures. Experiments show that for cooling-water flows at the beginning of the transition regime, the maximum potential in the absorption mass flux is not reached if compared with results for a fully developed turbulent flow.

Although the heat transfer resistance was dominant in the solution side rather than in the water side in all our experiments, increasing the water side heat transfer coefficient also increases the absorption mass flux. The same behavior was observed in the experiments with the plate absorber H-type and also by Cerezo et al. (2009, 2010) with an NH_3/H_2O mixture and Oronel et al. (2013) with an $NH_3/LiNO_3$ mixture, both using a plate absorber

L-type. In general terms, the absorption mass flux values achieved in the advanced surface tube represent a significant improvement over the values obtained with the smooth tube. For instance, at low cooling-water Reynolds numbers and solution mass flows of 40 and 50 kg.h^{-1}, the absorption mass fluxes using the advanced surface tube are 1.46 and 1.57 times higher, respectively, than the values achieved using the smooth tube. At high cooling-water Reynolds numbers, improvements in the absorption mass fluxes with the advanced surface tube are around 1.71 and 1.54 times higher than the values achieved using the smooth tube.

Figure 4.29 and Figure 4.30 shows the solution heat transfer coefficient and thermal load as a function of the solution mass flow at low cooling-water flows, respectively. As mentioned earlier, solution heat transfer coefficients when high cooling-water flows were used are not shown because the uncertainty propagations for the absorber thermal load values were high, and were therefore also high for the solution heat transfer coefficient values. However, Figure 4.29 shows that the solution heat transfer coefficient increases from 1.25 to 2.55 kW.m^{-2}K^{-1} when the solution mass flow in the advanced surface tube is changed from 20 to 70 kg.h^{-1}. On the other hand, the solution heat transfer coefficient in the smooth tube increases slightly from 1.13 to 1.64 kW.m^{-2}K^{-1}. Therefore, the solution heat transfer coefficient values from the advanced surface tube are 1.11 and 1.55 times higher than the values from the smooth surface tube when the solution mass flow is set to 40 and 70 kg.h^{-1}.

Contrary to what is seen in the results of the absorption mass flux, the solution heat transfer coefficients obtained with the advanced surface tube are lower than those reported by Oronel et al. (2013) with the corrugated plate heat exchanger absorber. This difference in behavior may be related to the deficient use of the tube area for the heat transfer and also due to the use of the plate area for heat transfer in contrast with the plate area used for the mass transfer. Infante Ferreira (1985) obtained a maximum value of 2.53 kW.m^{-2}K^{-1} for the solution heat transfer coefficient using a 10 mm inner smooth tube diameter.

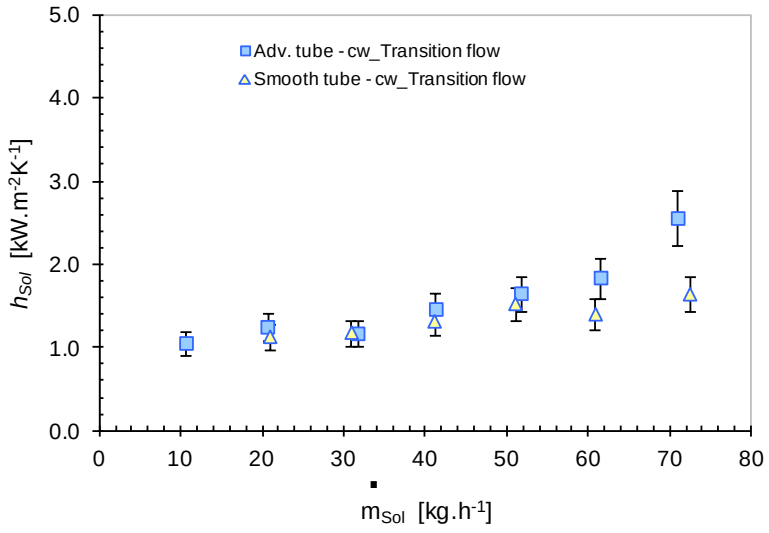

Figure 4.29 - Effect of advanced surfaces on solution heat transfer coefficient.

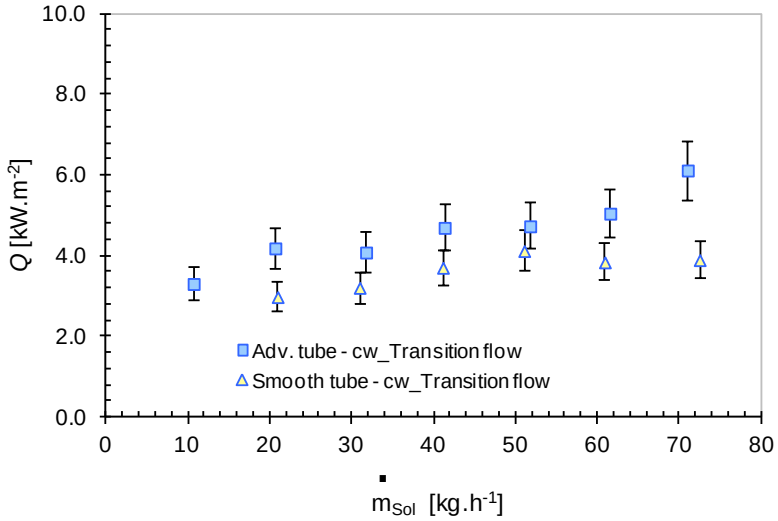

Figure 4.30 - Effect of advanced surfaces on absorber thermal load.

Regarding the thermal load, Figure 4.30 shows that values increase from 4.19 to 6.13 kW.m^{-2} using the advanced surface tube and from 2.99 to 3.90 kW.m^{-2} using the smooth surface tube. The thermal load values using the advanced surface tube are around 1.26 and 1.57 times higher than the values from experiments in the smooth surface tube when the solution mass flow is set varied from 20 and 70 kg.h^{-1}.

Figure 4.31 shows the mass transfer coefficient as a function of the solution mass flow. As expected, mass transfer coefficient values show a similar trend to those of the absorption mass flux values. At low cooling-water Reynolds numbers and solution mass flows between 20 and 70 kg.h^{-1}, the mass transfer coefficient in the absorber with the advanced surface tube increases from 1.49 to 1.85 m.h^{-1} while mass transfer coefficient using the smooth tube is around 1 m.h^{-1}. Moreover, when a fully turbulent cooling-water regime is set and solution mass flows is changed between 20 and 60 kg.h^{-1}, mass transfer coefficients in the advanced and smooth surface tubes increase from 1.56 to 2.58 m.h^{-1} and from 1.1 to 1.7 m.h^{-1}, respectively. The higher mass transfer coefficient achieved in the advanced surface tube is 1.49 times higher than values in the smooth tube.

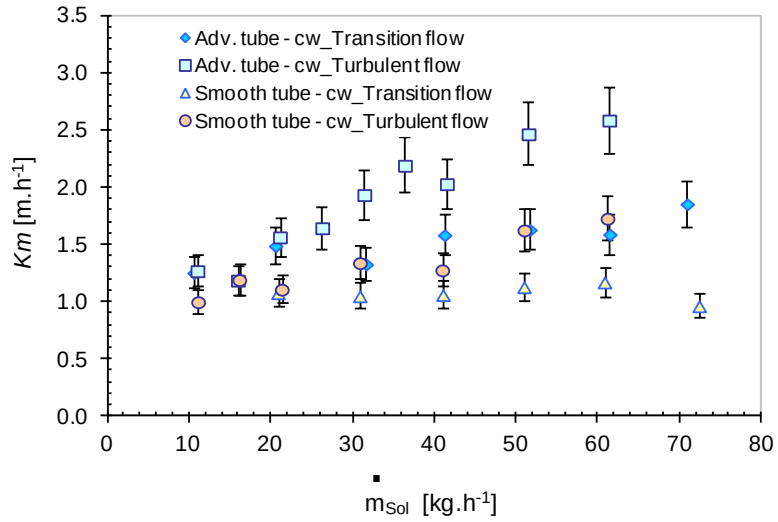

Figure 4.31 - Effect of advanced surfaces on solution mass transfer coefficient.

While the results obtained using the smooth tube at low cooling-water Reynolds numbers are similar to those obtained in the plate absorber H-type and by Oronel et al. (2013) with plate absorber L-type. The maximum mass transfer coefficient value obtained with the advanced surface tube and a fully turbulent cooling-water flow is 2.5 times higher than the maximum coefficient obtained in the plate heat exchanger. The maximum value reported by Infante Ferreira (1985) was 0.79 $m.h^{-1}$ with an inner smooth tube measuring 20.5 mm in diameter.

It was initially expected that the use of the advanced surfaces would have a predominant effect on heat transfer; however results show that the use of advanced surfaces in the configurations under study involve an additional factor that enhances mass transfer more than heat transfer. These greater improvements in mass transfer are probably due to the fact that advanced surfaces not only act as turbulators, but the centrifugal effect of helical micro-fins may also force the bubbles into contact with the rough and micro-finned wall, allowing that the ammonia bubbles break more easily, and therefore their absorption is more easy.

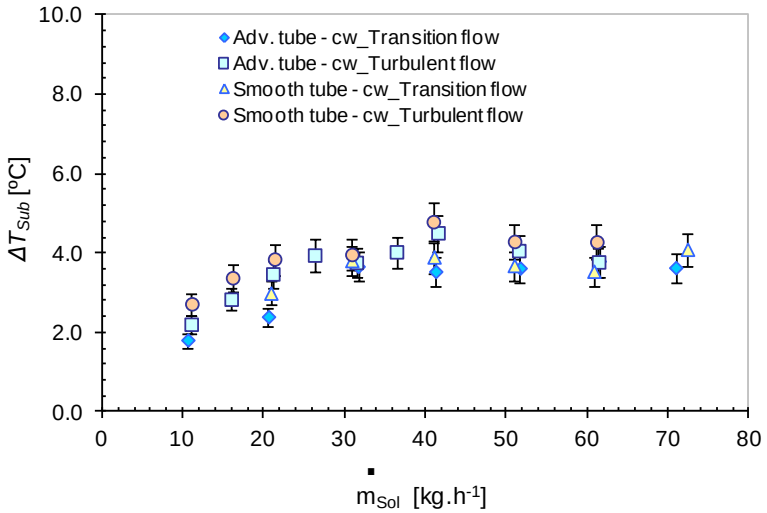

Figure 4.32 - Effect of advanced surfaces on subcooling at the absorber outlet.

The subcooling degree of the solution leaving the absorber in this case study increases when the solution mass flow is changed from 10 to 30 $kg.h^{-1}$, for higher solution flows subcoolings are almost constant (Figure 4.32). The figure also shows that subcooling in the absorber with advanced surfaces yields slightly lower values than with the smooth tube. All subcooling values obtained were below 5 ºC, which indicates that the tested absorbers operated at near optimal performance at the selected operating conditions.

Figure 4.33 shows the total pressure drop in both the advanced surface tube and smooth surface tube. Since one would expect that the insertion of micro-fins in the plain tube also increases the pressure drop along the absorber and thereby reduces the absorber pressure and thus the absorption capacity, the effect of micro-fins on pressure drop is also required to be investigated. It can be noticed that pressure drops in the advanced surface tube are slightly lower that pressure drops in the smooth tube. Therefore, for the operating conditions selected in this sub-section, the advantage of using advanced

surface tubes for bubble absorbers is clearly justified since they enhance heat and mass transfer processes without penalizing pressure drop. Lower pressure drop in the advanced surface tube can be attributed to the fact that this tube presents a wall thickness thinner in comparison with smooth tube which in turn results in a slightly higher passage area and a lower flow velocity.

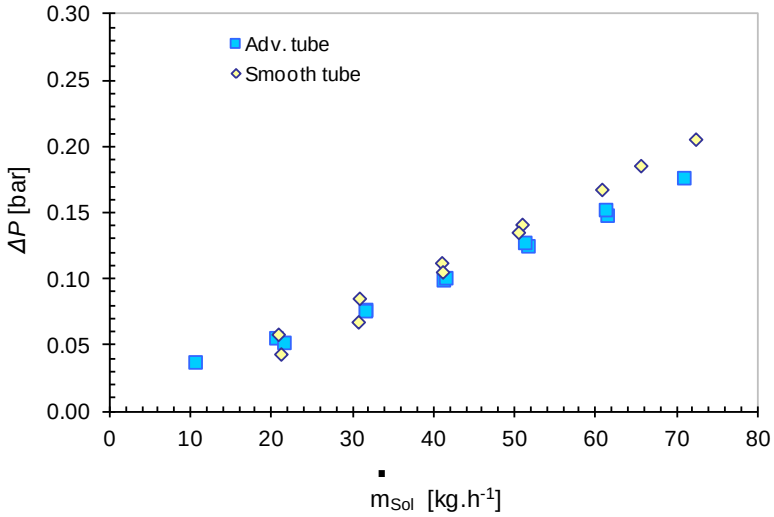

Figure 4.33 - Total pressure drop comparison.

4.3.2.4 Effect of the length of the advanced surface tube

An experimental characterization of an $NH_3/LiNO_3$ tubular absorber with an advanced surface tube of 8.0 mm (OD) with three tube lengths (1, 2 and 3 meters in series) was performed. In these experiments, operating parameters such as solution mass flow and cooling-water temperature were varied as shown in the next Figures. Cooling-water flow was kept in a transition regime and inlet solution temperature was set to 45 °C for all the experiment to keep an equal initial absorption potential.

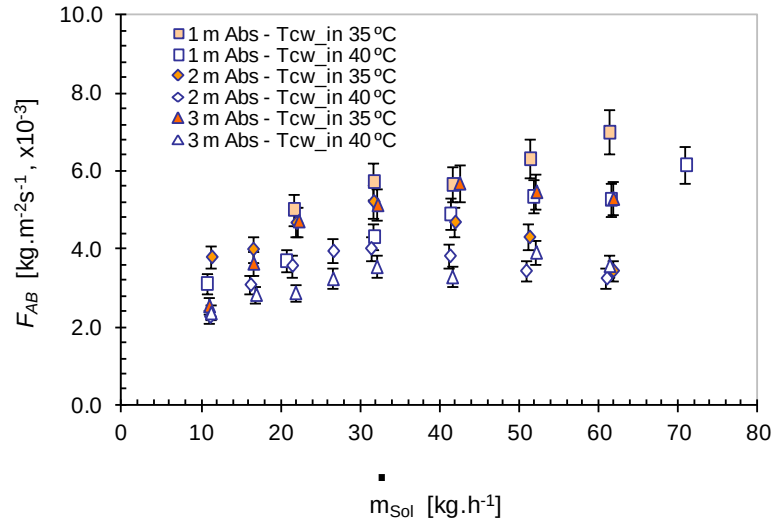

Figure 4.34 - Effect of advanced surface tube length on NH_3 absorption mass flux.

Figure 4.34 shows the effect of the absorber length on the NH_3 absorption mass flux, for the cooling-water temperatures at 40 °C and 35 °C. In Figure 4.34 can be observed that absorption mass flux values decrease when the absorbers of two or three meters are set if compared with the absorber of one meter. In contrast, Figure 4.35 reveals that the increment of the tube length results in a sharp rise in the solution concentration difference between the outlet and inlet of the absorber. It indicates that an important increment in the NH_3 mass absorption flow is obtained. However, the improvement of the absorption mass flux is not proportional to the increment of the tube length while increasing the solution mass flow. It is also observed that the absorption mass flux tends to gradually decrease for solution mass flows over 40 $kg.h^{-1}$ in the absorber of two and three meters. In addition, absorption mass flux values at a cooling-water temperature of 35 °C show similar trends in comparison with results at a cooling-water temperature of 40 °C.

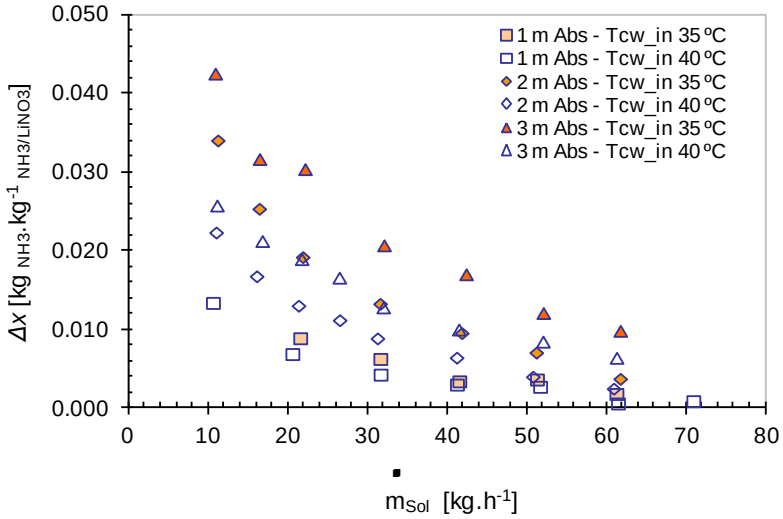

Figure 4.35 - Effect of advanced surface length on solution concentration difference.

Additionally, when the cooling-water temperature is set to 35 °C, higher absorption mass fluxes are achieved due to the wider temperature gradient between the solution and cooling-water temperatures, which improve the heat transferred to the cooling-water side (Figure 4.36), and therefore it results in an increment on the solution capacity to absorb more ammonia. As shown in Figure 4.34, the maximum absorption mass flux values are achieved in the one meter tube at a cooling-water temperature of 35 °C. According to experiments at these conditions, absorption mass flux increases from 0.0050 to 0.0070 $kg.m^{-2}s^{-1}$ by changing the solution mass flow from 20 to 60 $kg.h^{-1}$.

Figure 4.36 shows that the absorber thermal load increases when the absorber length is increased. Besides, thermal load results for the absorber of two and three meters are relatively similar. The higher heat transfer areas of absorbers of two and three meters are capable to dissipate the heat released by the absorption process which is not proportional to the tube length increment. In addition, it also allows dissipating more sensible heat from the solution which results in a solution temperature at the outlet of the absorber lower that the inlet solution temperature.

In the cases of the absorber of one meter in length, solution temperatures at the outlet of the absorber in most of the experiments were higher that the inlet solution temperatures. This means that as commented in sub-section 4.3.2.3, heat transfer area of the 1 meter was not enough to dissipate all the heat released by the absorption process.

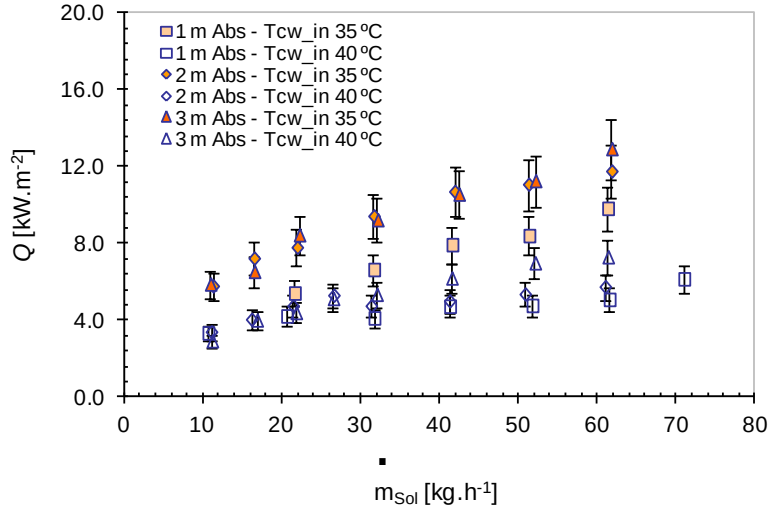

Figure 4.36 - Effect of advanced surface tube length on absorber thermal load.

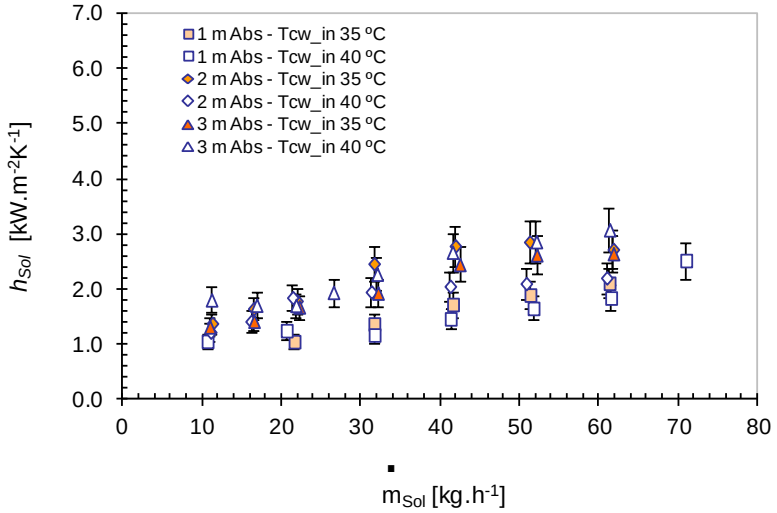

Figure 4.37 - Effect of advanced surface tube length on solution heat transfer coefficient.

Figure 4.37 shows that as expected, the increment in the heat transfer area resulted in a cooler solution at the absorber outlet and in a significant increment in the absorber thermal load, and therefore in the solution heat transfer coefficient as well. For instance, at a cooling-water temperature to 40 ºC, solution heat transfer coefficients range approximately from 1.10 to 1.80 $kW.m^{-2}K^{-1}$, from 1.21 to 2.20 $kW.m^{-2}K^{-1}$, and from 1.80 to 3.10 $kW.m^{-2}K^{-1}$ in the one, two and three meters absorber, respectively, when increasing the solution mass flow from 10 to 60 $kg.h^{-1}$. Increment of the solution heat transfer coefficient is also due the fact that the LMTD in the absorbers of two and three meters are much lower than values in the absorber of one meter (Figure 4.38). The reason is that

less vapor is absorbed in the final section of the absorber, and therefore less absorption heat is dissipated which allows cooling the solution closer to coolant inlet temperature.

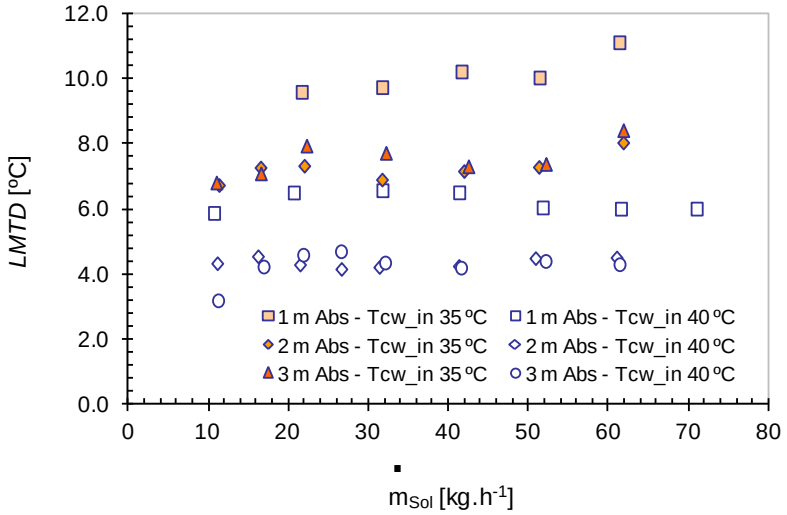

Figure 4.38 - Effect of advanced surface tube length on LMTD.

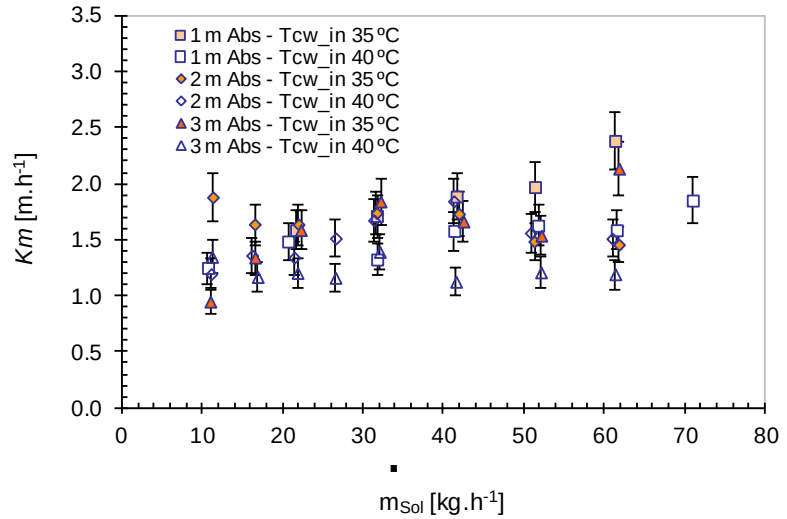

Figure 4.39 - Effect of advanced surface tube length on solution mass transfer coefficient.

As mentioned in Chapter 3, LMTD used in this study is based on the measured solution and cooling-water temperature at the inlet and outlet of the absorber. Another option used for the LMTD is based on saturation temperatures; however, this definition represents an idealized driving temperature difference for heat transfer in the absorption process. In consequence, LMTD based on saturation temperatures results considerably higher than an LMTD based on measured temperatures and may not correctly represent the heat transfer performance of the absorber (Garimella, 2007).

Figure 4.39 illustrates the effect of the advanced surface tube length on the mass transfer coefficient. In this figure can be noted that mass transfer coefficient values follow a more irregular trend in comparison with the absorption mass flux results, however, values for the 1 meter tube absorber remain larger achieving a maximum of 2.4 $m.h^{-1}$ at a cooling-water temperature of 35 ^{o}C. Finally, Figure 4.40 reports the subcooling degree of the

solution leaving the absorber for the configurations under study. For this case study, all values achieved were below 5.0 °C, which indicates that the absorber was operated near its maximum efficiency at the operating conditions established.

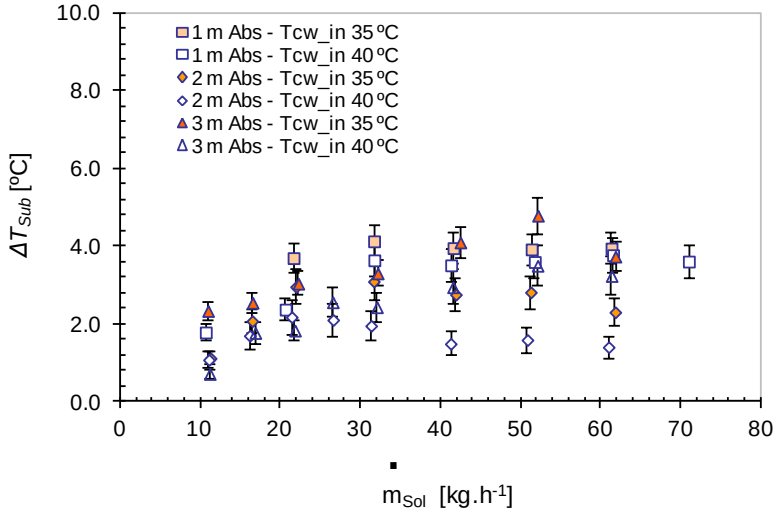

Figure 4.40 - Effect of advanced surface tube length on subcooling at the absorber outlet.

4.3.2.5 Experimental uncertainty of results

Based on the accuracy of the measuring instruments and the method for calculating uncertainties propagation described in Chapter 4, Table 4.4 shows the uncertainty intervals of the calculated parameters presented above for the tubular absorbers configurations taking into consideration a 95 % confidence interval.

Table 4.4 - Summary of uncertainty of the calculated parameters.

Parameters	Uncertainty
Tube diameter, mm	0.02
Tube length	± 0.5 %
Calculated parameters	
NH_3 absorption mass flux, F_{AB}	± 5.7 %
Thermal Load, Q_{AB}	± 12.5 %
Solution mass transfer coefficient, *Km*	± 11.2 %
Solution heat transfer coefficient, h_S	± 13.4 %
Subcooling, ΔT_{Sub}	± 18.7 %

4.3.2.6 Experimental correlations

Equations (4.12), (4.13) and (4.14) are the empirical correlations for the NH_3 absorption mass flux, solution Nusselt and Sherwood number, respectively, based on experimental results of the NH_3 absorption process into $NH_3/LiNO_3$ in the 1 meter tubular absorber using the inner smooth surface tube. In the same way, Equations (4.15), (4.16) and (4.17) are the empirical correlations for the NH_3 absorption mass flux, solution

Nusselt and Sherwood number, respectively, based on experimental results of the NH_3 absorption process into $NH_3/LiNO_3$ in the 1 meter tubular absorber using the inner advanced surface tube. Correlations that are presented below were developed using the same structure than correlations presented from studies in the plate absorber H-type and are valid for the studied conditions with cooling water in transition regime.

For the tubular absorber with smooth surfaces

$$F_{AB} = F_0 \cdot \mathrm{Re}^{0.09} \cdot \left(\frac{T_{Sol,Eq,in}}{T_{Sol,in}} \right)^{5.59} \cdot \left(\frac{T_{Sol,in}}{T_{Cw,in}} \right)^{1.37}, F_0 = 69.65 \times 10^{-5}\,\mathrm{kg.m^{-2}s^{-1}} \quad (4.12)$$

$$\mathrm{Nu}_{Sol} = 0.42 \cdot \mathrm{Re}^{0.34} \cdot \mathrm{Pr}^{1/3} \cdot \left(\frac{T_{Sol,Eq,in}}{T_{Sol,in}} \right)^{4.58} \cdot \left(\frac{T_{Sol,in}}{T_{Cw,in}} \right)^{-0.1} \quad (4.13)$$

$$\mathrm{Sh}_{Sol} = 800 \cdot \mathrm{Re}^{0.09} \cdot \mathrm{Sc}^{0.043} \cdot \left(\frac{T_{Sol,Eq,in}}{T_{Sol,in}} \right)^{0.03} \cdot \left(\frac{T_{Sol,in}}{T_{Cw,in}} \right)^{-0.37} \quad (4.14)$$

For the tubular absorber with advanced surfaces

$$F_{AB} = F_0 \cdot \mathrm{Re}^{0.35} \cdot \left(\frac{T_{Sol,Eq,in}}{T_{Sol,in}} \right)^{5.75} \cdot \left(\frac{T_{Sol,in}}{T_{Cw,in}} \right)^{1.60}, F_0 = 20.62 \times 10^{-5}\,\mathrm{kg.m^{-2}s^{-1}} \quad (4.15)$$

$$\mathrm{Nu}_{Sol} = 0.80 \cdot \mathrm{Re}^{0.56} \cdot \mathrm{Pr}^{1/3} \cdot \left(\frac{T_{Sol,Eq,in}}{T_{Sol,in}} \right)^{-5.83} \cdot \left(\frac{T_{Sol,in}}{T_{Cw,in}} \right)^{-1.41} \quad (4.16)$$

$$\mathrm{Sh}_{Sol} = 872358 \cdot \mathrm{Re}^{0.49} \cdot \mathrm{Sc}^{-1.13} \cdot \left(\frac{T_{Sol,Eq,in}}{T_{Sol,in}} \right)^{3.87} \cdot \left(\frac{T_{Sol,in}}{T_{Cw,in}} \right)^{2.97} \quad (4.17)$$

Figure 4.41a,b,c depicts the correlated data for each one of the parameters of interest using the smooth surface and advanced surface tube into the tubular absorber.

Based in results presented in Figure 4.41, it can be clearly observed the significant enhancements achieved in the absorption mass flux, solution mass transfer coefficient and solution mass transfer coefficient using a tubular absorber with advanced surfaces with respect to those values with smooth surfaces at the same operating conditions. In consequence, all absorption mass flux values in the tubular absorber with smooth surfaces are within an interval that ranges between 0.0031 and 0.0042 $kg.m^{-2}s^{-1}$ while with advanced surfaces, values are within a more extensive interval that ranges between 0.0031 and 0.0070 $kg.m^{-2}s^{-1}$.

Regarding the solution heat transfer coefficient, all values in the tubular absorber with smooth surfaces are within an interval that ranges from 1.1 to 1.7 $kW.m^{-2}K^{-1}$, while with advanced surfaces values are within a range between 1.1 and 2.6 $kW.m^{-2}K^{-1}$. Finally, all mass transfer coefficient values in the tubular absorber with smooth surfaces are in interval that ranges from 0.9 to 1.3 $m.h^{-1}$, while with advanced surfaces values are within a range between 1.2 and 2.4 $m.h^{-1}$.

Additionally, Figure 4.41a,b,c shows that correlations obtained predict the experimental results satisfactorily. For the tubular absorber with smooth surfaces, 94 %, 86 % and 93 % of the experimental absorption mass fluxes, solution heat transfer coefficients and solution mass transfer coefficient, respectively, were predicted with an error lower than 15 %.

For the tubular absorber with advanced surfaces, 98 %, 94 % and 94 % of the experimental absorption mass fluxes, solution heat transfer coefficients and solution mass transfer coefficient, respectively, were predicted with an error lower than 21 %.

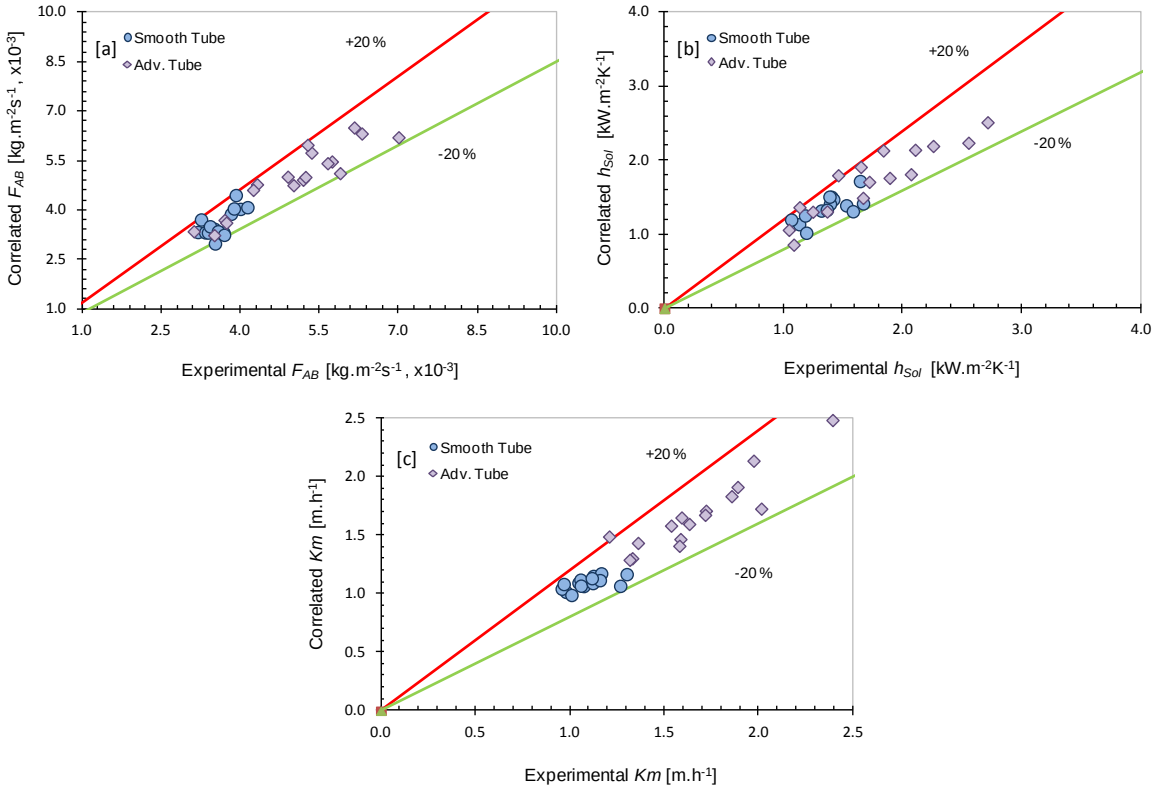

Figure 4.41 - Correlated data in the tubular absorber with smooth and advanced surfaces for: [a] NH_3 absorption mass flux, [b] solution heat transfer coefficient; and [c] solution mass transfer coefficient.

4.3.3 NH_3 absorption process in a tubular absorber with nanoparticles

In this sub-section, experimental results using a tubular heat exchanger with smooth surfaces with and without carbon nanotubes (CNTs) suspended in the base mixture NH_3/$LiNO_3$ are shown. Then, comparison from using inner smooth and advanced surface tubes with the base mixture and nanofluids mixture are also depicted. Finally, experiments with two CNTs concentrations in the base mixture and two cooling-water temperatures using the advanced surface tube are presented. The advance surface tube used in these experiments corresponds to the same tube used for the experimental study presented in sub-section 4.3.2 with an outer tube diameter of 8.0 mm. In appendix C can be found a summary of tests performed.

4.3.3.1 Operating conditions

Experimental results of the absorber evaluation parameters with $NH_3/LiNO_3$ mixture and CNTs (binary nanofluids, Kim et al. 2006a,b) are presented below. During the experiments, cooling-water flows were kept in transitions regimes to avoid too high uncertainty propagations in the absorber thermal load and solution heat transfer coefficient, caused by small differences in the water-side temperature.

Table 4.5 - Experimental operating conditions.

Parameters	Range
Solution temperature at the absorber inlet, °C	45
Cooling-water temperature at the absorber inlet, °C	35 and 40
Ammonia mass fraction in the solution at the absorber inlet, $kg_{NH3}.kg^{-1}_{NH3/LiNO3}$	0.45
Absorber pressure, kPa	510
Solution mass flow rate, $kg.h^{-1}$	10-70
Cooling-water flow rate in the tubular absorber, $m^3.h^{-1}$	0.080-0.100
Carbon nanotubes concentration into de base solution, wt. %	0.00-0.02

4.3.3.2 Carbon nanotubes

In order to study the effect of nanoparticles on the NH_3 absorption process with the $NH_3/LiNO_3$ solution, multi walled carbon nanotubes were selected.

CNTs have outstanding thermal and mechanical properties (Eastman et al. 2004). Additionally, due to the fact the CNTs do not chemically react with ammonia as may happen with metal based nanoparticles (Ma et al., 2007, 2009 and Yang et al., 2012), CNTs seem more suitable for use in ammonia based working fluids.

Taking into account experimental results using CNTs into the conventional working fluids found in the literature (Kang et al., 2008 and Lee et al., 2010) and stability tests of the CNTs in the base mixture $NH_3/LiNO_3$ carried out for this study, concentration of CNTs in the base mixture was initially set to 0.01 wt. %. Figure 4.42 shows a TEM image of the tested multi walled carbon nanotubes. Specifications of the CNTs are shown in Table 4.6.

Table 4.6 - Specifications of the carbon nanotubes.

Multi Walled Carbon Nanotubes	
Nanoparticles supplier	Cheap tubes inc.
Outer Diameter	20-30nm
Inside Diameter	5-10nm
Purity	>95 wt. %
Bulk density	$0.28\ g.cm^{-3}$
Length	10-30um

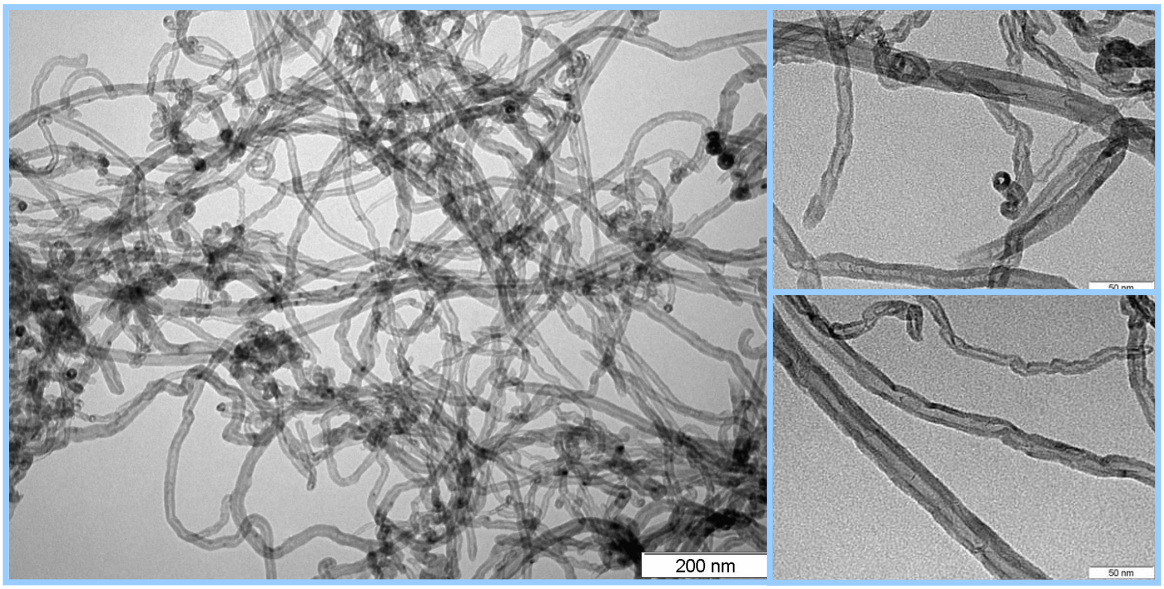

Figure 4.42 - TEM picture of tested carbon nanotubes.

4.3.3.3 Chemical treatment

Before the CNTs were introduced into the base solution $NH_3/LiNO_3$, they were subjected to a chemical treatment to achieve a better dispersion and suspension. CNTs were treated in a beaker with nitric acid (70 %) and hydrogen peroxide (35 %) added drop wise (10 % of the amount of nitric acid), at a temperature of 70 ^oC during two hours. Then, carbon nanotubes were washed with deionized water until a neutral pH-value of 7 was reached and dried at a temperature of 120 ^oC (Datsyuk et al., 2008). In Figure 4.43 can be observed the CNTs (0.01 wt. %) used in an $NH_3/LiNO_3$ solution. This figure shows that just a minor sedimentation start to be slightly notable after 24 hrs in a motionless state. Due to the fact that during the experimental study, the binary nanofluids were in constant recirculation, sedimentation was not a problem. Once test facility was stopped and passed 3 days (weekends), sedimentation was observed; however, when turning on the solution recirculation pump and after some minutes, the binary nanofluids become again homogeneous.

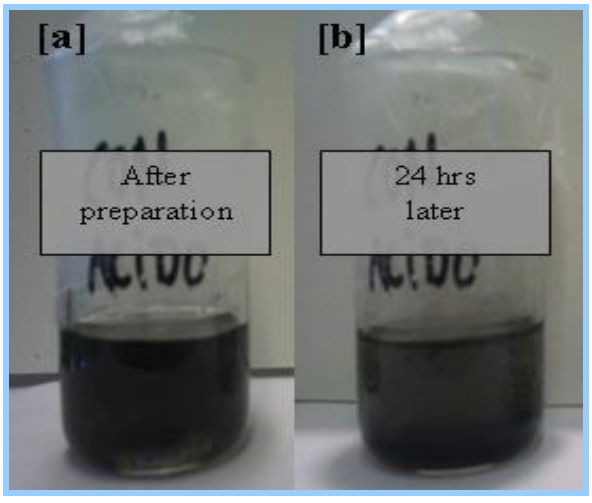

Figure 4.43 - CNTs in the base mixture $NH_3/LiNO_3$.

4.3.3.4 Effect of carbon nanotubes on the absorber performance

In this subsection, the effect of the CNTs addition into the base mixture $NH_3/LiNO_3$ on the absorber performance is studied. Concentration of the CNTs was set to 0.01 wt. %. Experiments were conducted varying the solution mass flow and cooling-water temperature. Results with the binary nanofluids and base mixture $NH_3/LiNO_3$ using the tubular absorber with an inner smooth surface tube are compared.

Figure 4.44 compares NH_3 absorption mass fluxes in a vertical smooth tube absorber using the base mixture and the nanofluids solution. Figure 4.44 shows that at a cooling-water temperature of 40 °C, NH_3 absorption mass flux for the base mixture $NH_3/LiNO_3$ slightly varies between 0.0032 to a maximum of 0.0035 $kg.s^{-1}m^{-2}$, however it is observed an important difference when the nanofluids are under study. In that case, the NH_3 absorption mass flux improves from 0.0038 to a maximum of 0.0054 $kg.s^{-1}m^{-2}$ when the solution mass flow is changed from 20 to 70 $kg.h^{-1}$. Moreover, at a cooling-water temperature of 35 °C, NH_3 absorption mass flux values for the base mixture increase from 0.0039 to 0.0042 $kg.s^{-1}m^{-2}$ while from 0.005 to a maximum of 0.0063 $kg.s^{-1}m^{-2}$ for the nanofluids when the solution mass flow is changed from 20 to 65 $kg.h^{-1}$. The maximum values achieved with the nanofluids were around 1.64 and 1.48 times higher than results with the base mixture at cooling-water temperatures of 40 °C and 35 °C, respectively. Results in this figure agree with observations reported by Kim et al. (2006b), who concluded that the lower absorption potential is, the higher effect the addition of nanoparticles is.

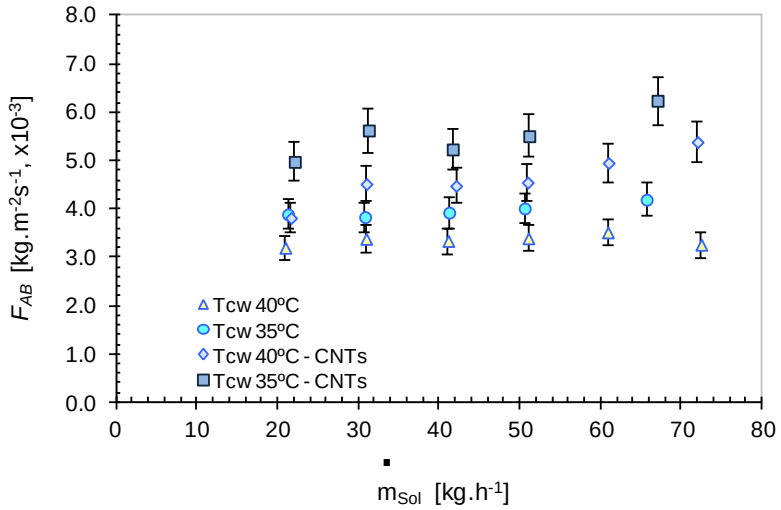

Figure 4.44 - Effect of carbon nanotubes on NH_3 absorption mass flux.

Moreover, Figure 4.45 shows that at a cooling-water temperature of 35 °C, the heat transfer coefficient increases from 0.88 to a maximum of 1.50 $kW.m^{-2}K^{-1}$ for the base mixture and from 1.07 to a maximum of 2.09 $kW.m^{-2}K^{-1}$ for the binary nanofluids when the solution mass flow was varied from 20 to 65 $kg.h^{-1}$. In addition, results at a cooling-water temperature of 40 °C range between 1.20 and 1.78 $kW.m^{-2}K^{-1}$ for the base mixture and between 1.13 and 2.06 $kW.m^{-2}K^{-1}$ for the binary nanofluids. According to these results, difference between results with the nanofluids and base mixture is clearer at a cooling-water temperature of 35 °C because of the wider difference between inlet

temperatures for these experiments. The maximum solution heat transfer coefficient value obtained with the binary nanofluids is around 1.39 times higher than with the base mixture at a cooling-water temperature of 35 °C and a solution mass flow of 65 kg.h^{-1}. As depicted in Figure 4.45, solution heat transfer coefficients for each case study are close due to a similar increment the absorber thermal load (Figure 4.46) and also in the LMTD (Figure 4.47).

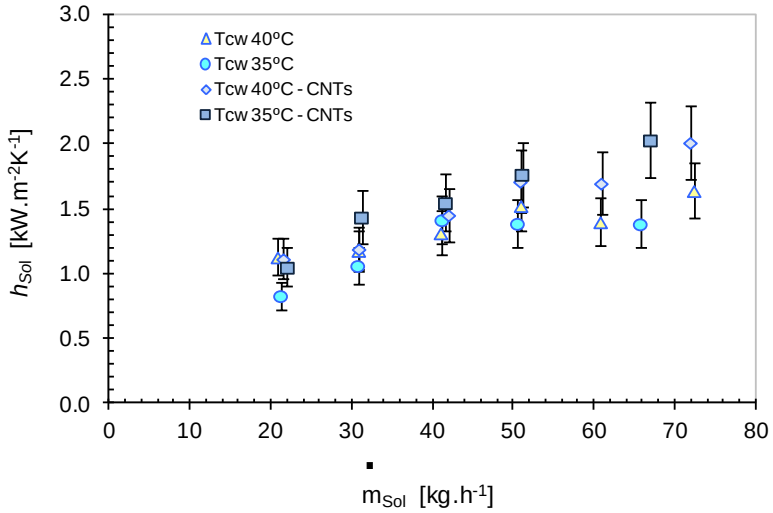

Figure 4.45 - Effect of carbon nanotubes on solution heat transfer coefficient.

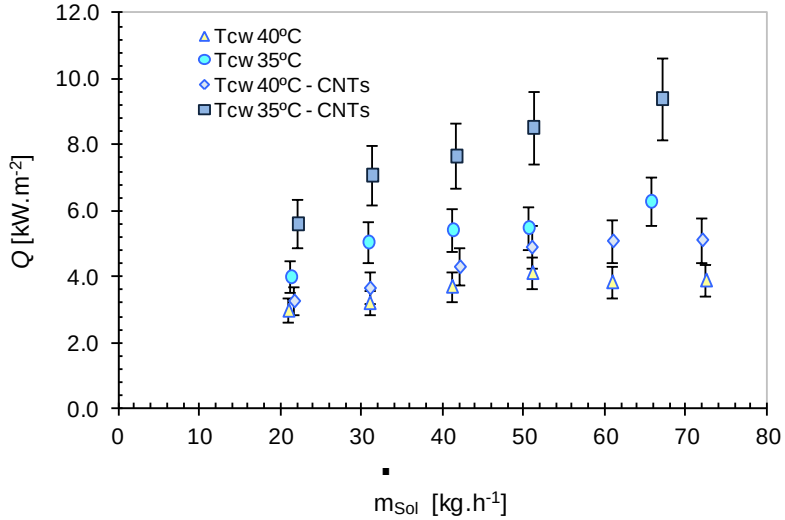

Figure 4.46 - Effect of carbon nanotubes on absorber thermal load.

Figure 4.46 illustrates the absorber thermal load with the binary nanofluids reports an upper value around 1.32 and 1.49 times higher than with the base mixture at cooling-water temperatures of 40 and 35 °C, respectively. Figure 4.46 presents that at a cooling-water temperature of 40 °C, thermal load increases from 3.0 to 3.9 kW.m^{-2} using the base mixture and from 3.3 to 5.1 kW.m^{-2} with the nanofluids by changing the solution low from 20 to 71 kg.h^{-1}. In contrast, at a cooling-water temperature of 35 °C, thermal load using the nanofluids increases from 5.6 to 9.4 kW.m^{-2} and from 4.0 to 6.3 kW.m^{-2} with the base mixture when the solution flow is varied from 20 to 65 kg.h^{-1}.

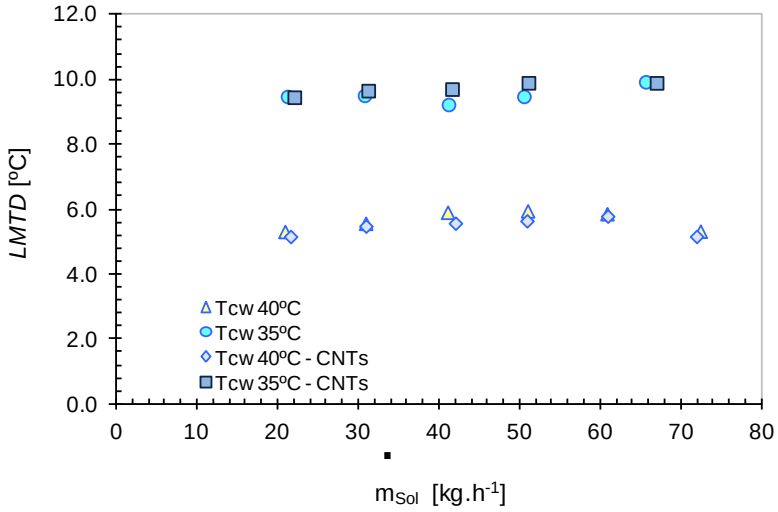

Figure 4.47 - Effect of carbon nanotubes on LMTD.

According to thermal load results, CNTs have a more positive effect on heat transfer when the inlet solution and cooling-water temperature difference is wider. Results also indicate that the addition of CNTs has a higher effect on the absorption rates than in the thermal load and also that cooling-water temperature showed a more important effect on the thermal load than on the absorption rates.

In relation to the LMTD, Figure 4.47 shows values obtained with both binary nanofluids and base mixtures are similar. These results are attributed to increments noted in the outlet cooling-water temperatures for the binary nanofluids which are balanced with increments observed in the outlet solution temperature resulting in similar LMTD if compared with those of the base fluid.

Regarding the subcooling degree of the solution leaving the absorber, Figure 4.48 shows that subcooling values, which are below 6 ºC, are relatively higher for a cooling-water temperature of 35 ºC and also that subcooling is slightly affected by the solution mass flow at the studied operating conditions.

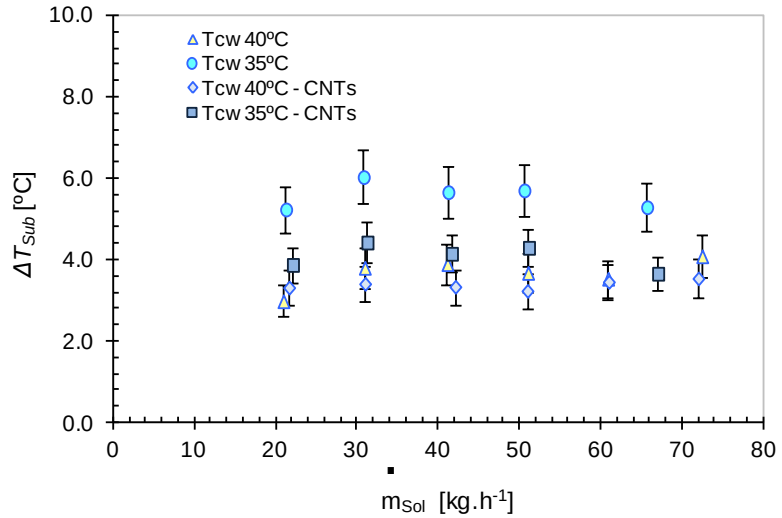

Figure 4.48 - Effect of carbon nanotubes on subcooling at the outlet of the absorber.

Figure 4.49 shows the experimentally measured pressure drops in the smooth tube absorber with the base mixture of $NH_3/LiNO_3$ and nanofluids as a function of solution mass flow rate. It is evidenced that pressure drops in the smooth tube and the base mixture with and without CNTs are similar so at the operating conditions selected in this work, the use of low CNTs fraction represents important advantages without penalizing pressure drop.

Since experimentation was performed from a macroscopic point of view to quantify the effect of CNTs in a bubble absorber with the $NH_3/LiNO_3$ mixture, study on the mechanisms involved in the heat and mass transfer enhancement by adding nanoparticles to a base fluid was not possible. According to studies found in the open literature (Keblinski et al., 2002, Buongiorno, 2006, Krishnamurthy et al., 2006, and Torres Pineda et al., 2012), It has been observed that nanoparticles slip mechanisms could explain these phenomena but the effect of each mechanism will differ depending of the conditions and approaches of each investigation. According to the study reported by Cuenca et al. (2013b), CNTs improve the thermal conductivity of the base mixture under study but the improvement obtained (up to 7.5 % at a CNTs concentration of 0.01 %) was not so high to be considered as the main reason that explain the results achieved in the present experimental study. Anyhow, results presented show clear evidences and confirm that CNTs significantly improve heat and mass transfer processes.

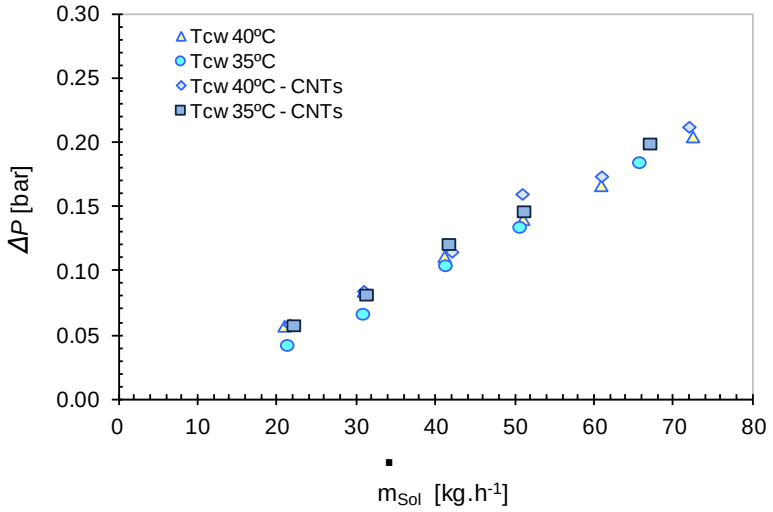

Figure 4.49 - Effect of carbon nanotubes on total pressure drop.

4.3.3.5 Simultaneous effect of nanoparticles and advanced surfaces

In this subsection, comparison between experimental results of the single and simultaneous effect of carbon nanotubes and advanced surfaces on the absorber evaluation parameters is presented. The inner tubes have an outer diameter of 8.0 mm and measure 1 meter in length. For this study, the CNTs concentration in the base mixture $NH_3/LiNO_3$ was set to 0.01 wt. % while the cooling-water temperature was set to 40 ^oC.

Figure 4.50 shows NH_3 absorption mass flux values for each experimentally evaluated case study. It can be observed that NH_3 absorption mass flux values for the base mixture

$NH_3/LiNO_3$ in the advanced surface tube are close to those with binary nanofluids in the internal smooth tube at low solution flows. However, at high solution flows, the effect of the advanced surfaces on the NH_3 absorption mass flux is more pronounced. NH_3 absorption mass flux values for base mixture $NH_3/LiNO_3$ in the advanced surface tube are around 1.09, 1.17 and 1.14 times higher than those with the binary nanofluids in the smooth tube at solution mass flows of 40, 50, and 70 $kg.h^{-1}$, respectively. In addition, simultaneous effect of the CNTs and advanced surfaces on the absorber performance was also investigated. Figure 4.50 also shows that combination of both intensification techniques resulted in a sharp increment in the absorption capacity of the solution. For this case, absorption mass flux increases from 0.0041 to a maximum of 0.0063 $kg.s^{-1}m^{-2}$ which represents values around 1.61 and 1.80 times higher than those results with the base mixture $NH_3/LiNO_3$ in the smooth tube. Nevertheless, it can be seen that the benefit achieved by the combined effect of the carbon nanotubes and advanced surfaces is more significant at low solution mass flows and also that this benefit is gradually less pronounced at high solution mass flows getting close to those results obtained with the base mixture and advanced surfaces which would mean that at these conditions of solution flows, the nanofluids achieves its maximum NH_3 absorption capacity.

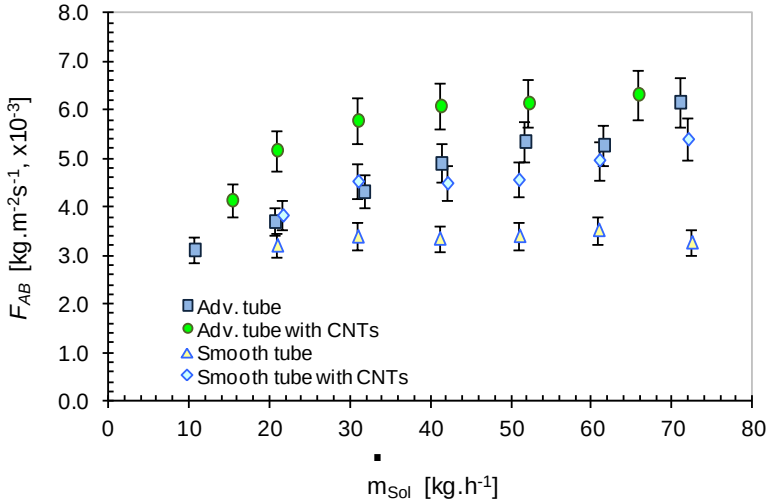

Figure 4.50 - Effect of carbon nanotubes and advanced surfaces on NH_3 absorption mass flux.

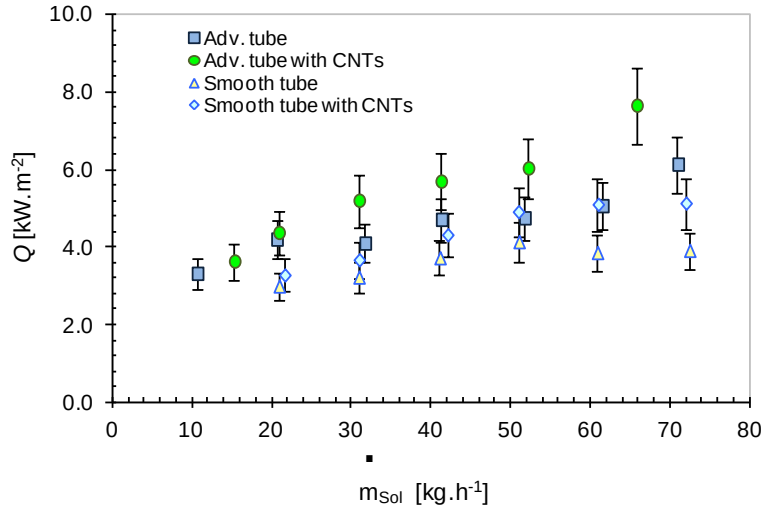

Figure 4.51 - Effect of carbon nanotubes and advanced surfaces on absorber thermal load.

Regarding the absorber thermal load and solution heat transfer coefficient, Figure 4.51 shows that as in the absorption mass flux, similar tendencies in the thermal loads were obtained when using the binary nanofluids with the smooth surface tube and base mixture $NH_3/LiNO_3$ with the advanced surface tube. Besides, Figure 4.52 shows that solution heat transfer coefficient values using the binary nanofluids in the smooth tube were slightly lower than values with the base mixture in the advanced tube. Moreover, it can be noted a more significant increase in the thermal load and solution heat transfer coefficient mainly at the highest solution flow rates when the CNTs and advanced surface tube were simultaneously implemented.

Results with the simultaneous implementation of CNTs and the advanced surface tube show a clear sign of a synergistic effect. According to Figure 4.52, thermal load and solutions heat transfer coefficient values increase from 3.6 to 7.6 $kW.m^{-2}$ and from 1.1 to 3.2 $kW.m^{-2}.K^{-1}$, respectively, in which the highest thermal load and heat transfer coefficient values are around 1.35 and 1.40 times higher, respectively, than those values achieved with the base mixture $NH_3/LiNO_3$ using the advanced surface tube. In this case, improvements on the heat transfer coefficient at high solution flows were more pronounced due to the increase in the thermal load and also because the logarithmic mean temperature differences obtained by implementing CNTs and the advanced surfaces were slightly lower. Induced turbulence by the tube advanced surface and constant nanoparticles interaction with the boundary wall may facilitate the bubble breaking, its absorption and an important increment in the heat transfer.

Subcoolings at the absorber outlet for the studied conditions were lower than 4 °C (Figure 4.53). Simultaneous implementation of the CNTs and advanced surfaces improves the absorption rates, and therefore the higher concentration difference obtained at the outlet of the absorber with respect to the base cases, results in a lower equilibrium temperature at the outlet of the absorber, which at the same time kept low the difference with respect to the actual outlet solution temperature.

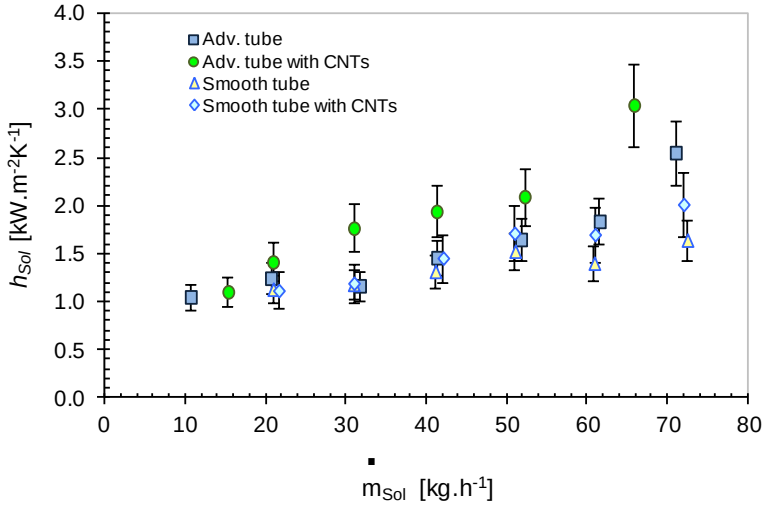

Figure 4.52 - Effect of carbon nanotubes and advanced surfaces on solution heat transfer coefficient.

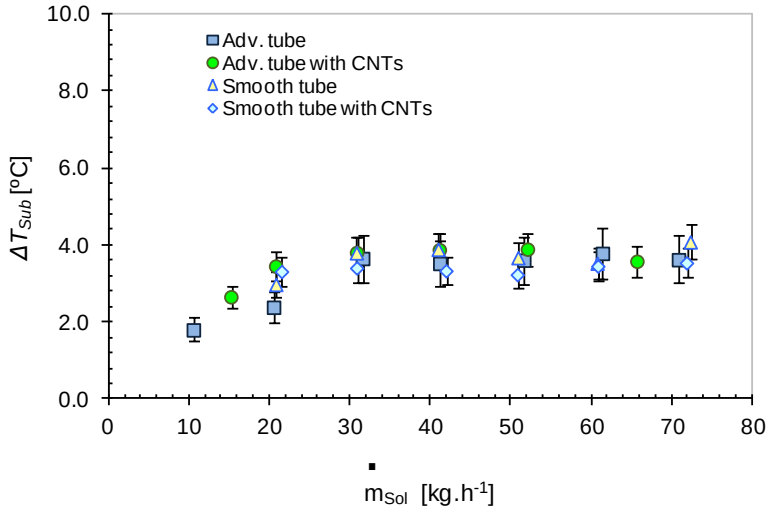

Figure 4.53 - Effect of carbon nanotubes and advanced surfaces on subcooling at the outlet of the absorber.

4.3.3.6 Effect of carbon nanotubes concentration

This sub-section shows results from experiments conducted to study the effect of CNTs with concentration of 0.01 and 0.02 wt. % on the absorber performance using the advanced surface tube. For the experiments, cooling-water temperature was set to 40 and 35 ºC changing the solution mass flow from 15 to 65 kg.h^{-1}. Experiments were not performed using higher CNTs concentration due to the fact that CNTs stability in the base fluid was poor. Same stability results were obtained in the thermal conductivity study conducted by Cuenca et al. (2013b) with the $NH_3/LiNO_3$ mixture with CNTs.

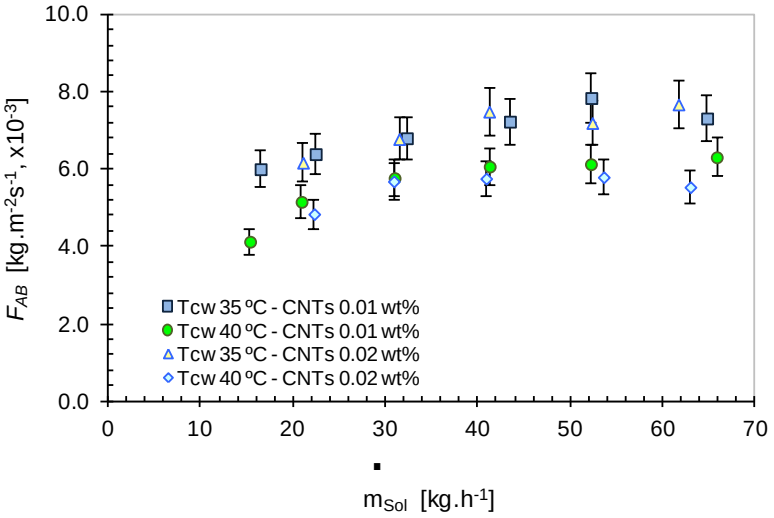

Figure 4.54 - Effect of carbon nanotubes concentration on NH_3 absorption mass flux.

In Figure 4.54 can be observed that no significant variations are obtained on the NH_3 absorption mass flux when CNTs concentrations of 0.01 to 0.02 wt. % are used in the base mixture. The absorption mass flux at a cooling-water temperature of 40 ºC and CNTs concentration of 0.02 wt. % increases from 0.0049 to a maximum of 0.0058 kg.s^{-1}m^{-2}.

Furthermore, at a cooling-water temperature of 35 ºC and CNTs concentration of 0.01 wt. %, NH_3 absorption mass flux shows an increase from 0.006 to a maximum of 0.0078 $kg.s^{-1}m^{-2}$. According to results, absorption mass flux values at a cooling-water temperature of 35 ºC are in average around 1.28 times higher than those results at a cooling-water temperature of 40 ºC.

Similarly, absorber thermal load results show no important differences when CNTs concentration is changed from 0.01 to 0.02 wt. % (Figure 4.55). At cooling-water temperature of 35 ºC, thermal load increases from 6.5 to 13.4 $kW.m^{-2}$ when the solution mass flow is varied from 15 to 65 $kg.h^{-1}$. According to results at cooling-water temperature of 35 ºC and CNTs concentration of 0.01 wt. %, values are 1.75 times higher than thermal load results at cooling-water temperature of 40 ºC.

Regarding the solution heat transfer coefficient, values depicted in Figure 4.57 at the two cooling-water temperature and CNTs concentration established are similar and follow a similar trend. The solution heat transfer coefficient values range between 1.12 and 3.65 $kW.m^{-2}K^{-1}$.

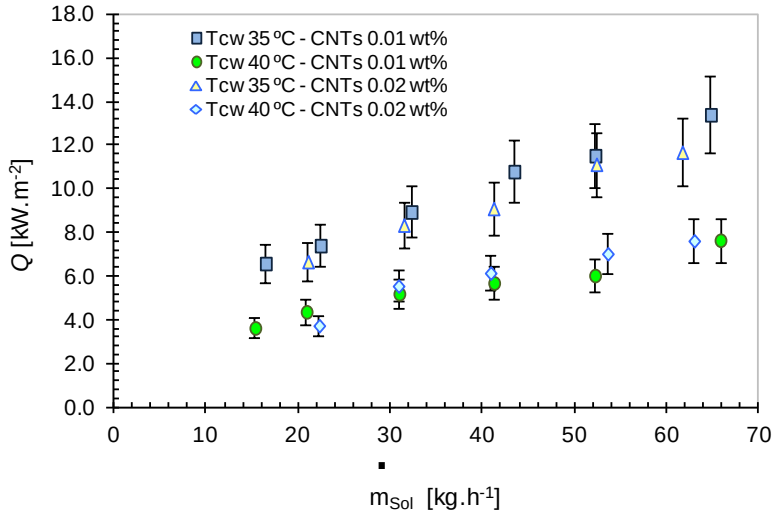

Figure 4.55 - Effect of carbon nanotubes concentration on absorber thermal load.

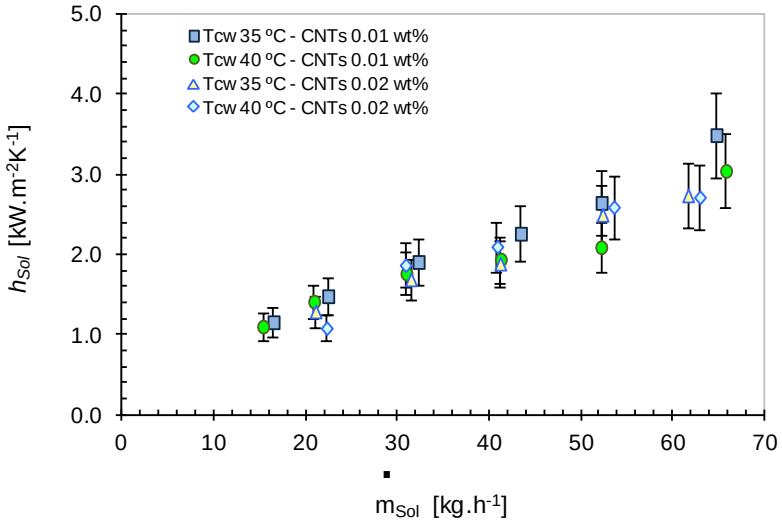

Figure 4.56 - Effect of carbon nanotubes concentration on solution heat transfer coefficient.

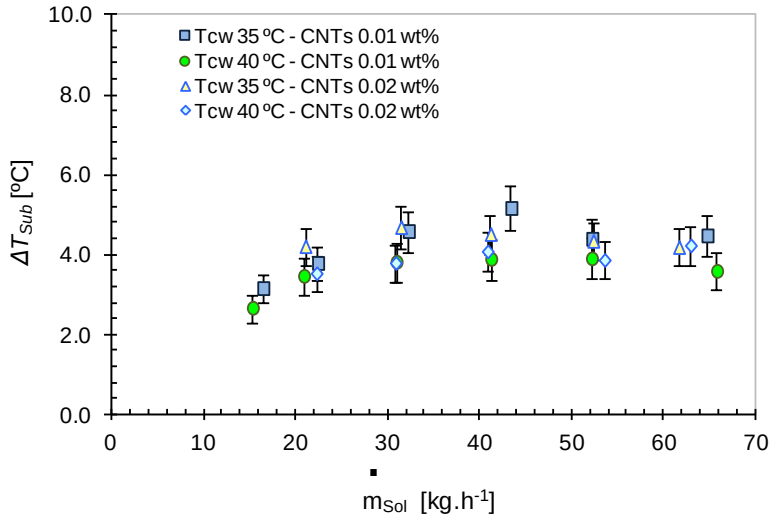

Figure 4.57 - Effect of carbon nanotubes concentration on subcooling at the outlet of the absorber.

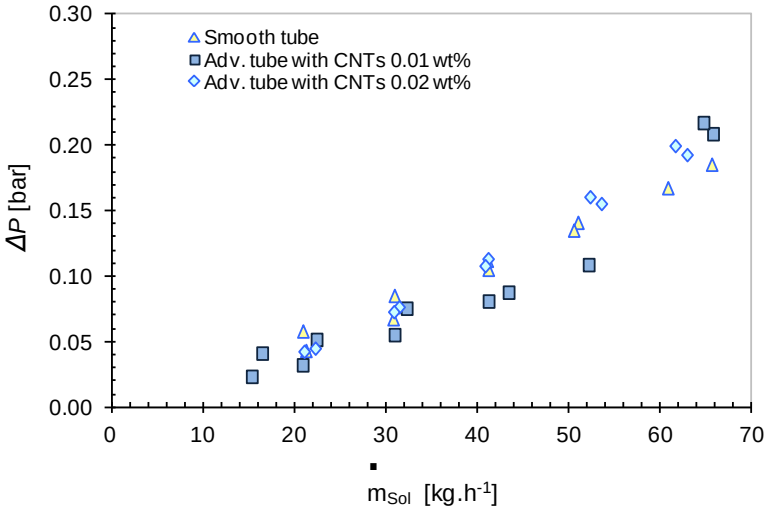

Figure 4.58 - Effect of carbon nanotubes concentration on total pressure drop.

In addition, Figure 4.57 shows that for all the experiment presented in this sub-section, subcooling values of the nanofluids solution at the outlet of the absorber were lower than 5.5 ºC achieving in all the experiments the maximum solution capacity to absorb ammonia.

Finally, Figure 4.58 depicts total pressure drop values obtained in the tubular absorber using the advanced surfaces and the CNTs with concentration 0.01 and 0.02 wt. %. Results with CNTs concentration of 0.01 wt. % show pressure drop values slightly lower than those values with the smooth tube and the base mixture. However, pressure drop when the CNTs concentration is set to 0.02 wt. % results slightly higher than values with the base mixture in the smooth tube absorber.

4.3.3.7 Experimental uncertainty of results

Based on the accuracy of the measuring instruments and the method for calculating uncertainties propagation described in Chapter 4, Table 4.7 shows the uncertainty

intervals of the calculated parameters presented in sub-section 4.3.3 for the tubular absorber configurations studied implementing CNTs and advanced surfaces. Uncertainty intervals were calculated taking into consideration a 95 % confidence interval.

Table 4.7 - Summary of uncertainty of the calculated parameters.

Parameters	Uncertainty
Tube diameter, mm	0.02
Tube length	± 0.5 %
Calculated parameters	
NH_3 absorption mass flux, F_{AB}	± 7.1 %
Thermal Load, Q_{AB}	± 13.6 %
Solution heat transfer coefficient, h_S	± 17.0 %
Subcooling, ΔT_{Sub}	± 11.7 %

4.3.4 Summary of the improvements achieved

Figure 4.59 and Figure 4.60 show the improvements achieved on the absorption mass flux, thermal load and solution heat transfer coefficient at solution mass flows of 40 and 60 $kg.h^{-1}$ by applying the passive intensification techniques previously described. Figure 4.59 shows the improvements obtained at an inlet cooling-water temperature of 40 °C while Figure 4.60 illustrates the improvements obtained at an inlet cooling-water temperature of 35 °C.

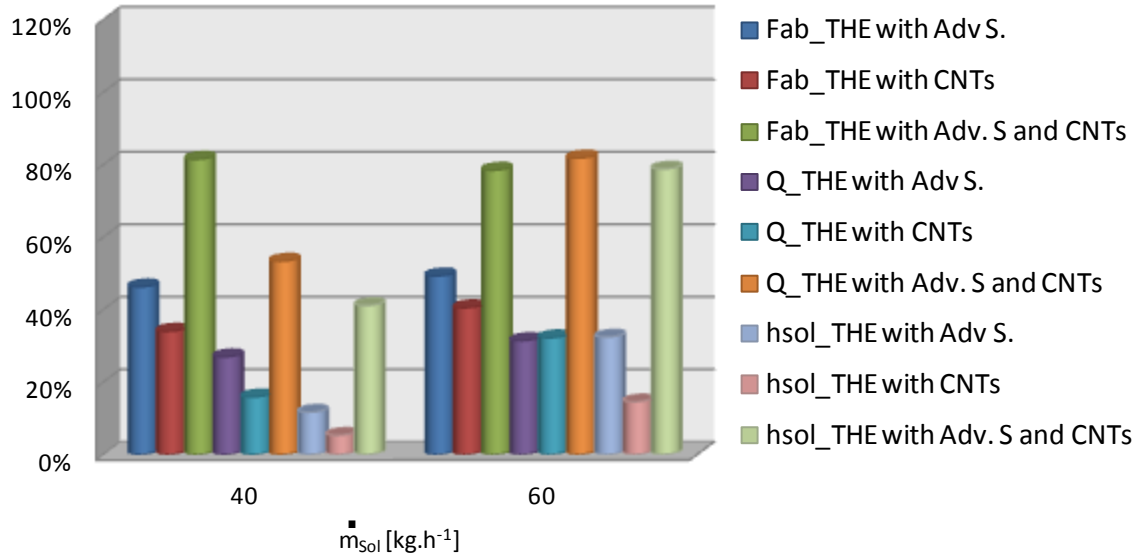

Figure 4.59 - Improvement of the NH_3 absorption mass flux (Fab), thermal load (Q) and solution heat transfer coefficient (hsol) applying passive intensification techniques at an inlet cooling-water temperature of 40 °C.

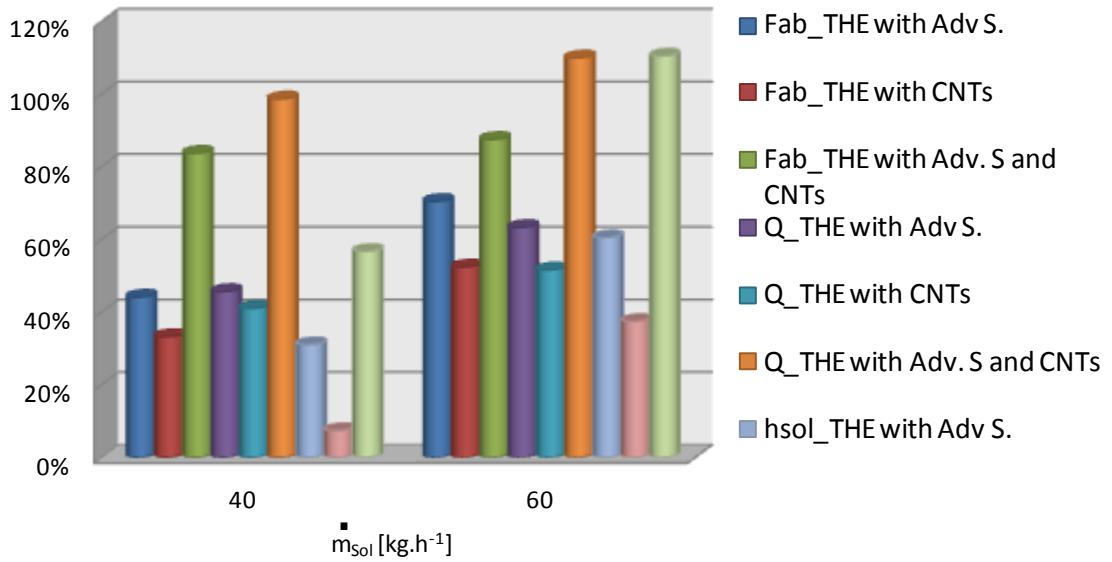

Figure 4.60 - Improvement of the NH_3 absorption mass flux (Fab), thermal load (Q) and solution heat transfer coefficient (hsol) applying passive intensification techniques at an inlet cooling-water temperature of 35 ^oC.

From these figures can be drawn the next points:

- When the inlet temperature difference between the solution and cooling-water is narrow, individual use of advanced surfaces and CNTs with direct contact with the solution side affects more positively the mass transfer than the heat transfer.
- Effect of advanced surfaces is more intense than the effect of nanoparticles (CNTs).
- Effect of the studied intensification techniques is more intense by increasing the solution mass flow.
- At these conditions, simultaneous use of advanced surfaces and CNTs shows an important synergic effect on mass and heat transfer.
- Individual effects of advanced surfaces and CNTs are more intense when reducing the cooling-water temperature due to the greater potential for the heat dissipation.
- When reducing the cooling-water temperature, effect of the simultaneous use of advanced surfaces and CNTs is higher on the heat transfer than in the mass transfer.

4.4 Conclusions

Results from experiments on the NH_3 absorption process in bubble absorbers with the $NH_3/LiNO_3$ mixture have been presented and discussed.

Operating conditions of the experiments were obtained from a thermodynamic simulation of a single stage absorption refrigeration cycle with $NH_3/LiNO_3$ at absorption/condensation, evaporation and generation temperatures of 40 ^oC, 5 ^oC and 90 ^oC, respectively. At these conditions, COP of the cycle was of 0.6 which makes the absorption refrigeration cycle with $NH_3/LiNO_3$ suitable to be air-cooled and operated at low temperature heat sources such as solar or waste heat.

Experiments were aimed to the intensification of the NH_3 absorption process in bubble absorbers using passive techniques. For this, two types of heat exchangers working as bubble absorbers were tested; a plate heat exchanger with H-type corrugations and a tubular heat exchanger with advanced surfaces.

Experimental results involved the analysis of parameters such as overall NH_3 absorption mass flux, absorber thermal load, solution heat transfer coefficient, solution mass transfer coefficient and degree of subcooling at the absorber outlet.

Initially, results from the NH_3 absorption process in the plate heat exchanger with H-type corrugations with an angle of 30 degree from its horizontal axis were presented. Previously to evaluation of the NH_3 absorption process, experiments using water in both hot and cold sides were conducted and experimental heat transfer coefficients were correlated and presented. Then, main results using the plate absorber H-type were compared with results found in the literature with a plate absorber with Chevron L-type corrugations with an angle of 60 degree from its horizontal axis.

Experiments on the NH_3 absorption process using the plate absorber H-type resulted in maximum absorption mass fluxes of 0.0038 and 0.0072 $kg.m^{-2}s^{-1}$ at inlet cooling-water temperatures of 40 and 35 ^oC, respectively, and at a solution mass flow of 40 $kg.h^{-1}$.

At an inlet cooling-water temperature of 40 ^oC, the maximum absorption mass flux obtained in the plate H-type was similar to that value in the plate absorber L-type. However, the maximum absorption mass flux in the plate absorber H-type at a cooling-water temperature of 35 ^oC was 1.26 times higher than those values obtained in the plate heat exchanger L-type when the solution Reynolds number is varied from 15 to 40. In contrast, solution heat transfer coefficients in the plate absorber L-type were higher than those values in the plate absorber H-type at an inlet cooling-water temperature of 35 ^oC. Moreover, it was observed that experiments in the plate absorber H-type were performed at a higher cooling-water flow rate which has a positive effect on the absorption rate and according to this, effect of the angle of corrugation in the plate H-type on the absorption rates with respect to the plate L-type is rather insignificant.

In general terms, absorption mass flux and thermal load in the plate absorber increased when increasing the solution mass flow and cooling-water flow and by reducing the cooling-water temperature. From experimental results of the absorption process in the plate absorber H-type, parameters such as absorption mass flux, solution Nusselt number and Sherwood number were correlated satisfactorily predicting around 93 %, 90 % and 90 % of the experimental data of the absorption mass flux, solution heat and mass transfer coefficients with lower error than 15 %.

Experiments on the NH_3 absorption performance of a tubular bubble absorber using advanced and smooth surfaces were also conducted.

Experiments with the tubular absorber showed that the advanced surfaces used significantly improve the absorption process in the tubular bubble absorber analyzed in comparison with using a smooth tube. The effect of the advanced surfaces was larger when increasing the solution mass flow. At low cooling-water Reynolds numbers and solution mass flows of 40 and 50 $kg.h^{-1}$, absorption mass fluxes for the tube with advanced surfaces were around 1.46 and 1.57 times higher than the values achieved using the smooth tube. At high values of the cooling-water Reynolds number, absorption

mass flux values for the tube with advanced surfaces were around 1.71 and 1.54 times higher than those achieved using the smooth tube.

Improvements in the solution heat transfer coefficient were also obtained with advanced surface tube. These improvements, more pronounced at high solution mass flows, were around 1.11 and 1.55 times higher than values achieved using the smooth surface tube when the solution mass flow was set between 40 and 70 $kg.h^{-1}$. In addition, the advanced surface tubes tested increase heat and mass transfer coefficients without penalizing pressure drop.

The absorption mass flux, solution Nusselt number and Sherwood number were also correlated from experimental results of the absorption process in the tubular absorber with advanced and smooth surfaces.

Geometry parameters such as tube diameter and tube length are absolutely important in the tubular absorbers design. The absorber performance with two advanced surface tube diameters and three different lengths was analyzed. According to experimental results, absorption mass flux increased when reducing the tube diameter and decreased with the tube length extension. However, the larger area of the tube with higher diameter allows keeping the absorber thermal load. On the other hand, the increase in the tube length achieves a significant increase in the absorption capacity but in a smaller proportion to the increase of area.

Experiments on the performance of the tubular bubble absorber with multi walled carbon nanotubes in the base mixture $NH_3/LiNO_3$ and the smooth and advanced surface tube were also conducted. Results showed that carbon nanotubes significantly improve the NH_3 absorption process in the tubular bubble absorber with the $NH_3/LiNO_3$ mixture. With respect to the reference values, the maximum enhancements achieved on the absorption mass flux with binary nanofluids were around 1.64 and 1.48 times higher at cooling-water temperature of 40 and 35 ^oC, respectively, while the maximum solution heat transfer coefficient value obtained with the binary nanofluids was around 1.39 times higher.

It is clearly observed that effects of the intensification techniques on heat and mass transfer processes are more significant when increasing the solution mass flow. Additionally, it is evidenced that pressure drops was not affected by the CNTs fraction set at the operating conditions under study.

Effect of the simultaneous use of the carbon nanotubes and advanced surfaces was also studied. Results depicted an outstanding improvement in the absorption mass flux at low solution mass flow. However, at high solution mass flows, enhancements were less pronounced getting close to those results with the base mixture in the advanced surface tube. Moreover, an important synergic effect was observed in the solution heat transfer coefficient.

The implementation of passive intensification techniques directly to the solution side can affect more positively the mass transfer than the heat transfer reducing the limitation imposed by this last one.

The absorber performance with CNTs concentrations of 0.01 and 0.02 wt. % showed no remarkable differences. Low CNTs concentrations used in this work, showed good stability in the base fluid during experiments.

Chapter 5

Simplified Model for Bubble Absorbers

5.1 Introduction

This chapter focuses on the numerical study of a one-dimensional simplified model of the ammonia absorption process in bubble absorbers with the $NH_3/LiNO_3$ mixture.

It includes a review of the main numerical bubble absorber models found in the literature. Then, main aspects of the numerical model developed in this chapter are explained. Finally, results obtained from the numerical model are directly compared with those from the experiments using plate and tubular bubble absorbers with the $NH_3/LiNO_3$ mixture for the model validation.

In the numerical model, the absorber is discretized in consecutive small control volumes where energy and mass balances are solved simultaneously to obtain the output values which will be the input values of the immediately next control volume. For that, it is required the use of empirical heat and mass transfer correlations to perform energy and mass balances. Correlations were obtained from results of the experimental study showed in chapter 4. The numerical model allows predicting not only the overall heat and mass transfer in the bubble absorber but also concentration and temperature profiles along the absorber length.

The model is then divided in three main parts: first part includes input of the absorber geometry and input of parameters such as pressure, temperature, mass flow rate and concentration of the solution at the absorber inlet; pressure, temperature and mass flow rate of the cooling-water at the absorber inlet; and ammonia mass flow. Second part involves the thermodynamic properties and heat and mass transfer correlations, and the last part describes energy and mass balances in the control volume and the resolution method.

5.2 Literature Review of Bubble Absorbers Models

Bubble absorbers provide higher heat and mass transfer coefficients, have a better mixing between solution and refrigerant, and absorption process is simpler in comparison to falling film absorbers (Kang et al., 2000). Some numerical models of the absorption process have been developed for a better interpretation of the transport phenomena that take place in bubble absorbers. In this section, main numerical models of bubble absorbers for absorption refrigeration systems found in the literature are reviewed.

Infante Ferreira et al. (1984) developed a model that simultaneously calculates heat and mass transfer processes in a vertical tubular bubble absorber with different heights and diameters with NH_3/H_2O mixture for absorption refrigeration systems. In this model, mixture of NH_3/H_2O and ammonia vapor flow upward in co-current configuration and cooling fluid flows downward in the annulus in counter-current configuration. Authors considered that the vapor goes up through the absorber showing three flow patterns; churn flow, slug flow, and bubbly flow. In this numerical study, the model iterative calculations start from the defined inlet conditions taking into account also the outlet conditions from previous experimental studies carried out by the same authors. During the iterative calculations, model assumes arbitrary values for the heat and mass transfer

coefficients along the absorber length. Model iterative calculations finishes when calculated outlet conditions are equal to the experimental ones. Modeled overall heat and mass transfer coefficients presented good agreement with respect to experimental results; however, local values for parameters such as temperature and concentration were not showed. Subsequently, Infante Ferreira (1985a) reported numerical and experimental results of a vertical tubular bubble absorber, this time for the $NH_3/LiNO_3$ and NH_3/NaSCN mixtures. For the development of the numerical model, author applied Nusselt`s theory and penetration theory represented in partial differential equations to evaluate the heat and mass transfer coefficients, respectively, from the interface to the bulk solution and temperature profiles during the absorption process. According to data shown in this work for $NH_3/LiNO_3$, relation between the mass transfer coefficients predicted in this study and those values obtained experimentally ranged between 0.64 and 1.60.

Herbine and Perez-Blanco (1995) reported a numerical model of the absorption process in an NH_3/H_2O vertical tubular bubble absorber which yielded one dimensional temperature and concentration profiles along the absorber length for both liquid and vapor phase. Model used correlations from the literature for local heat and mass transfer coefficients for the liquid phase, bubble velocity and bubble diameter. In this study authors also assumed that the mass transfer for ammonia vapor was always in direction to the solution and a small amount of water moving in direction to the interface, which imply water desorption. Authors explained that it could occur due to the heat transfer rate in the liquid phase and latent heat released during the absorption process due to the ammonia phase change at the interface. With respect to the bubble diameter along the absorber length, authors obtained an initial increase of the bubble diameter, followed by a decrease. Finally, results were compared with experiments at the studied conditions resulting in reasonable agreements.

Sujatha et al. (1997a,b) developed a model of the absorption process in a vertical tubular bubble absorber working with R22-DMF, R22-DMA, R22-DMETEG, R22-DMEDEG and R22-NMP where heat and mass transfer equation are solved using a finite element method. In this model, solution and vapor flows upward in co-current in the inner tube, while coolant flows downward in the annulus. The numerical model developed was validated with experimental data for an ammonia-water absorption system reported by Keizer (1982). A correlation for the mass transfer coefficient obtained from the numerical analysis was suggested for vertical tubular bubble absorbers.

Merrill and Perez-Blanco (1997) analytically studied the bubble behavior from inception to its absorption into a liquid solution. Model developed, which was used to study the effect of the liquid subcooling, initial bubble diameter, liquid flow and other parameters on bubble collapse rates, use a finite difference method to solve the governing equations and their associated boundary. For this, authors assumed the bubble to be spherical during the absorption process, uniform vapor temperature and concentration and neglected inertial effects associated with liquid motion into the bubble. In this study authors explained that bubble collapses after a steady decline in its diameter due to the absorption. Otherwise, model was not validated with experimental studies.

Kang et al. (1998,2000) designed a numerical model for a plate heat exchanger working as a bubble absorber with NH_3/H_2O to simultaneously study the heat and mass transfer processes in the interface between vapor phase and bulk solution. The plate absorber had

an offset strip fin (OSF) in the coolant side, and the solution and vapor flows in counter-current configuration with vapor flowing upwards into the channel where the absorption process took place. In this model, correlations found in the open literature to estimate the heat and mass transfer rates in both liquid and vapor phases, the bubble size and gas hold-up were used. This model allowed analyzing parameters such as gas hold-up, bubble diameter, bubble slip velocity for counter flow and the interfacial area along the absorber length. In this study was found that heat transfer resistance is dominant in the vapor region while mass transfer resistance is dominant in liquid phase. Also that the gas hold-up, bubble size, and thus the mass transfer area decreased along the absorber length as a result of the vapor absorption. In addition, it was concluded that mass transfer area is more important that the heat transfer area in bubble mode and also that the bubble mode allows higher absorption rate, and thus smaller absorbers size in comparison the falling film mode. Model developed used heat and mass transfer correlations found in the open literature and furthermore, numerical results were not validated with experimental results.

Terasaka et al. (2002) modeled the ammonia absorption during the growth of bubble through an orifice into water. Model, which estimates the bubble growth curves, the bubble shapes, the bubble volume at its detachment and mass transfer, takes into account mass transfer resistances in the gas phase, at the gas-liquid interface and in the liquid phase. Study showed that the mass transfer in the liquid phase dominated the mass transfer rate throughout the bubble formation. Results from the model showed good accuracy with respect to experimental results carried out by the same author.

Lee et al. (2003) numerically studied the ammonia mass transfer process along a cylindrical bubble mode absorber with NH_3/H_2O and results were compared with experimental ones showing good agreement. In this work, authors neglected mass transfer in the vapor phase and use correlations found in the literature to estimate the bubble diameter and the heat and mass transfer coefficients in the liquid phase. The effect of parameters such input gas and solution, temperature and concentration of solution, and direction of flow on the absorption process were analyzed.

Kim et al. (2003b) theoretically studied the ammonia absorption process and flow characteristics in a bubble absorber with NH_3/H_2O obtaining local heat and mass transfer coefficients on the liquid side from equations found in the literature, however, comparison with experimental results was not done.

Elperin and Fominykh (2003) designed an analytical model which uses general diffusion and energy balance equations to study heat and mass transfer process at all stages of bubble formation and rise in a bubble absorber. For this, authors considered four stages of bubble formation and rise as follows; bubble formation at the orifice described by equations of non-steady convective diffusion, accelerating motion of a bubble after detachment described by unsteady convective diffusion under unsteady flow conditions, bubble rise with constant velocity described by equations of unsteady convective diffusion under steady flow conditions and bubble rise described by equations of constant velocity and steady convective diffusion under steady flow conditions. The initial bubble diameters calculated by this author at different solution concentrations are compared with measured values reported Kang et al. (2002). Values obtained with this model were found to have errors up to 15 % and 30 % for solution concentration of 0.00 and 0.20, respectively with respect to data of Kang et al. (2002).

Fernández-Seara et al. (2005) presented a differential mathematical model to analyze the heat and mass transfer process in a shell and tubes type heat exchanger working as a tubular bubble absorber with NH_3/H_2O. Model, which is solved using the finite-difference method, is based on mass and energy balances, employs local heat and mass transfer coefficients using correlations found in the literature and takes into account separately the churn, slug and bubbly flow patterns during the bubble rise along the absorber. In this study, authors evaluated the effects of tube diameter, length, solution concentration and coolant temperature on the absorber performance and confirm that heat and mass transfer in the vapor phase have an insignificant effect on the absorption process. Fernández-Seara et al., (2007) also presented a differential mathematical model of the absorption process in an air cooled tubular bubble absorber with NH_3/H_2O and evaluated the influence of fin spacing, tube row distribution, diameter, length and cooling air temperature and the air-facing velocity on the absorber performance.

Kim et al. (2007b) numerically analyzed the effect of nanoparticles and surfactants on the combined heat and mass transfer processes in a plate bubble absorber with NH_3/H_2O. The considered surfactants are 2-ethyl-1-hexanol (2E1H), n-octanol, and 2-octanol and nano-particles are copper (Cu), copper oxide (CuO), and alumina (Al_2O_3). In this study, aqueous solution and ammonia vapor flows upward in co-current configuration and cooling fluid flows in the same direction through coolant side. Authors included the effect of nanoparticles and/or surfactants in the numerical model by applying effective absorption ratios obtained from experimental studies performed by the same author (Kim et al. 2006a,b, 2007a) for each case. However, heat and mass transfer coefficients along the absorber for the solution and vapor phase were calculated from correlations found in the literature. Authors of this study concluded that the implementation of binary nanofluids and surfactants can reduce significantly the size of absorber.

Castro et al. (2009) modeled two air cooled NH_3/H_2O absorbers. One in bubble mode and the other in falling film mode. Mass absorbed and temperature profiles obtained from the bubble absorber model was compared with results from the model presented by Herbine and Pérez-Blanco (1995) and additionally, effect of air and solution flow on the absorber thermal load was presented.

Cerezo (2006) and Cerezo et al. (2010) theoretically studied the heat and mass transfer processes in an NH_3/H_2O bubble absorber. The bubble absorber was a plate heat exchanger formed by four plates with L type corrugations. Model is based on heat and mass transfer coefficients in the liquid and vapor phase interface calculated from correlations found in the literature. Studies by these authors involved parametric evaluation of temperatures, solution concentration, absorption rates, heat transfer coefficients in the solution and vapor interface, mass transfer coefficients in the solution and vapor interface, bubble diameter, bubble velocity, gas hold-up and mass transfer interface along the absorber length. It also includes quantification of the effect of parameters such as absorber pressure, solution and coolant flow, solution and coolant inlet temperature and initial solution concentration on the overall absorption rate and absorber thermal load. Overall values were compared with experimental results reported by the same authors and maximum differences of 28.4 % and 11.1 % for the overall absorption rate and absorber thermal load were obtained respectively. Additionally, Cerezo et al. (2011) reported a mathematical model of the absorption process in the plate bubble absorber with the NH_3/H_2O, $NH_3/LiNO_3$ and $NH_3/NaSCN$ mixtures as working

fluids. Authors performed a comparative analysis of the absorber performance with the three mixtures. Profiles along the absorber of parameters such as temperatures and thermal load for each mixture are presented; however, results with $NH_3/LiNO_3$ and NH_3/NaSCN mixtures were not validated with experimental data.

Suresh and Mani (2010) applied a phenomenological theory of heat and mass transfer initially proposed by Staicovici (2000a,b) to model the absorption of the R134a gas bubble in liquid R134a-dimethyl formamide (DMF) solution. With this model, the bubble dynamics during bubble growth and collapse were studied as well as the estimation of the liquid concentration, temperature, heat and mass transfer rates, and local heat and mass transfer coefficients at the bubble interface. For this, the heat and mass transfer in liquid phase were considered using Navier-Stokes equations. In the gas phase, first law of thermodynamics and Bernoulli's equation were applied, and in the in the gas–liquid interface, equations of motion, energy equation, gas mass balance and liquid mass balance equations were considered. Authors assumed the physical and thermo-physical properties of liquid medium as functions of liquid temperature. From this study, authors concluded that absorption efficiency increases as gas mass flow rate increases. Also, that the gas inlet temperature has little effect on the parameters under study. Finally, authors concluded that absorption efficiency decreases when solution pressure increases. Results from this model were validated with good agreement using experimental results of NH_3/H_2O solution.

5.3 Description of the Simplified Numerical Model

A one-dimensional simplified model for bubble absorbers was developed to analyze the performance of $NH_3/LiNO_3$ bubble absorbers at the conditions of interest. The model gives direct use to empirical heat and mass transfer correlations based on the experimental mean overall heat and mass transfer coefficients presented in Chapter 4.

Bubble absorber geometries analyzed with the model include plate and tubular absorbers which involved smooth and advanced surfaces. The plate absorbers consist in four plates (Chevron L and H type corrugations, see chapter 3) forming three channels where the solution and ammonia vapor flow in the central channel from the bottom of the absorber to up in concurrent configuration and cooling-water flow in countercurrent on both sides of the channel. The tubular absorbers consist of a double pipe heat exchanger (with internal smooth and advanced surfaces) where the solution and ammonia vapor flow in the internal tube from the bottom of the absorber to up in concurrent configuration while the cooling-water flow in countercurrent in the annular space (detailed geometrical characteristics are shown in Table 5.1).

The modeling of bubble absorber is performed by the discretization of the absorber in small control volumes where mass and energy balances are solved simultaneously. The control volumes are localized consecutively between the absorber inlet and outlet as shown in Figure 5.1.

The numerical model allows predicting concentration and temperatures profiles along the absorber and overall heat and mass transfer in the bubble absorber with the $NH_3/LiNO_3$ mixture.

For each case study, it is necessary the definition of the empirical heat and mass transfer correlations which were obtained from results of the experimental study presented in chapter 4, the bubble absorber geometry and input values such as pressure, temperature, mass flow rate, ammonia concentration in the $NH_3/LiNO_3$ mixture at the absorber inlet; pressure, temperature, mass flow rate of the cooling-water at the absorber inlet; and ammonia mass flow. Thermodynamic properties of the $NH_3/LiNO_3$ such as vapor pressure, heat capacity, density and viscosity reported by Libotean et al. (2007, 2008) were used for this study. Correlation used to determine the thermal conductivity of the $NH_3/LiNO_3$ was reported by Cuenca et al. (2013a). Equations for the determination of the thermodynamic and thermophysical properties are summarized in appendix B.

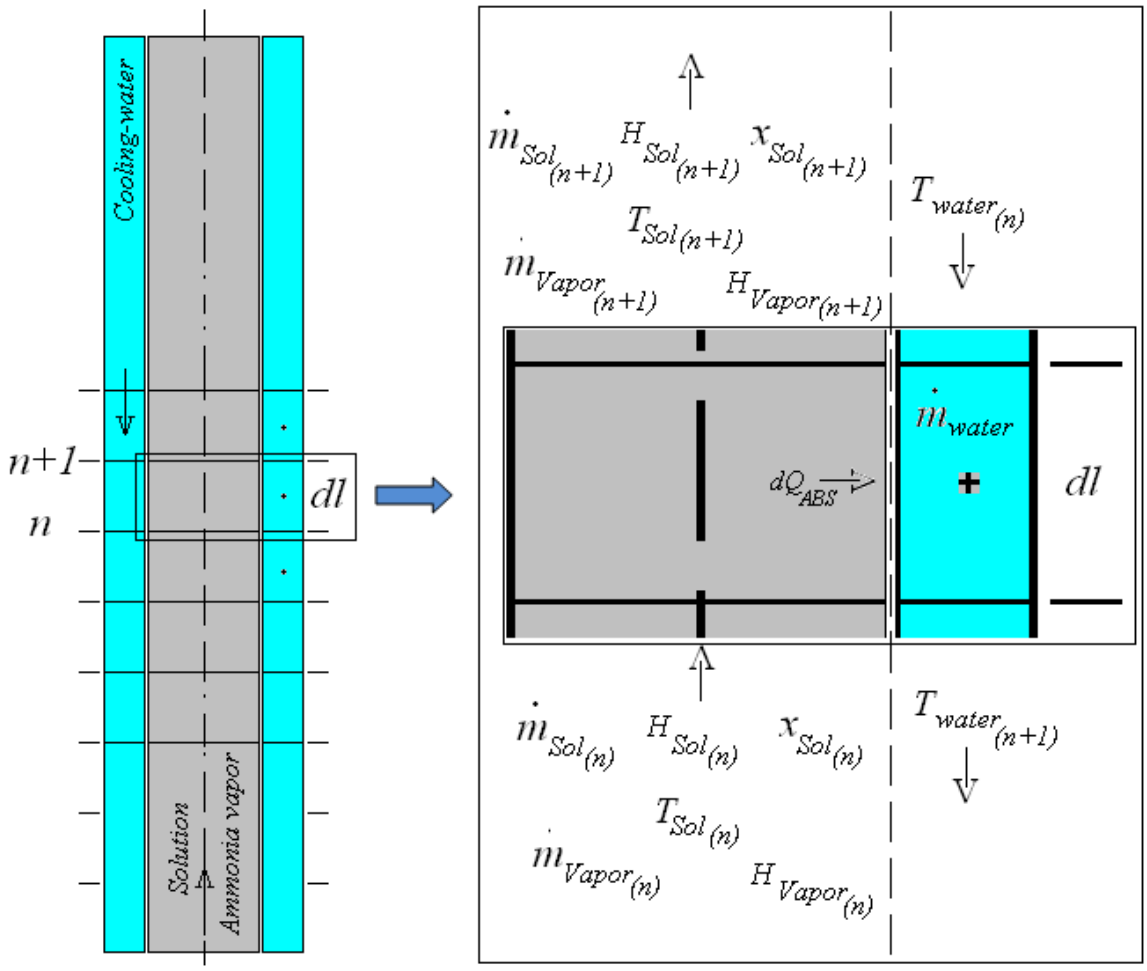

Figure 5.1 - Geometric discretization of the bubble absorber.

5.3.1 Assumptions for the numerical model design

The main assumptions considered for the design of the simplified bubble absorber numerical model are listed as follows:

- One-dimensional model.
- The absorption process is in steady state.
- The system pressure is constant.

- Only heat and mass transfer in the liquid phase is considered.
- Homogeneous solution at the inlet.
- Heat and mass transfer areas are considered equal.
- Ammonia vapor temperature equal to the bulk solution temperature.
- In the transversal section of each discrete volume, the cooling-water, solution and ammonia vapor properties are assumed to be constant.
- There is no heat loss to the surroundings.

5.3.2 Discretized governing equations

The numerical model developed for absorption process analysis in bubble absorbers is mainly based on equations for calculating thermodynamic properties of the $NH_3/LiNO_3$ solution and water, empirical correlations of overall heat and mass transfer (reported in Chapter 4) and energy and mass balances, which take into account the $NH_3/LiNO_3$ solution and ammonia vapor mass flows ($\dot{m}$), solution concentrations (x) and enthalpies (h) at the inlet and outlet of each discretized control volume.

Global mass balance:

$$\dot{m}_{Sol}(n+1)+\dot{m}_{Vap}(n+1)-\dot{m}_{Sol}(n)-\dot{m}_{Vap}(n)=0 \tag{5.1}$$

Partial mass balance:

$$\dot{m}_{Sol}(n+1)\cdot x_{Sol}(n+1)-\dot{m}_{Sol}(n)\cdot x_{Sol}(n)-d\dot{m}_{Sol}=0 \tag{5.2}$$

$$d\dot{m}_{Sol}=-d\dot{m}_{AB\_Vap} \tag{5.3}$$

$$x_{Sol}(n+1)=x_{Sol}(n)+dx_{Sol} \tag{5.4}$$

$$\dot{m}_{Sol}(n+1)=\dot{m}_{Sol}(n)+d\dot{m}_{Sol} \tag{5.5}$$

$$\dot{m}_{Vap}(n+1)=\dot{m}_{Vap}(n)-d\dot{m}_{AB\_Vap} \tag{5.6}$$

$$d\dot{m}_{Sol}=F_{AB}\cdot dTa \tag{5.7}$$

where F_{AB} is the NH_3 absorption mass flux, which was obtained for each case study by calculating first the Sherwood number (Sh) and then the mass transfer coefficient (k_m), Equations (5.8) and (5.9). Correlations used for calculating the Sherwood number are those presented in chapter 4. dTa is a differential transfer area for each control volume. In a plate absorber, the differential transfer area is calculated as $dTa_{PA}=2\cdot w\cdot dl$ while in a tubular absorber, $dTa_{TA}=\pi\cdot D_{outer}\cdot dl$. w refers to the plate width, dl is the differential length of each control volume and D_{outer} is the outer diameter of the inner tube.

$$\mathrm{Sh}_{Sol,Exp} = \frac{K_m \cdot D_h}{\beta_{Sol}} \tag{5.8}$$

$$K_m = \frac{F_{AB}}{LMXD} \tag{5.9}$$

Energy balance:

$$\dot{m}_{Sol}(n)H_{Sol}(n) + \dot{m}_{Vap}(n)H_{Vap}(n) - \dot{m}_{Sol}(n+1)H_{Sol}(n+1) - \dot{m}_{Vap}(n+1)H_{Vap}(n+1) = dQ_{AB} \tag{5.10}$$

where the absorber thermal load (dQ_{AB}) is expressed as in the next equation:

$$dQ_{AB} = U \cdot dTa \cdot (T_{Sol}(n) - T_{Cw}(n)) \tag{5.11}$$

The overall heat transfer coefficient (U) is found based in the heat transfer resistances from the bulk solution to the cooling-water side at the conditions of each control volume.

$$\frac{1}{U \cdot A} = \frac{1}{h_{Sol} \cdot A_{Sol\_Side}} + R_{Wall} + \frac{1}{h_{Cw} \cdot A_{Cw\_Side}} \tag{5.12}$$

h_{Sol} and h_{Cw} are the solution and cooling-water heat transfer coefficients, respectively. R_{Wall} refers to resistance of the wall material between the fluids. The convective heat transfer coefficients are calculated from Equations (5.13) and (5.14).

$$h_{Sol} = \frac{\mathrm{Nu}_{Sol} \cdot \lambda_{Sol}}{D_{h\_Sol\_Side}} \tag{5.13}$$

$$h_{Cw} = \frac{\mathrm{Nu}_{Cw} \cdot \lambda_{Cw}}{D_{h\_Cw\_Side}} \tag{5.14}$$

In this case, λ refers to the thermal conductivity of the fluids and D_h is the hydraulic diameter for each case.

Nusselt numbers (Nu) and Sherwood number (Sh) for each case study are those correlations experimentally obtained and presented in chapter 4. Correlations for the solution Nusselt number and Sherwood number for each absorber configuration are summarized below.

Correlations obtained from studies in the Plate absorber L-type (Oronel, 2010).

$$\mathrm{Sh}_{Sol} = 733 \cdot \mathrm{Re}^{0.36} \cdot \mathrm{Sc}^{-0.12} \cdot \left(\frac{T_{Sol,Eq,in}}{T_{Sol,in}}\right)^{-0.59} \cdot \left(\frac{T_{Sol,in}}{T_{Cw,in}}\right)^{1.99} \tag{5.15}$$

$$\mathrm{Nu}_{Sol} = 0.24 \cdot \mathrm{Re}^{0.80} \cdot \mathrm{Pr}^{1/3} \cdot \left(\frac{T_{Sol,Eq,in}}{T_{Sol,in}}\right)^{6.60} \cdot \left(\frac{T_{Sol,in}}{T_{Cw,in}}\right)^{-0.90} \tag{5.16}$$

Correlations obtained from studies in the Plate absorber H-type.

$$\mathrm{Sh}_{Sol} = 872358 \cdot \mathrm{Re}^{0.51} \cdot \mathrm{Sc}^{-1.08} \cdot \left(\frac{T_{Sol,Eq,in}}{T_{Sol,in}} \right)^{3.87} \cdot \left(\frac{T_{Sol,in}}{T_{Cw,in}} \right)^{2.97} \tag{5.17}$$

$$\mathrm{Nu}_{Sol} = 1.24 \cdot \mathrm{Re}^{0.60} \cdot \mathrm{Pr}^{1/3} \cdot \left(\frac{T_{Sol,Eq,in}}{T_{Sol,in}} \right)^{1.12} \cdot \left(\frac{T_{Sol,in}}{T_{Cw,in}} \right)^{-1.41} \tag{5.18}$$

Correlations obtained from studies in the 1 meter tubular absorber with smooth surfaces.

$$\mathrm{Sh}_{Sol} = 800 \cdot \mathrm{Re}^{0.09} \cdot \mathrm{Sc}^{0.043} \cdot \left(\frac{T_{Sol,Eq,in}}{T_{Sol,in}} \right)^{0.03} \cdot \left(\frac{T_{Sol,in}}{T_{Cw,in}} \right)^{-0.37} \tag{5.19}$$

$$\mathrm{Nu}_{Sol} = 0.42 \cdot \mathrm{Re}^{0.34} \cdot \mathrm{Pr}^{1/3} \cdot \left(\frac{T_{Sol,Eq,in}}{T_{Sol,in}} \right)^{4.58} \cdot \left(\frac{T_{Sol,in}}{T_{Cw,in}} \right)^{-0.1} \tag{5.20}$$

Correlations obtained from studies in the 1 meter tubular absorber with advanced surfaces.

$$\mathrm{Sh}_{Sol} = 872358 \cdot \mathrm{Re}^{0.49} \cdot \mathrm{Sc}^{-1.13} \cdot \left(\frac{T_{Sol,Eq,in}}{T_{Sol,in}} \right)^{3.87} \cdot \left(\frac{T_{Sol,in}}{T_{Cw,in}} \right)^{2.97} \tag{5.21}$$

$$\mathrm{Nu}_{Sol} = 0.80 \cdot \mathrm{Re}^{0.56} \cdot \mathrm{Pr}^{1/3} \cdot \left(\frac{T_{Sol,Eq,in}}{T_{Sol,in}} \right)^{-5.83} \cdot \left(\frac{T_{Sol,in}}{T_{Cw,in}} \right)^{-1.41} \tag{5.22}$$

Energy balances are also performed on the cooling-water side to calculate the cooling-water temperature at the outlet of each control volume.

$$dQ_{AB} = \dot{m}_{Cw} \cdot Cp_{Cw} \cdot [T_{Cw}(n+1) - T_{Cw}(n)] \tag{5.23}$$

Thermodynamic and transport properties of the $NH_3/LiNO_3$ mixture were calculated in function of the temperature and solution concentration.

$$P, H_{Sol}, \rho_{Sol}, \lambda_{Sol}, \mu_{Sol}, Cp_{Sol} \rightarrow f(T_{Sol}, x_{Sol}) \tag{5.24}$$

5.3.3 Resolution procedure

The resolution procedure follows a step by step process in which energy and mass balances in every control volume are solved sequentially. Resolution process starts from the first control volume, continuing with the immediately next section in the same solution flow direction until the last control volume.

Due to the fact that the solution and cooling-water flows are in counter current configuration, solution temperature at the outlet of the control volume and cooling-water

temperature at the inlet of the control volume need to be calculated by an interactive process.

Interaction process in each control volume ends when the energy balances achieve equilibrium and the initially defined inlet cooling temperature is equal to the calculated inlet cooling temperature. Software used for the numerical study was the Engineering Equation Solver (EES).

The resolution procedure of the model is summarized as follow and represented in a diagram, Figure 5.2 :

- Input of geometrical characteristics of the absorber and empirical correlations of heat and mass transfer.
- Input of operating conditions at the absorber inlet such as solution temperature $T_{Sol}(n)$, ammonia concentration in the $NH_3/LiNO_3$ mixture $x_{Sol}(n)$, solution mass flow $\dot{m}_{Sol}(n)$, solution-side pressure P_{Sol}, ammonia mass flow $\dot{m}_{Vap}(n)$, cooling-water temperature $T_{Cw}(n)$, cooling-water volumetric flow rate $V_{Cw}(n)$ and water-side pressure $P_{Cw}(n)$.

  Due to the configuration in counter-current, algorithm assumes an initial outlet cooling-water temperature higher than defined inlet cooling-water temperature.
- Evaluation of the control volume.
  - Call of thermodynamic properties.
  - Calculation of absorption mass flux F_{AB} and resolution of mass transfer balances in the control volume.
  - Evaluation of outlet solution and inlet cooling-water temperatures, heat transfer coefficients (h_{Sol}, h_{Cw}), and energy balances in the control volume. Model assumes an initial solution temperature at the outlet of the control volume *(n+1)* to calculate enthalpies, to perform the energy balances, and to determine the inlet cooling-water temperature of this section.

    If energy balances in the control volume achieve equilibrium, model resolution procedure continues with the study of the next control volume, if not, a new outlet solution temperature is assumed until energy balances achieve equilibrium. Secant method was used to obtain the solution temperature at the outlet of the control volumes.
- Once analysis achieves the last control volume, evaluation of cooling-water temperature at the absorber inlet is performed. Calculated inlet cooling temperature is compared with initially defined Inlet cooling-water temperature.

  If temperatures are equal, iterative process finishes and results of the absorber performance can be analyzed, if not, a new cooling-water temperature at the absorber outlet is assumed and calculation of the whole absorber through the control volumes start again.

  Secant method was used to obtain the cooling-water temperature.

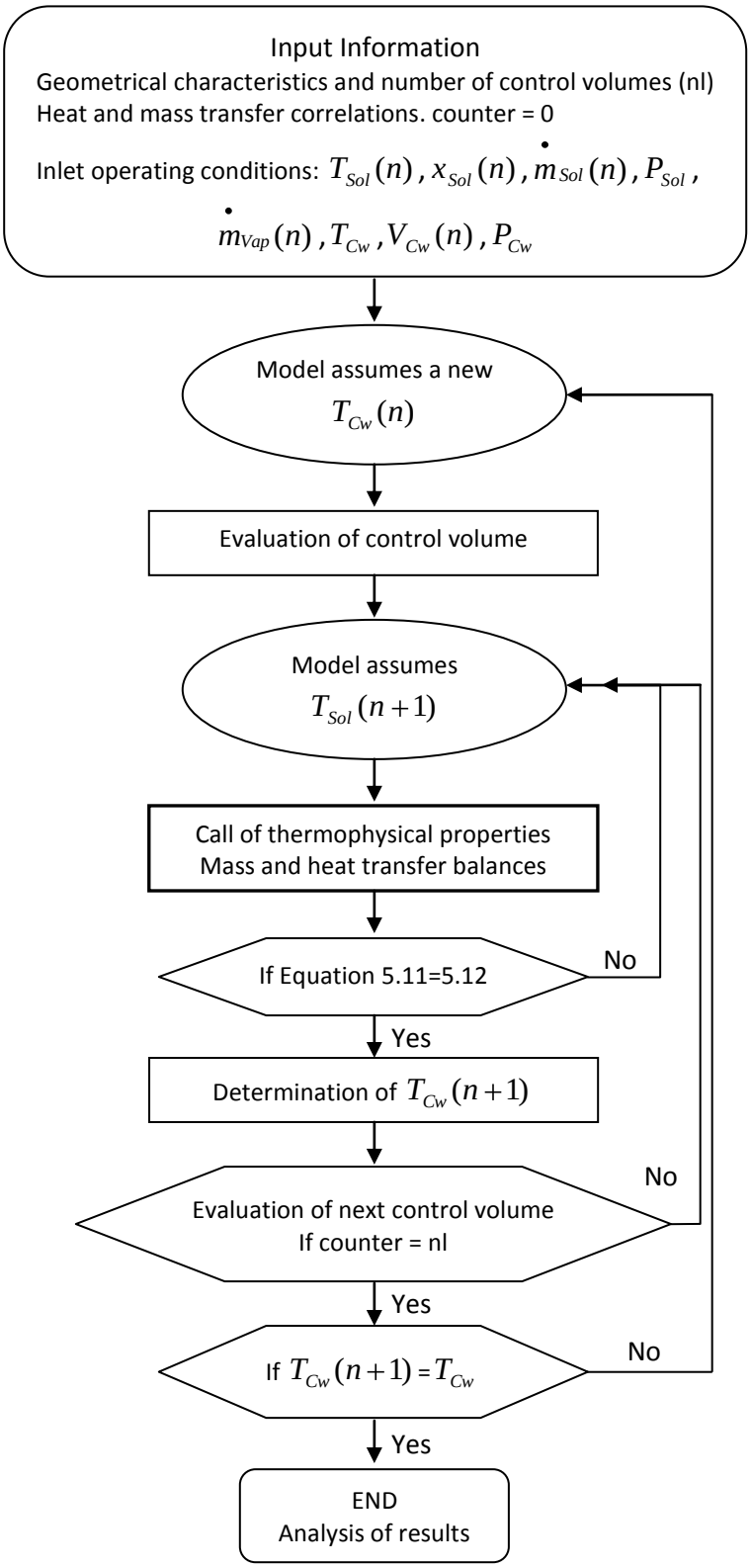

Figure 5.2 - Diagram of the model resolution procedure.

5.4 Results from the Simplified Model

In this section, results of the heat and mass transfer processes in bubble absorbers from the simplified model are compared with experimental result for its validation. Temperatures and ammonia concentration profiles in the absorbers are also predicted. Geometrical characteristics of two plate absorbers (Chevron H and L type corrugations) and two tubular absorbers (with smooth and advanced surfaces) are used for this study. Experimental results of heat and mass transfer processes $NH_3/LiNO_3$ mixture with the L type plate absorber were reported by Oronel (2010) while results with the H type absorber and tubular absorber are reported in chapter 4 of this thesis.

Main geometrical characteristics of the absorbers under study are presented in Chapter 3 and summarized in Table 5.1. Plate absorbers H and L differ in the angle of corrugations on the plate surfaces with respect to its horizontal axis. An angle of 30 ^{o} for the H-type plate while 60 ^{o} for the L-type plate. In the case of the tubular absorber, both advanced and smooth surfaces tubes present the same geometrical specification. The inner diameter (internal hydraulic diameter) of the advanced surface tube was measured at the fin tip diameter which resulted equal to the smooth tube.

Table 5.1 - Specifications of the plate and tubular absorbers.

Plate Absorbers	
Model	Type H-L
Absorbers Length, m	0.53
Absorber Width, m	0.112
Heat exchange area, m^2	0.1
Channel hydraulic diameter, m	0.004
Plate thickness, m	0.0004
Tubular Absorbers	
Absorbers Length, m	1.0
Heat exchange area, m^2	0.025
Internal hydraulic diameter, m	0.006
Annular hydraulic diameter, m	0.005

5.4.1 Prediction of overall heat and mass transfer rates

In this subsection, it is compared both experimental (Exp) and numerical (Mod) results from the simplified model at the same operating conditions. Inputs of operating conditions for the absorbers modelling are resumed in Table 5.2. Operating conditions are those of interest for a single-effect absorption refrigeration cycle with $NH_3/LiNO_3$ at evaporation and condensation/absorption temperatures of 5 ^{o}C and 40 ^{o}C, respectively.

In the next figures can be observed that results from the simplified model illustrate similar trends to experimental results. Detailed discussion of trends in the experimental results at the conditions under study was done in chapter 4. In addition, experimental errors presented in Chapter 4 are also shown in bars for the experimental results.

Table 5.2 - Operating conditions of the absorbers.

Parameters	Range
Solution temperature at the absorber inlet, °C	45
Cooling-water temperature at the absorber inlet, °C	35 and 40
Ammonia mass fraction in solution at the absorber inlet, $kg_{NH3}.kg^{-1}_{NH3/LiNO3}$	0.45
Absorber pressure, kPa	510
Solution mass flow rate, $kg.h^{-1}$	10-70
Cooling-water flow rate in the tubular absorber, $m^3.h^{-1}$	0.090-0.110
Cooling-water flow rate in the plate absorber, $m^3.h^{-1}$	0.130-0.450

5.4.1.1 Plate absorber H-type

Figure 5.3 shows the effect of cooling-water temperature, solution mass flow and cooling-water volumetric flow rate on absorption mass flux and absorber thermal load in the plate bubble absorber **H-type**. Results in Figure 5.3a,c were performed at a cooling-water volumetric flow rate of 0.268 $m^3.h^{-1}$ and in Figure 5.3b,d at a solution mass flow of 40 $kg.h^{-1}$.

Results from the numerical model in Figure 5.3a,c show that the absorption mass flux increases from 0.0028 to 0.0062 $kg.m^{-2}.s^{-1}$ and from 0.0019 to 0.0041 $kg.m^{-2}.s^{-1}$ at cooling-water temperatures of 35 and 40 °C, respectively, when solution mass flow is varied from 10 (Re 10) to 50 (Re 50) $kg.h^{-1}$. For the thermal load, values range from 4.7 to 12.2 $kW.m^{-2}$ and from 3.2 to 7.2 $kW.m^{-2}$ at cooling-water temperatures of 35 and 40 °C, respectively.

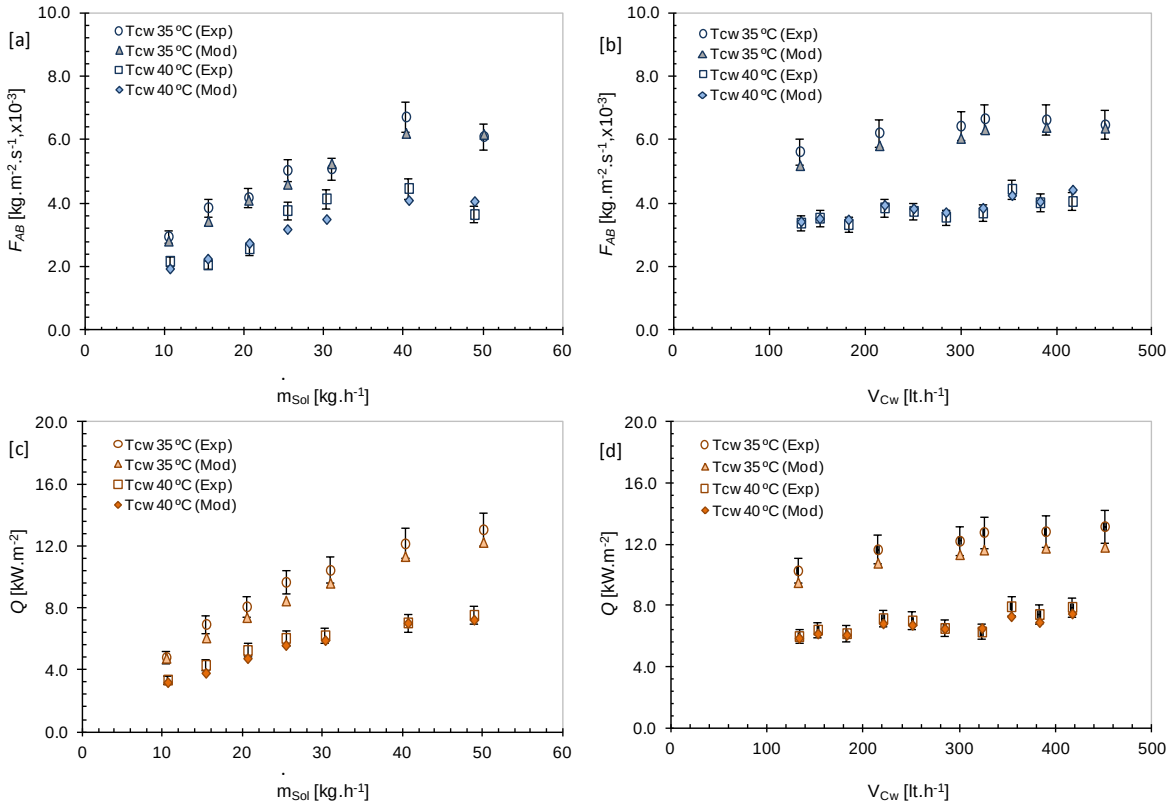

Figure 5.3 - Effect of cooling-water temperature, solution mass flow and cooling-water volumetric flow rate on: [a,b] Absorption mass flux and [c,d] Thermal load in a **Plate Absorber H-type.**

It is also observed in Figure 5.3b,d that the absorption mass flux from the model ranges between 0.0052 and 0.0064 $kg.m^{-2}.s^{-1}$, and between 0.0034 to 0.0044 $kg.m^{-2}.s^{-1}$ at cooling-water temperatures of 35 and 40 ^{o}C, respectively, when cooling-water flow rate is varied from 0.130 (Re 534) to 0.450 $m^{3}.h^{-1}$ (Re 1760).

For the thermal load, values range from 9.5 to 11.6 $kW.m^{-2}$ and from 6.1 to 7.4 $kW.m^{-2}$ at cooling-water temperatures of 35 and 40 ^{o}C, respectively. Once Reynolds numbers in turbulent flows are achieved, it can be noted that effect of the cooling-water flow rate on absorption mass flux and thermal load is not significant.

Results from the numerical model showed a maximum and a mean error with respect to experimental results of 15.8 % and 6.0 %, respectively, for the absorption mass flux. From all results, 83.3 % of the points showed an error lower than 10.0 %.

For the thermal load, a maximum and a mean error of 12.5 % and 6.4 %, respectively, were obtained where 86.7 % of the points showed an error lower than 10.0 %. In addition, in Figure 5.3 can be noted that errors between experimental and modelled results are higher at a cooling-water temperature of 35 ^{o}C.

5.4.1.2 Plate absorber L-type

Figure 5.4 shows a comparison between main experimental and modelled results of the heat and mass transfer processes in the **plate bubble absorber L-type**. It is also quantified the effect of cooling-water temperature and solution mass flow on absorption mass flux and absorber thermal load.

For this study, only heat and mass transfer correlations were changed into the model for the plate absorber H-type since geometrical specifications assumed of both plates are equal. Effects of the corrugations are involved in the heat and mass transfer correlations which were obtained experimentally.

Figure 5.4a shows that modelled absorption mass flux increases from 0.0024 to 0.0056 $kg.m^{-2}.s^{-1}$ and from 0.0021 to 0.0041 $kg.m^{-2}.s^{-1}$ at cooling-water temperatures of 35 and 40 ^{o}C, respectively, when solution mass flow is varied from 15 (Re 15) to 50 $kg.h^{-1}$ (Re 50).

Results from the numerical model showed a maximum and a mean error of 21.2 % and 9.3 %, respectively, for the absorption mass flux. From all absorption mass flux values, 66.6 % of the points showed an error lower than 10.0 %.

Figure 5.4b illustrates that modelled thermal load values range from 4.1 to 11.0 $kW.m^{-2}$ at a cooling-water temperature of 35 ^{o}C and from 3.4 to 6.8 $kW.m^{-2}$ at a cooling-water temperature of 40 ^{o}C.

In this case, thermal load obtained from the numerical study showed a maximum and a mean error of 9.5 % and 5.4 %, respectively; so 100.0 % of the points showed an error lower than 10.0 %.

Modelled absorption mass flux and thermal load values at a cooling-water temperature of 35 ^{o}C are around 1.42 and 1.60 higher than values at a cooling-water temperature of 40 ^{o}C showing a similar proportionality than in experimental results.

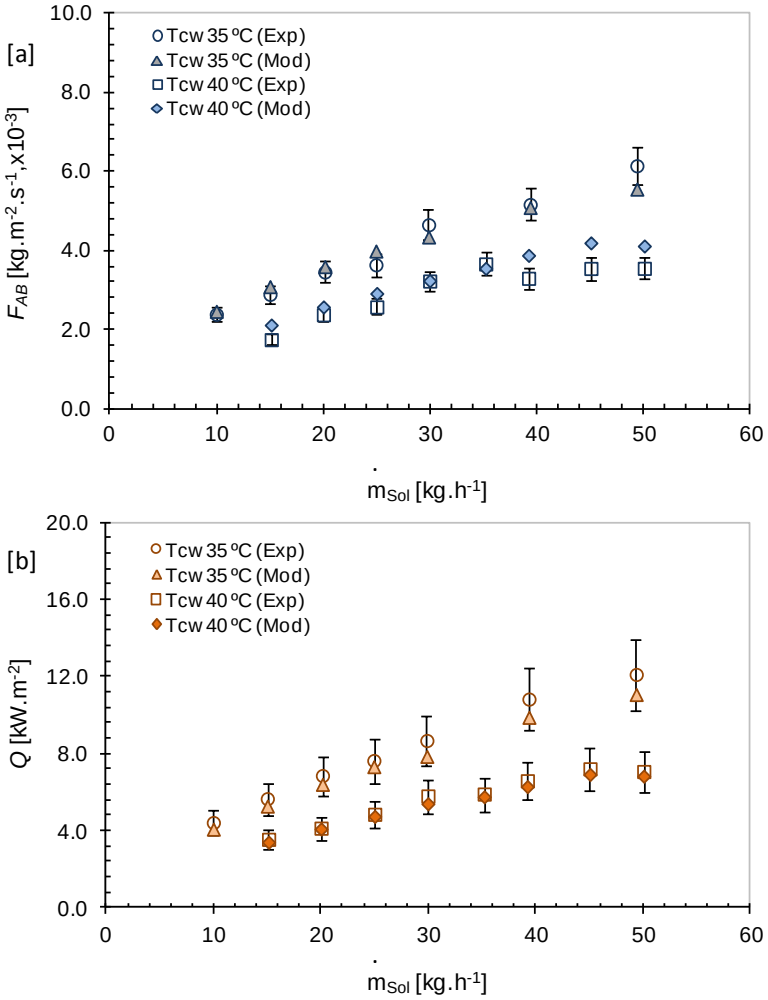

Figure 5.4 - Effect of cooling-water temperature and solution mass flow on: [a] Absorption mass flux and [b] Thermal load in a **Plate Absorber L-type**.

5.4.1.3 Tubular absorber with smooth surface

Figure 5.5 shows a comparison between experimental and modelled results in the **tubular bubble absorber with smooth surfaces**. To study the absorption process in the tubular absorber with smooth surface, heat and mass transfer correlations and geometrical specifications were set into the model.

Effect of cooling-water temperature and solution mass flow on absorption mass flux and absorber thermal load are illustrated in Figure 5.5. Modelled absorption mass flux varies from 0.0035 to 0.0044 kg.m^{-2}.s^{-1} and from 0.0032 to 0.0039 kg.m^{-2}.s^{-1} at cooling-water temperatures of 35 and 40 ºC, respectively, when solution mass flow is varied from 20 (Re≈220) to 65 kg.h^{-1} (Re≈670). For the thermal load, values range from 4.5 to 6.3 kW.m^{-2} and from 2.7 to 3.6 kW.m^{-2} at cooling-water temperatures of 35 and 40 ºC, respectively.

Results in Figure 5.5 from the numerical model for the smooth tube absorber showed a maximum and a mean error of 16.1 % and 7.5 %, respectively, for the absorption mass flux. From all results, 60.0 % of the points showed an error lower than 10.0 %. For the thermal load, a maximum and a mean error of 14.2 % and 6.5 %, respectively, were obtained where 80.0 % of the points showed an error lower than 10.0 %.

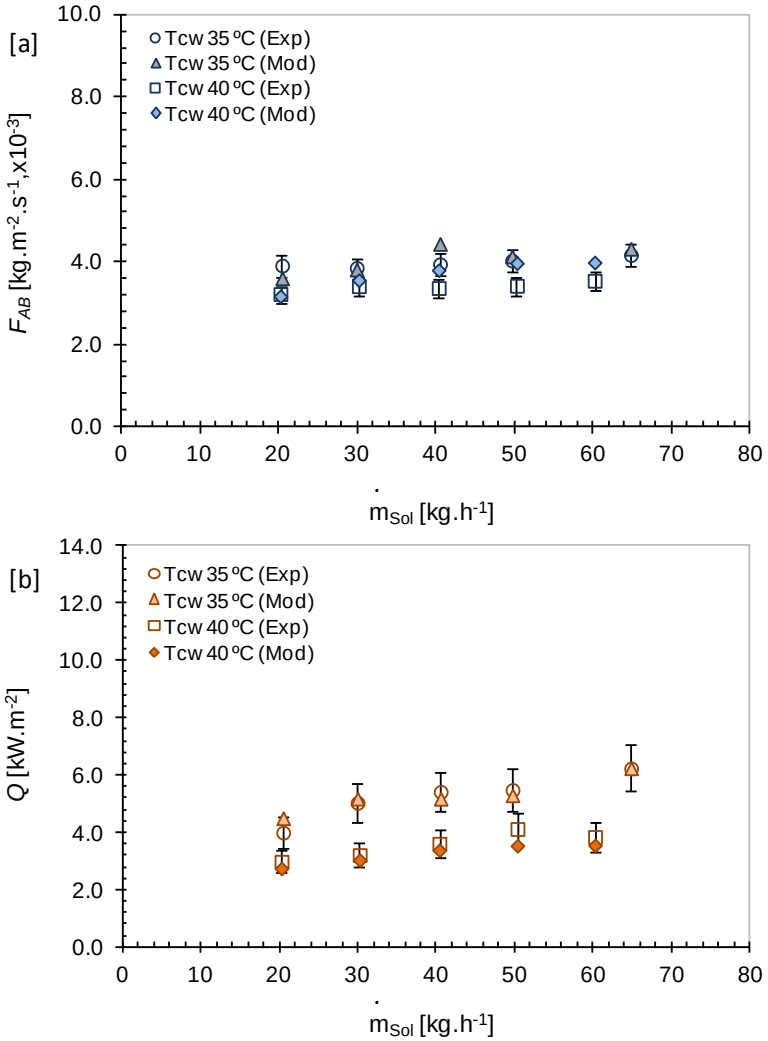

Figure 5.5 - Effect of cooling-water temperature and solution mass flow on: [a] Absorption mass flux and [b] Thermal load in **Tubular absorber with smooth surfaces**.

5.4.1.4 Tubular absorber with advanced surfaces

Numerical modeling of the absorption process in the **tubular absorber with advanced surfaces** was also performed. To study the absorption process in the tubular absorber with advanced surfaces, heat and mass transfer correlations for this case study were specified into the model designed for the tubular absorber with smooth surface. Effects of the advanced surfaces are involved in the heat and mass transfer correlations.

Main results are presented in Figure 5.6. It is observed that results from the numerical model, modeled absorption mass flux varies from 0.0043 to 0.0072 kg.m^{-2}.s^{-1} and from 0.0030 to 0.0060 kg.m^{-2}.s^{-1} at cooling-water temperatures of 35 and 40 ºC, respectively, when solution mass flow is varied from 20 (Re≈222) to 60 kg.h^{-1} (Re≈640).

Modelled thermal load ranges from 6.2 to 10.0 kW.m^{-2} and from 3.2 to 5.8 kW.m^{-2} at cooling-water temperatures of 35 and 40 ºC, respectively. Results from the numerical model of tubular absorber with advanced surfaces showed a maximum and a mean error of 16.2 % and 7.7 % for the absorption mass flux. From all results, 63.6 % of the points showed an error lower than 10.0 %. For the thermal load, a maximum and a mean error of 17.3 % and 9.4 %, respectively, were obtained where 54.6 % of the points showed an error lower than 10.0 %.

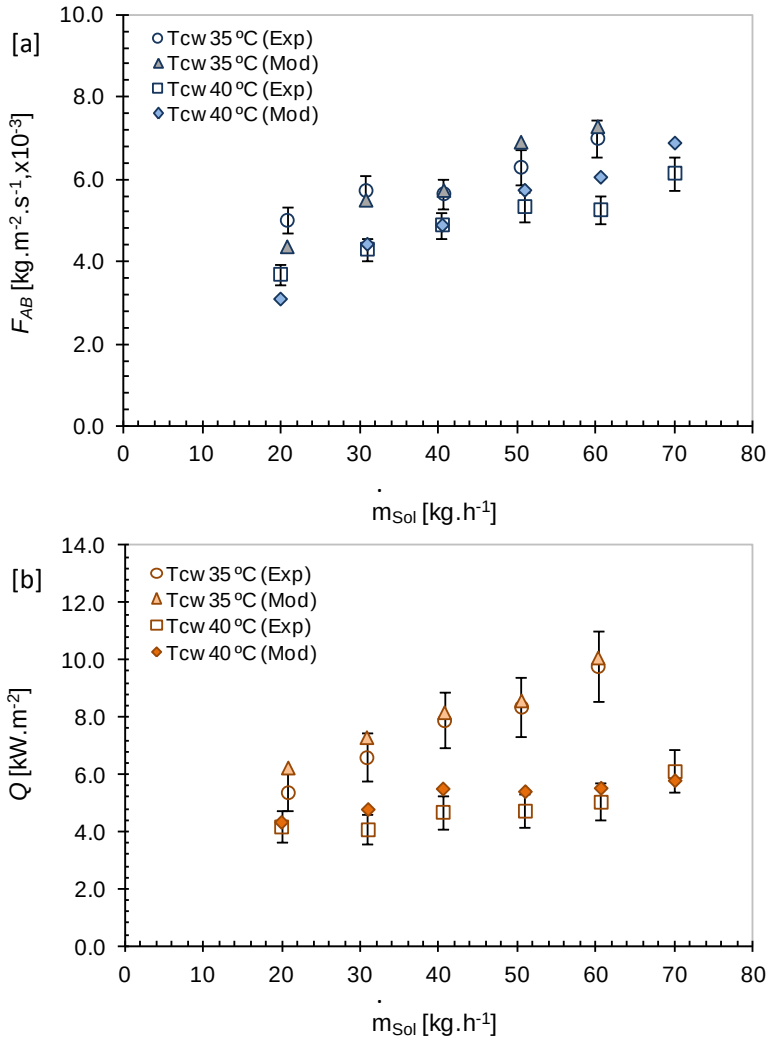

Figure 5.6 - Effect of cooling-water temperature and solution mass flow on: [a] Absorption mass flux and [b] Thermal load in **Tubular absorber with advanced surfaces**.

5.4.1.5 Sensitivity study

Once the simplified model has been validated and comparison with experimental data has shown good agreement, results shown in sub-section 5.4.1.1 using the plate absorber H-type are complemented with a sensitivity study presented in this sub-section.

In this case, effects of parameters such as inlet pressure, initial solution concentration and inlet solution temperature on the absorption mass flux and absorber thermal load are analyzed. The reference operating conditions for the modeling of the absorber were; inlet pressure of 510 kPa, inlet solution temperature of 45 ºC, inlet solution concentration of 0.45, inlet cooling-water temperature and flow rate of 35 ºC and 0.266 $m^3.h^{-1}$, respectively. Parameters under study are varied for each case as shown in Figure 5.7.

Figure 5.7a,b shows the effect of the inlet pressure on the absorption mass flux and absorber thermal load. Absorption mass flux in Figure 5.7a ranges between 0.0036 and 0.0086 $kg.m^{-2}.s^{-1}$ and between 0.0017 and 0.0039 $kg.m^{-2}.s^{-1}$ at inlet pressures of 550 and 450 kPa, respectively, when varying the solution mass flow from 10 to 50 $kg.h^{-1}$.

Thermal load in Figure 5.7b ranges between 5.9 and 14.9 $kW.m^{-2}$ and between 3.4 and 9.3 $kW.m^{-2}$ at inlet pressures of 550 and 450 kPa, respectively. Results show that as

expected, increasing the inlet pressure in the absorber, higher absorption mass fluxes and thermal load are achieved. This effect is caused due to the fact the equilibrium solution concentration also increases when increasing the pressure allowing to solution a higher capacity to absorb ammonia and thus, more heat is released.

An opposite effect occurs when the solution concentration is increased. Figure 5.7c,d shows that when increasing the inlet solution concentration, concentration difference between actual and equilibrium concentration gets smaller so ammonia absorption capacity of the solution is reduced. Absorption mass flux in Figure 5.7c ranges between 0.0040 and 0.0096 $kg.m^{-2}.s^{-1}$ and between 0.0018 and 0.0043 $kg.m^{-2}.s^{-1}$ at inlet solution concentrations of 0.40 and 0.48 $kg_{NH3}.kg^{-1}_{NH3/LiNO3}$, respectively, when varying the solution mass flow from 10 to 50 $kg.h^{-1}$.

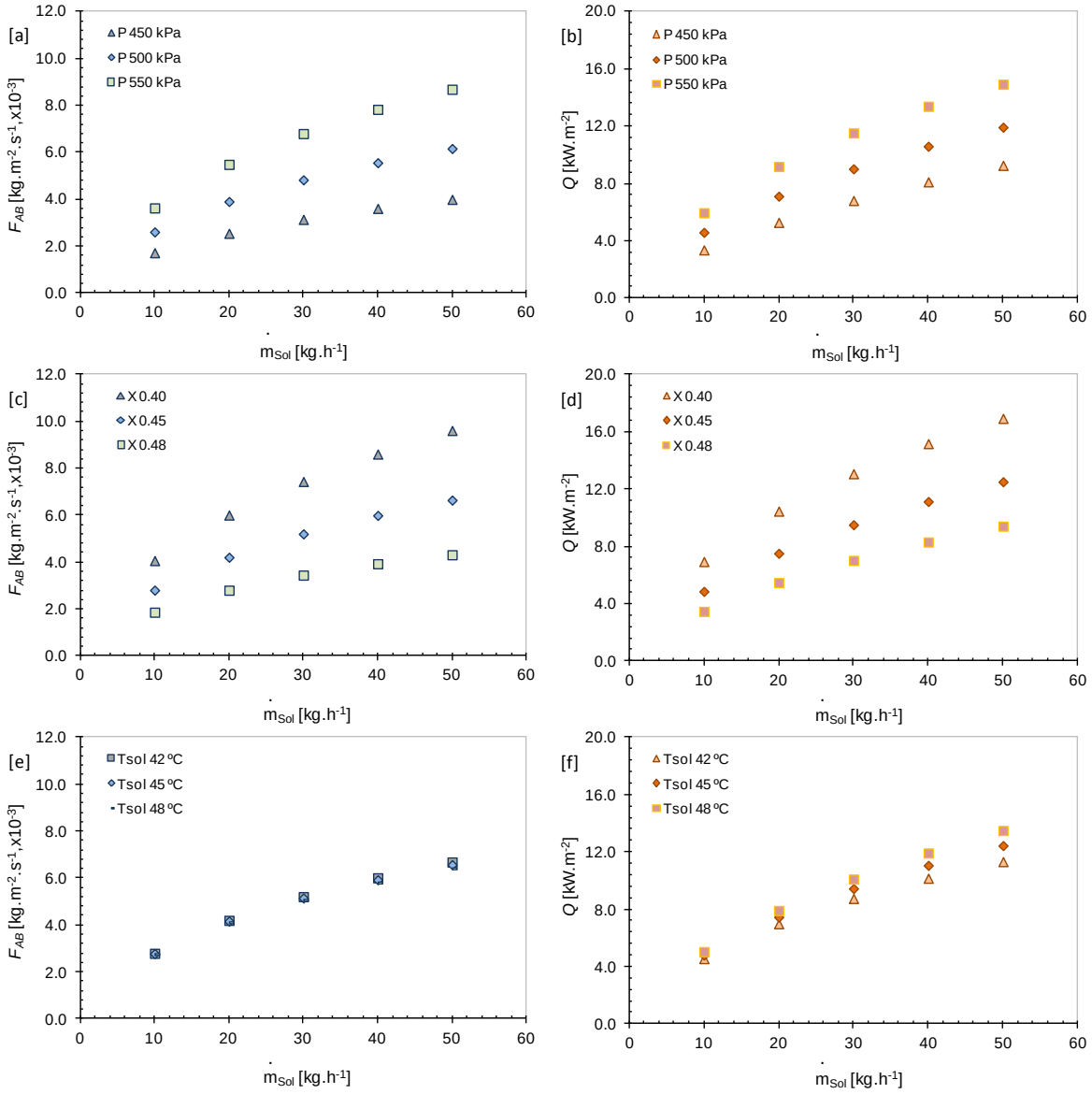

Figure 5.7 - Sensitivity study on the plate absorber H-type.

Thermal load in Figure 5.7d ranges between 6.9 and 16.9 $kW.m^{-2}$ and between 3.5 and 9.4 $kW.m^{-2}$ at inlet solution concentrations of 0.40 and 0.48 $kg_{NH3}.kg^{-1}_{NH3/LiNO3}$, respectively. Moreover, even though low inlet solution concentrations allow achieving higher absorption rates, higher activation temperatures in the generator are required. Otherwise, Figure 5.7e,f shows that effect of the inlet solution temperature on the absorption mass flux is negligible and effect on the thermal load is rather small. Behavior of results agrees with the trends of results reported by Cerezo et al. (2009) and Oronel (2010) with NH_3/H_2O and $NH_3/LiNO_3$, respectively.

5.4.2 Prediction of temperature and concentration profiles

In this subsection, numerical prediction of the temperatures and concentration profiles along the length of the plate absorber L-Type and the tubular absorber with inner advanced surfaces are presented. Modeling of the absorbers was performed at the conditions shown in Table 5.3. Specifications of the plate and tubular absorbers are described in Table 5.1. Experimental temperatures and concentration at the absorbers inlet and outlet are also shown in the next figures in order to compare those with results from models.

Table 5.3 - Operating conditions.

Parameters	Range
Solution temperature at the absorber inlet, °C	45
Cooling-water temperature at the absorber inlet, °C	30-40
Ammonia mass fraction in solution at the absorber inlet, $kg_{NH3}.kg^{-1}_{NH3/LiNO3}$	0.45
Absorber pressure, kPa	510
Solution mass flow rate, $kg.h^{-1}$	30 and 40

In the case of the plate absorber L-Type, results from the model were also compared with those results from the model found in the literature reported by Cerezo et al. (2011) with $NH_3/LiNO_3$. Comparison was performed at the same operating conditions.

This model was reported by Cerezo et al. (2011) and took into account the interface transfer areas between both solution and vapor, and also the heat transfer in both phases. In the case of the mass transfer, it was only considered in the solution side as in the present simplified model.

In that model, the transfer area of the bubbles in each control volume was obtained as shown in Equation (5.25) where a_i and Ap are the specific interfacial area and the cross-sectional area of the absorber, respectively. The specific interfacial area relation was approached as shown by Treybal (1981), Equation (5.26). In this equation, author related the gas hold up (E_G) and volume made up of n bubbles of diameters d_p. The gas hold up was determined as presented by Hikita et al. (1980) for bubble columns, Equation (5.27).

The heat transfer correlations used for the solution and vapor phase at the interface were those reported by Deckwer (1980)(Equation 5.28) and by Colburn and Drew (1937)(Equation 5.29), respectively.

The adimensional mass transfer correlation was that reported by Hughmark (1967) for bubble columns, Equation (5.30). It was later used to determine the absorption mass flux in each control volume, Equation (5.31). Since the absorbent is a salt, $F_{AB,ABS}$ is equal to 0 and z (ratio of ammonia mass flux to the total mass flux absorbed) is 1.

Moreover, Cerezo et al. (2011) used Equation (5.32), which was proposed by Herbine and Perez-Blanco (1995), to determine the heat transferred from the solution bulk to the absorber wall. In this case authors explained that due to the fact that there were not experimental values of heat transfer for the plate absorber studied with $NH_3/LiNO_3$, α_{Sol} was obtained using experimental values for water and correlated in Equation (5.33).

In addition, Cerezo et al. (2011) calculated the total energy transferred between the vapor and solution bulk as shown in Equations (5.34), (5.35) and (5.36), where the constants of heat transfer of the vapor and solution bulk were deduced as reported by Treybal (1981), Equation (5.37).

Differential transfer area, specific interfacial area and gas hold up.

$$dTa = a_i \cdot Ap_{AB} \cdot dl \tag{5.25}$$

$$a_i = \frac{6 \cdot E_G}{d_p} \tag{5.26}$$

$$E_G = 0.672 \cdot 1.1 \cdot \left(\frac{vel_{vap,AB} \cdot \mu_{Sol}}{\sigma_{Sol}} \right)^{0.578} \cdot \left(\frac{\mu_{Sol}^4 \cdot \mathrm{g}}{\rho_{Sol} \cdot \sigma_{Sol}^3} \right)^{-0.131} \cdot \left(\frac{\rho_{Vap}}{\rho_{Sol}} \right)^{0.062} \cdot \left(\frac{\mu_{Vap}}{\mu_{Sol}} \right)^{0.107} \tag{5.27}$$

Heat transfer coefficients correlations for the solution and vapor phase in the interface.

$$h_{Int,Sol} = 0.1 \left(\frac{\rho_{Sol} \cdot vel_{vap} \cdot d_p}{\mu_{Sol}} \right)^{-0.25} \cdot \left(\frac{vel_{vap}^2}{g \cdot d_p} \right)^{-0.25} \cdot \left(\frac{\mu_{Sol} \cdot Cp_{Sol}}{\lambda_{Sol}} \right)^{-0.5} \cdot \rho_{Sol} Cp_{Sol} vel_{vap} \tag{5.28}$$

$$h_{Int,vap} = 0.0075 \cdot Cp_{vap} \cdot \dot{V}_{vap} \cdot \left(\frac{\lambda_{vap}}{Cp_{vap} \cdot \mu_{vap}} \right)^{2/3} \tag{5.29}$$

Mass transfer correlations for the solution phase in the interface.

$$\mathrm{Sh}_{Int,Sol} = 2 + 0.0187 \cdot \mathrm{Re}_b^{0.779} \cdot \mathrm{Sc}_{Sol}^{0.546} \cdot \left(\frac{d_b \cdot \mathrm{g}^{1/3}}{\beta_{Sol}^{2/3}} \right)^{0.116} \tag{5.30}$$

$$F_{AB,REF} + F_{AB,ABS} = Km_{Sol} \left(Ln \frac{z - x}{z - x_{\mathrm{int}}} \right) \tag{5.31}$$

Solution and cooling water heat transfer coefficients.

$$h_{Sol} = h_{liq} (1 - E_G)^{-0.5} \tag{5.32}$$

$$h_{Cw} = 0.99 \cdot \mathrm{Re}_{Cw}^{0.529} \cdot \mathrm{Pr}_{Cw}^{1/3} \cdot \frac{\lambda_{Cw}}{D_h} \tag{5.33}$$

Energy balances between the vapor and solution bulk.

$$Q_{AB} = Q_{SEN,Sol} + Q_{SEN,vap} \tag{5.34}$$

$$Q_{SEN,vap} = cte_{Vap}(T_{vap} - T_{\mathrm{int}}) \tag{5.35}$$

$$Q_{SEN,Sol} = cte_{Sol}(T_{\mathrm{int}} - T_{Sol}) \tag{5.36}$$

$$cte_{Sol,vap} = \frac{\frac{m_{REF} \cdot Cp_{liq,vap} + m_{ABS} \cdot Cp_{liq,vap}}{h_{\mathrm{int},Sol,vap}}}{1 - e^{\frac{m_{REF} \cdot Cp_{liq,vap} + m_{ABS} \cdot Cp_{liq,vap}}{h_{\mathrm{int},Sol,vap}}}} \cdot h_{\mathrm{int},Sol,vap} \cdot dA_M \tag{5.37}$$

It is important to highlight that correlations for heat and mass transfer used by Cerezo et al. (2011), which were found in the open literature, were obtained from other applications different that for absorbers in absorption systems where heat and mass transfer are simultaneous. However, some of these correlations have been also used by other authors such as Herbine and Perez-Blanco (1995), Kang et al. (1998, 2000), Kim et al. (2007b) and Cerezo et al. (2010) in NH_3/H_2O systems.

5.4.2.1 Plate absorber L-Type

Figure 5.8 and Figure 5.9 show that even when overall heat and mass transfer correlations were used in the model presented in this thesis, temperature and concentration profiles along the absorbers were reasonably predicted and values at the outlet of the absorbers are significantly close to those experimentally obtained.

Figure 5.8 illustrates temperature and solution concentration profiles along the plate absorbers L-type at a solution mass flow of 40 $kg.h^{-1}$. Results in Figure 5.8a show that at an inlet cooling-water temperature of 40 ^oC, solution temperature is relatively constant until a length of 15 cm from the inlet of the absorber and then temperature tends to gradually decrease. It is then observed that from an absorber length of 15 cm, cooling-water flow is able to sensible cool the solution flow and more latent heat from the absorption process is removed. Moreover, solution temperature profile from the model reported by Cerezo et al. (2011) presents a more remarked increase at the beginning of the absorber but after 10 cm from the absorber inlet, solution temperature presents a sharp decrease.

Outlet temperature from the model reported by Cerezo et al. (2011) is 1.7 ^oC lower than result from the model described in this thesis and 2.2 ^oC lower than the experimental result. With regards to results at a cooling-water temperature of 35 ^oC, Figure 5.8d illustrates an instantaneous decrease in the solution temperature by using the model described in this thesis. In the case of the model proposed by Cerezo et al. (2011), solution temperature shows a slight increase until a length of 4 cm and then it decreases.

At these conditions, solution temperature from the model of Cerezo et al. (2011) is 0.9 ºC lower than results from the model described in this thesis and 3.2 ºC lower than the experimental result.

In addition, Figure 5.8a,d shows that outlet cooling-water temperatures increase almost lineally for both models but results obtained by using the present model are closer to those achieved experimentally.

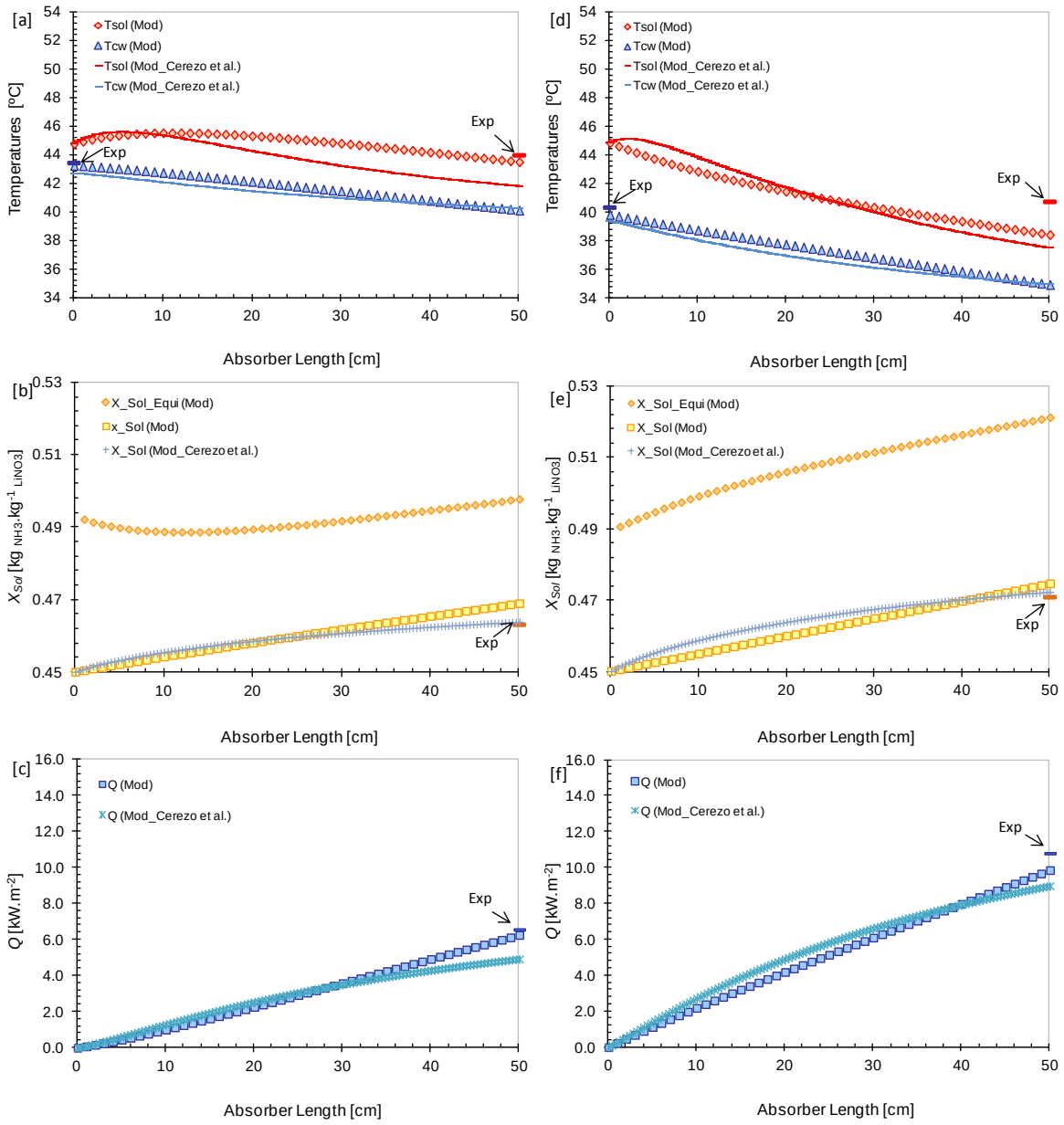

Figure 5.8 - Temperatures [a], solution concentration [b] and thermal load [c] profiles at cooling-water temperatures of 40 ºC. Temperatures [d], solution concentration [e] and thermal load [f] profiles at cooling-water temperatures of 35 ºC.

With respect to the concentration profiles, model proposed by Cerezo et al. (2011) predict the outlet solution concentration better than the present model. In the case of the present model, concentration values are over predicted, however errors with respect to experiments do not exceed 1.3 %.

It is important to remark that in Figure 5.8b,e can be noted the effect of the cooling-water temperature on the actual and equilibrium concentration profiles. The wider temperature difference between the solution and cooling-water allows cooling more the solution and a higher heat extraction from the absorption process which extend the difference between the actual and equilibrium states at the studied conditions and therefore, the solution is able to absorb much more ammonia.

Figure 5.8c,f show the thermal load profiles along the length of the plate absorber L-type. It is observed that trends of the thermal load values along the absorber length for both models are similar; however, results achieved with the present model are closer to those values obtained by the experiments.

Overall absorption mass flux errors with respect to experimental data for these case studies using the present model were of 1.4 % and 17.6 % at temperatures of 35 and 40 ^{o}C, respectively, while 8.7 % and 4.6 % for the thermal load at temperatures of 35 and 40 ^{o}C, respectively.

In the cases of the model proposed by Cerezo et al. (2011), overall absorption mass flux errors were of 11.2 % and 16.8 % at temperatures of 35 and 40 ^{o}C, respectively, while 16.7 % and 24.9 % for the thermal load at temperatures of 35 and 40 ^{o}C, respectively.

Although the present model is not as detailed as the model proposed by Cerezo et al. (2011), which takes into account the liquid-vapor interface area, results predicted are closer to those experimentally obtained. As described earlier, model reported by Cerezo et al. (2011) is based on series of correlations from the literature which were obtained from systems without simultaneous heat and mass transfer. Cerezo et al. (2011) used these correlations to calculate the absorption mass flux and mass transfer area between the vapor bubble and solution bulk when the vapor bubble goes upward through the absorber.

In the case of the model proposed in the thesis, correlations obtained from the experimental study in chapter 4 for calculating the absorption mass flux and solution heat transfer coefficient are implemented into the model. Therefore, the absorption mass flux can be calculated from the Sherwood correlation or the specific correlation for this parameter giving to these correlations an important use.

5.4.2.2 Tubular absorber with advanced surfaces

Figure 5.9 depicts temperature and solution concentration profiles along the tubular bubble absorber with advanced surfaces at a solution mass flow of 30 kg.h^{-1}. Figure 5.9a shows that at inlet cooling-water temperatures of 40 and 35 ^{o}C, solution temperature tends to gradually increase due to the fact that the cooling-water flow is not able to cool the solution flow. In consequence, heat released from the absorption process is not completely removed. This behavior is due to the low heat transfer area of the tubular absorber which is not enough for transferring a higher amount of heat to the cooling-water side. Furthermore, Figure 5.9b shows that the limited heat transfer to the cooling-

side implies that solution gets close to its equilibrium conditions not being able to absorb a larger amount of ammonia.

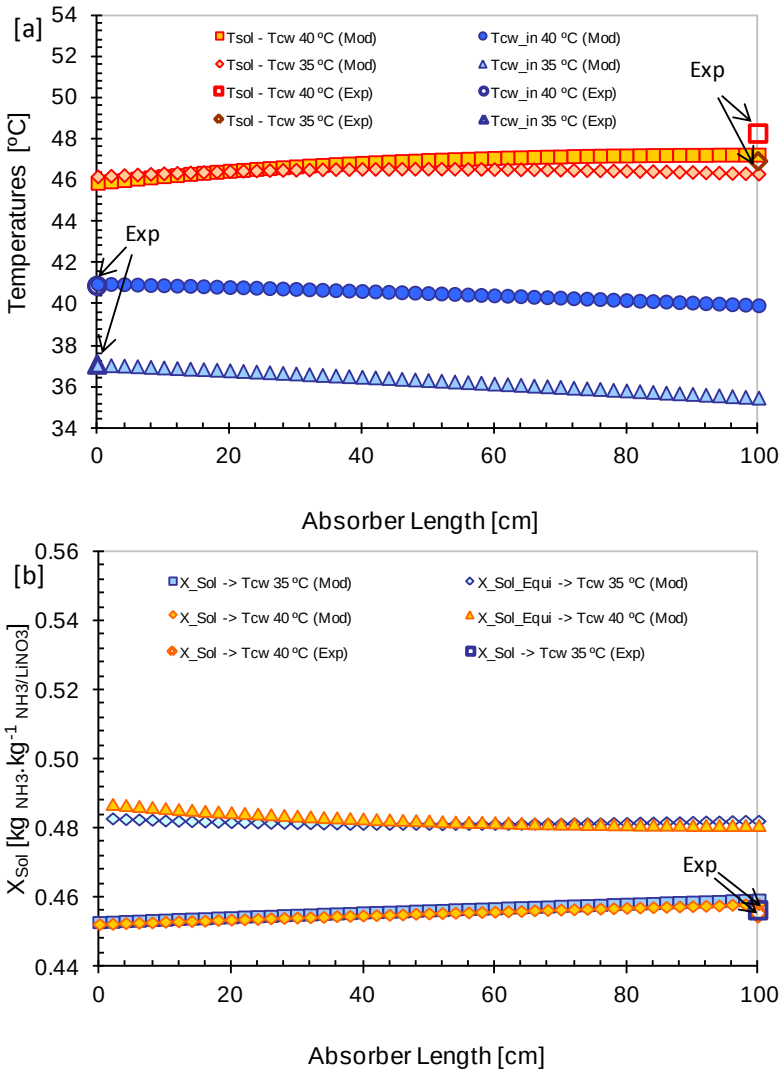

Figure 5.9 - Temperatures [a] and solution concentration [b] profiles along the tubular absorber using an inner tube with advanced surface.

5.5 Conclusions

In this chapter, a one-dimensional simplified model of the ammonia absorption process in bubble absorbers with the $NH_3/LiNO_3$ mixture is described and evaluated.

Numerical model was used to study the performance of four absorber configurations: two plate absorbers with H and L-type corrugations and two tubular absorbers with smooth and advanced surfaces.

Numerical model is mainly based on heat and mass transfer correlations obtained from the experimental study presented in Chapter 4. In the numerical model, the absorber was discretized in consecutive small control volumes where energy and mass balances were

solved simultaneously to obtain the output values which were the input values of the immediately next control volume.

Results from the numerical model for each case study were compared with results from the experimental study showing good agreement. Furthermore, numerical model allows having an approach to temperature and concentration profiles. In this case, temperature and concentration at outlet of the absorber showed good agreement with those values obtained by experimentation. In addition, results with the plate absorber L-type from the present model were compared with the numerical model proposed by Cerezo et al. (2011). Results from the present model predict better the experimental outlet solution, cooling-water temperature, the total absorption mass flux and thermal load.

Model can be easily adapted to the desired absorber configurations and simulate with good accuracy the ammonia absorption process in bubble mode absorbers. In addition, results showed that correlations used to calculate overall heat and mass transfer values can be used to have a good approach to local values of heat and mass transfer along the absorber. Numerical results evidenced that model can be used as a useful tool to design bubble absorbers.

Chapter 6

Conclusions and Future Work

6.1 Conclusions

Experiences resulting from this research work allowed to study and quantify the ammonia absorption process in bubble absorbers for $NH_3/LiNO_3$ absorption chillers. Different process intensification techniques were employed in order to improve the absorption process at the operating conditions of an air-cooled $NH_3/LiNO_3$ absorber. Also, a numerical study of the absorption process in various bubble absorbers geometries was conducted.

Main conclusions about the results of this thesis are drawn as follows:

With regard to the review on the absorption refrigeration technology and absorption process:

Thermally driven absorption refrigeration technologies have been identified as an attractive option to replace conventional electrically driven mechanical compression systems because they provide great opportunities for energy savings. In addition, absorption technologies use environmentally friendly working fluids which do not deplete the ozone layer and do not contribute to global warming.

$NH_3/LiNO_3$ is found to be a promising working fluid for air-cooled absorption refrigeration systems driven by low temperature heat sources such as solar or waste heat.

Ammonia is an exemplar refrigerant due to its excellent thermodynamic properties and a great potential for use in low charge systems with compact components such as plate heat exchangers or advanced surface heat exchangers.

Bubble absorbers are found to have a better absorption performance than falling film absorbers and spray absorbers, and thus less volume and smaller sizes can be achieved.

Intensification techniques such as the use of advanced surfaces and nanoparticles have shown outstanding heat and mass transfer enhancements in the absorption process for absorption systems.

With regard to the experimental study of the NH_3 absorption process:

The experimental study was conducted in a test facility modified and adapted for studying the performance of bubble absorbers.

Operating conditions of the experiments were obtained from a thermodynamic simulation of a single stage absorption cycle with $NH_3/LiNO_3$ at a generation temperature of 90 ^oC and heat released by air.

Experiments were aimed to the intensification of the NH_3 absorption process in bubble absorbers using passive techniques. For this, two types of heat exchangers working as bubble absorbers were tested; a plate heat exchanger H-type and a tubular heat exchanger with advanced surfaces.

Experimental results involved the analysis of absorber performance parameters such as overall NH_3 absorption mass flux, absorber thermal load, solution heat transfer coefficient, solution mass transfer coefficient and degree of subcooling at the absorber outlet.

Experiments on the NH_3 absorption process in the **plate absorber** H-type resulted in maximum absorption mass flux of 0.0038 and 0.0072 $kg.m^{-2}s^{-1}$ at an inlet cooling-water temperature of 40 and 35 ^oC, respectively, and at a solution mass flow of 40 $kg.h^{-1}$ (Re 40).

At an inlet cooling-water temperature of 40 ^oC, maximum absorption mass flux obtained in the plate H-type was similar to that value in the plate absorber L-type. However, maximum absorption mass flux in the plate absorber H-type at a cooling-water temperature of 35 ^oC was 1.26 times higher than those values obtained in the plate heat exchanger L-type when the solution Reynolds number was varied from 15 to 40. In contrast, solution heat transfer coefficients in the plate absorber L-type were higher than those values in the plate absorber H-type at an inlet cooling-water temperature of 35 ^oC. Moreover, it was observed that experiments in the plate absorber H-type were performed at a higher cooling-water flow rate which has a positive effect on the absorption rate and according to this, effect of the angle of corrugation in the plate H-type on the absorption rates with respect to the plate L-type is rather insignificant.

From experimental results of the absorption process in the plate absorber H-type, parameters such as absorption mass flux, solution Nusselt number and Sherwood number were correlated satisfactorily predicting around 93 %, 90 % and 90 % of the experimental data of the absorption mass flux, solution heat and mass transfer coefficients with lower error than 15 %.

With respect to experiments with the **tubular absorber**, results showed that the **advanced surfaces** used significantly improve the absorption process in the tubular bubble absorber analyzed in comparison with using a smooth tube.

The effect of the advanced surfaces was larger when increasing the solution mass flow. At low cooling-water Reynolds numbers and solution mass flows of 40 (Re≈439) and 50 $kg.h^{-1}$ (Re≈545), absorption mass fluxes for the tube with advanced surfaces were around 1.46 and 1.57 times higher than the values achieved for the smooth tube. At high values of the cooling-water Reynolds number, absorption mass flux values for the tube with advanced surfaces were around 1.71 and 1.54 times higher than those achieved for the smooth tube. Improvements in the solution heat transfer coefficient were also obtained with advanced surface tube. These improvements, more pronounced at high solution mass flows, were around 1.11 and 1.55 times higher than values achieved for the smooth surface tube when the solution flow was set between 40 and 70 $kg.h^{-1}$, respectively. In addition, the advanced surface tubes tested increase heat and mass transfer coefficients without penalizing pressure drop.

Absorption mass flux, solution Nusselt number and Sherwood number were also correlated from experimental results of the absorption process in the tubular absorber with advanced and smooth surfaces.

Tubular absorber with advanced surfaces was also tested with two tube diameters and three tube lengths. According to experimental results, absorption mass flux increased when the tube diameter was reduced and decreased with the tube length extension.

Experiments on the performance of a smooth **tubular absorber** with multi walled **carbon nanotubes** into the base mixture $NH_3/LiNO_3$ were also conducted. Results

showed that carbon nanotubes improve the NH_3 absorption process in the tubular bubble absorber with the $NH_3/LiNO_3$ mixture. With respect to the reference values, the maximum enhancements achieved in the absorption mass flux with binary nanofluids (0.01 wt. % of CNTs) were around 1.64 and 1.48 times higher, at cooling-water temperature of 40 and 35 ^oC, respectively, while the maximum solution heat transfer coefficient value obtained with the binary nanofluids was around 1.39 times higher. It is also evidenced that pressure drops was not affected by the CNTs fraction set at the operating conditions under study.

Effect of the combined use of the **carbon nanotubes** and **advanced surfaces** in the **tubular absorber** was also studied. It showed an outstanding improvement in the absorption mass flux at low solution mass flow. However, at high solution mass flows, enhancements were less pronounced getting close to those results with the base mixture in the advanced surface tube. Moreover, an important synergic effect was observed in the solution heat transfer coefficient. Otherwise, absorber performance with CNTs concentrations of 0.01 and 0.02 wt. % showed no remarkable differences.

With respect to the simplified model for bubble absorbers:

The simplified model was developed to study numerically the performance of the absorber configurations experimentally evaluated. The simplified numerical model included the heat and mass transfer correlations obtained from experiments in order to predict the heat and mass transfer rates, and temperatures and concentration profiles during the absorption in the studied configurations. Results showed that correlations used to calculate overall heat and mass transfer values can be used to have a good approach to local values of heat and mass transfer along the absorber. Results from the numerical model for each case study were compared with results from the experimental study showing good agreement. Numerical results evidenced that the simplified model can be used as a useful tool to design bubble absorbers.

6.2 Future Work

For the future, the next tasks can be explored for further advances on the development of $NH_3/LiNO_3$ absorption chillers driven by low temperature heat sources such as solar or waste heat:

- It is of great interest the build-up of test facility in order to study experimentally the boiling process with $NH_3/LiNO_3$ in a tubular heat exchanger as a generator using smooth and advanced surfaces and develop experimental correlations for further generator designs.
- It is also of attention to evaluate the effect of the addition of carbon nanotubes on the boiling process in a tubular heat exchanger as a generator with smooth and advanced surfaces.
- The mechanical design and testing of an air cooled tubular bubble absorber with inner advanced surfaces as well as its refrigerant vapor distributor, and adaptation of this absorber in an absorption chiller working with $NH_3/LiNO_3$ and carbon

nanotubes are the final step to quantify the performance and viability of the absorption chiller using these intensification techniques.

References

References

Abdulateef J.M., Sopian K., Alghoul M.A., Optimum design for solar absorption refrigeration systems and comparison of the performances using ammonia-water, ammonia-lithium nitrate and ammonia-sodium thiocyanate solutions, International Journal of Mechanical and Materials Engineering 3 (1) (2008) 17-24.

Absorsistem, www.absorsistem.com/Tecnologia, (Consulted in 2013).

Acuña A., Velázquez N., Cerezo J., Energy analysis of a diffusion absorption cooling system using lithium nitrate, sodium thiocyanate and water as absorbent substances and ammonia as the refrigerant, Applied Thermal Engineering 51 (2013) 1273-1281.

Aggarwal M.K. and Agarwal, R.S., Thermodynamic properties of lithium nitrate-ammonia and mixtures, Energy Research 10 (1986) 59-68.

Altamush M., Economic analyses of absorption systems: part b-optimization of operating parameters, Energy Conversion and Management 38 (9) (1997) 905-918.

Altenkirch E. and Tenckhoff B., Absorptionskaeltemaschine zur kontinuierlichen Erzeugung vonKaelte und Waerme oder acuh von Arbeit, (1914), German Patent 278,076.

Alvarez M.E., Estudio teórico y experimental de la solución acuosa de nitratos de litio, sodio y potasio como fluido de trabajo en enfriadoras de agua de absorción con accionamiento a alta temperatura, Doctoral Thesis, Universitat Rovira i Virgili, Tarragona, Spain, 2013.

Amaris C., Bourouis M., Vallès M., Effect of advanced surfaces on heat and mass transfer processes in a tubular bubble absorber with NH_3/$LiNO_3$ for absorption refrigeration cycles, 10th IIR Gustav Lorentzen Conference on Natural Refrigerant, (2012), Delft, The Netherlands.

Antonopoulos K.A. and Rogdakis E.D., Performance of solar driven ammonia lithium nitrate and ammonia-sodium thiocyanate absorption systems operating as coolers or heat pumps in Athens, Applied Thermal Engineering 16 (1996) 127-147.

Arzoz D., Venegas M., Rodriguez P., Izquierdo M., Solar absorption refrigeration using $LiNO_3$-NH_3 solution and Flat Plate collectors, International Sorption Heat Pump Conference, (2002), Shangai, China.

Ayala R., Frías J.L., Heard C.L., Holland F.A., Experimental assessment of and ammonia/lithium nitrate absorption cooler operated on low temperature geothermal energy, Heat Recovery Systems & CHP 14 (1994) 437-446.

Ayala R., Heard C.L. and Holland F.A., Ammonia/lithium nitrate absorption/compression refrigeration cycle. part I. Simulation, Applied Thermal Engineering 17 (3) (1997) 223-233.

Ayala R., Heard C.L. and Holland F.A., Ammonia/lithium nitrate absorption/compression refrigeration cycle. part II. Experimental, Applied Thermal Engineering 18 (8) (1998) 661-670.

Ayala R., Heard C.L., Holland F.A., Development in geothermal energy in Mexico-Part 26, Experimental assessment of an ammonia/lithium nitrate absorption cooler operated on low temperature geothermal energy, Heat Recovery Systems & CHP 14 (4) (1994) 437-466.

Bergman T.L., Lavine A.S., Incropera F.P., Dewitt D.P., Fundamentals of heat and mass transfer, Seventh edition, John Wiley & Sons, Inc., 2011.

Best R. and Pilatowsky I., Solar assisted cooling with sorption systems: status of the research in Mexico and Latin America, International Journal of Refrigeration 21 (2) (1998) 100-115.

Blytas G.C., Kertesz D.J., Daniels F., Concentrated Solutions in Liquid Ammonia: Solubility of $NaNO_3$ and KBr and Other Salts; Vapor Pressures of $LiNO_3$-NH_3 Solutions, Journal of American Chemical Society 84 (1962) 1083-1085.

Bokelmann H., Presentation of new working fluids for absorption heat pumps, Proceedings of Absorption Heat Pump Congress, (1985), Paris, France.

Bothe A., Das Stoffsystem NH_3-$LiNO_3$/H_2O für den Einsatz in Absorptionskreisläufen, Doctoral Thesis, Universität Duisburg-Essen, Essen, Germany, 1989.

Bourouis M., Coronas A., Valles M.; Zamora M., Air/water or water/water absorption water cooler using ammonia and lithium nitrate, (2011), Patent PCT/ES2010/070608.

Bourouis M., Vallès M., Coronas A., Absorption refrigeration cycles driven by thermal energy at low temperature, Proceeding of Eurotherm Seminar No 72, (2003) 383-388.

Buongiorno J., Convective transport in nanofluids, Journal of Heat Transfer 128 (2006) 240-250.

Castro J., Oliet C., Rodríguez I., Oliva A., Comparison of the performance of falling film and bubble absorbers for air-cooled absorption systems, International Journal of Thermal Sciences 48 (2009) 1355-1366.

Cerezo J., Best R., Bourouis M., Coronas A., Comparison of numerical and experimental performance criteria of an ammonia-water bubble absorber using plate heat exchangers, International Journal of Heat and Mass Transfer 53 (2010) 3379-3386.

Cerezo J., Best R., Romero R.J., A study of a bubble absorber using a plate heat exchanger with NH_3-H_2O, NH_3-$LiNO_3$ and NH_3-NaSCN, Applied Thermal Engineering 31 (2011) 1869-1876.

Cerezo J., Bourouis M., Valles M., Coronas A., Best R., Experimental study of an ammonia-water bubble absorber using a plate heat exchanger for absorption refrigeration machines, Applied Thermal Engineering 29 (2009) 1005-1011.

Cerezo J., Estudio del proceso de absorción con amoníaco-agua en intercambiadores de placas para equipos de refrigeración por absorción, Doctoral Thesis, Universitat Rovira i Virgili, Tarragona, Spain, 2006.

Cheng W-L, Houda K., Chen Z-S, Akisawa A., Hu P., Kashiwagi T., Heat transfer enhancement by additive in vertical falling film absorption of H_2O/LiBr, Applied Thermal Engineering 24 (2004) 281-298.

Choi U.S., Enhancing thermal conductivity of fluids with nanoparticles, ASME Fluids Engineering Division, 231 (1995) 99-105.

Colburn A.P. and Drew T.B., The condensation of mixed vapors, Transactions of American Institute of Chemical Engineers 33 (1937) 197-215.

Cuenca Y., Salavera D., Vernet A., Teja A.S., Vallès M., Thermal Conductivity of Ammonia + Lithium Nitrate and Ammonia + Lithium Nitrate + Water Solutions over a Wide Range of Concentrations and Temperatures, International Journal of Refrigeration (2013a), doi: 10.1016/j.ijrefrig.2013.08.010.

Cuenca Y., Vernet A., Vallès M., Enhanced thermal conductivity of new working fluid (NH_3 + $LiNO_3$) using CNTs binary nanofluid, International Workshop on New Working Fluids for Absorption Heat Pumps and Refrigeration Systems, Eurotherm Seminar nº 100, (2013b), Tarragona, Spain.

Das S., Putra N., Thiesen P., Roetzel W., Temperature dependence of thermal conductivity enhancement for nanofluids, Journal of Heat Transfer 125 (2003) 567-574.

Datsyuk V., Kalyva M., Papagelis K., Parthenios J., Tasis D., Siokou A., Kallitsis I., Galiotis C., Chemical oxidation of multiwalled carbon nanotubes, Carbon 4 (6) (2008) 833-840.

Davis R.O.E., Olmstead L. B., Lundstrum F.O., Vapor Pressure of Lithium Nitrate/Ammonia System, Journal of American Chemical Society 43 (1921) 1575-1580.

Deckwer W.D., On the mechanism of heat transfer in bubble column reactor, Chemical Engineering Sciences 35 (1980) 1341-1349.

Ding Y., Chen H., He Y., Lapkin A., Yeganeh M., Siller L., Butenko Y.V., Forced convective heat transfer of nanofluids, Advanced Powder Technology 18 (6) (2007) 813-824.

Eastman J.A., Phillpot S.R., Choi S.U.S., Keblinski P., Thermal transport in nanofluids, Annual Review of Materials Research 34 (2004) 219-246.

Ehmke H.J. and Renz M., Ternary Working Fluids for Absorption Systems with Salt-Liquid Mixtures as Absorber, IIF - IIR Congress, Comission B1, (1983), Paris, France.

Elperin T.A. and Fominykh A., Four stages of the simultaneous mass and heat transfer during bubble formation and rise in a bubbly absorber, Chemical Engineering Science 58 (2003) 3555-3564.

Eysseltová J. and Orlova V.T., IUPAC-NIST solubility data series. 89. Alkali metal nitrates. Part 1. Lithium nitrate, Journal of Physical and Chemical Reference Data 39 (2010) 033-104.

Fang X., Xuan Y., Li Q., Experimental investigation on enhanced mass transfer in nanofluids, Applied Physics Letters 95 (2009) 203108.

Fernández-Seara J., Sieres J., Rodríguez C., Vázquez M., Ammonia-water absorption in vertical tubular absorbers, International Journal of Thermal Sciences 44 (2005) 277-288.

Fernández-Seara J., Uhía F., Sieres J., Analysis of an air cooled ammonia–water vertical tubular absorber, International Journal of Thermal Sciences 46 (2007) 93-103.

Garimella S., Fundamental understanding of heat and mass transfer in the ammonia/water absorber, Report, Air-conditioning and refrigeration technology institute, 2007.

Ge Y.T., Tassou S.A., Chaer I., Suguartha N., Performance evaluation of a tri-generation system with simulation and experiment, Applied Energy 86 (2009) 2317-2326.

Gensch K., Lithiumnitratammoniakat als Absorptionsflüssigkeit für Kältemaschinen, Zeitschrift für die gesamte Kälte, Industrie (1937) S24-S30 (Heft 2).

Gluesenkamp K. Radermacher R., Y. Hwang Y., Trends in absorption machines, International Sorption Heat Pump Conference, (2011), Padua, Italy.

Gnielinski V., Heat transfer coefficients for turbulent flow in concentric annular ducts, Heat Transfer Engineering, 30 (6) (2009) 431-436.

Gnielinski V., New equations for heat and mass transfer in turbulent pipe and channel flow, International Chemical Engineering 16 (1976) 359-368.

Haddad Z., Abu-Nada E., Oztop H.F., Mataoui A., Natural convection in nanofluids: Are the thermophoresis and Brownian motion effects significant in nanofluid heat transfer enhancement?, International Journal of Thermal Sciences 57 (2012) 152-162.

Haltenberger W., Enthalpy-concentration charts from vapor pressure data, Industrial and Engineering Chemistry 31 (6) (1939)783-786.

Heard C.L., Ayala R., Best R., An experimental comparison of an absorption refrigerator using ammonia/water and ammonia/lithium nitrate, in: Proceedings of the International Absorption Heat Pump Conference, Montreal, Canada, (1996) 245-252.

Heard C.L., Ayala R., Carbon and stainless steel in solutions of lithium nitrate in ammonia at moderate temperature, Materials and Corrosion 54 (2003) 609-611.

Heat Exchanger Design Handbook (HEDH), Sect. 2.5.1., Begell House Inc., 1983.

Helbing U., Würfel R., Fratzscher W., Comparative Investigations of Non-adiabatic Absorption in Film Flow and Bubble Flow, Chemical Engineering Technology 23 (2000) 1081-1085.

Herbine G.S. and Perez-Blanco H., Model of an ammonia-water bubble absorber, ASHRAE Transactions 101 (1) (1995) 1324-1334.

Herrera J.V., García-Valladares O., Gómez V.H., Best R. Numerical simulation and experimental results of horizontal tube falling film generator working in a $NH_3/LiNO_3$ absorption refrigeration system, Applied Thermal Engineering 30 (2010) 1751-1763.

Hikita H., Asai S., Tanigawa K., Segawa K., Kitao M., Gas Hold-Up in Bubble Columns, Chemical Engineering Journal 20 (1980) 59-67.

Hughmark G.A. Holdup and mass transfer in bubble columns, Industrial & Engineering Chemistry Process Design and Development 6 (2) (1967) 218-220.

Infante Ferreira C.A., Combined momentum, heat and mass transfer in vertical slug flow absorbers, International Journal of Refrigeration 8 (6) (1985a) 326-334.

Infante Ferreira C.A., Keizer C., Machielsen C.H.M., Heat and mass transfer in vertical tubular bubble absorbers for ammonia-water absorption refrigeration systems, International Journal of Refrigeration 7 (6) (1984) 348-357.

Infante Ferreira C.A., Operating characteristics of NH_3-$LiNO_3$ and NH_3-NaSCN absorption refrigeration machines, in: Proceedings of The Nineteenth International Congress of Refrigeration, (1995) 321-328.

Infante Ferreira C.A., Thermodynamic and physical property data equations for ammonia-lithium nitrate and ammonia-sodium thiocyanate solutions, Solar Energy (32) (1984) 231-236.

Infante Ferreira C.A., Vertical tubular absorbers for ammonia-salt absorption refrigeration, Doctoral Thesis, Delft University of Technology, Delf, Netherlands, 1985.

International Energy Agency (IEA), Energy Technology Perspectives 2010.

Issa M., Ishida K., Monde M., Mass and heat transfer during absorption of ammonia into ammonia water mixture, International Communication in Heat and Mass Transfer 29 (6) (2002) 773-786.

Kalogirou S.A. and Florides G.A., Solar Space Heating and Cooling Systems, Comprehensive Renewable Energy, 3.13 (2012) 449-480.

Kang Y.T. and Kashiwagi T., Heat transfer enhancement by Marangoni convection in the NH_3-H_2O absorption process, International Journal of Refrigeration 25 (2002) 780-788.

Kang Y.T., Akisawa A., Kashiwagi T., Analytical investigation of two different absorption modes: falling film and bubble types, International Journal of Refrigeration 23 (2000) 430-443.

Kang Y.T., Akisawa A., Kashiwagi T., Experimental correlation of combined heat and mass transfer for NH_3-H_2O falling film absorption, International Journal of Refrigeration 22 (1999a) 250-262.

Kang Y.T., Akisawa A., Kashiwagi T., Visualization and model development of Marangoni convection in NH_3-H_2O system, International Journal of Refrigeration 22 (8) (1999b) 640-649.

Kang Y.T., Christensen R.N., Kashiwagi T., Ammonia–water bubble absorber with a plate heat exchanger, ASHRAE Transaction 104 (1998) 956-966.

Kang Y.T., Kim H.J., Lee K.I., Heat and mass transfer enhancement of binary nanofluids for H_2O/LiBr falling film absorption process, International Journal of Refrigeration 31 (2008) 850-856.

Kang Y.T., Nagano T., Kashiwagi T., Mass transfer correlation of NH_3-H_2O bubble absorption, International Journal of Refrigeration 25 (2002a) 878-886.

Kang Y.T., Nagano T., Kashiwagi T., Visualization of bubble behavior and bubble diameter correlation for NH_3-H_2O bubble absorption, International Journal of Refrigeration 25 (2002b) 127-135.

Keblinski P., Phillpot S.R., Choi S.U.S., Eastman J.A., Mechanism of heat flow in suspensions of nano-sized particles (nanofluids), International Journal of Heat and Mass Transfer 45 (2002) 855-863.

Keizer C., Absorption Refrigeration Machines, Report, Laboratory of Refrigeration and Indoor Climate Technology, Delft University of Technology, Netherlands, 1982.

Kim H., Jeong J., Kang Y.T., Heat and mass transfer enhancement for falling film absorption process by SiO_2 binary nanofluids, International Journal of Refrigeration 35 (2012) 645-651.

Kim H.Y., Saha B.B., Koyama S., Development of a slug flow absorber working with ammonia-water mixture: part I—flow characterization and experimental investigation, International Journal of Refrigeration 26 (2003a) 508-515.

Kim H.Y., Saha B.B., Koyama S., Development of a slug flow absorber working with ammonia–water mixture: part II—data reduction model for local heat and mass transfer characterization, International Journal of Refrigeration 26 (2003b) 698-706.

Kim J-K, Akisawa A., Kashiwagi T., Kang Y.T., Numerical design of ammonia bubble absorber applying binary nanofluids and surfactants, International Journal of Refrigeration 30 (2007b) 1086-1096.

Kim J-K., Jung J.Y., Kang Y.T., Absorption performance enhancement by nano-particles and chemical surfactants in binary nanofluids, International Journal of Refrigeration 30 (2007a) 50-57.

Kim J-K., Jung J.Y., Kang Y.T., The effect of nano-particles on the bubble absorption performance in a binary nanofluids, International Journal of Refrigeration 29 (2006b) 22-29.

Kim J-K., Jung J.Y., Kim J.H., Kim M.G., Kashiwagi T., Kang Y.T., The effect of chemical surfactants on the absorption performance during NH_3/H_2O bubble absorption process, International Journal of Refrigeration 29 (2006a) 170-177.

Kim J-K., Park C.W., Kang Y.T., The effect of micro-scale surface treatment on heat and mass transfer performance for a falling film H_2O/LiBr absorber, International Journal of Refrigeration 36 (2003) 575-585.

Kim K.J., Berman N.S., Wood B.D., The interfacial turbulence in falling film absorption: effects of additives, International Journal of Refrigeration 19 (5) (1996) 322-330.

Klein S.A., Engineering Equation Solver (EES) (1992-2012), v9.174.

Krishnamurthy S., Bhattacharya P., Phelan P.E., Enhanced mass transport in nanofluids, Nano Letters 6 (3) (2006) 419-423.

Kwon K. and Jeong S., Effect of vapor flow on the falling-film heat and mass transfer of the ammonia/water absorber, International Journal of Refrigeration 27 (2004) 955-964.

Labus J., Modelling of small capacity absorption chillers driven by solar thermal energy or waste heat, Doctoral Thesis, Universitat Rovira i Virgili, Tarragona, Spain, 2011.

Lee J. W., Jung J-Y., Lee S-G., Kang Y. T., CO_2 bubble absorption enhancement in methanol-based nanofluids, International Journal of Refrigeration 34 (2011) 1727-1733.

Lee J.K., Koo J., Hong H., Kang Y.T., The effects of nanoparticles on absorption heat and mass transfer performance in NH_3/H_2O binary nanofluids, International Journal of Refrigeration 33 (2010) 269-275.

Lee J-C., Lee K-B., Chun B-H., Lee C.H., Ha J.J., Kim S.H., A study on numerical simulations and experiments for mass transfer in bubble mode absorber of ammonia and water, International Journal of Refrigeration 26 (2003) 551-558.

Lee K.B., Chun B.H., Lee J.C., Hyun J.C., Kim S.H., Comparison of Heat and Mass Transfer in Falling Film and Bubble Absorbers of Ammonia-Water, Experimental Heat Transfer 15 (2002b) 191-205.

Lee K.B., Chun B.H., Lee J.C., Lee C.H., Kim S.H., Experimental analysis of bubble mode in a plate-type absorber, Chemical Engineering Science 57 (2002a) 1923-1929.

Libotean S., Martin A., Salavera D., Vallès M., Esteve X., Coronas, A., Densities, viscosities, and heat capacities of ammonia + lithium nitrate and ammonia + lithium nitrate + water solutions between (293.15 and 353.15) K, Journal of Chemical and Engineering Data 53 (10) (2008) 2383-2388.

Libotean S., Salavera D., Vallès M., Esteve X., Coronas A., Vapour-liquid equilibrium of ammonia + lithium nitrate + water and ammonia + lithium nitrate solutions from (293.15 to 353.15) K, Journal of Chemical and Engineering Data 52 (2007) 1050-1055.

Linek V., Korda M., Soni M., Mechanism of gas absorption enhancement in presence of fine solid particles in mechanically agitated gas–liquid dispersion. Effect of molecular diffusivity, Chemical Engineering Science 63 (2008) 5120-5128.

Ma X., Su F., Chen J., Zhang Y., Heat and mass transfer enhancement of the bubble absorption for a binary nanofluids, Journal of Mechanical Science and Technology 21 (2007) 1813-1818.

Ma X., Su F., Chen J., Bai T., Han Z., Enhancement of bubble absorption process using a CNTs-ammonia binary nanofluid, International Communication in Heat and Mass Transfer 36 (2009) 657–660.

McNelly L.A., Thermodynamic properties of aqueous solutions of lithium bromide, ASHRAE Transactions 85 (1) (1979) 413-434.

Medrano M., Bourouis M., Coronas A., Double-lift absorption refrigeration cycles driven by low-temperature heat sources using organic fluid mixtures as working pairs, Applied Energy 68 (2001) 173-185.

Merrill T.L. and Perez-Blanco H., Combined heat and mass transfer during bubble absorption in binary solutions, International Journal of Heat and Mass Transfer 40 (3) (1997) 589-603.

Merrill T.L., Setoguchi T., Perez-Blanco H., Passive Heat Transfer Enhancement Techniques Applied to Compact Bubble Absorber Design, Journal of Enhanced Heat Transfer 2 (3) (1995) 199-208.

Miller W.A., The experimental analysis of aqueous lithium bromide vertical falling film absorption, Doctoral Thesis, Universidad de Tennessee, Knoxville, USA, 1998.

Miller W.A., The synergism between heat and mass transfer additive and advanced surfaces in aqueous LiBr horizontal tube absorbers, Proceedings of the International Sorption Heat Pump Conference, (1999), Munich, Germany.

Moller R. and Knoche K.F., Surfactants with NH_3-H_20, International Journal of Refrigeration 19 (5) (1996) 317-321.

Moreno-Quintanar G., Rivera W., Best R., Comparison of the experimental evaluation of a solar intermittent refrigeration system for ice production operating with the mixtures $NH_3/LiNO_3$ and $NH_3/LiNO_3/H_2O$, Renewable Energy 38 (1) (2012) 62-68.

Nakoryakov V.E., Grigoryeva N.I., Bufetov N.S., Dekhtyar R.A., Heat and mass transfer intensification at steam absorption by surfactant additives, International Journal of Heat and Mass Transfer 51 (2008) 5175-5181.

Nordgrent M. and Setterwall F., An experimental study of the effects of surfactant on a falling liquid film, International Journal of Refrigeration 19 (5) (1996) 310- 316.

Oouchi T., Usui S., Fukuda T., Nishiguchi A. Multi-stage absorption refrigeration system, 1985, Patent No. 4520634.

Oronel C., Amaris C., Bourouis M., Vallès M., Boiling heat transfer in a plate heat exchanger of ammonia based working fluids for absorption refrigeration systems, 6th European Thermal Science Conference (EUROTHERM), (2012), Poitiers, France.

Oronel C., Amaris C., Bourouis M., Vallès M., Heat and mass transfer in a bubble plate absorber with $NH_3/LiNO_3$ and $NH_3/(LiNO_3+H_2O)$ mixtures, International Journal of Thermal Sciences 63 (2013) 105-114.

Oronel C., Amaris C., Vallès M., Bourouis M., Experiments on the characteristics of saturated boiling heat transfer in a plate heat exchanger for ammonia/lithium nitrate and ammonia/ (lithium nitrate + water), Third International Conference on Thermal Issues in Emerging Technologies (ThETA 3), (2010), El Cairo, Egypt.

Oronel C., Estudio experimental de los procesos de absorción y generación de las mezclas $NH_3/LiNO_3$ y $NH_3/(LiNO_3+H_2O)$ en intercambiadores de placas para equipos de refrigeración solar por absorción, Doctoral Thesis, Universitat Rovira i Virgili, Tarragona, Spain, 2010.

Pang C., Wu W., Sheng W., Zhang H., Kang Y.T., Mass transfer enhancement by binary nanofluids (NH_3/H_2O + Ag nanoparticles) for bubble absorption process, International Journal of Refrigeration 35 (8) (2012) 2240-2247.

Pang C., Wu W., Wu R., Chen S., The effect of Al_2O_3 nanoparticles on the NH_3/H_2O bubble absorption performance in binary nanofluids, International Conference on Computer Distributed Control and Intelligent Environmental Monitoring, (2011), Changsha, Hunan, China.

Park C. W., Kim S. S., Cho H. C, Kang Y.T., Experimental correlation of falling film absorption heat transfer on micro-scale hatched tubes, International Journal of Refrigeration 26 (2003) 75-763.

Park C.W., Cho H.C., Kang Y.T., The effect of heat transfer additive and surface roughness of micro-scale hatched tubes on absorption performance, International Journal of Refrigeration 27 (2004) 264-270.

Pearson A., Market successes of natural refrigerants: twenty years of progress, 10th IIR Gustav Lorentzen Conference on Natural Refrigerant, (2012), Delft, The Netherlands.

Perez-Lombard L., Ortiz J., Pout C., A review on buildings energy consumption information, Energy and Buildings 40 (2008) 394-398.

Petukhov B.S. and Roizen L.I., Generalized Relationships for Heat Transfer in a Turbulent Flow of a Gas in Tubes of Annular Section, High temperature (USSR) 2 (1964) 65-68.

Petukhov B.S., Heat transfer and friction in turbulent pipe flow with variable physical properties, Advances in Heat Transfer 6 (1970) 503-564.

Reiner R.H. and Zaltash A., Densities and Viscosities of ternary Ammonia/Water Fluids. ASME Winter Annual Meeting, (1993), New Orleans, US.

Reiner R.H. and Zaltash A., Evaluation of ternary ammonia-water fluids for GAX and regenerative absorption cycles. Report ORNL/CF-91/263, 1991.

Rivera C.O. and Rivera W., Modeling of an intermittent solar absorption refrigeration system operating with ammonia-lithium nitrate mixture, Solar Energy Materials & Solar Cells 76 (2003) 417-427.

Rivera W., Best R., Boiling heat transfer coefficients inside a vertical smooth tube for water:ammonia and ammonia:lithium nitrate mixtures, International Journal of Heat and Mass Transfer 42 (1999) 905-921.

Rivera W., Moreno-Quintanar G., Rivera C.O., Best R., Martinez F., Evaluation of a solar intermittent refrigeration system for ice production operating with ammonia/lithium nitrate, Solar Energy 85 (2011) 38-45.

Rivera W., VeHlez V., Xicale A., Heat transfer coefficients in two-phase flow for mixtures used in solar absorption refrigeration systems, Solar Energy Materials & Solar Cells 63 (2000) 401-411.

Srikhirin P., Aphornratana S., Chungpaibulpatana S., A review of absorption refrigeration Technologies, Renewable and Sustainable Energy Reviews 5 (2001) 343-372.

Staicovici M.D., A non-equilibrium phenomenological theory of the mass and heat transfer in physical and chemical interactions Part II - modeling of the NH_3/H_2O bubble absorption, analytical study of absorption and experiments, International Journal of Heat and Mass Transfer 43 (2000a) 4175-4188.

Staicovici M.D., A non-equilibrium phenomenological theory of the mass and heat transfer in physical and chemical interactions Part I - application to NH_3/H_2O and other working systems, International Journal of Heat and Mass Transfer 43 (2000b) 4153-4173.

Sujatha K.S., Mani A., Murthy S.S., Analysis of a bubble absorber working with R22 and five organic absorbents, Heat and Mass Transfer 32 (1997b) 255-259.

Sujatha K.S., Mani A., Murthy S.S., Finite element analysis of a bubble absorber, International Journal for Numerical Methods for Heat & Fluid Flow 7 (7) (1997a) 737-750.

Sujatha K.S., Mani A., Srinivasa Murthy S., Experiments on a bubble absorber, International Communication on Heat and Mass Transfer 26 (7) (1999) 975-984.

Sun D.W., Comparison of the performances of NH_3-H_2O, NH_3-$LiNO_3$ and NH_3-NaSCN absorption refrigeration systems, Energy Conversion and Management 39 (1998) 357-368.

Suresh M. and Mani A., Experimental studies on bubble characteristics for R134a–DMF bubble absorber, Experimental Thermal and Fluid Science 39 (2012a) 79-89.

Suresh M. and Mani A., Experimental studies on heat and mass transfer characteristics for R134a-DMF bubble absorber, International Journal of Refrigeration 35 (2012b) 1104-1114.

Suresh M. and Mani A., Heat and mass transfer studies on a compact bubble absorber in R134a-DMF solution based vapour absorption refrigeration system, International Journal of Refrigeration 36 (2013) 1004-1014.

Suresh M. and Mani A., Heat and mass transfer studies on R134a bubble absorber in R134a/DMF solution based on phenomenological theory, International Journal of Heat and Mass Transfer 53 (2010) 2813-2825.

Taylor B.N. and Kuyatt C.E., Guidelines for Evaluating and Expressing the Uncertainty of NIST Measurement Results, National Institute of Standards and Technology Technical Note 1297, 1994.

Terasaka K., Oka J., Tsuge H., Ammonia absorption from a bubble expanding at a submerged orifice into wáter, Chemical Engineering Science 57 (2002) 3757-3765.

Tillner-Roth R., Harms-Watzenberg F., and Baehr H.D., Eine neue Fundamentalgleichung fur Ammoniak, DKV-Tagungsbericht 20 (1993) 167-181.

Torres Pineda I., Lee J.W., Jung I., Kang Y. T., CO_2 absorption enhancement by methanol-based $Al2O_3$ and SiO_2 nanofluids in a tray column absorber, International Journal of Refrigeration 35 (2012) 1402-1409.

Treybal R.E., Mass transfer operations, McGraw-hill, 3rd edition, 1981.

Uchibayashi K., Niibe M., Nakamura Y., Viscosity and lithium-7 nuclear magnetic resonance relaxation time of concentrated lithium nitrate-ammonia solutions, Journal of chemical and engineering data (30) (1985) 214-216.

United Nations Environment Programme, www.unep.org/ClimateChange, (Consulted in 2013).

Valles M. and Salavera D., Enthalpy of NH_3/$LiNO_3$, Internal report, Crever, Universitat Rovira i virgili, 2011.

Veilleux J. and Coulombe S., A dispersion model of enhanced mass diffusion in nanofluids, Chemical Engineering Science 66 (2011) 2377-2384.

Venegas M., Arzoz P., Rodríguez M., Izquierdo M., Heat and mass transfer in NH_3-$LiNO_3$ spray absorption system, International Communication on Heat Mass Transfer 30 (6) (2003) 805-815.

Venegas M., Izquierdo M., De Vega M., A. Lecuona A., Thermodynamic study of multistage absorption cycles using low-temperature heat, International Journal of Energy Research 26 (2002) 775-791.

Venegas M., Izquierdo M., Rodríguez P., Lecuona A., Heat and mass transfer during absorption droplets, International Journal of Heat and Mass Transfer 47 (2004) 2653-2667.

Venegas M., Rodriguez P., Lecuona A., Izquierdo M., Spray absorbers in absorption systems using lithium nitrate–ammonia solution, International Journal of Refrigeration 28 (2005) 554-564.

Venegas M., Zacarías A., Vereda C., Lecuona A., Ventas R., Subcooled and saturated boiling of ammonia–lithium nitrate solution in a plate-type generator for absorption machines, International Journal of Heat and Mass Transfer 55 (2012) 4914-4922.

Ventas R., Lecuona A., Legrand M., Rodríguez-Hidalgo M.C., On the recirculation of ammonia-lithium nitrate in adiabatic absorbers for chillers, Applied Thermal Engineering 30 (2010b) 2770-2777.

Ventas R., Lecuona A., Zacarías A., Venegas M., Ammonia-lithium nitrate absorption chiller with an integrated low-pressure compression booster cycle for low driving temperatures, Applied Thermal Engineering 30 (2010a) 1351-1359.

Ventas R., Vereda C., Lecuona A., Venegas M., Rodríguez-Hidalgo M.C., Effect of the NH_3-$LiNO_3$ concentration and pressure in a fog-jet spray adiabatic absorber, Applied Thermal Engineering 37 (2012) 430-437.

Vereda C., Ventas R., Lecuona A., Venegas M., Study of an ejector-absorption refrigeration cycle with an adaptable ejector nozzle for different working conditions, Applied Energy 97 (2012) 305-312.

Wang J., Chen G., Jiang H., Study on a solar-driven ejection absorption refrigeration cycle, International Journal of Energy Research 22 (1998) 733-739.

Wang J.F., Gao G.C., Chen G.M., An improved absorption refrigeration cycle driven by unsteady thermal sources below 100 ^{o}C, International Journal of Energy Research 24 (2000) 633-640.

Wang K., Abdelaziz O., Kisari P., Vineyard E.A., State-of-the-art review on crystallization control technologies for water/LiBr absorption heat pumps, International Journal of Refrigeration 34 (2011) 1325-1337.

Wang X. and Chua H.T., Absorption Cooling: A Review of Lithium Bromide-Water Chiller Technologies, Recent Patents on Mechanical Engineering 2009, 2, 193-213.

Wang X., Bierwirth A., Christ A., Whittaker P., Regenauer-Lieb K., Chua H.T., Application of geothermal absorption air-conditioning system: A case study, Applied Thermal Engineering 50 (2013) 71-80.

Yang L., Du K., Bao S., Wu Y., Investigations of selection of nanofluids applied to the ammonia absorption refrigeration systems, International Journal of Refrigeration 35 (2012) 2248-2260.

Yang L., Du K., Niu X.F., Cheng B., Jiang Y.F., Experimental study on enhancement of ammonia-water falling film absorption by adding nano-particles, International Journal of Refrigeration 34 (2011) 640-647.

Yoon J.I., Kim E., Choi K.H., Seol W.S., Heat transfer enhancement with a surfactan on horizontal bundle tubes of an absorber, International Journal of Heat and Mass Transfer, 45 (2002) 735-741.

Zacarías A., Venegas M., Lecuona A., Ventas R., Experimental evaluation of ammonia adiabatic absorption into ammonia-lithium nitrate solution using a fog jet nozzle, Applied Thermal Engineering 50 (2013) 781-790.

Zacarías A., Venegas M., Ventas R., Lecuona A., Experimental assessment of ammonia adiabatic absorption into ammonia-lithium nitrate solution using a flat fan nozzle, Applied Thermal Engineering 31 (2011) 3569-3579.

Zacarías A., Ventas R., Venegas M., Lecuona A., Boiling heat transfer and pressure drop of ammonia-lithium nitrate solution in a plate generator, International Journal of Heat and Mass Transfer 53 (2010) 4768-4779.

Appendix

Appendix A. Model Description of Single Stage Absorption Refrigeration Cycle with the $NH_3/LiNO_3$ Mixture

In this section, description of energy and mass balances in each one of the components of a single stage absorption refrigeration system is presented. $\dot{m}$, H and x refer to mass flow, enthalpy and solution concentration in ammonia, respectively. Numbers as subscript refer to the position of the currents according to Figure 4.1 in Chapter 4.

Evaporator

Mass Balance
$$\dot{m}_{[11]} = \dot{m}_{[10]} \tag{A.1}$$

Energy Balance
$$Q_{Evap} = \dot{m}_{[10]} \cdot (H_{[11]} - H_{[10]}) \tag{A.2}$$

Absorber

Mass Balance
$$\dot{m}_{[1]} = \dot{m}_{[12]} + \dot{m}_{[6]} \tag{A.3}$$

$$\dot{m}_{[1]} \cdot x_{[1]} = \dot{m}_{[12]} + \dot{m}_{[6]} \cdot x_{[6]} \tag{A.4}$$

Energy Balance
$$Q_{Abs} + \dot{m}_{[1]} \cdot H_{[1]} = \dot{m}_{[12]} \cdot H_{[12]} + \dot{m}_{[6]} \cdot H_{[6]} \tag{A.5}$$

Solution Pump

Mass Balance
$$\dot{m}_{[2]} = \dot{m}_{[1]} \tag{A.6}$$

$$x_{[2]} = x_{[1]} \tag{A.7}$$

Energy Balance
$$W_{Pump} = \dot{m}_{[1]} \cdot (H_{[2]} - H_{[1]}) \tag{A.8}$$

$$\eta_{Pump} = \frac{v_{[1]} \cdot (P_{High} - P_{Low})}{H_{[2]} - H_{[1]}} \tag{A.9}$$

Solution Heat Exchanger

Mass Balance
$$\dot{m}_{[3]} = \dot{m}_{[2]} \tag{A.10}$$

$$\dot{m}_{[5]} = \dot{m}_{[4]} \tag{A.11}$$

$$x_{[3]} = x_{[2]} \tag{A.12}$$

$$x_{[5]} = x_{[4]} \tag{A.13}$$

Energy Balance

$$Q_{Strong\_Sol} = \dot{m}_{[2]} \cdot (H_{[3]} - H_{[2]})$$
$$Q_{Weak\_Sol} = \dot{m}_{[4]} \cdot (H_{[4]} - H_{[5]}) \quad \text{(A.14)}$$

$$\eta_{SHE} = \frac{\dot{m}_{[2]} \cdot (H_{[3]} - H_{[2]})}{C_{\min} \cdot (T_{[4]} - T_{[2]})} \quad \text{(A.15)}$$

Valve in the Solution Circuit

Mass Balance

$$\dot{m}_{[6]} = \dot{m}_{[5]} \quad \text{(A.16)}$$

$$x_{[6]} = x_{[5]} \quad \text{(A.17)}$$

$$H_{[6]} = H_{[5]} \quad \text{(A.18)}$$

Generator

Mass Balance

$$\dot{m}_{[4]} + \dot{m}_{[7]} = \dot{m}_{[3]} \quad \text{(A.19)}$$

$$\dot{m}_{[4]} \cdot x_{[4]} + \dot{m}_{[7]} = \dot{m}_{[3]} \cdot x_{[3]} \quad \text{(A.20)}$$

Energy Balance

$$\dot{m}_{[4]} \cdot H_{[4]} + \dot{m}_{[7]} \cdot H_{[7]} = Q_{Gen} + \dot{m}_{[3]} \cdot H_{[3]} \quad \text{(A.21)}$$

Condenser

Mass Balance

$$\dot{m}_{[8]} = \dot{m}_{[7]} \quad \text{(A.22)}$$

Energy Balance

$$Q_{Cond} = \dot{m}_{[7]} \cdot (H_{[7]} - H_{[8]}) \quad \text{(A.23)}$$

Valve in the Refrigerant Circuit

Mass Balance

$$\dot{m}_{[10]} = \dot{m}_{[9]} \quad \text{(A.24)}$$

Energy Balance

$$H_{[10]} = H_{[9]} \quad \text{(A.25)}$$

Refrigerant Heat Exchanger

Mass Balance

$$\dot{m}_{[9]} = \dot{m}_{[8]} \quad \text{(A.26)}$$

$$\dot{m}_{[12]} = \dot{m}_{[11]} \quad \text{(A.27)}$$

Energy Balance

$$Q_{\mathrm{REF1}} = \dot{m}_{[8]} \cdot (H_{[8]} - H_{[9]})$$
$$Q_{\mathrm{REF2}} = \dot{m}_{[12]} \cdot (H_{[12]} - H_{[11]}) \quad \text{(A.28)}$$

$$\eta_{RHE} = \frac{\dot{m}_{[8]} \cdot (H_{[8]} - H_{[9]})}{C_{\min} \cdot (T_{[8]} - T_{[11]})} \quad \text{(A.29)}$$

Coefficient of Performance (COP)

$$COP = \frac{Q_{Evap}}{Q_{Gen}} \quad \text{(A.30)}$$

System Pressures

$$P_{Low} = P_{[1,6,10,11,12]} \rightarrow f(T_{[11]})_{Saturated\_vapor} \quad \text{(A.31)}$$

$$P_{High} = P_{[2,3,4,5,7,8,9]} \rightarrow f(T_{[7]})_{Saturated\_vapor} \quad \text{(A.32)}$$

Calculation of Properties

In position 1 and 4	$x_{Sol} \rightarrow f(T_{Sol}, P_{Sol})$	(A.33)
From position 1 to 6	$H_{Sol}, \rho_{Sol}, Cp_{Sol} \rightarrow f(T_{Sol}, x_{Sol})$	(A.34)
In position 7	$H_{NH3} \rightarrow f(q_{NH3}, P_{NH3})_{Saturated\_vapor}$	(A.35)
In position 8	$H_{NH3} \rightarrow f(q_{NH3}, P_{NH3})_{Saturated\_liquid}$	(A.36)
In position 11	$H_{NH3} \rightarrow f(q_{NH3}, P_{NH3})_{Saturated\_vapor}$	(A.37)
In position 9, 10 and 12	$T_{NH3} \rightarrow f(H_{NH3}, P_{NH3})$	(A.38)

Equations of state for calculating the thermodynamic properties for ammonia were those developed by Tillner-Roth et al. (1993) and implemented in the software Engineering Equations Solver (EES).

Appendix B. Correlations of Thermophysical Properties of the $NH_3/LiNO_3$ Mixture

Crystallization limits of $NH_3/LiNO_3$ reported by Infante Ferreira et al. (1984).

$$XCRIS \rightarrow f(T_{Sol}[^{o}\mathrm{C}], x_{Sol})$$

IF (X<0.2911) THEN XCRIS =0.3021-0.00034*T-0.00000272*T^2
IF (0.2911<X<0.3) THEN XCRIS =X
IF (0.3<X <0.3076) THEN XCRIS =-0.000608*T+0.3152
IF (0.3076<X<0.3362) THEN XCRIS =0.0143*T+0.12885
IF (0.3362<X<0.4304) THEN XCRIS =-0.005402*T+0.41318
IF (0.4304<X<0.5072) THEN XCRIS =0.443413+0.0069*T+0.000854*T^2
IF (0.5072<X<0.6434) THEN XCRIS =0.527643-0.003126*T-0.000019*T^2
IF (0.6434<X<0.6649) THEN XCRIS =-0.004605*T+0.40761
IF (0.6649<X<0.7826) THEN XCRIS =0.0000309*T^2+0.57452
IF (0.7826<X<1.0000) THEN XCRIS =0.07378*T+6.7214

Vapor pressure of $NH_3/LiNO_3$ measured and correlated by Libotean et al. (2007).

$$P_{Sol}[\mathrm{kPa}] \rightarrow f(T_{Sol}[\mathrm{K}], x_{Sol})$$

pa0=4.99470524658178	pb0=-1793.21854659273
pa1=88.5490906185871	pb1=-22317.1158016582
pa2=-197.698944465798	pb2=61289.3128925447
pa3=134.938665891525	pb3=-45238.5915843719

$$\mathrm{pa} = \mathrm{pa0} + \mathrm{pa1}\cdot \mathrm{x} + \mathrm{pa2}\cdot \mathrm{x}^2 + \mathrm{pa3}\cdot \mathrm{x}^3$$
$$\mathrm{pb} = \mathrm{pb0} + \mathrm{pb1}\cdot \mathrm{x} + \mathrm{pb2}\cdot \mathrm{x}^2 + \mathrm{pb3}\cdot \mathrm{x}^3$$
$$P_{Sol} = \mathrm{e}^{\left(\mathrm{pa} + \frac{(\mathrm{pb})}{T}\right)}$$

Heat capacity of $NH_3/LiNO_3$ measured and correlated by Libotean et al. (2008).

$$Cp_{Sol}\left[\mathrm{J}\cdot \mathrm{g}^{-1}\cdot \mathrm{K}^{-1}\right] \rightarrow f(T_{Sol}[\mathrm{K}], x_{Sol})$$

cpa0=0.559273057	cpb0=0.00207796
cpa1=3.241167393	cpb1=0.001846907

$$cpa = cpa0 + cpa1 \cdot x$$
$$cpb = cpb0 + cpb1 \cdot x$$
$$Cp_{Sol} = cpa + cpb \cdot T(K)$$

Density of $NH_3/LiNO_3$ measured and correlated by Libotean et al. (2008).

$$\rho_{Sol}[kg \cdot m^{-3}] \rightarrow f(T_{Sol}[K], x_{Sol})$$

da0=1.521	db0=-0.00001961
da1= -0.4528	db1=-0.001726

$$da = da0 + da1 \cdot x$$
$$db = db0 + db1 \cdot x$$
$$\rho_{Sol} = (da + db \cdot T \cdot 1000$$

Dynamic viscosity of $NH_3/LiNO_3$ measured and correlated by Libotean et al. (2008).

$$\mu_{Sol}[mPa \cdot s] \rightarrow f(T_{Sol}[K], x_{Sol})$$

va0=1.918	vb0=-1.205
va1=10.094	vb1=-35.627
va2=-18.394	vb2=51.529

$$va = va0 + va1 \cdot x + va2 \cdot x^2$$
$$vb = vb0 + vb1 \cdot x + vb2 \cdot x^2$$
$$\mu_{Sol} = e^{\left(\frac{1000 \cdot va}{T} + vb\right)}$$

Thermal conductivity of $NH_3/LiNO_3$ measured and correlated by Cuenca et al. (2013).

$$k_{Sol} \rightarrow f(T_{Sol}[K], x_{Sol})$$

ka1=0.446088003	ka3=2.13849E-07
ka2=-0.000350326	ka4=0.006538043

$$k_{Sol} = ka1 + ka2 \cdot T + ka3 \cdot T^2 \cdot x + ka4 \cdot x$$

Enthalpy of $NH_3/LiNO_3$ (Internal report, Valles M. and Salavera D. 2011).

The liquid enthalpy for $NH_3/LiNO_3$ mixture was obtained following the method of Haltenberger (1939) used by McNeely (1979). This method was developed for binary

mixtures with only one component in the vapour phase. In addition, it should be noted that the enthalpy reference value for ammonia is 0 kJ.kg^{-1} at 0 ºC, and the reference state for the $NH_3/LiNO_3$ mixture is 0 kJ.kg^{-1} at 0 ºC with an ammonia mass fraction of 0.5.

$$H_{Sol} \rightarrow f(T_{Sol}[K], x_{Sol})$$

ha0=249.1567745	hb0=2.481273559	hc0=-0.004240786
ha1=-1628.297463	hb1=-5.184392344	hc1=0.025111292
ha2=-464.3464344	hb2=-0.775202139	hc2=-0.013342843
ha3=-105.6321057	hb3=18.98142102	hc3=-0.025956064

$$ha = ha0 + ha1 \cdot x + ha2 \cdot x^2 + ha3 \cdot x^3$$
$$hb = hb0 + hb1 \cdot x + hb2 \cdot x^2 + hb3 \cdot x^3$$
$$hc = hc0 + hc1 \cdot x + hc2 \cdot x^2 + hc3 \cdot x^3$$
$$H_{Sol} = ha + hb \cdot T + hc \cdot T^2$$

Appendix C. Test Results

Table C.1 - Experimental results from the study water/water in the plate absorber H-type.

Exp.	m_{H_in} kg.h^{-1}	T_{H_in} ºC	T_{H_out} ºC	m_{C_in} kg.h^{-1}	T_{C_in} ºC	T_{C_out} ºC	LMTD ºC	Re_H	Nu_H	h_H W.m^{-2}K^{-1}	Re_C	Nu_C	h_C W.m^{-2}K^{-1}	UA_{exp} W.K^{-1}	UA W.K^{-1}	error
A1	50.25	50.06	32.26	69.80	30.01	42.78	4.29	382.66	37.96	5981.82	242.50	30.49	4752.99	241.90	245.73	1.56 %
A2	50.36	50.04	31.01	111.20	30.09	38.78	4.12	379.18	37.92	5968.53	372.04	39.22	6085.70	271.39	276.78	1.95 %
A3	55.07	50.44	31.92	110.83	30.82	39.99	4.15	419.33	39.94	6293.60	378.27	39.29	6111.23	284.95	284.14	0.28 %
A4	60.07	50.85	31.74	110.43	30.17	40.67	4.61	458.24	41.92	6609.00	376.92	39.21	6099.17	290.55	290.14	0.14 %
A5	60.09	50.84	31.19	141.32	30.16	38.62	4.53	456.66	41.90	6602.31	471.85	44.78	6946.98	304.79	307.86	1.00 %
A6	65.19	51.06	32.12	109.43	30.13	41.51	4.82	500.06	43.92	6927.31	376.46	39.07	6082.01	299.08	295.71	1.14 %
A7	65.18	50.99	31.48	141.23	30.19	39.31	4.72	497.28	43.87	6915.91	475.32	44.83	6961.64	315.34	314.81	0.17 %
A8	65.19	50.91	31.10	171.51	30.16	37.80	4.62	495.43	43.84	6907.89	568.03	49.79	7716.57	326.95	329.18	0.68 %
A9	70.14	50.46	32.84	111.88	30.77	41.79	4.60	539.05	45.75	7218.32	387.96	39.61	6172.14	311.58	303.10	2.80 %
A10	70.73	50.03	31.64	140.26	30.11	39.46	4.68	535.54	45.84	7219.44	472.04	44.66	6934.95	324.49	320.39	1.28 %
A11	70.76	50.03	31.21	170.34	30.08	37.97	4.61	533.81	45.82	7212.96	565.33	49.63	7693.14	336.83	335.50	0.40 %
A12	70.70	49.92	31.00	201.67	30.13	36.83	4.50	531.36	45.77	7202.08	661.19	54.38	8417.82	346.82	348.31	0.43 %
A13	50.49	55.67	32.58	70.33	29.80	46.22	5.46	406.04	38.44	6096.59	252.53	30.80	4820.44	247.00	249.51	1.01 %
A14	50.35	55.71	31.97	109.89	30.92	41.75	4.99	402.80	38.34	6077.61	381.77	39.23	6115.02	277.99	279.80	0.65 %
A15	60.50	55.32	34.47	68.76	30.03	48.26	5.65	492.67	42.59	6765.55	252.12	30.53	4790.64	258.55	259.20	0.25 %
A16	60.61	55.30	31.71	118.07	30.03	42.15	5.58	482.25	42.46	6725.78	407.79	40.78	6351.98	297.71	298.10	0.13 %
A17	60.53	55.32	31.02	158.77	30.00	39.32	5.43	478.06	42.37	6705.76	533.31	47.83	7425.36	315.81	319.32	1.10 %
A18	70.23	55.33	35.84	70.16	30.01	49.54	5.81	578.99	46.37	7375.48	260.20	30.94	4860.91	273.71	269.87	1.42 %
A19	70.23	55.32	32.48	119.50	30.03	43.57	5.93	562.82	46.14	7314.45	419.26	41.17	6425.48	315.64	310.88	1.53 %
A20	70.23	55.29	31.55	159.06	30.02	40.60	5.82	557.80	46.06	7295.40	541.76	47.99	7463.30	334.60	332.86	0.52 %
A21	70.22	55.28	31.04	200.12	29.97	38.56	5.70	554.62	46.01	7282.30	666.77	54.31	8422.70	348.66	350.34	0.48 %
A22	50.04	59.86	37.59	68.65	35.05	50.85	5.11	436.09	38.82	6213.08	270.16	30.90	4888.82	249.86	253.41	1.40 %
A23	55.97	60.64	37.07	110.80	35.85	47.57	5.00	488.58	41.32	6614.69	426.57	40.15	6335.31	304.41	295.72	2.94 %
A24	60.44	59.97	39.17	68.70	35.04	52.94	5.45	533.91	43.21	6926.79	275.27	31.02	4917.20	264.89	265.39	0.19 %
A25	60.51	59.95	36.78	109.31	35.05	47.74	5.37	523.81	43.08	6890.36	417.75	39.80	6274.75	301.83	299.71	0.71 %
A26	60.56	59.88	35.98	149.71	35.02	44.62	5.18	520.56	43.05	6878.80	556.33	47.15	7408.61	323.40	323.07	0.10 %
A27	70.08	59.94	37.28	118.66	35.04	48.32	5.69	609.61	46.78	7485.40	455.98	41.69	6577.80	322.72	317.71	1.58 %
A28	70.21	60.71	36.67	182.30	35.64	44.85	5.42	610.78	46.83	7493.37	682.53	52.67	8284.13	360.56	352.96	2.15 %
A29	70.10	59.96	36.00	190.72	35.01	43.73	5.44	602.62	46.69	7461.22	702.08	53.84	8450.39	357.01	355.16	0.52 %
A30	70.08	54.94	35.82	191.17	35.00	41.97	4.39	496.80	42.65	6781.40	691.73	53.74	8418.38	329.09	338.40	2.75 %

Continuation of the experimental results from the study water/water in the plate absorber H-type.

Exp.	m_{H_in} kg.h^{-1}	T_{H_in} ºC	T_{H_out} ºC	m_{C_in} kg.h^{-1}	T_{C_in} ºC	T_{C_out} ºC	LMTD ºC	Re_H	Nu_H	h_H W.m^{-2}K^{-1}	Re_C	Nu_C	h_C W.m^{-2}K^{-1}	UA_{exp} W.K^{-1}	UA W.K^{-1}	error
A31	70.09	54.98	36.25	148.42	35.01	43.80	4.52	578.95	46.35	7373.25	547.36	46.86	7356.99	336.26	332.46	1.14 %
A32	70.02	55.66	37.72	111.19	35.78	46.92	4.52	588.56	46.47	7406.41	424.92	40.18	6334.30	320.79	310.50	3.31 %
A33	60.47	55.05	35.49	192.40	34.98	41.05	4.08	495.96	42.64	6778.52	690.86	53.86	8428.76	334.98	338.49	1.04 %
A34	60.31	55.66	35.63	161.50	34.89	42.37	4.33	498.13	42.63	6782.65	586.63	48.97	7674.78	324.05	325.74	0.52 %
A35	60.32	55.54	36.35	109.82	34.88	45.38	4.49	500.88	42.68	6792.91	410.40	39.74	6249.05	298.86	297.22	0.55 %
A36	50.63	55.49	35.55	109.84	34.67	43.83	4.18	417.45	38.67	6150.50	403.56	39.62	6217.37	280.42	283.55	1.11 %
A37	50.33	55.51	36.65	79.63	35.04	46.82	4.20	418.66	38.61	6147.51	302.03	33.33	5250.11	260.88	261.55	0.26 %
A38	55.25	50.46	31.20	209.69	30.83	35.90	3.87	418.35	39.97	6294.46	686.09	55.55	8596.27	319.15	328.24	2.77 %
A38	69.98	50.46	31.33	255.37	30.77	36.02	4.26	529.89	45.57	7177.09	835.57	61.98	9590.43	365.33	366.22	0.24 %
A39	70.02	50.43	31.26	282.72	30.78	35.52	4.21	530.21	45.59	7179.48	921.21	65.53	10134.44	370.55	373.95	0.91 %
A40	69.82	50.42	31.22	312.58	30.79	35.07	4.15	528.68	45.51	7167.96	1014.31	69.23	10702.21	374.10	381.09	1.83 %
A41	69.89	55.82	36.34	209.34	35.67	42.14	4.31	581.28	46.33	7376.21	764.75	56.62	8878.94	365.71	360.44	1.46 %
A42	70.15	55.66	36.17	307.77	35.80	40.19	4.05	582.48	46.41	7386.69	1102.98	69.89	10934.94	390.25	390.49	0.06 %
A43	70.13	60.69	36.31	250.09	35.71	42.48	5.17	609.08	46.79	7485.25	915.38	62.52	9806.16	382.43	377.69	1.26 %
A44	70.10	60.66	36.18	308.03	35.73	41.28	5.02	607.75	46.76	7479.67	1116.74	70.06	10976.91	395.84	393.71	0.54 %
A45	70.02	60.70	36.11	352.21	35.75	40.61	4.93	607.02	46.73	7474.68	1267.09	75.37	11799.06	404.81	403.62	0.29 %

Table C.2 - Experimental results from the study of NH_3 absorption process in the plate absorber H-type.

Exp.	m_{Sol_in} $kg.h^{-1}$	T_{Sol_in} ºC	P_{abs_in} kPa	V_{water_in} $m^3.h^{-1}$	T_{water_in} ºC	m_{Sol_out} $kg.h^{-1}$	T_{Sol_out} ºC	P_{abs_out} kPa	T_{water_out} ºC	x_{NH3_in} wt. %	x_{NH3_out} wt. %	F_{AB} $kg.m^{-2}s^{-1}$	Q $kW.m^{-2}$	h_{Sol} $kW.m^{-2}K^{-1}$	k_m $m.h^{-1}$	$\Delta T_{Sub\text{-}cooling\_out}$ ºC
1	40,23	45,35	516,91	0,353	40,41	42,20	43,53	505,68	42,37	0,4491	0,4672	0,00445	7,97	3,64	1,15	4,82
2	40,56	44,98	516,15	0,382	40,41	42,41	43,13	505,19	42,10	0,4526	0,4681	0,00402	7,46	3,69	1,07	4,96
3	40,46	45,14	521,46	0,416	40,45	42,16	43,18	510,60	42,10	0,4500	0,4677	0,00406	7,93	3,80	0,99	5,34
4	40,26	45,42	517,80	0,220	40,19	41,97	43,50	507,02	43,03	0,4520	0,4678	0,00386	7,19	3,82	1,06	4,79
5	40,11	45,74	515,79	0,182	40,74	41,52	43,86	505,30	43,70	0,4531	0,4678	0,00333	6,21	3,75	1,01	4,30
6	40,21	45,11	518,72	0,323	40,73	41,96	42,81	508,55	42,43	0,4539	0,4677	0,00370	6,32	3,80	0,95	5,57
7	39,84	45,62	514,80	0,284	40,70	41,10	43,39	504,30	42,70	0,4528	0,4713	0,00357	6,55	3,23	1,13	3,81
8	40,11	46,07	518,92	0,250	40,83	41,89	44,07	507,87	43,27	0,4515	0,4656	0,00375	7,05	3,29	1,06	4,82
9	39,99	45,67	519,94	0,133	40,57	41,64	44,19	509,22	44,52	0,4532	0,4657	0,00338	6,03	5,14	0,96	4,78
10	40,40	45,94	516,95	0,152	40,61	42,04	44,11	506,11	44,28	0,4519	0,4656	0,00354	6,45	4,37	1,02	4,68
11	40,36	45,37	518,32	0,132	35,68	42,75	41,50	506,37	42,48	0,4501	0,4734	0,00563	10,31	4,18	1,41	5,29
12	40,55	45,45	515,33	0,214	35,57	43,14	40,62	503,10	40,30	0,4497	0,4756	0,00622	11,69	3,32	1,56	5,41
13	40,19	45,22	514,11	0,299	35,21	43,01	39,91	502,05	38,76	0,4525	0,4777	0,00644	12,25	3,00	1,66	5,51
14	40,02	45,18	515,92	0,325	35,22	42,63	40,06	503,62	38,65	0,4502	0,4800	0,00667	12,83	3,07	1,73	4,87
15	40,18	45,21	517,65	0,389	35,41	42,89	40,06	505,24	38,28	0,4512	0,4792	0,00663	12,88	2,96	1,70	5,15
16	40,28	45,61	517,40	0,450	35,74	42,95	40,30	504,91	38,29	0,4506	0,4778	0,00648	13,21	2,92	1,68	5,26
17	10,39	44,93	521,24	0,272	35,94	11,95	36,93	516,06	37,48	0,4524	0,4966	0,00295	4,84	1,86	0,79	4,57
18	15,38	45,70	513,86	0,271	36,00	17,26	38,31	507,94	38,23	0,4500	0,4903	0,00387	6,97	1,97	1,11	4,28
19	20,45	45,63	516,14	0,264	35,48	22,38	37,93	509,30	38,14	0,4538	0,4875	0,00418	8,12	2,32	1,14	5,44
20	25,34	45,69	510,34	0,267	35,48	27,54	39,16	502,24	38,63	0,4497	0,4834	0,00504	9,69	2,43	1,38	4,82
21	40,24	44,71	517,38	0,275	34,97	43,04	39,95	505,08	38,80	0,4528	0,4806	0,00673	12,18	3,08	1,76	4,91
22	30,88	45,64	519,63	0,267	35,58	32,97	39,43	510,55	38,98	0,4526	0,4820	0,00509	10,47	2,73	1,34	5,38
23	50,01	46,15	509,85	0,266	35,35	52,55	40,51	495,50	39,61	0,4533	0,4733	0,00611	13,08	3,10	1,73	5,64
24	10,57	45,39	521,39	0,267	40,36	11,91	41,44	516,67	41,46	0,4519	0,4813	0,00218	3,38	1,88	0,64	3,92
25	15,33	45,39	514,77	0,268	40,32	16,34	41,86	509,40	41,73	0,4530	0,4796	0,00207	4,34	2,25	0,67	3,51
26	20,55	45,85	515,80	0,268	40,20	21,80	42,22	509,62	41,92	0,4528	0,4753	0,00257	5,30	2,38	0,79	4,28
27	25,33	46,10	518,95	0,268	40,21	26,85	42,57	511,82	42,18	0,4523	0,4812	0,00378	6,08	2,60	1,44	2,53
28	30,25	45,00	518,21	0,267	40,22	31,90	42,67	509,97	42,25	0,4527	0,4788	0,00414	6,25	3,39	1,38	2,94
29	48,85	45,87	513,26	0,269	40,79	50,30	43,74	501,43	43,23	0,4518	0,4652	0,00365	7,56	4,01	1,04	4,88
30	40,59	45,32	515,08	0,269	40,39	42,33	43,34	504,69	42,68	0,4496	0,4703	0,00447	7,08	3,65	1,25	4,15

Table C.3 - Experimental results from the study of NH_3 absorption process in the tubular absorber.

Exp.	m_{Sol_in} kg.h^{-1}	T_{Sol_in} ºC	P_{abs_in} kPa	V_{water_in} m^3.h^{-1}	T_{water_in} ºC	m_{Sol_out} kg.h^{-1}	T_{Sol_out} ºC	P_{abs_out} kPa	T_{water_out} ºC	x_{NH3_in} wt. %	x_{NH3_out} wt. %	F_{AB} kg.m^{-2}s^{-1}	Q kW.m^{-2}	h_{Sol} kW.m^{-2}K^{-1}	k_m m.h^{-1}	$\Delta T_{Sub\text{-}cooling\_out}$ ºC
Observations: Surface: Smooth; Nanoparticles: -o- ; Tube lenght: 1 m.; Outer diam. of the abs. tube: 8.0 mm; Inner hydraulic diam. of the abs. tube: 6.0 mm																
31	10,49	45,50	514,08	0,432	40,48	11,09	47,19	523,42	40,68	0,4529	0,4653	0,00272	-	-	1,00	2,71
32	15,46	45,97	510,86	0,432	40,49	16,13	47,24	519,26	40,68	0,4525	0,4617	0,00340	-	-	1,19	3,37
33	20,75	45,56	519,33	0,432	40,38	21,32	47,28	526,73	40,59	0,4525	0,4613	0,00360	-	-	1,10	3,84
34	40,22	45,79	513,32	0,433	40,25	40,95	47,41	515,27	40,58	0,4520	0,4549	0,00444	-	-	1,27	4,78
35	50,23	46,06	509,39	0,433	40,49	51,00	47,56	507,90	40,85	0,4520	0,4545	0,00517	-	-	1,62	4,28
36	60,39	46,14	512,46	0,434	40,56	61,16	47,74	508,31	40,96	0,4520	0,4540	0,00552	-	-	1,72	4,27
37	30,23	45,48	514,02	0,435	40,57	30,88	47,25	518,54	40,82	0,4535	0,4593	0,00425	-	-	1,33	3,95
38	20,24	45,13	515,31	0,102	40,68	20,86	47,80	509,53	41,31	0,4524	0,4589	0,00319	2,97	1,13	1,07	2,98
39	30,21	45,56	515,56	0,102	40,67	30,87	47,83	507,06	41,36	0,4520	0,4551	0,00338	3,20	1,18	1,05	3,80
40	40,37	46,00	513,90	0,105	40,65	41,04	48,09	502,72	41,42	0,4517	0,4529	0,00333	3,69	1,32	1,06	3,89
41	50,32	46,06	516,20	0,107	40,62	50,96	48,12	502,11	41,46	0,4529	0,4534	0,00339	4,11	1,53	1,13	3,68
42	60,21	46,04	517,76	0,106	40,81	60,80	48,34	501,03	41,60	0,4525	0,4529	0,00351	3,83	1,40	1,17	3,53
43	71,53	45,23	516,58	0,110	40,78	72,38	48,14	496,06	41,55	0,4527	0,4505	0,00326	3,88	1,64	0,96	4,09
44	29,94	45,58	514,31	0,105	35,56	30,74	45,58	507,58	36,60	0,4530	0,4553	0,00382	5,03	1,06	0,98	6,03
45	40,54	45,00	516,86	0,091	35,62	41,15	46,04	506,36	36,90	0,4516	0,4547	0,00392	5,40	1,42	0,96	5,66
46	49,70	45,63	514,84	0,091	35,69	50,50	46,04	501,34	37,00	0,4532	0,4535	0,00400	5,46	1,39	1,06	5,70
47	64,82	46,07	514,17	0,106	35,70	65,70	46,50	495,64	36,99	0,4521	0,4510	0,00414	6,22	1,39	1,12	5,56
48	20,46	45,23	517,41	0,091	35,52	21,19	45,71	513,11	36,47	0,4522	0,4590	0,00388	3,98	0,83	1,01	5,24
49	20,84	45,95	511,68	0,084	40,57	21,58	47,59	505,43	41,54	0,4531	0,4580	0,00352	3,75	1,19	1,27	3,18
50	31,43	45,50	514,73	0,086	40,62	32,08	47,53	505,64	41,71	0,4507	0,4537	0,00343	4,29	1,58	0,97	4,39
51	40,47	45,65	510,22	0,086	40,57	41,17	47,57	498,74	41,58	0,4522	0,4537	0,00368	4,01	1,36	1,16	3,94
52	50,38	46,11	511,21	0,091	40,46	51,04	47,71	496,87	41,70	0,4514	0,4521	0,00358	5,22	1,78	1,12	4,15
53	60,60	46,33	511,84	0,090	40,47	61,20	47,91	494,49	41,71	0,4527	0,4532	0,00369	5,14	1,67	1,30	3,50

Continuation of the experimental results from the study of NH_3 absorption process in the tubular absorber.

Exp.	m_{Sol_in} kg.h^{-1}	T_{Sol_in} ºC	P_{abs_in} kPa	V_{water_in} m^3.h^{-1}	T_{water_in} ºC	m_{Sol_out} kg.h^{-1}	T_{Sol_out} ºC	P_{abs_out} kPa	T_{water_out} ºC	x_{NH3_in} wt. %	x_{NH3_out} wt. %	F_{AB} kg.m^{-2}s^{-1}	Q kW.m^{-2}	h_{Sol} kW.m^{-2}K^{-1}	k_m m.h^{-1}	$\Delta T_{Sub\text{-}cooling\_out}$ ºC
Observations: Surface: Adv.; Nanoparticles: -o- ; Tube lenght: 1 m.; Outer diam. of the abs. tube: 9.5 mm; Inner hydraulic diam. of the abs. tube: 7.5 mm																
54	10,41	44,79	520,10	0,460	40,88	11,28	46,07	525,07	41,04	0,4531	0,4656	0,00346	-	-	1,01	3,84
55	15,18	45,77	519,19	0,461	40,82	16,08	46,51	524,14	41,02	0,4531	0,4621	0,00379	-	-	1,14	4,27
56	40,15	45,31	508,34	0,464	40,81	41,09	46,32	510,49	41,09	0,4524	0,4557	0,00477	-	-	1,29	5,35
57	49,96	45,71	520,92	0,464	40,82	51,04	47,22	522,18	41,18	0,4493	0,4526	0,00599	-	-	1,42	5,97
58	20,36	45,54	521,03	0,464	40,52	21,25	46,50	525,00	40,77	0,4523	0,4607	0,00427	-	-	1,18	4,70
59	30,38	46,00	524,14	0,464	40,44	31,37	46,71	527,06	40,72	0,4523	0,4574	0,00484	-	-	1,27	5,48
60	25,57	45,78	518,13	0,459	40,27	26,42	46,38	521,46	40,53	0,4522	0,4585	0,00417	-	-	1,13	5,19
Observations: Surface: Adv.; Nanoparticles: -o- ; Tube lenght: 1 m.; Outer diam. of the abs. tube: 9.5 mm; Inner hydraulic diam. of the abs. tube: 2.5 mm																
61	10,48	45,74	515,08	0,448	40,55	11,24	44,76	514,58	40,78	0,4522	0,4679	0,00331	-	-	1,03	3,93
62	15,22	45,30	518,72	0,448	40,55	16,07	45,30	515,91	40,84	0,4517	0,4642	0,00410	-	-	1,14	4,44
63	25,30	45,65	511,45	0,448	40,07	26,32	45,31	506,83	40,48	0,4508	0,4587	0,00523	-	-	1,38	5,36
64	20,34	45,68	513,52	0,446	40,33	21,20	45,61	513,77	40,74	0,4531	0,4650	0,00477	-	-	1,54	3,81
65	30,32	45,12	510,02	0,445	40,14	31,39	45,94	504,55	40,61	0,4525	0,4613	0,00629	-	-	1,92	3,91
66	35,36	45,24	511,95	0,445	40,16	36,54	46,22	503,94	40,69	0,4521	0,4608	0,00732	-	-	2,28	3,71
67	40,44	45,20	514,28	0,445	40,64	41,65	46,46	503,29	41,16	0,4531	0,4621	0,00811	-	-	2,75	3,11

Continuation of the experimental results from the study of NH_3 absorption process in the tubular absorber.

Exp.	m_{Sol_in} kg.h^{-1}	T_{Sol_in} ºC	P_{abs_in} kPa	V_{water_in} m^3.h^{-1}	T_{water_in} ºC	m_{Sol_out} kg.h^{-1}	T_{Sol_out} ºC	P_{abs_out} kPa	T_{water_out} ºC	x_{NH3_in} wt. %	x_{NH3_out} wt. %	F_{AB} kg.m^{-2}s^{-1}	Q kW.m^{-2}	h_{Sol} kW.m^{-2}K^{-1}	k_m m.h^{-1}	$\Delta T_{Sub\text{-}cooling\_out}$ ºC
Observations: Surface: Adv.; Nanoparticles: -o- ; Tube lenght: 1 m.; Outer diam. of the abs. tube: 8.0 mm; Inner hydraulic diam. of the abs. tube: 6.0 mm																
68	10,39	45,56	515,00	0,433	40,40	11,01	46,83	523,45	40,58	0,4528	0,4686	0,00319	-	-	1,27	2,20
69	20,30	45,45	511,68	0,433	40,42	21,10	47,16	517,59	40,67	0,4518	0,4612	0,00484	-	-	1,57	3,46
70	25,39	45,87	514,46	0,433	40,48	26,27	47,24	519,18	40,73	0,4532	0,4595	0,00512	-	-	1,65	3,94
71	30,51	45,54	511,91	0,432	40,47	31,42	47,33	515,39	40,75	0,4519	0,4590	0,00615	-	-	1,94	3,75
72	60,38	46,55	514,18	0,433	40,60	61,44	47,67	508,47	41,07	0,4528	0,4562	0,00795	-	-	2,75	3,77
73	50,41	45,84	516,76	0,432	40,34	51,53	47,54	514,81	40,80	0,4527	0,4570	0,00801	-	-	2,48	4,05
74	35,31	45,59	515,37	0,433	40,34	36,39	47,24	517,80	40,63	0,4529	0,4589	0,00711	-	-	2,19	4,02
75	15,40	45,50	514,36	0,432	40,26	15,98	47,34	522,28	40,48	0,4512	0,4640	0,00358	-	-	1,24	2,83
76	40,37	45,85	514,97	0,433	40,48	41,62	47,63	515,86	40,90	0,4512	0,4552	0,00763	-	-	2,21	4,50
77	9,93	45,02	520,18	0,105	39,87	10,60	47,46	516,48	40,56	0,4528	0,4662	0,00312	3,32	1,05	1,26	1,80
78	19,87	45,90	513,35	0,109	39,91	20,57	47,99	507,83	40,74	0,4531	0,4600	0,00370	4,20	1,25	1,49	2,39
79	50,91	45,17	520,85	0,112	39,89	51,68	48,02	508,37	40,81	0,4527	0,4554	0,00535	4,75	1,65	1,63	3,61
80	60,56	45,08	516,01	0,113	39,84	61,46	48,03	501,22	40,81	0,4525	0,4532	0,00528	5,06	1,84	1,59	3,79
81	30,90	45,80	521,90	0,112	39,92	31,65	48,26	514,24	40,71	0,4514	0,4557	0,00432	4,10	1,17	1,33	3,66
82	40,44	45,88	520,88	0,111	39,95	41,24	48,24	510,97	40,87	0,4525	0,4555	0,00490	4,71	1,46	1,59	3,53
83	69,98	45,08	520,32	0,114	39,81	70,92	48,25	502,70	40,98	0,4524	0,4533	0,00616	6,13	2,55	1,86	3,62
84	20,72	45,19	511,25	0,110	35,44	21,56	46,02	506,08	36,50	0,4530	0,4620	0,00501	5,39	1,05	1,58	3,74
85	30,73	45,41	515,88	0,112	35,50	31,62	46,46	508,30	36,78	0,4530	0,4593	0,00574	6,62	1,37	1,72	4,15
86	40,62	46,19	510,21	0,108	35,48	41,54	46,90	500,15	37,06	0,4530	0,4564	0,00566	7,91	1,72	1,89	3,98
87	50,43	45,79	513,65	0,112	35,55	51,29	47,17	500,93	37,17	0,4521	0,4557	0,00631	8,38	1,89	1,97	3,94
88	60,18	47,32	517,31	0,111	35,51	61,27	47,96	502,10	37,42	0,4511	0,4530	0,00700	9,80	2,11	2,39	3,96
89	10,73	45,18	519,59	0,079	40,60	11,49	47,24	515,52	41,49	0,4532	0,4649	0,00351	3,23	1,09	1,32	2,29
90	20,56	46,18	514,97	0,084	40,67	21,25	47,52	509,40	41,65	0,4527	0,4596	0,00373	3,81	1,13	1,36	3,06
91	30,89	45,63	512,31	0,087	40,71	31,68	47,71	504,49	41,91	0,4496	0,4532	0,00424	4,77	1,67	1,21	4,29
92	40,87	45,86	514,22	0,088	40,86	41,81	48,01	503,75	42,24	0,4503	0,4525	0,00519	5,59	2,07	1,54	4,14
93	50,78	45,93	514,98	0,091	40,81	51,61	47,84	502,22	42,24	0,4525	0,4545	0,00524	6,01	2,26	1,72	3,67
94	60,08	46,62	515,99	0,091	40,71	61,12	48,27	500,77	42,48	0,4520	0,4526	0,00589	7,47	2,71	2,01	3,67

Continuation of the experimental results from the study of NH_3 absorption process in the tubular absorber.

Exp.	m_{Sol_in} kg.h^{-1}	T_{Sol_in} ºC	P_{abs_in} kPa	V_{water_in} m^3.h^{-1}	T_{water_in} ºC	m_{Sol_out} kg.h^{-1}	T_{Sol_out} ºC	P_{abs_out} kPa	T_{water_out} ºC	x_{NH3_in} wt. %	x_{NH3_out} wt. %	F_{AB} kg.m^{-2}s^{-1}	Q kW.m^{-2}	h_{Sol} kW.m^{-2}K^{-1}	k_m m.h^{-1}	$\Delta T_{Sub\text{-}cooling\_out}$ ºC
Observations: Surface: Adv.; Nanoparticles: -o- ; Tube lenght: 2 m.; Outer diam. of the abs. tube: 8.0 mm; Inner hydraulic diam. of the abs. tube: 6.0 mm																
95	10,25	45,73	515,01	0,137	40,32	11,00	44,68	497,68	41,41	0,4530	0,4753	0,00231	3,44	1,22	1,22	1,09
96	15,11	45,70	515,19	0,137	40,28	16,09	45,29	492,59	41,58	0,4526	0,4694	0,00315	4,10	1,41	1,39	1,71
97	20,23	45,29	515,60	0,136	40,40	21,34	45,81	487,49	41,94	0,4513	0,4644	0,00365	4,82	1,84	1,38	2,19
98	30,05	45,44	512,07	0,122	40,46	31,25	45,82	472,82	42,18	0,4529	0,4617	0,00410	4,83	1,95	1,71	1,97
99	59,99	45,86	515,77	0,136	40,63	60,92	46,53	443,22	42,50	0,4515	0,4540	0,00332	5,84	2,20	1,55	1,42
100	49,80	45,81	515,08	0,121	40,54	50,77	46,46	455,16	42,49	0,4525	0,4565	0,00351	5,45	2,10	1,60	1,61
101	40,13	45,66	509,21	0,123	40,54	41,20	45,87	457,54	42,32	0,4532	0,4597	0,00390	5,08	2,05	1,89	1,51
102	10,14	45,11	513,00	0,136	35,66	11,21	41,63	496,11	37,53	0,4527	0,4868	0,00388	5,88	1,38	1,92	1,13
103	20,63	45,71	514,49	0,137	35,77	21,87	43,01	484,18	38,29	0,4521	0,4713	0,00477	7,93	1,79	1,68	2,97
104	30,21	45,28	512,44	0,137	35,86	31,59	43,33	465,88	38,90	0,4519	0,4652	0,00533	9,60	2,46	1,78	3,11
105	40,72	45,63	511,01	0,136	35,60	41,84	43,40	450,19	39,06	0,4528	0,4624	0,00479	10,90	2,78	1,77	2,77
106	60,92	46,49	512,08	0,135	35,31	61,74	44,13	429,67	39,16	0,4525	0,4563	0,00352	11,98	2,72	1,49	2,32
107	50,23	45,06	508,40	0,137	35,08	51,20	43,35	436,13	38,65	0,4518	0,4589	0,00440	11,28	2,86	1,52	2,83
108	15,39	45,61	516,06	0,136	35,59	16,42	42,49	492,18	37,93	0,4533	0,4787	0,00408	7,35	1,64	1,68	2,09
Observations: Surface: Adv.; Nanoparticles: -o- ; Tube lenght: 3 m.; Outer diam. of the abs. tube: 8.0 mm; Inner hydraulic diam. of the absorber tube: 6.0 mm																
109	9,93	45,14	515,33	0,138	40,94	11,11	44,57	504,94	42,34	0,4530	0,4788	0,00236	2,91	1,80	1,35	0,73
110	15,54	45,17	515,17	0,176	39,92	16,79	44,68	502,14	41,43	0,4524	0,4736	0,00283	3,99	1,71	1,18	1,79
111	20,63	45,54	517,38	0,183	39,91	21,74	45,12	502,10	41,50	0,4527	0,4717	0,00288	4,38	1,70	1,21	1,85
112	25,23	45,73	516,79	0,210	39,95	26,47	45,24	498,16	41,57	0,4509	0,4675	0,00324	5,11	1,94	1,17	2,58
113	30,55	45,86	513,86	0,211	40,44	31,98	45,47	492,16	42,11	0,4529	0,4658	0,00355	5,33	2,27	1,40	2,45
114	40,29	45,08	511,26	0,274	40,11	41,48	45,14	482,75	41,61	0,4529	0,4629	0,00328	6,18	2,67	1,13	2,96
115	50,61	45,31	513,26	0,299	40,05	52,04	45,23	478,29	41,60	0,4510	0,4594	0,00392	6,97	2,86	1,22	3,51
116	60,05	45,33	513,98	0,317	40,13	61,28	45,14	473,36	41,65	0,4532	0,4596	0,00357	7,28	3,08	1,20	3,25
117	9,98	45,61	520,50	0,357	34,63	10,89	39,09	508,27	35,72	0,4524	0,4950	0,00254	5,86	1,31	0,96	2,35
118	20,50	45,86	517,44	0,358	34,75	22,16	41,30	499,40	36,31	0,4509	0,4813	0,00472	8,43	1,68	1,59	3,05
119	40,43	45,30	514,84	0,356	35,51	42,39	42,33	481,84	37,47	0,4520	0,4690	0,00569	10,55	2,45	1,67	4,11
120	50,14	45,62	512,77	0,357	35,58	52,09	42,44	473,99	37,67	0,4520	0,4641	0,00547	11,25	2,62	1,54	4,80
121	15,07	45,62	519,43	0,356	35,62	16,46	41,26	505,57	36,83	0,4531	0,4848	0,00363	6,52	1,42	1,35	2,56
122	30,24	46,47	516,01	0,356	35,82	32,08	42,45	490,14	37,53	0,4528	0,4736	0,00513	9,21	1,93	1,85	3,32
123	59,94	47,86	508,17	0,357	35,68	61,75	42,89	457,29	38,08	0,4525	0,4624	0,00530	12,92	2,64	2,14	3,75

Exp.	m_{Sol_in} kg.h^{-1}	T_{Sol_in} ºC	P_{abs_in} kPa	V_{water_in} m^3.h^{-1}	T_{water_in} ºC	m_{Sol_out} kg.h^{-1}	T_{Sol_out} ºC	P_{abs_out} kPa	T_{water_out} ºC	x_{NH3_in} wt. %	x_{NH3_out} wt. %	F_{AB} kg.m^{-2}s^{-1}	Q kW.m^{-2}	h_{Sol} kW.m^{-2}K^{-1}	k_m m.h^{-1}	$\Delta T_{Sub\text{-}cooling\_out}$ ºC
Observations: Surface: Smooth; Nanoparticles: 0.01 wt. % of CNTs ; Tube lenght: 1 m ; Outer diam. of the abs. tube: 8.0 mm; Inner hydraulic diam. of the abs. tube: 6.0 mm																
124	50,17	45,74	520,12	0,086	40,53	50,88	48,24	504,06	41,77	0,4531	0,4551	0,00456	4,90	1,71	-	3,23
125	60,10	45,88	520,67	0,091	40,55	60,89	48,38	503,24	41,77	0,4525	0,4535	0,00497	5,09	1,70	-	3,46
126	71,10	45,07	518,77	0,092	40,62	71,92	48,29	497,49	41,82	0,4516	0,4523	0,00540	5,13	2,01	-	3,54
127	41,28	45,67	518,07	0,085	40,64	42,01	48,21	506,52	41,73	0,4525	0,4554	0,00449	4,31	1,46	-	3,34
128	30,02	45,58	511,56	0,085	40,62	30,91	47,85	503,06	41,56	0,4526	0,4557	0,00453	3,66	1,19	-	3,41
129	20,83	45,04	518,98	0,084	40,65	21,56	47,82	513,10	41,49	0,4521	0,4583	0,00383	3,27	1,12	-	3,32
130	21,19	45,12	515,44	0,084	35,48	22,02	46,29	509,62	36,93	0,4524	0,4612	0,00499	5,61	1,05	-	3,87
131	30,26	45,45	517,64	0,081	35,39	31,19	46,67	509,43	37,28	0,4523	0,4577	0,00564	7,09	1,44	-	4,42
132	40,78	45,63	514,36	0,086	35,49	41,59	46,83	502,21	37,42	0,4528	0,4565	0,00525	7,67	1,55	-	4,15
133	50,22	45,77	519,20	0,086	35,47	51,06	47,32	504,50	37,63	0,4522	0,4546	0,00552	8,54	1,77	-	4,29
134	66,09	45,83	512,18	0,087	35,44	66,96	47,39	492,20	37,77	0,4522	0,4540	0,00625	9,41	2,03	-	3,66
Observations: Surface: Adv.; Nanoparticles: 0.01 wt. % of CNTs ; Tube lenght: 1 m ; Outer diam. of the abs. tube: 8.0 mm; Inner hydraulic diam. of the abs. tube: 6.0 mm																
135	14,43	45,28	511,48	0,089	40,28	15,26	47,20	509,15	41,16	0,4528	0,4623	0,00414	3,63	1,10	-	2,66
136	19,89	45,15	520,80	0,089	40,26	20,83	47,48	517,60	41,33	0,4519	0,4601	0,00517	4,37	1,41	-	3,46
137	29,94	45,45	519,52	0,087	40,25	30,90	47,55	514,01	41,55	0,4518	0,4577	0,00579	5,20	1,77	-	3,81
138	40,16	45,67	516,74	0,087	40,17	41,19	47,54	508,67	41,60	0,4531	0,4563	0,00609	5,69	1,94	-	3,88
139	51,17	45,59	513,76	0,090	40,16	52,14	47,61	502,91	41,63	0,4523	0,4547	0,00615	6,03	2,09	-	3,90
140	64,72	45,92	517,39	0,088	40,16	65,75	47,72	496,53	42,05	0,4531	0,4540	0,00633	7,65	3,05	-	3,58
141	42,36	45,60	516,94	0,099	35,17	43,38	45,76	508,19	37,56	0,4526	0,4580	0,00725	10,80	2,26	-	5,16
142	15,41	45,42	509,70	0,098	35,04	16,40	44,93	505,60	36,51	0,4534	0,4682	0,00602	6,58	1,16	-	3,15
143	21,37	45,22	518,69	0,098	35,96	22,36	45,75	513,55	37,61	0,4532	0,4645	0,00641	7,40	1,48	-	3,78
144	31,19	45,56	518,49	0,095	35,94	32,22	45,98	510,96	37,99	0,4528	0,4600	0,00682	8,95	1,91	-	4,58
145	51,09	45,73	517,93	0,101	35,91	52,18	46,30	500,67	38,41	0,4530	0,4573	0,00786	11,53	2,65	-	4,39
146	63,73	45,91	520,99	0,096	35,93	64,71	46,86	499,29	38,98	0,4517	0,4545	0,00733	13,40	3,49	-	4,47
Observations: Surface: Adv.; Nanoparticles: 0.02 wt. % of CNTs ; Tube lenght: 1 m ; Outer diam. of the abs. tube: 8.0 mm; Inner hydraulic diam. of the abs. tube: 6.0 mm																
147	29,87	45,57	518,80	0,095	40,53	30,81	47,96	511,54	41,81	0,4499	0,4557	0,00570	5,55	1,87	-	3,78
148	39,88	45,73	518,24	0,095	40,36	40,81	47,71	507,47	41,77	0,4509	0,4547	0,00577	6,15	2,10	-	4,07
149	52,64	45,83	517,79	0,092	40,29	53,53	47,76	502,27	41,95	0,4518	0,4541	0,00581	7,03	2,59	-	3,86
150	21,33	45,15	518,69	0,096	39,98	22,21	47,00	514,21	40,83	0,4535	0,4609	0,00486	3,74	1,08	-	3,52
151	61,99	45,97	521,53	0,094	40,10	62,90	47,86	502,27	41,87	0,4516	0,4524	0,00555	7,62	2,72	-	4,22
152	20,00	45,17	521,28	0,095	35,90	20,99	45,76	517,04	37,43	0,4524	0,4636	0,00619	6,67	1,29	-	4,20
153	30,37	45,54	518,08	0,095	35,77	31,39	45,78	510,45	37,68	0,4526	0,4603	0,00680	8,35	1,69	-	4,68
154	40,05	45,71	518,64	0,097	35,92	41,13	46,11	507,34	37,97	0,4532	0,4590	0,00750	9,11	1,89	-	4,51
155	51,29	45,87	517,35	0,095	35,76	52,29	46,40	501,31	38,30	0,4532	0,4572	0,00721	11,13	2,50	-	4,34
156	60,55	46,04	514,25	0,096	35,93	61,61	46,44	494,30	38,59	0,4530	0,4561	0,00769	11,69	2,74	-	4,18

Publications and Conferences

Contributions in refereed Journals

- C. Oronel, C. Amaris, M. Bourouis, M. Vallès, Heat and mass transfer in a bubble plate absorber with $NH_3/LiNO_3$ and $NH_3/(LiNO_3+H_2O)$ mixtures, International Journal of Thermal Sciences, 63 (2013) 105-114.
- C. Amaris, M. Bourouis, M. Vallès, D. Salavera, A. Coronas, Thermophysical properties and heat and mass transfer of new working fluids in plate heat exchangers for absorption refrigeration systems, Heat Transfer Engineering, (2013). (Accepted)
- C. Amaris, M. Bourouis, M. Vallès, Effect of advanced surfaces on the ammonia absorption process with $NH_3/LiNO_3$ in a tubular bubble absorber, International Journal of Heat and Mass Transfer, (2013). (Accepted)
- C. Amaris, M. Bourouis, M. Vallès, Passive intensification of the NH_3 absorption process with $NH_3/LiNO_3$ using carbon nanotubes and advanced surfaces in a tubular bubble absorber, Energy – The International Journal, (2013). (Accepted)
- C. Amaris, M. Bourouis, M. Vallès, Performance evaluation of the absorption process in a $NH_3/LiNO_3$ bubble absorber with different models. (In preparation)

Contributions in refereed Conferences

- C. Oronel, C. Amaris, M. Vallès, M. Bourouis, Experiments on the characteristics of saturated boiling heat transfer in a plate heat exchanger for ammonia/lithium nitrate and ammonia/(lithium nitrate + water), Third International Conference on Thermal Issues in Emerging Technologies (ThETA 3), December 19 - 22, 2010, El Cairo, Egypt. Oral Communication.
- C. Oronel, C. Amaris, M. Vallès, M. Bourouis, A. Coronas, Performance comparison of a bubble absorber with ammonia/lithium nitrate and ammonia/(lithium nitrate + water) for absorption chillers, International Sorption Heat Pump Conference (ISHPC11), April 6 - 8, 2011, Padua, Italy. Oral Communication.
- C. Amaris, C. Oronel, M. Vallès, M. Bourouis, Estudio experimental de la ebullición forzada de la mezcla $NH_3/(LiNO_3+H_2O)$ en intercambiadores de placas, VII Congreso Nacional de Ingeniería Termodinámica (CNIT7), June 15 - 17, 2011, Bilbao, Spain. Oral Communication.
- C. Amaris, M. Vallès, M. Bourouis, A. Coronas, Experimental analysis on heat and mass transfer processes in a tubular bubble absorber with ammonia/lithium nitrate for absorption chillers, 21^{ST} National & 10^{TH} ISHMT-ASME Heat and Mass Transfer Conference, December 27 - 30, 2011, Chennai, India. Oral Communication.
- C. Amaris, M. Bourouis, M. Vallès, D. Salavera, A. Coronas, Thermophysical properties and heat and mass transfer in plate heat exchangers of new absorption mixtures with

special reference to solar cooling applications, 21ST National & 10TH ISHMT-ASME Heat and Mass Transfer Conference, December 27 - 30, 2011, Chennai, India. Oral Communication.

- C. Amaris, M. Bourouis, M. Vallès, Effect of advanced surfaces on heat and mass transfer processes in a tubular bubble absorber with NH_3-$LiNO_3$ for absorption refrigeration cycles, 10th IIR Gustav Lorentzen Conference on Natural Refrigerant, June 25 - 28, 2012, Delft, The Netherlands. Oral Communication.
- C. Oronel, C. Amaris, M. Bourouis, M. Vallès, Boiling heat transfer in a plate heat exchanger of ammonia based working fluids for absorption refrigeration systems, 6th European Thermal Science Conference, September 4 - 7, 2012, Poitiers, France. Oral Communication.
- C. Amaris, M. Bourouis, M. Vallès, Experimental study of absorption process in a tubular bubble absorber with NH_3/$LiNO_3$, International Workshop on New Working Fluids for Absorption Heat Pumps and Refrigeration Systems (EUROTHERM Seminar No 100), July 22 - 23, 2013, Tarragona, Spain. Oral Communication.